Rapid Changes in the Global Carbon Cycle

Thesis submitted to the University of Oxford
for the degree of D.Phil.

Trinity 2008

Department of Earth Sciences, Faculty of Physical Sciences
Supervised by Rosalind E. M. Rickaby

Paul R. Halloran

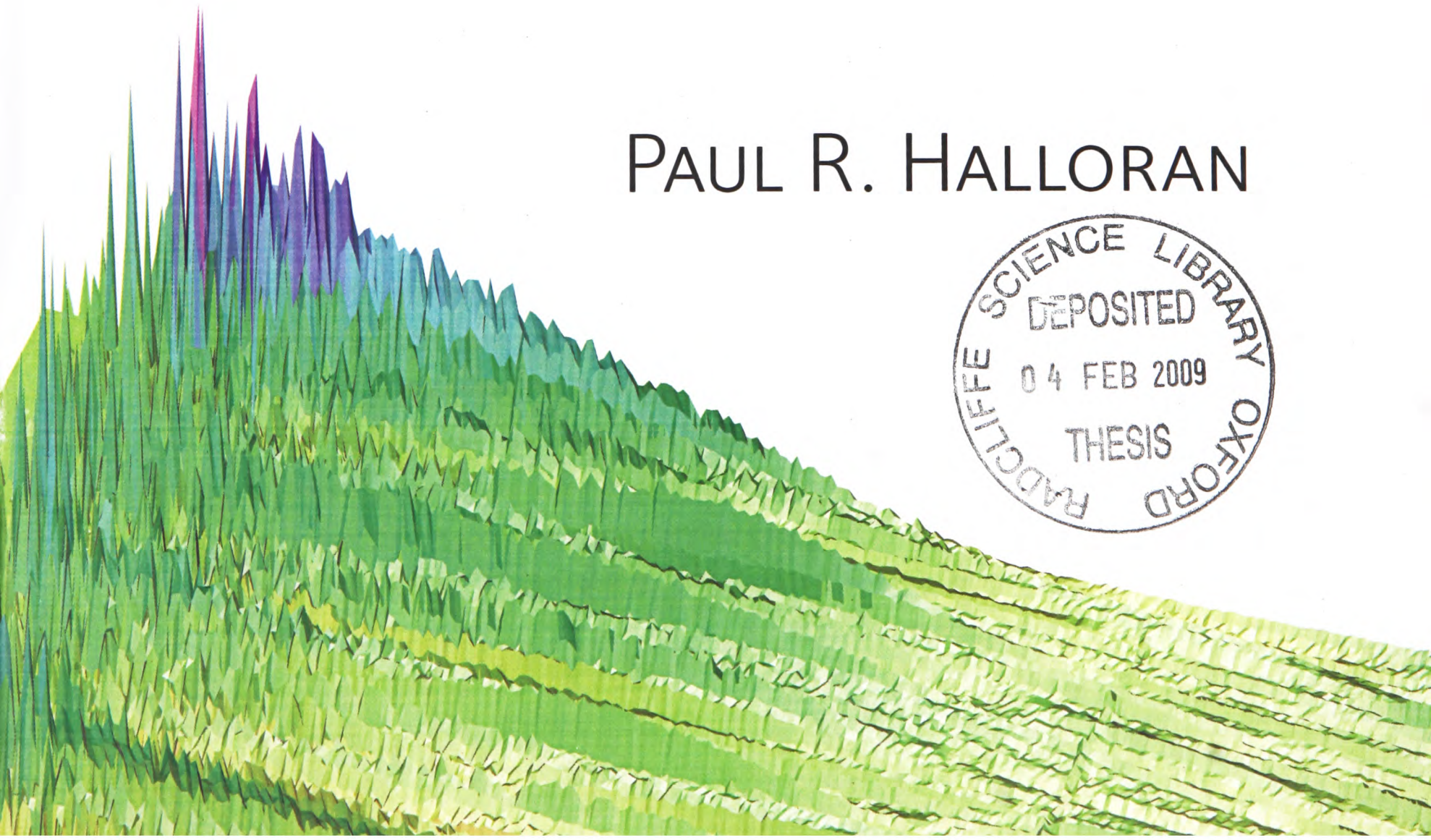

Rapid Changes in the Global Carbon Cycle

Paul Halloran, Department of Earth Sciences and Hertford College

Submitted for the degree of D. Phil. Trinity term 2008

Abstract

The flux of carbon in to and out of the atmosphere exerts a fundamental control over the Earth's climate. The oceans contain almost two orders of magnitude more carbon than the atmosphere, and consequently, small fluctuations within the oceanic carbon reservoir can have very significant effects on air-sea CO_2 exchange, and the climate of the planet. Pelagic carbonates represent a major long-term flux of carbon from the surface ocean to deep-sea sediments. Within sediments, the biologically produced carbonates act as a long-term carbon store, but also as chemical recorders of past surface ocean conditions. Counter-intuitively, despite the production and sedimentation of carbonate acting as a CO_2 sink, over periods shorter than the mixing-time of the ocean, the pH change associated with calcium carbonate precipitation enriches the surface waters in CO_2 and elevates the equilibrium value of gaseous exchange with the atmosphere.

Coccolithophores, ubiquitous marine photosynthetic plankton, produce calcium carbonate plates, coccoliths, which account for around one third of all marine calcium carbonate production. Sedimentary coccoliths therefore represent a valuable repository of surface ocean geochemical data, as well as a very significant carbon-cycle flux. This thesis examines how the mass of calcium carbonate produced by coccolithophores has changed in response to rising levels of atmospheric CO_2. A ~40% increase in average coccolith mass over the last 230 years, paralleling anthropogenic CO_2 release, is demonstrated within a high-accumulation rate North Atlantic sediment core.

Additionally, a flow-cytometry method is presented, which enables the automatic separation of coccoliths from clay particles in sedimentary samples, representing the first step in a coccolith cleaning procedure, which should ultimately enable down-core measurements of coccolith trace-element/calcium ratios. Complementing this work I describe results from continuous dissolution analysis of cultured coccoliths which allows a first-order evaluation of trace-element partitioning into coccoliths produced by the species *Coccoliths pelagicus*, and present a conceptual methodology to allow the determination of single-species coccolith chemical data.

Extended Abstract

The equilibrium state of the Earth's climate has been evolving in response to tectonic, chemical, biological or astronomical forcing since the planet's formation around four and a half billion years ago. A number of times throughout this evolution, catastrophic events have rapidly pushed the system into a state of significant disequilibrium, which has provoked dramatic re-organisation of both physical and biological processes in allowing the system to return to a steady-state. As a result of large-scale fossil-fuel combustion and the associated CO_2 release, the Earth is currently in one of these phases. To forecast and mitigate the effect that this re-equilibriation will have on human-kind, the community must understand how the biological and physical world are changing today, and how they have changed in the past.

This thesis considers how photosynthesising plankton are responding to the present non-equilibrium climatic state, and what part this response plays in mediating CO_2 exchange between the ocean and atmosphere. Also examined is how past climatic conditions can be recorded by the chemistry of marine organisms and stored in the geological record, then how this data can be measured and interpreted.

The reduction in pH of the surface ocean in response to absorption of anthropogenic CO_2, and formation of carbonic acid (commonly termed ocean-acidification) has widely been expected to reduce calcification by marine organisms (e.g. Bijma et al., 2002, Langdon et al., 2000, Ridgwell et al., 2006, Riebesell et al., 2000). The production of $CaCO_3$ causes a reduction in the surface ocean's total alkalinity (the buffering capacity of the seawater), and a fall in seawater pH. At any given pH, the relative proportion of the inorganic carbon species (HCO_3, CO_3 and CO_2) in seawater are fixed, however if the pH changes, the proportion of each of the dissolved carbon species changes. Consequently, the formation of carbonate is accompanied by an increase in the concentration of aqueous CO_2 at the expense of CO_3 (Ridgwell and Zeebe, 2005). $CaCO_3$ produced by pelagic organisms, of which the photosynthetic algae coccolithophores are a major component (Schiebel, 2002), is thought to account for almost half of present open-marine $CaCO_3$ production (Iglesias-Rodriguez et al., 2002). Recent experiments challenge whether calcification by all coccolithophore species will decrease under rising levels of atmospheric CO_2 (Langer et al., 2006). Chapter 2 presents the first deep ocean field investigation of coccolith calcification over the past two centuries, obtained from an open ocean sediment core of uniquely high accumulation rate. An increase of around 40% in the average coccolith mass is demonstrated, coincident with an increasing partial pressure of atmospheric CO_2 since the beginning of the industrial revolution. Measurements made on coccoliths, produced in cultures maintained under different CO_2 levels, indicate that the increase in coccolith mass is symptomatic of an overall increase in calcium carbonate production. This thesis considers how the described increase in calcification, and an apparent parallel increase in organic-carbon production, may influence carbon-cycle dynamics.

To understand how the Earth has responded to similar periods of rapid climate change in the past, environmental conditions must be reconstructed from proxy measurements. An environmental proxy is a parameter measurable in the geological record, which at the time

of formation co-varied with the climatic or physical parameter of interest. Of the chemical proxies utilised in the marine realm, arguably the most valuable are those which examine the isotopic abundance and trace-element composition of biologically produced carbonates. The ratio of two isotopes trapped in a biologically precipitated crystal lattice may, for example, vary with the ambient energy (i.e. temperature) during formation, or the pH and therefore chemical speciation within the liquid from which the crystal grows. The trace-element composition of the bio-crystal may co-vary with the composition of the ambient liquid, or the rate of growth of the crystal into which that element was trapped. The trace-element composition of foraminifera shells (tests) are widely used to reconstruct many past environmental parameters, including the temperature, nutrient concentrations, pH, or geographical origin, of the water in which they grew (e.g. Lear et al., 2000, Rickaby and Elderfield, 1999, Yu and Elderfield, 2007), yet symbiosis, heterotrophy and vertical migration complicate how these chemical signals are recorded. To avoid some of these issues and add a new dimension to trace-element analysis, it would be of considerable benefit to extend our trace-element measurement of biogenic calcite to the second major reservoir of pelagic $CaCO_3$, coccoliths. However, no technique has yet been proposed to facilitate the removal of detrital clay grains, the major source of trace-element contamination, from sedimentary coccolith samples. Chapters 3 and 4 present and demonstrate a technique which utilises the fluorescent and birefringent properties of calcite when examined by flow-cytometry, to identify and sort sedimentary coccoliths from detrital clays. Application of this technique produces large reductions in the elemental/calcium ratios of elements highly concentrated in clays (Mg, Mn, Al and Fe). Prior to purification, down-core samples from the North Atlantic showed highly statistically significant relationships between Mg/Ca, Mn/Ca and Al/Ca and Fe/Ca ($R^2 > 0.9$ and p-values $< 1 \times 10^{-7}$). After purification, the same analysis showed no statistical significance ($R^2 < 0.3$ and p-values > 0.8). Consideration of the trace-element composition of the clay-cleaned samples indicates that further chemical cleaning steps are probably required before down-core coccolith trace-element data can be measured with confidence. This must now be tested.

Chapter 5 examines the use of Flow-through Time Resolved Analysis, a technique developed to facilitate and monitor the cleaning and analysis of foraminiferal samples (Haley and Klinkhammer, 2002), to examine coccolith chemistry. The technique utilises a High Performance Liquid Chromatography pump to precisely control the passage of cleaning fluids and acids over a sample, held in a small filter housing, then directly into a mass spectrometer for analysis. The technique offers three major advantages over traditional batch cleaning and dissolution of samples. Firstly, because the solutions are continuously flowing past the sample, re-sorbtion of contaminants onto the sample surface after removal is prevented. Secondly, after cleaning, the rate of sample dissolution can be controlled by varying the pH and flow-rate of the final acid. Finally, because data is collected throughout the process of dissolution, it is possible to examine the spatial distribution of trace-elements within the sample. The FT-TRA protocol previously utilised for foraminiferal analysis is examined, and the procedure adapted for use with cultured coccolith samples. In contrast to the previously published methodology, it is propose that final sample dissolution should be undertaken at a constant pH of 2.5 units. Using this modification, preliminary values for the trace-element distribution coefficients between seawater and coccolith calcite are obtained, and the possibility of inhomogeneous distributions of Sr, Cd and Zn within a single coccolith considered.

As an understanding of the distribution of trace-elements into coccoliths is built up, and the method for cleaning sedimentary samples refined to allow accurate measurement of these trace-element concentrations, one final problem must be tackled; how to separate the chemistries of individual coccolith species. Chapter 6 presents a conceptual solution to this long-standing problem. It is proposed that by combining absolute coccolith species counts from different fractions of a coccolith-rich sample, with measurements of the calcium carbonate mass within each fraction, the average mass of a coccolith of each species can be calculated. If this data is then combined, again with species counts, but also with bulk

chemical measurements from each sample, the individual species chemistries can be obtained. Potential applications of this technique are considered.

Declaration

I declare that all the work presented in this thesis, other than where explicitly stated to the contrary, is my own. Unless otherwise attributed, all the ideas and opinions presented in this thesis belong to me.

Paul R. Halloran

Acknowledgements

It is a pleasure to thank the whole of the Oxford Earth Sciences Department, but in particular my supervisor **Ros Rickaby** for allowing me so much freedom and providing me with so many opportunities. I would like to thank **John Arden**, **Cees-Jan de Hoog**, **Norman Charnley** and **Jeremy Hyde** for making everything possible in the lab, **Kate Hendry** and **Dave Harding** for moral and geochemical support, and **John Elliott** and **Tom Fricker** for understanding statistics in a way I never could. I kindly thank all my co-authors on the ocean acidification publication, especially **Ian Hall** for giving up so much time, mud and lab-space and **Elena Colmenero-Hidalgo** for identifying and counting so many coccoliths! I would like to thank **Debora Iglesias-Rodriguez** for letting me analyse her cultured samples. My thanks go to **Alan and Sue Cooke** for accommodating my impromptu visits to Cardiff and **the Nissens** and **all of the inhabitants of Marlborough Road** for accommodating and entertaining me in Oxford. I sincerely thank everyone who helped in the development of the clay-coccolith sorting technique, from **Simon Jackman** for talking about flow-cytometry, **Mark Wallace** and **Claire Valance** for helping measure coccolith fluorescence, and ultimately **Nigel Rust**, who actually did the hard work. I wish to warmly thank **Brian Haley** for introducing me to Flow-Through, and **Sverre Myhra** and **Alison Crossley** for allowing me to use their equipment and giving up so much time to teach me how to use the atomic force microscope. I am deeply grateful to **Harry Elderfield**, **Mike Hall**, **Ian Hackman**, **the Plymouth Marine Labs** and **the Oxford University Museum** for supplying samples, and the Oxford Earth Sciences **Workshop** for accommodating my whims and producing various labour-saving devices. I thank gratefully **Derek Vance**, **Dani Schmidt**, **Rich Pancost** and **Dan Lunt** for believing that single-species coccolith chemistry has a future and putting so much time and effort into trying to persuade others! My gratitude goes to **Mum**, **Dad** and **NERC** for preventing me from slipping too far into the red, and **Mum** and **Dad** for much, much, more; including making me question my reason, science, and spelling. Many thanks to **Luc Beaufort** and **Heather Bouman** for carefully examining and enthusiastically discussing this thesis.

I owe the deepest loving thanks to **the chickens** for their nutritional contribution, and **Gemma** for keeping everything in context and fun! Thank you.

Table of Contents

Table of Figures and Tables

Chapter 1

Chapter 2

Chapter 3

Chapter 4

Chapter 5

Chapter 6

1 Introduction

'Climate change threatens the basic elements of life for people around the world – access to water, food, health, and use of land and the environment' (Stern and Great Britain Treasury, 2007).

The extent and consequences of anthropogenically forced climate change are perhaps the greatest unknowns our society must address. Under a 'business as usual' scenario the problems humanity are likely to face in response to a changing environment are comparable in scale to major disease and territorial threats. A thorough understanding of the Earth's response to climate forcing requires the ability either, to model perfectly every physical process on the planet with a deep understanding of the chaotic variables within the system, or, to look for analogies in the past where the world has already undergone these changes. Climate modelling is presently far from (and arguably can never be) perfect, yet where carefully applied is already providing accurate predictions and highlighting important questions. Palaeoclimate reconstruction can bring to our attention important physical processes in the climate system and provide test-scenarios for models, but critically can answer many of the questions that climate models stimulate. Both modelling and reconstruction have many inherent problems, from sampling bias to poorly understood physics, but both are required, and require each other if our changing climate is going to be understood and the correct mitigation strategies are to be enforced.

The CO_2 concentration of the atmosphere exerts an important control over the Earth's climate on all time-scales (IPCC, 2007; Royer et al., 2007; Weaver et al., 1998). Through understanding the role played by the atmospheric concentration of CO_2 in the changing climate of the past, we can narrow the uncertainty in how it might change climate in the future. To appreciate the mechanisms and consequences of changing atmospheric CO_2 concentrations we must reconstruct the past carbon cycle and concomitant environmental conditions. Marine microorganisms are responsible for almost half of the Earth's primary production, and as such play a substantial role in global carbon and nutrient cycling (Arrigo, 2005). Changes in the carbon cycle are therefore reflected by changes in the biogenic cycles of the oceans. This thesis examines the response of the phytoplankton coccolithophores, an important component of the marine planktonic community, to changes in the carbon cycle and considers the consequences of these changes. Complementing this work, the chemistry and potential of coccoliths, the fossilised remains of coccolithophores, to record past environmental change is investigated.

1.2 What are coccolithophores?

Coccolithophores are approximately-spherical unicellular planktonic algae (Division *Haptophyta*, Class *Prymnesiophyceae*) of diameter 1 to 20 μm which produce and surround themselves within an exoskeleton of calcium carbonate plates called coccoliths (Figure 1). Coccoliths first appeared in the geological record in the Late Triassic ~220 Ma (Bown, 1998), peaked in diversity during the Cretaceous and are presently produced by over 200 extant species (Jordan and Chamberlain, 1997). Coccoliths vary considerably in morphology and size, but form clusters around that of a discoid of diameter 2 to 10 μm. Coccolithophores are autotrophic photosynthesisers and as such inhabit the photic zone. In high nutrient oceanic settings, with limited competition, coccolithophore density can exceed 100,000 cells per litre (Armstrong and Brasier, 2005).

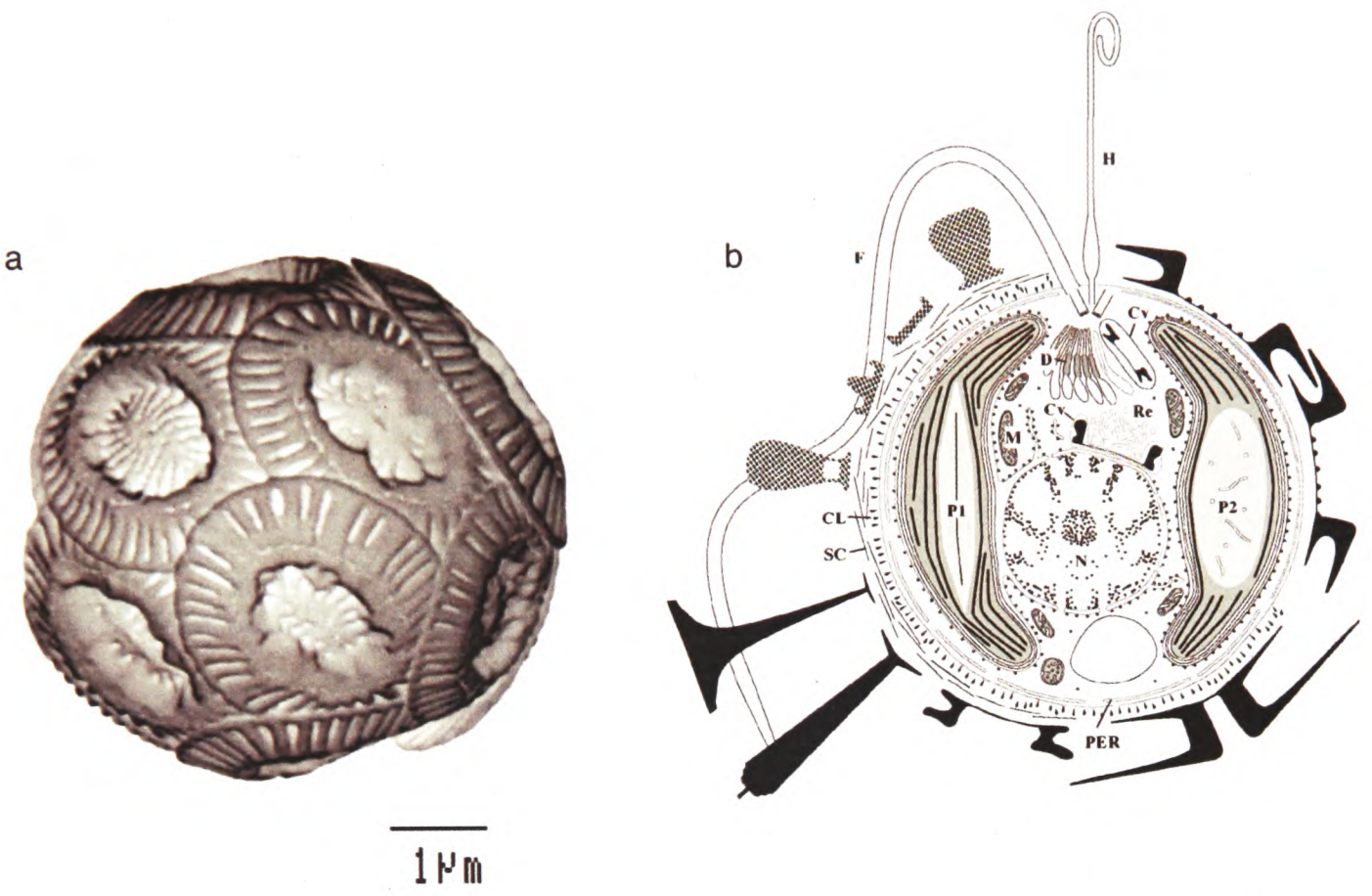

Figure 1. a. An inverted Scanning Electron Microscope (SEM) image of the coccolithophore *Emiliania huxleyi*. b. A diagrammatic representation of the cell and coccolith structures of a range of coccolithophores. The two types of coccolith-forming vesicles, found in *Pleurochrysis* (top), and *Emiliania* (bottom) are illustrated. Pyrenoid (P1) is typical in the coccolithophores and pyrenoid (P2) is seen in *Emiliania* and *Gephyrocapsa*. Heterococcoliths are shaded black and holococcoliths are highlighted by a lattice pattern. Abbreviations CL: co-lumnar deposit, Cv: coccolith forming vesicle, D: peculiar dilation of Golgi body, F: flagellum, H: haptonema, M: mitochondrial profiles, N: nucleus, P1: pyrenoid traversed by thylakoids, P2: pyrenoid traversed by tubular structures, PER: peripheral endoplasmic reticulum, Re: reticular body, SC: unmineralsed organic scales. B is taken from Billard and Inouye (2004).

After death the coccoliths settle, and assuming the underlying ocean floor lies above the carbonate compensation depth (CCD - the depth in the ocean at which the rate of supply of $CaCO_3$ equals its rate of dissolution), are well preserved in the sediment, where they are believed to constitute the largest single component of pelagic ooze (Young et al., 1999). Excellent preservation and extensive temporal and spatial existence have resulted in the detailed study of coccolithophores by both biologists and palaeontologists.

1.3 Coccolithophore Biology

Figure 1 outlines the broad physiological features of coccolithophores. The outer surface of the coccolithophore is made up of the coccoliths. There are two types of coccoliths, heterococcoliths and holococcoliths. Heterococcoliths are formed from interlocking crystal units of various morphologies, whereas holococcoliths are formed from numerous single micro-crystals (Figure 8). Heterococcoliths are produced during the diploid life-stage after the fusion of two holococcolith bearing haploid cells (Geisen et al., 2002). The two (diploid and haploid) life-stages can both reproduce through mitosis. The stimulus for sexual reproduction is poorly understood but may reflect nutrient availability or seawater viscosity (Marsh, 2003). The distinctive morphologies of heterococcoliths allow quick recognition, and have resulted in extensive study. Comparatively, holococcoliths are poorly studied, and large questions remain about their role in oceanic carbon cycling.

The biological purpose of the coccoliths remains unknown, but possible functions include:

- Protection from physical damage, predation or bacterial attack
- Light regulation resulting from the lens-like or scatter producing structures
- Buoyancy regulation
- Chemical excretion of calcium or associated metabolic by-products
- The provision of a large external surface area as a site for biological reactions

No strong evidence exists to suggest which, if any, of these functions explain coccolith formation.

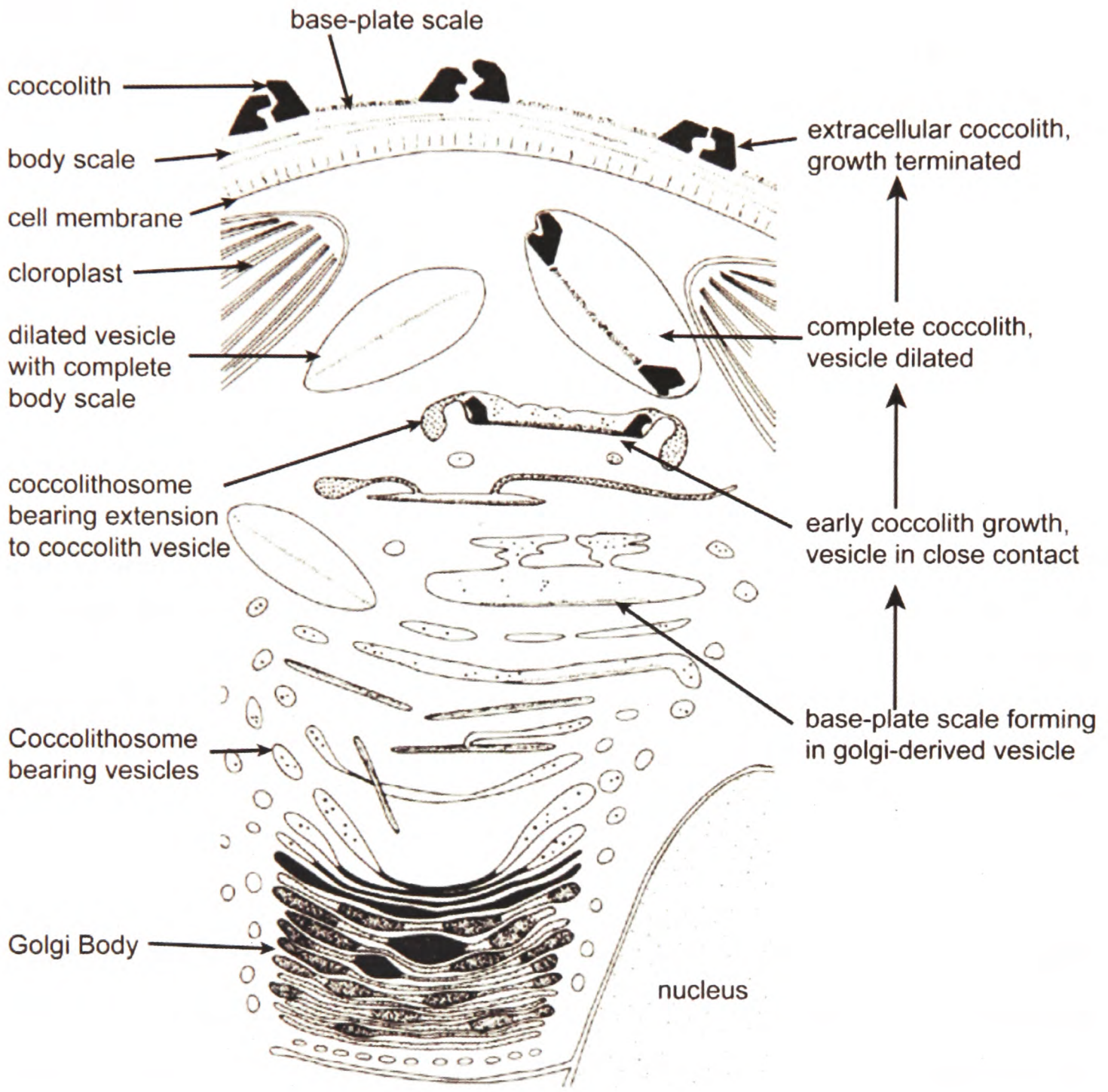

Figure 2. A diagrammatic representation of *Pleurochrysis carterae* coccolith formation and export to the cell surface. From van der Wal (1983).

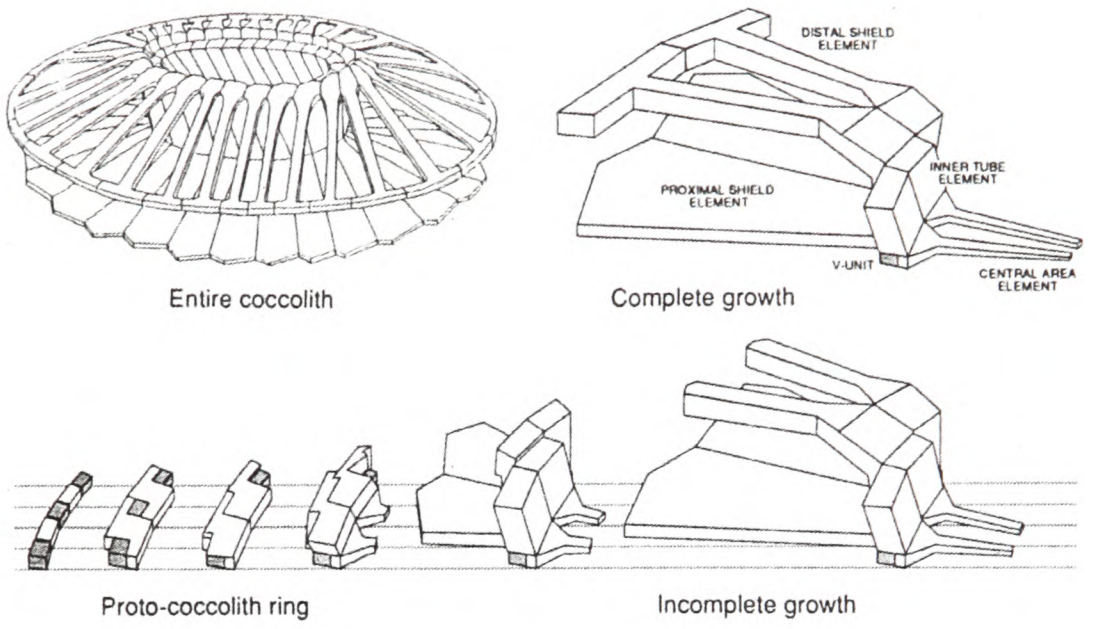

Figure 3. Crystallographic formation steps of *Emiliania huxleyi* coccoliths. Initially a proto-coccolith ring of alternating V and R crystals (crystals with their optical axis vertically 'V' and radially 'R' aligned to the plain of the coccolith) is precipitated from the vesicle fluid. In the case of *E. huxleyi* the R-crystals then grow upwards and outwards to produce the final complex coccolith morphology, and the V-crystals undergo no further growth. In different species the relative degree of growth, and morphological development of V or R-units vary. From Young et al. (1992).

Heterococcolith are produced intracellularly within a golgi-derived vesicle and exported to the surface, whereas holococcoliths are calcified extracellularly (Rowson et al., 1986). The facts that heterococcoliths are produced intracellularly, and that the process likely evolved independently from other biomineralisation mechanisms (Dove et al., 2003) distinguishes them from the many contrasting bio-calcified structures observed in the ocean and sediment, and therefore may explain some of the unusual characteristics to be discussed in subsequent chapters. The mechanisms behind the calcification process through which the delicately ornamented heterococcoliths are precipitated, although carefully studied and visually observed, are poorly understood. Firstly, the golgi-body produces, and releases into the cytoplasm, a vesicle and within that vesicle an organic base plate will form. Rhombohedral calcite nucleation takes place in a ring around the base plate, then morphologically restricted calcification progresses as the vesicle expands, upwards and outwards from these nucleation sites (Figure 2). Crystallographically the growth is strongly controlled. Figure 3 highlights

the coccolith crystal growth progression and coccolith units in *Emiliania huxleyi*. This simple diagram brings to light some of the poorly-understood questions associated with coccolith calcification:

- What causes nucleation at specific sites around the organic base-plate?
- How does the base-plate control the optical orientation of the nucleating crystals?
- Why does subsequent coccolith growth occur differently from different nucleation crystals depending on their optical orientation?
- How does the coccolithophore control the crystal morphology?

Conclusive answers to these questions are not yet available, although possible explanations, including nucleation on a well-defined template, followed by sculpting at the vesicle edge or calcium binding polysaccharides, all have their problems [see Chapter 7 in Dove et al. (2003) and Marsh (1999) for detailed discussion].

Beneath the coccolith layer exists the cell wall. The cell wall is made up of layered organic scales, again produced in vesicles associated with the golgi or reticular bodies and exported to the cell surface. Within the cells of all coccolithophore species, there are golden-brown chlorophyll-a and chlorophyll-c chloroplasts providing photosynthetic energy. The genetics and proteomics of coccolithophore cells are only now being studied, and will hopefully begin to provide answers to many of the so-far unresolved questions.

1.4 Coccolith Chemistry

The isotopic and trace-element chemistry of planktonic carbonates has been providing exemplary palaeo-climatological and oceanographic data for many decades (e.g. Hall et al., 2001; Shackleton et al., 1990). Mixed-layer open ocean organisms experience some of the most climatologically important conditions (i.e. near-surface water temperatures,

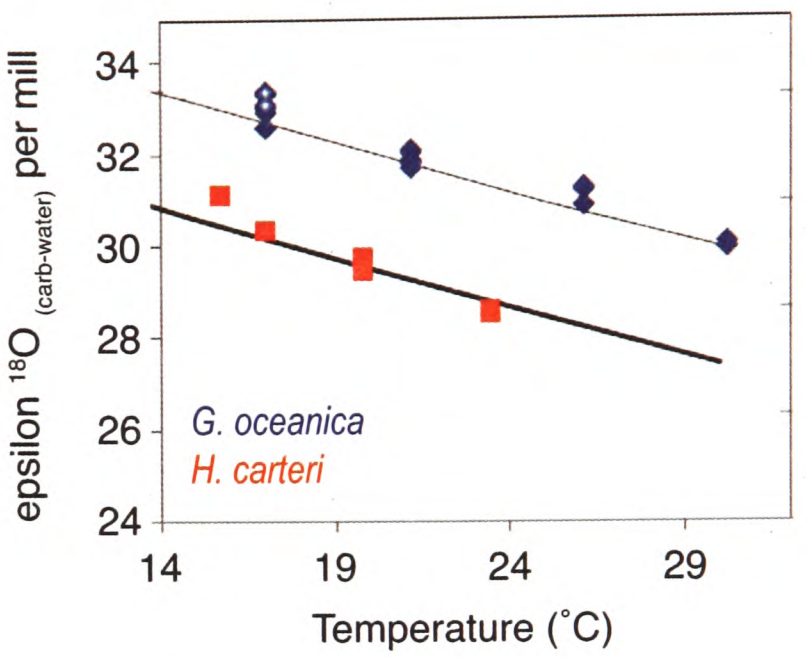

Figure 4. Epsilon ^{18}O versus temperature for the calcite of two coccolithophore species *Gephyrocapsa oceanica* and *Helicosphaera carterai*. Solid lines represent equilibrium palaeothermometry relationships. Modified from Ziveri et al. (2003).

salinities and nutrient conditions, away from the complicating coastal processes) and as such, the chemistry of their preserved remains arguably records the most valuable of climatic data-sets available in palaeoceanography. The tests (shells) of planktonic foraminifera are geochemically analysed in many labs around the world for their oxygen and carbon isotopes, Mg/Ca, Sr/Ca, Ba/Ca, Cd/Ca, U/Ca, B/Ca, and many other trace-element calcium ratios. The range of data produced from these examinations ranges from temperature and salinity to carbonate-ion and phosphate concentrations and is of immense value. The carbonate of coccolithophores, despite accounting for around half of the open ocean carbonate production and theoretically considerably more of that preserved in sediment, is only analysed at present for Sr/Ca (an intriguing but poorly understood productivity proxy). The primary reason for this is that coccoliths are too small to be manually separated from clays and from other coccolith species. The climate data is recorded, but cannot be obtained.

Thirty years ago one of the first investigations into coccolith chemistry suggested that measurement of their oxygen isotope composition represented the addition of 'a new and

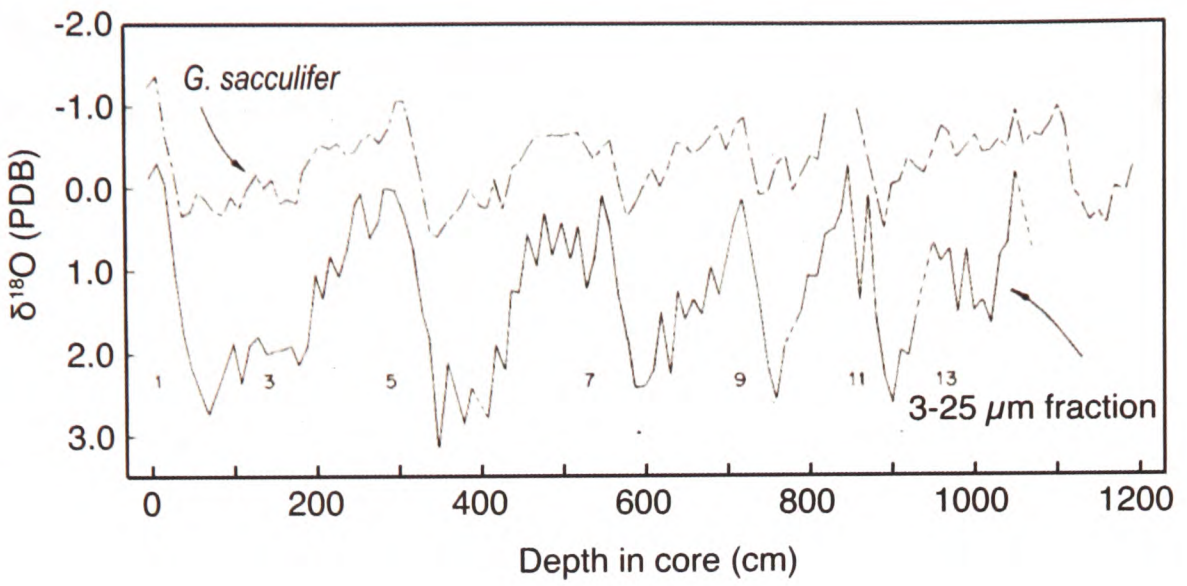

Figure 5. Oxygen isotope records from bulk sediment filtered to the 3-25 μm (coccolith) size fraction and the foraminifera *Globigerinoides sacculifer* from the central Caribbean. Modified from Anderson and Steinmetz (1981).

potentially important method to the palaeoclimatologist's arsenal' (Margolis et al., 1975). The authors compared polyspecific down-core coccolith, and foraminiferal $\delta^{18}O$, and concluded that coccolith calcium carbonate was precipitated at, or near to, equilibrium with oceanic surface waters, providing a new and valuable palaeosalinity and palaeotemperature recorder. Further work confirmed the $\delta^{18}O$ – temperature correlation in culture experiments, although this was found to hold only when growth-rate remained constant (Dudley and Goodney, 1979; Ziveri et al., 2003) (Figure 4). However, later, Dudley et al. (1986; 1980) discovered species-specific effects recorded in coccolith calcite. Despite evidence that polyspecific coccolith material could tell us little about past climates, Anderson and Steinmatz (1981) produced a polyspecific Pleistocene coccolith $\delta^{18}O$ record indicating an oxygen isotope sensitivity considerably greater than that existing in foraminifera (Figure 5).

Despite the similarities observed between bulk fine fraction and foraminiferal isotopic ratios, Paull and Thierstein (1987) recognised that near monospecific sediment samples were needed to rigorously develop coccolith palaeoproxies. To allow size separation the authors developed an automated decanting device that mixed and extracted the supernatant from

their suspension at predefined intervals as calculated using Stokes Law. Although some degree of species concentration was achieved, the authors concluded that overlap in the size ranges of coccolith species prevented true monospecific samples from being obtained. In 2001 Minoletti et al. developed a more precise technique allowing the concentration and size sorting of coccoliths. This method was, in part, made possible by the introduction of filter membranes in which the pores were 'punched' by a laser, enabling very accurate size and shape control. The method of Minoletti et al. (2001) involves repeated ultrasonic suspension and decanting, centrifuging and decanting, and filtering.

A number of further attempts have been made to produce species-specific coccolith Sr/Ca and isotopic records. Stoll and Ziveri (2002) applied repeated decanting and settling techniques to help purify coccolith sediment. These authors achieved "separation of sediment fractions whose carbonate is highly dominated (> 70% but in most cases > 90%) by coccoliths from a single species". These separated fractions displayed oxygen and carbon isotopic ratios ranging by up to 1.5‰ and 2.5‰ respectively, demonstrating a first-order separation of the chemical signatures of the different species. Stoll (2005) took this method further by attempting to quantify the mass of calcium carbonate attributed to each coccolithophore species based on species counts, coccolith volume estimates, and the density of calcite. These mass estimates were then used to assign a chemical signature to each species. Using this technique, Stoll (2005) produced oxygen and carbon isotopic records over the Palaeocene Eocene Thermal Maximum and concluded that similarities in the records produced by different species indicated only small species isotopic offsets. Culture experiments examining the inter-species variability in coccolith isotopic compositions indicated otherwise (Dudley et al., 1980; Ziveri et al., 2003). Unfortunately, volume estimates of coccoliths are subject to considerable errors (Young and Ziveri, 2000) which are greatly propagated when multiplied by the number of coccoliths in a sample. Additionally, as we show in Chapter 2, average coccolith mass from any given species is not constant, even over short timescales. Together, temporal mass variation and volume estimate errors, can explain the disparity between the down-core and

cultured range of coccolith oxygen and carbon isotopic values. More recently, a method has been developed to hand pick the coccoliths of individual species using a sharpened tungsten needle (Stoll et al., 2007a; Stoll et al., 2007b; Stoll et al., 2007c). Using this method, 12 to 20 coccoliths (~1.8 – 3.0 ng of calcium carbonate) are mounted in epoxy and their Sr/Ca ratio analysed with an ion probe. This technique reveals a considerably greater range of Sr/Ca values than those measured in sub-samples produced by filtering, settling and decanting, indicating that more information exists within down-core species specific Sr/Ca than was previously utilised. Although individual coccolith picking has the potential to highlight interspecific differences in coccolith chemistry, it is slow, and compromised by the small coccolith populations studied, and therefore unsuitable for producing high resolution, high precision records. Furthermore, the technique of Stoll et al. is suitable only for large coccoliths, preventing analysis of many Pleistocene species.

1.5 Coccolith Sr/Ca

Strontium is presently the only known trace-element incorporated into the calcite structure for which abundance in the coccolith exceeds that associated with clays, and which can be

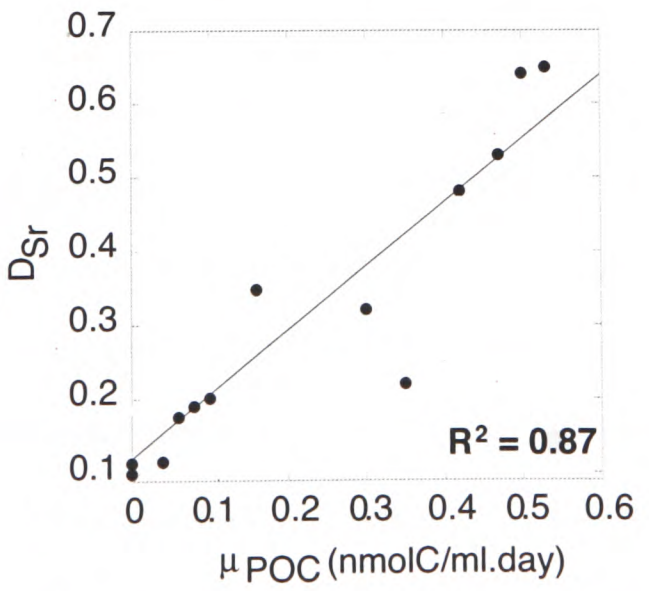

Figure 6. Sr partitioning coefficients (Dsr) plotted against growth rate (μ) in *Emiliania huxleyi*. From Rickaby et al. (2002).

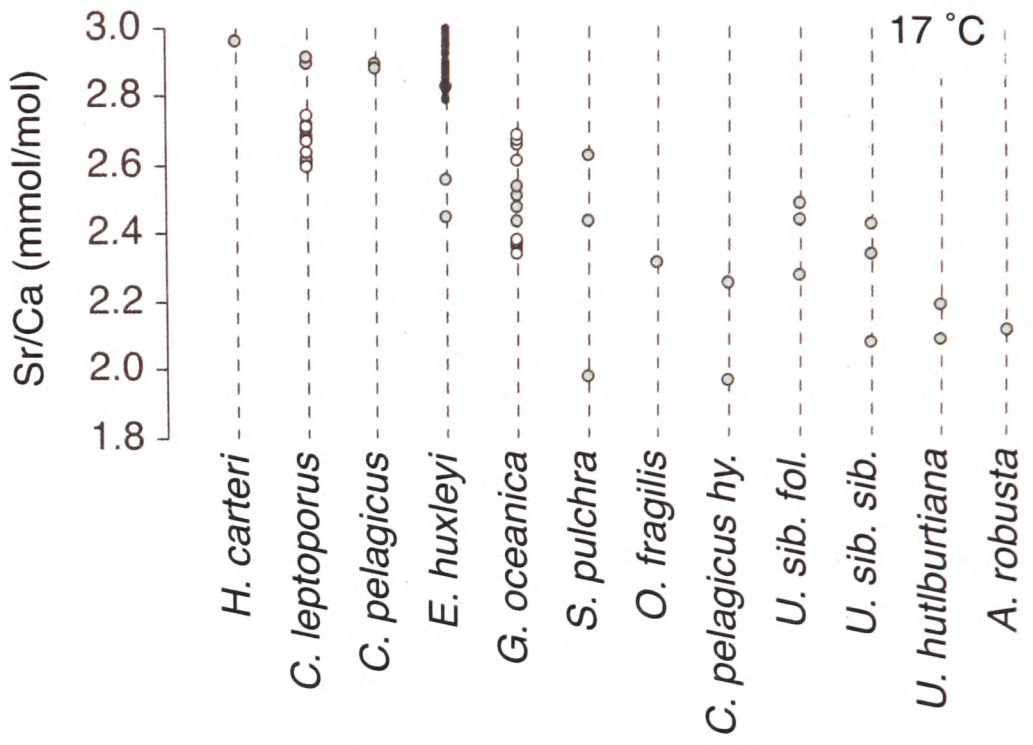

Figure 7. Sr/Ca of 12 different coccolithophore species cultured under identical conditions. Redrawn from Stoll et al. (2002)

removed from clays with reasonable success by ion-exchange. Variations in polyspecific coccolith Sr/Ca ratios observed by Stoll and Schrag (2000), from a range of latitudes, were in excess of changes expected from variations in surface water composition alone, instead correlating with differences in upwelling and primary productivity. Rickaby et al. (2002) confirmed this relationship in culture, although calculate a distribution coefficient an order of magnitude greater than that calculated by Stoll and Schrag (2000) for the open ocean (Figure 6). In 2002 Stoll and co-authors (Stoll et al., 2002a; Stoll et al., 2002b) discovered a significant temperature effect on coccolith Sr/Ca, however they also propose a seemingly elegant answer to the problem; because the relationship between coccolith Sr/Ca and calcification rate appeared to be linear, by measuring the element ratio in both slow calcifying and rapidly calcifying species, a simple equation should allow calculation of both the calcification rate and temperature. This research emphasised the need for a reliable method for species separation, a point exemplified by the ion-probe examination of Sr/Ca in individual coccoliths of various species (Shimizu and Stoll, 2004; Stoll et al., 2005) and highlighted by culture measurements (Stoll et al., 2002a) (Figure 7).

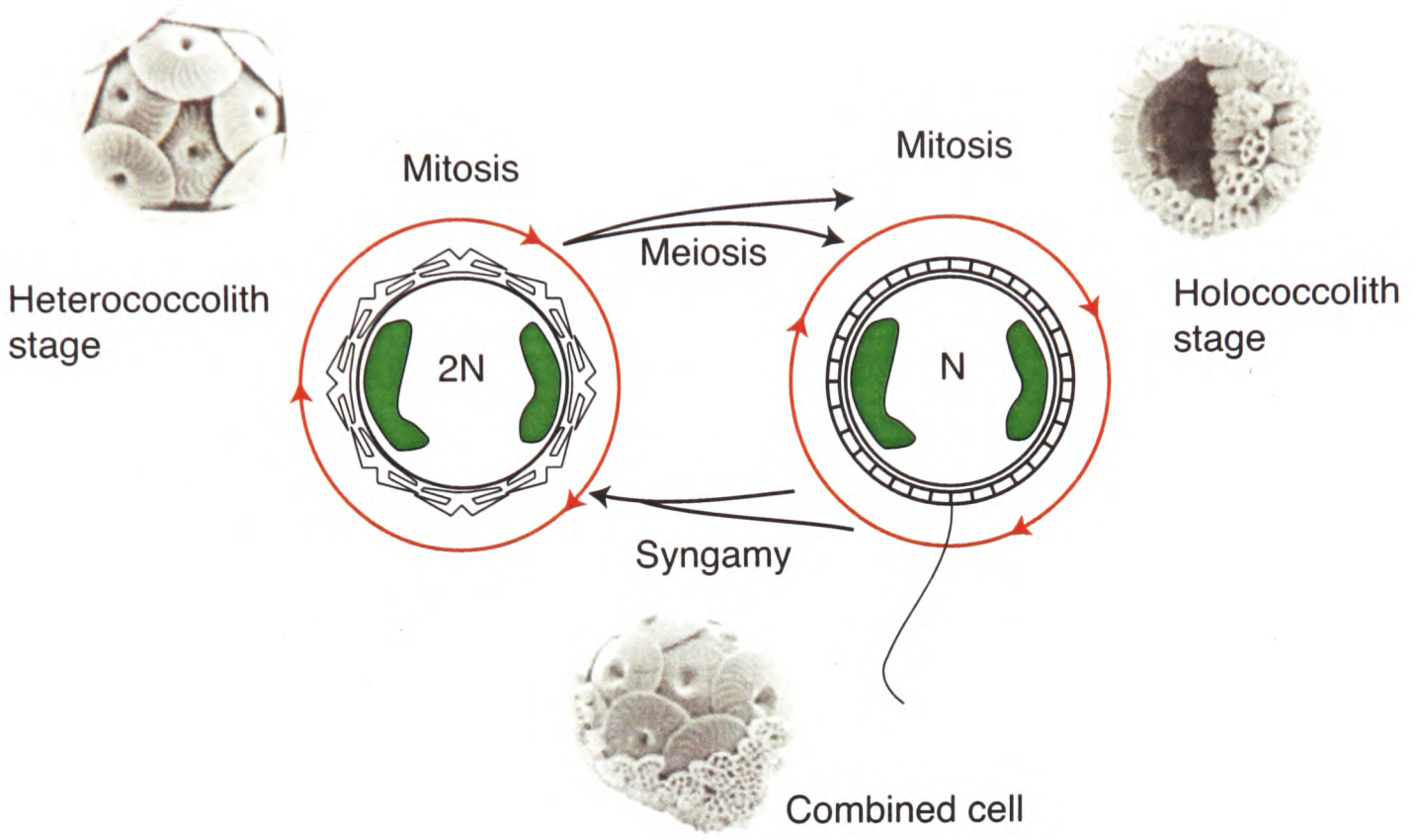

Figure 8. Diagrammatic representation of the diploid and haploid life-cycle stages of coccolithophores, during which the cell is covered with heterococcoliths and holococcoliths respectively. Modified from (Geisen et al., 2002).

In addition to strontium, magnesium is the only trace-element to be investigated as a potential coccolith palaeoproxy. In an initial investigation by Stoll et al. (2001), Mg/Ca appeared to show a significant temperature control, as would be predicted from analogy with foraminiferal calcite. However, due to the apparent low incorporation of magnesium into coccoliths, and binding of organic matter to the samples, the authors concluded that with current cleaning methods, palaeoceanographic application of the proxy was limited. A further study by Hasegawa et al. (2003) investigated x-ray diffraction observations by Takano et al. (1993) which implied the presence of Fe, Mg, Na, Sr, Si, Zn and K in the calcite of *E. huxleyi* and *H. carterae*. The data presented by Hasegawa et al. (2003) provides an interesting insight into trace-element incorporation into coccoliths, although unfortunately measurements made on the culture medium are insufficient to calculate distribution coefficients for these elements into the coccolith.

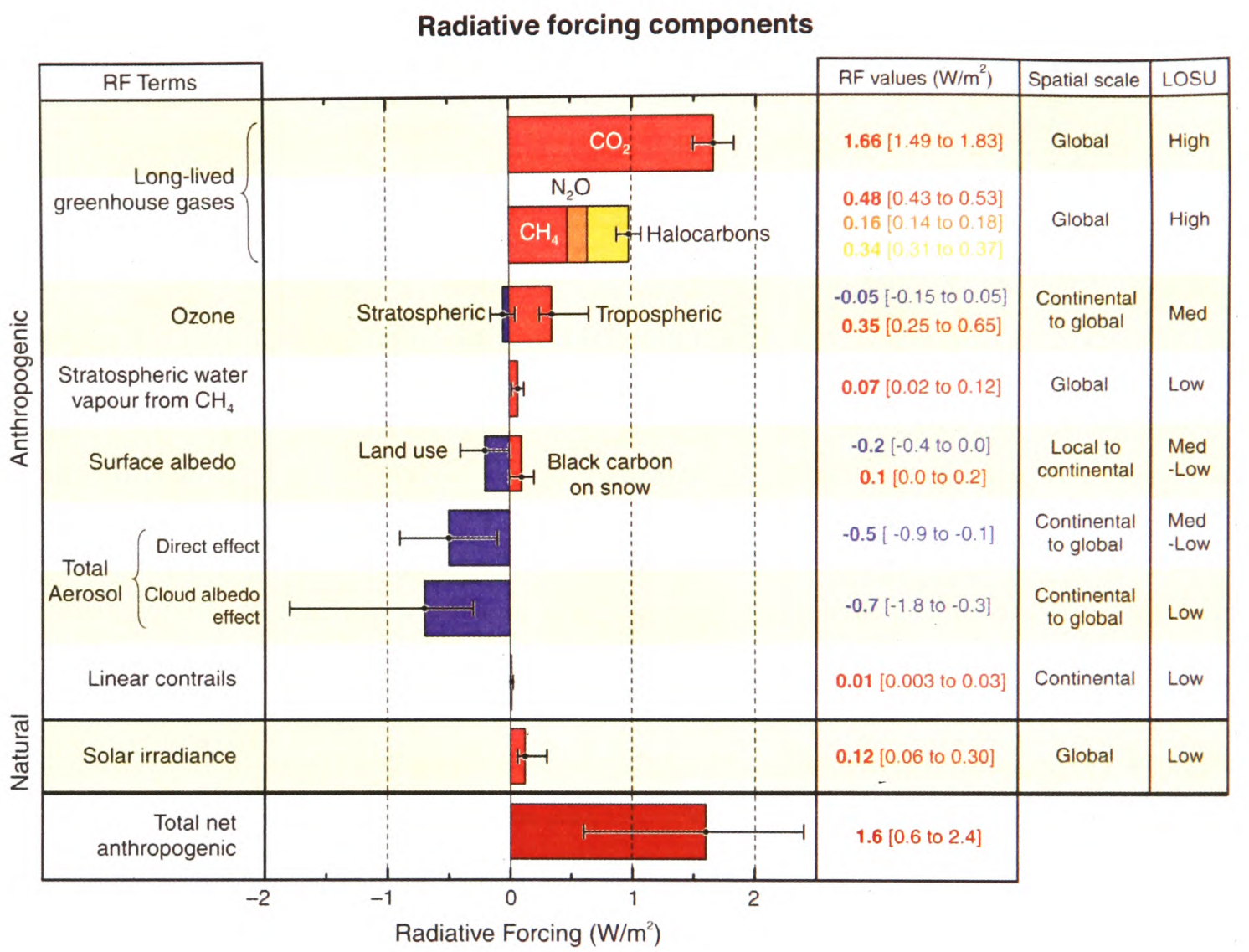

Figure 9. IPCC estimates of global-average radiative forcing (changes in the global energy balance) in 2005 from what are believed to be the seven major components of the climate system. Error bars represent 5-95% uncertainty. From the Intergovernmental Panel on Climate Change. Working Group II (2007).

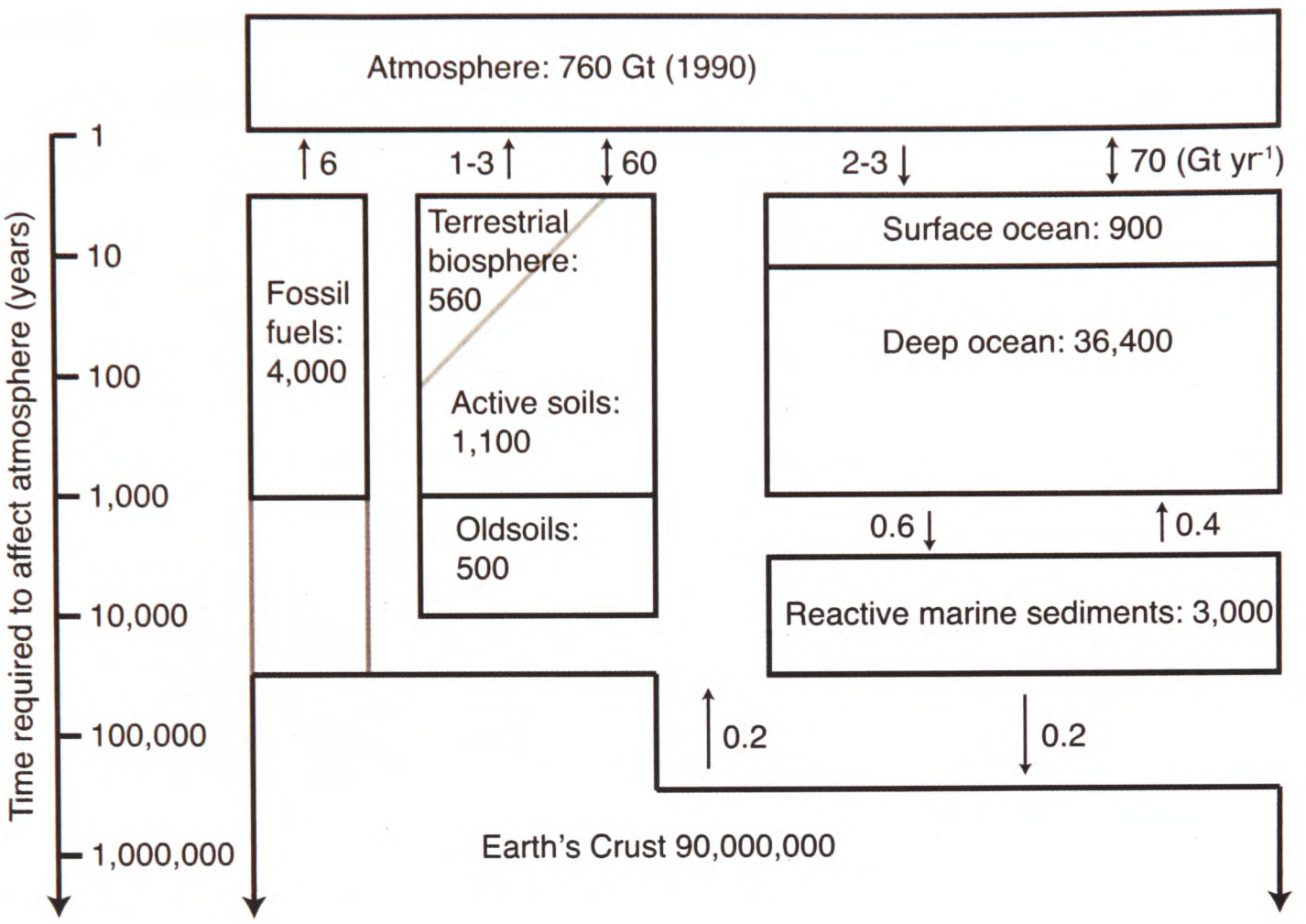

Figure 10. Principle global fluxes and reservoirs of carbon and approximate timescales over which those reservoirs can affect atmospheric CO_2. Reservoir units; Gt, flux units = Gt yr^{-1}. Re-drawn from Sundquist (1993).

1.6 Coccoliths and the Carbon Cycle

The carbon cycle involves the flux of around 150 Gt of carbon between numerous reservoirs within the atmosphere, biosphere and lithosphere every year. Figure 10 highlights the major reservoirs and illustrates the time-scales over which these carbon-stores interact with atmospheric CO_2. It is clear that on time-scales of social and political perception (years to hundreds of years) chemical and biological activity within the terrestrial and marine realms are of great importance to atmospheric CO_2 levels, and it is firstly on these time-scales that we must understand the response of the natural world to the rapidly increasing input of anthropogenic carbon into the system if we are to address the issues of anthropogenically

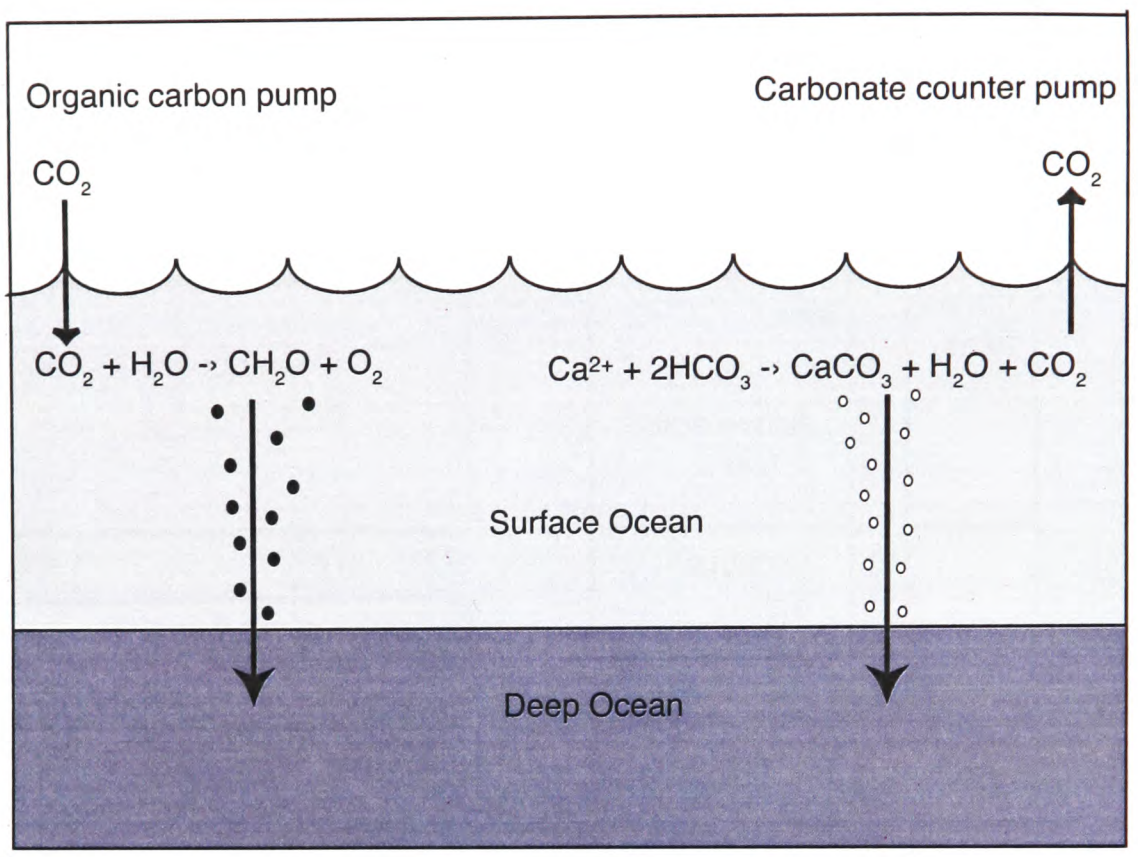

Figure 11. A simple schematic representation of the biological pump.

influenced global change. Of the ~13 Gt of carbon annually emitted by human activity during the last decade (Based on the year 2004. IPCC, 2007), less than half has ended up in the atmosphere, with the rest being taken up by the terrestrial and marine ocean sinks (Houghton and Intergovernmental Panel on Climate Change, 1997). Globally, the gradient of dissolved inorganic carbon between the sunlit surface waters to the deep ocean, carried by sinking organic matter, amounts to ~2500 Gt of carbon, over three times the atmospheric carbon budget (Riebesell et al., 2007). Even minor perturbations to this system, moving it away from a steady-state, have the potential to profoundly influence climate. It is therefore of significant importance to understand the response of the open ocean biological pump, of which coccolithophores constitute a major component, to past and present climate change. Importantly, coccolithophores are also involved in a second carbon pump, often referred to as the 'carbonate counter pump' (Figure 11). The carbonate counter pump is so named because the precipitation of calcium carbonate ($CaCO_3$) in seawater modifies the seawater chemistry in such a way that it becomes enriched (rather than reduced) in CO_2 (see Chapter 2 for further details). The relative export of particulate organic carbon (the

biological pump) and particulate inorganic carbon (the carbonate counter pump), known as the 'Rain Ratio' therefore controls the efficiency of atmospheric CO_2 drawdown by marine biology on annual to centennial time-scales. Estimates of pelagic $CaCO_3$ production range from 0.29 to 1.10 Gt C yr^{-1}, and are of the same order of magnitude as continental-shelf carbonate production (0.02-0.12 Gt C yr^{-1}) (Iglesias-Rodriguez et al., 2002), however the export efficiency of carbonate by different species is poorly constrained. Climatologically, the importance of understanding export efficiency is to quantify the mass of material leaving the seasonally mixed layer (i.e. the water which is mixed to the surface at least once during the year) (Antia et al., 2001), and the quantity of carbon being transported into and stored in sediments. To quantify these fluxes the rates of re-mineralisation and rates of sinking for different particles by different processes must be understood. A theoretical appreciation of this comes from discussions regarding the concept of mineral ballasting, and a practical understanding from the deployment of sediment traps. Stokes Law states that the settling of a particle in a fluid is proportional to the squared (spherical) radius of the particle, the density difference between the fluid and the particle and the fluids viscosity. Organic matter can be approximately considered to have a constant density, as can the viscosity of the fluid in which any contemporaneous particles are settling. It has therefore commonly been assumed that larger particles will sink more rapidly than smaller particles. However, the effective size and density of particles can be increased by aggregation or the incorporation of more-dense mineral phases, and therefore these mechanisms are likely to play a more important role in carbon export than cell size (Barker et al., 2003; Richardson and Jackson, 2007).

1.7 Ocean Acidification

Ocean acidification has become the term used to describe the increased carbonic acid concentration of the surface-ocean in response to dissolution of anthropogenically produced CO_2 into the waters. The consequences of the resulting pH change have only really started

to be realised in the past decade, and are likely to range from the disruption of pH sensitive biological processes such as sexual fertilization, to the wide-scale dissolution of sedimentary carbonates. On time-scales greater than ~10 kyr the degree of seawater saturation with respect to calcium carbonate (the ion product of the calcium and carbonate ion concentrations) is believed to be buffered by vertical mobility in the carbonate compensation depth (CCD), the depth in the ocean below which the rate of supply of calcium carbonate is exceeded by the rate of dissolution (Tyrrell and Zeebe, 2004). On sub-kyr time-scales however, perturbations to the surface-ocean chemistry can have dramatic effects. Figure 12 shows how the saturation horizons (the depth below which the water is no longer saturated) for aragonite and calcite have changed in the Atlantic, Pacific and Indian Oceans between pre-industrial times and today, as a result of increased CO_2 absorption by surface waters. The dissolution of $CaCO_3$ resulting from this changing horizon depth is estimated to be 0.5 ± 0.2 Gt yr^{-1} (Feely et al., 2004). This significant carbonate dissolution, equivalent to about half the present oceanic $CaCO_3$ export production, has occurred in response to a reduction in surface water pH by ~0.1 units. By the end of the century, in response to reaching an atmospheric partial pressure of CO_2 (pCO_2) of 800 ppmv, surface water pH is likely to have fallen by a further 0.4 units (Caldeira and Wickett, 2003), potentially resulting in aragonite under-saturation reaching surface waters in cool, high latitude, basins (Feely et al., 2004). Changes in the saturation state of surface waters, even before they approach under-saturation, will affect the ability of surface-dwelling organisms to produce calcite shells or reefs. As a result we do not need to wait until acidified waters reach sedimentary carbonates before we see the effects of ocean acidification on the carbonate system. Laboratory, field and modelling experiments are beginning to elucidate some of the biological consequences of these changes (Kleypas et al., 1999; Langdon and Atkinson, 2005; Ridgwell et al., 2006; Riebesell et al., 2000; Zondervan et al., 2001), and the work described in Chapter 2 adds a further dimension to this, however, the full ecosystem cost and net CO_2 feedback are still far from being elucidated.

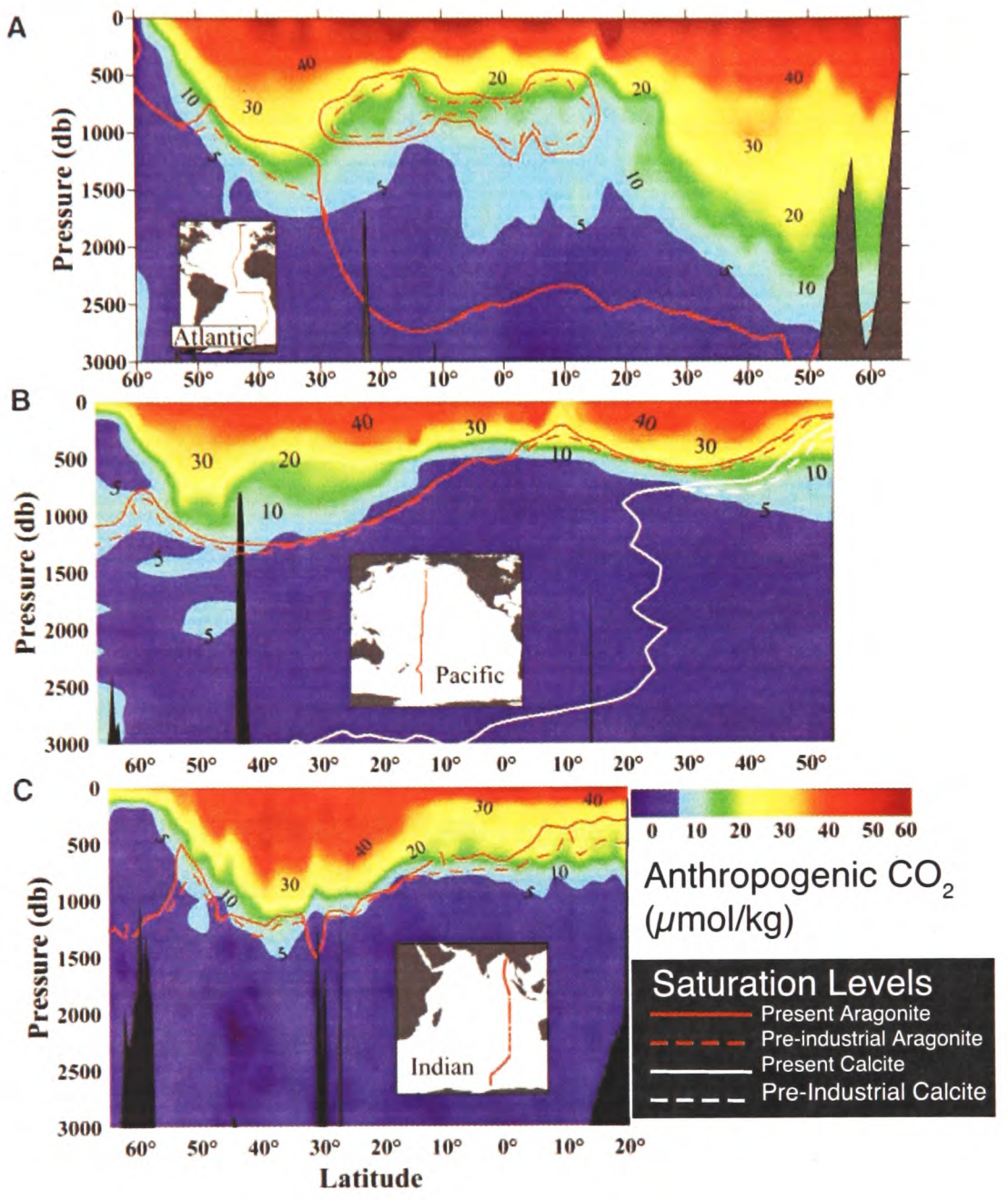

Figure 12. Sections through the Atlantic (A), Pacific (B) and Indian (C) Oceans showing anthropogenic CO_2 concentrations as colour intensity, together with aragonite (orange) and calcite (white) saturation horizons for pre-industrial (dashed lines) and present day (solid lines) conditions. From Feely et al. (2004).

1.7 Bibliography

ANDERSON, T. F. AND STEINMETZ, J. C. (1981) Isotopic and biostratigraphical records of calcareous nannofossils in a Pleistocene Core. Nature, 294, 741-744.

ANTIA, A. N., KOEVE, W., FISCHER, G., BLANZ, T., SCHULZ-BULL, D., SCHOLTEN, J., NEUER, S., KREMLING, K., KUSS, J., PEINERT, R., HEBBELN, D., BATHMANN, U., CONTE, M., FEHNER, U. AND ZEITZSCHEL, B. (2001) Basin-wide particulate carbon flux in the Atlantic Ocean: Regional export patterns and potential for atmospheric CO_2 sequestration. Global Biogeochemical Cycles, 15, 845-862.

ARMSTRONG, H. AND BRASIER, M. (2005) Microfossils, Oxford, Blackwell Publishers.

ARRIGO, K. (2005) Marine microorganisms and global nutrient cycles. Nature, 437, 349-355.

BARKER, S., HIGGINS, J. A. AND ELDERFIELD, H. (2003) The future of the carbon cycle: review, calcification response, ballast and feedback on atmospheric CO_2. Philos. Trans. R. Soc. London Ser. A, 361, 1977-1998.

BILLARD, C. AND INOUYE, I. (2004) What is new in coccolithophore biology? In THIERSTEIN, H. AND YOUNG, J. (Eds.) Coccolithophores From Molecular Processes to Global Impact. New York, Springer.

BOWN, R. (1998) Calcareous nannofossil biostratigraphy, London, Chapman AND Hall.

CALDEIRA, K. AND WICKETT, M. E. (2003) Anthropogenic carbon and ocean pH. Nature, 425, 365-365.

DOVE,M., DE YOREO, J. AND WEINER, S. (2003) Biomineralization, Washington, DC, Mineralogical Society of America.

DUDLEY, W. C., BLACKWELDER, P., BRAND, L. AND DUPLESSY, J. C. (1986) Stable isotopic composition of coccoliths. Mar. Micropaleontol, 10, 1-8.

DUDLEY, W. C., DUPLESSY, J. C., BLACKWELDER, P. L., AND BRAND, L. E. (1980) Coccoliths in Pleistocene-Holocene nannofossil assemblages. Nature, 285, 222-223.

DUDLEY, W. C. AND GOODNEY, D. E. (1979) Oxygen Isotope content of coccoliths grown in culture. Deep-Sea Research Part a-Oceanographic Research Papers, 26, 495-503.

FEELY, R. A., SABINE, C. L., LEE, K., BERELSON, W., KLEYPAS, J., FABRY, V. J. AND MILLERO, F. J. (2004) Impact of anthropogenic CO_2 on the $CaCO_3$ system in the oceans. Science, 305, 362-366.

GEISEN, M., BILLARD, C., BROERSE, A. T. C., CROS, L., PROBERT, I. AND YOUNG, J. R. (2002) Life-cycle associations involving pairs of holococcolithophorid species:

intraspecific variation or cryptic speciation? European Journal of Phycology, 37, 531-550.

HALL, I. R., MCCAVE, I. N., SHACKLETON, N. J., WEEDON, G. AND HARRIS, S. E. (2001) Intensified deep Pacific inflow and ventilation in Pleistocene glacial times. Nature, 412, 809-812.

HASEGAWA, H., MITO, S., NORISUYE, K., MATSUI, M., MAKI, T. AND UEDA, K. (2003) Determination of minor and trace elements in biogenic carbonate minerals of coccolithophores by high-resolution inductively coupled plasma mass spectrometry. Bulletin of the Chemical Society of Japan, 76, 115-120.

HOUGHTON, J. T. AND INTERGOVERNMENTAL PANEL ON CLIMATE CHANGE (1997) Climate change 1995 : the science of climate change, Cambridge, Cambridge University Press.

IGLESIAS-RODRIGUEZ, M. D., ARMSTRONG, R., FEELY, R., HOOD, R., KLEYPAS, J., SABINE, C. AND SARMIENTO, J. (2002) Progress made in study of ocean's calcium carbonate budget. EOS, Transactions, American Geophysical Union, 83, 365.

IPCC (2007) Summary for Policymakers. In: Climate Change 2007: The physical science basis. Contribution of working group I to the fourth assessment report of the Intergovernmental Panel on Climate Change. IN SOLOMON, S., QIN, D., MANNING, M., CHEN, Z., MARQUIS, M., AVERYT, K. B., TIGNOR, M. AND MILLER, H. L. (Eds.), Cambridge University Press.

JORDAN, R. W. AND CHAMBERLAIN, A. H. L. (1997) Biodiversity among haptophyte algae. Biodiversity and Conservation, 6, 131-152.

KLEYPAS, J. A., BUDDEMEIER, R. W., ARCHER, D., GATTUSO, J. P., LANGDON, C. AND OPDYKE, B. N. (1999) Geochemical consequences of increased atmospheric carbon dioxide on coral reefs. Science, 284, 118-120.

LANGDON, C. AND ATKINSON, M. J. (2005) Effect of elevated pCO_2 on photosynthesis and calcification of corals and interactions with seasonal change in temperature/ irradiance and nutrient enrichment. Journal of Geophysical Research-Oceans, 110, doi:10.1029/2004JC002576.

MARGOLIS, S. V., KROOPNICK, M., GOODNEY, D. E., DUDLEY, W. C. AND MAHONEY, M. E. (1975) Oxygen and Carbon Isotopes from Calcareous Nannofossils as Paleoceanographic Indicators. Science, 189, 555-557.

MARSH, M. E. (1999) Coccolith crystals of Pleurochrysis carterae: crystallographic faces, organization, and development. Protoplasma, 207, 54-66.

MARSH, M. E. (2003) Regulation of $CaCO_3$ formation in coccolithophores. Comparative Biochemistry and Physiology B-Biochemistry AND Molecular Biology, 136, 743-754.

MINOLETTI, F., GARDIN, S., NICOT, E., RENARD, M. AND SPEZZAFERR, S. (2001)

Mise au point d'un protocole experimental de separation granulometrique d'assemblages de nannofossiles calcaires; applications paleoecologiques et geochimiques. Bulletin de la SociÈtÈ GÈologique de France, 172, 437-446.

PAULL, C. AND THIERSTEIN, H. (1987) Stable isotopic fractionation among particles in Quaternary coccolith-sized deep sea sediments. Paleoceanography, 2, 423-429.

RICHARDSON, T. L. AND JACKSON, G. A. (2007) Small phytoplankton and carbon export from the surface ocean. Science, 315, 838-840.

RICKABY, R. E. M., SCHRAG, D. P., ZONDERVAN, I. AND RIEBESELL, U. (2002) Growth rate dependence of Sr incorporation during calcification of *Emiliania huxleyi*. Global Biogeochemical Cycles, 16, doi:10.1029/2001GB001408.

RIDGWELL, A., ZONDERVAN, I., HARGREAVES, J. C., BIJMA, J. AND LENTON, T. M. (2006) Significant long-term increase of fossil fuel CO_2 uptake from reduced marine calcification. Biogeosciences Discussions, 3, 1763-1780.

RIEBESELL, U., SCHULZ, K. G., BELLERBY, R. G. J., BOTROS, M., FRITSCHE, P., MEYERHOFER, M., NEILL, C., NONDAL, G., OSCHLIES, A., WOHLERS, J. AND ZOLLNER, E. (2007) Enhanced biological carbon consumption in a high CO_2 ocean. Nature, 450, 545-U10.

RIEBESELL, U., ZONDERVAN, I., ROST, B., TORTELL,D., ZEEBE, R. E. AND MOREL, F. M. M. (2000) Reduced calcification of marine plankton in response to increased atmospheric CO_2 Nature, 407, 364-367.

ROWSON, J. D., LEADBEATER, B. S. C. AND GREEN, J. C. (1986) Calcium-carbonate deposition in the motile (crystallolithus) phase of *Coccolithus pelagicus* (*Prymnesiophyceae*). British Phycological Journal, 21, 359-370.

ROYER, D. L., BERNER, R. A. AND PARK, J. (2007) Climate sensitivity constrained by CO_2 concentrations over the past 420 million years. Nature, 446, 530-532.

SHACKLETON, N. J., BERGER, A. AND PELTIER, W. R. (1990) An alternative astronomical calibration of the Lower Pleistocene timescale based on ODP Site 677. Transactions of the Royal Society of Edinburgh-Earth Sciences, 81, 251-261.

SHIMIZU, N. AND STOLL, H. (2004) Coccolith Sr/Ca ratios by ion probe analysis. Geochimica Et Cosmochimica Acta, 68, A206-A206 Suppl. S.

STERN, N. H. AND GREAT BRITAIN. TREASURY. (2007) The economics of climate change, Norwich, TSO.

STOLL, H. AND SCHRAG, D.(2000) Coccolith Sr/Ca as a new indicator of coccolithaphorid calcification and growth rate. Geochemistry Geophysics Geosystems, 1, Paper Number 1999GC000015.

STOLL, H., SHIMIZU, N., AREVALOS, A., MATELL, N., BANASIAK, A. AND ZEREN, S. (2007a) Insights on coccolith chemistry from a new ion probe method for analysis of individually picked coccoliths. Geochemistry Geophysics Geosystems, 8.

STOLL, H. M. (2005) Limited range of interspecific vital effects in coccolith stable isotopic records during the Palaeocene Eocene thermal maximum. Paleoceanography, 20, -.

STOLL, H. M., AREVALOS, A., BURKE, A., SHIMIZU, N., THEROUX, S. AND ZIVERI, P. (2005) Unraveling nutrient, growth rate, calcification, and diagenesis effects on the chemistry of coccolith calcite. Geochimica Et Cosmochimica Acta, 69, A127-A127.

STOLL, H. M., ENCINAR, J. R., ALONSO, J. I. G., ROSENTHAL, Y., PROBERT, I. AND KLAAS, C. (2001) A first look at paleotemperature prospects from Mg in coccolith carbonate: Cleaning techniques and culture measurements. Geochemistry Geophysics Geosystems, 2, doi:10.1029/2000GC000144.

STOLL, H. M., KLAAS, C. M., PROBERT, I., ENCINAR, J. R. AND ALONSO, J. I. G. (2002a) Calcification rate and temperature effects on Sr partitioning in coccoliths of multiple species of coccolithophorids in culture. Global and Planetary Change, 34, 153-171.

STOLL, H. M., ROSENTHAL, Y. AND FALKOWSKI, P. (2002b) Climate proxies from Sr/Ca of coccolith calcite: Calibrations from continuous culture of *Emiliania huxleyi*. Geochimica Et Cosmochimica Acta, 66, 927-936.

STOLL, H. M., SHIMIZU, N., ARCHER, D. AND ZIVERI, P. (2007b) Coccolithophore productivity response to greenhouse event of the Paleocene-Eocene Thermal Maximum. Earth and Planetary Science Letters, 258, 192-206.

STOLL, H. M. AND ZIVERI, P. (2002) Separation of monospecific and restricted coccolith assemblages from sediments using differential settling velocity. Marine Micropaleontology, 46, 209-221.

STOLL, H. M., ZIVERI, P., SHIMIZU, N., CONTE, M. AND THEROUX, S. (2007c) Relationship between coccolith Sr/Ca ratios and coccolithophore production and export in the Arabian Sea and Sargasso Sea. Deep-Sea Research Part Ii-Topical Studies in Oceanography, 54, 581-600.

SUNDQUIST, E. T. (1993) The Global Carbon-Dioxide Budget. Science, 259, 934-941.

TAKANO, H., MANABE, E., HIRANO, M., OKAZAKI, M., BURGESS, J. G., NAKAMURA, N. AND MATSUNAGA, T. (1993) Development of a Rapid Isolation Procedure for Coccolith Ultrafine Particles Produced by Coccolithophorid Algae. Applied Biochemistry and Biotechnology, 39, 239-247.

TYRRELL, T. AND ZEEBE, R. E. (2004) History of carbonate ion concentration over the last 100 million years. Geochimica Et Cosmochimica Acta, 68, 3521-3530.

VANDERWAL, P., DEJONG, E. W., WESTBROEK, P., DEBRUIJN, W. C. AND MULDERSTAPEL, A. A. (1983) Polysaccharide Localization, Coccolith Formation, and Golgi Dynamics in the Coccolithophorid Hymenomonas-Carterae. Journal of Ultrastructure Research, 85, 139-158.

WEAVER, A. J., EBY, M., AUGUSTUS, F. F. AND WIEBE, E. C. (1998) Simulated

influence of carbon dioxide, orbital forcing and ice sheets on the climate of the Last Glacial Maximum. Nature, 394, 847-853.

YOUNG, J., DAVIS, S., BOWN, P. R., AND MANN, S. (1999) Coccolith Ultrastructure and Biomineralisation. Journal of Structural Biology, 126, 195-215.

YOUNG, J. R., DIDYMUS, J. M., BOWN,R., PRINS, B. AND MANN, S. (1992) Crystal Assembly and phylogenetic evolution in heterococcoliths. Nature, 356, 516-518.

YOUNG, J. R. AND ZIVERI, P. (2000) Calculation of coccolith volume and its use in calibration of carbonate flux estimates. Deep-Sea Research Part II -Topical Studies in Oceanography, 47, 1679-1700.

ZIVERI, P., STOLL, H., PROBERT, I., KLASS, C., GEISEN, M., GANSSEN, G. AND YOUNG, J. (2003) Stable isotope vital effects in coccolith calcite. Earth and Planetary Science Letters, 210, 137-149.

ZONDERVAN, I., ZEEBE, R. E., ROST, B. AND RIEBESELL, U. (2001) Decreasing marine biogenic calcification: A negative feedback on rising atmospheric pCO_2. Global Biogeochem. Cycles, 15, 507-516.

Increased Coccolithophore Calcification Under Elevated CO_2 Concentrations

2

Ocean acidification has become the term used to describe the chemical response of the marine realm to the uptake of anthropogenically produced CO_2. This aspect of man-made global change has, until recently received considerably less attention than the effects of elevated CO_2 levels on global temperatures, although through the carbon cycle, both are strongly linked. The reduction in pH of the seawater in response to increased concentrations of dissolved CO_2 will not only affect the ability of the ocean to absorb further CO_2, but will also cause a decrease in the saturation state of carbonate minerals (Feely et al., 2004). Calcium carbonate ($CaCO_3$) is one of the most ubiquitously utilised biominerals, and it is widely believed that many organisms will calcify less under higher pCO_2 (Bijma et al., 2002; Orr et al., 2005; Ridgwell et al., 2006; Riebesell et al., 2000; Zondervan et al., 2001).

The major findings of this research have been combined with data from a laboratory study undertaken in Southampton University and were published in April 2008. See:

M. Debora Iglesias-Rodriguez and Paul R. Halloran et al. (2008) Phytoplankton calcification in a high CO_2 world. Science, 320 (5874), 336-340.

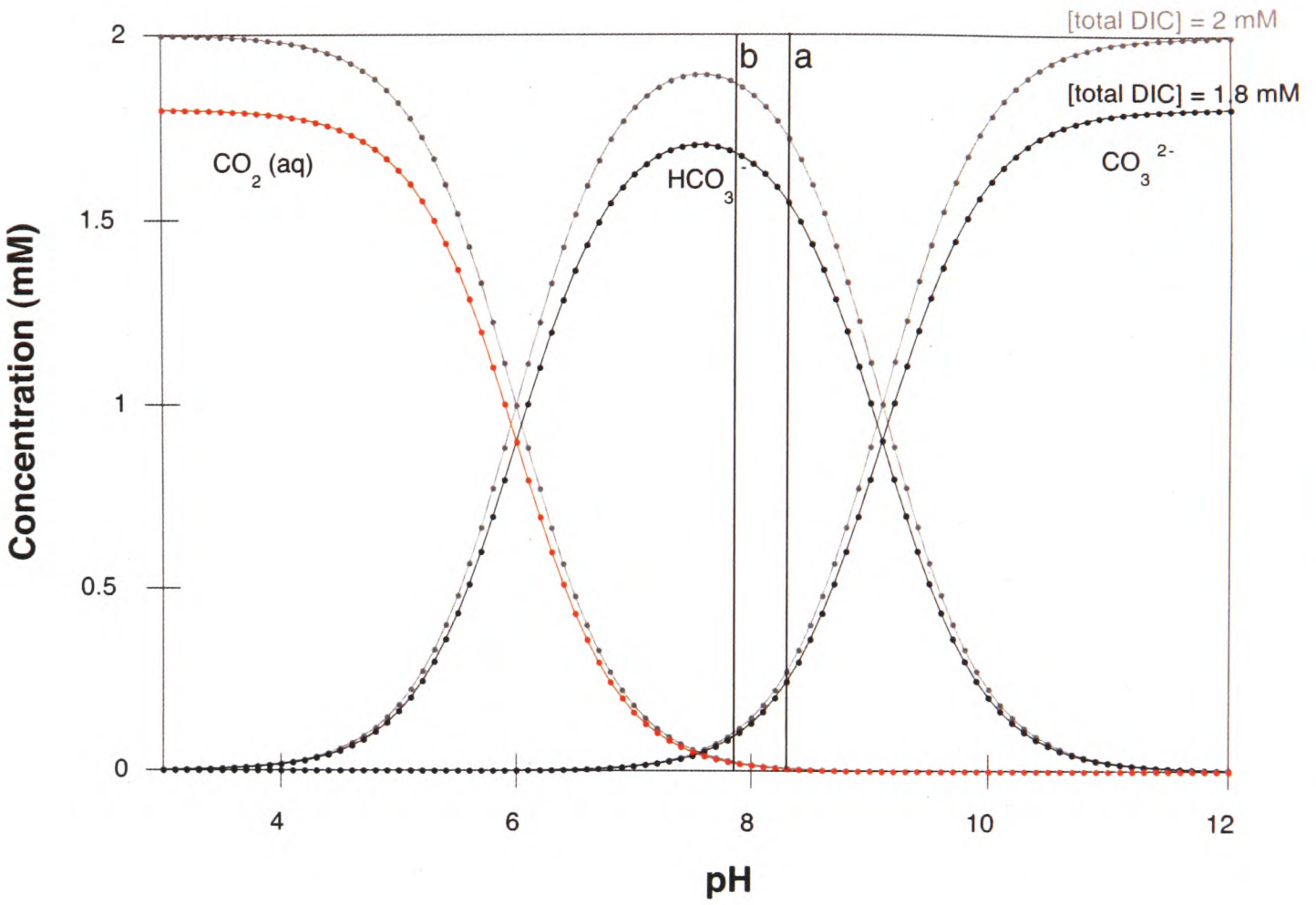

Figure 1. Bjerrum plots for 1.8 and 2 mM Dissolved Inorganic Carbon (DIC) (grey and black/red curves respectively) between pH 3 and 12. This diagram shows the major species of DIC in seawater, carbon dioxide, bicarbonate and carbonate. This diagram also shows how the relative proportions of these three species are fixed at any given pH. The formation of $CaCO_3$ requires calcium (Ca) and carbonate (CO_3). When $CaCO_3$ is precipitate, carbonate is removed from the seawater. This reduces the total DIC concentration ([DIC]), and the absolute quantity of the three species is reduced (i.e. moving from the grey curves to the black and red curves). However, at the same time, because carbonate, which has a double negative charge, is removed, the total alkalinity is reduced. The total alkalinity reflects the ability of the solution to buffer protons, so through its reduction, protons made available, and the pH reduced. Modern seawater pH is ~8.2 (vertical line 'a'). A reduction in pH moves the composition towards the left of the graph (vertical line 'b'), and changes the relative proportions of the DIC species in favour of CO_2. The positive change in [CO_2] resulting because the [CO_2] increase associated with the pH shift is greater than the reduction in [CO_2] associated with the [DIC] reduction, and therefore, there is a net [CO_2] increase and CO_2 can potentially be released to the atmosphere as the air and water equilibrate.

2.1 Ocean Acidification and the carbonate system

When CO_2 dissolves in to seawater, a small amount of carbonic acid (H_2CO_3) is formed. H_2CO_3 has a higher dissociation constant than H_2O ($K_{a(\text{carbonic acid})} = 4.30 \times 10^{-7}$, $K_{a(\text{Water})} = 1.0 \times 10^{-14}$), so the pH of the seawater will decrease. The speciation of dissolved carbon in seawater is highly pH sensitive. Figure 1 and the associated caption describe how the relative proportions of the main carbonate species, CO_2, HCO_3^- and CO_3^{2-} vary with pH at 25 °C and atmospheric pressure, for a total dissolved inorganic carbon (DIC) concentration of 1.8 mM (grey) and 2 mM (black and red). Typical modern mixed-layer seawater pH is ~8.2, at which, total DIC is comprised of 88.3% HCO_3^-, 11.1% CO_3^{2-} and 0.6% CO_2. By

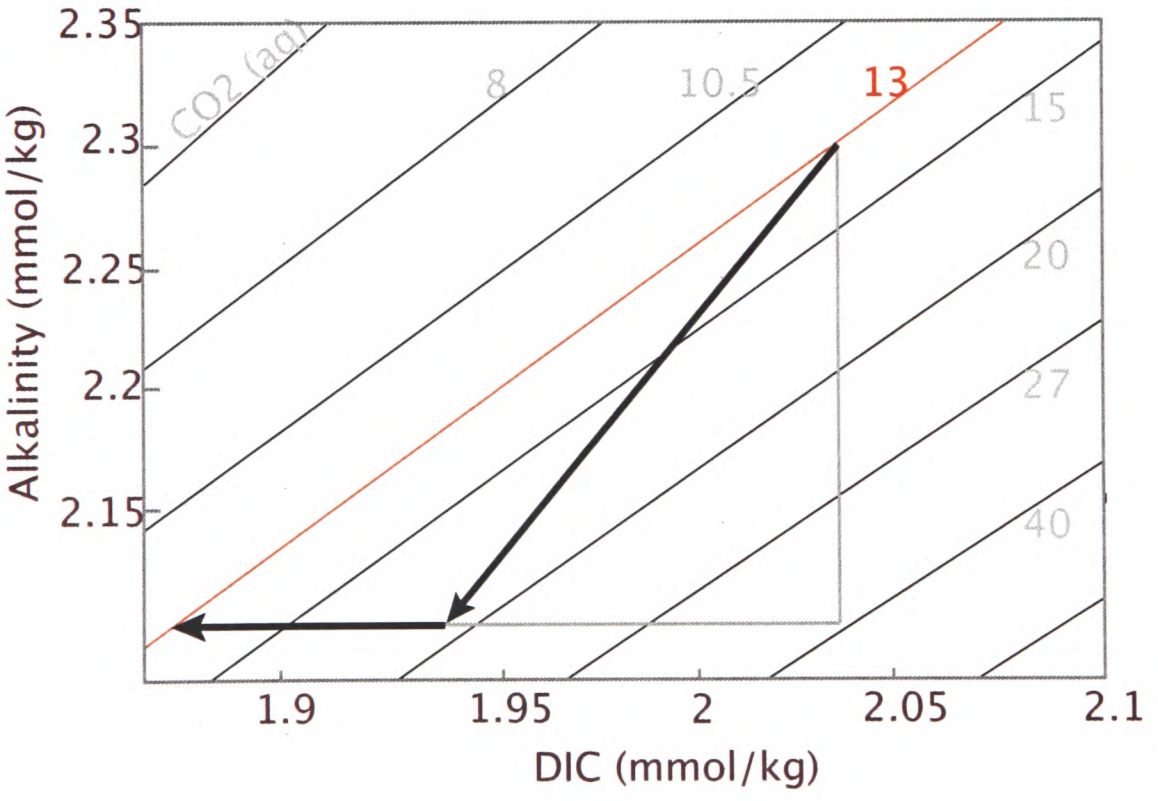

Figure 2. Plot explaining the release of CO_2 by calcification. Forming one mole of $CaCO_3$ reduces the DIC by one unit (because one carbonate ion has been consumed), and the alkalinity by two units (because Ca has a negative charge of two). Assuming the current seawater CO_2 concentration of 13 mmol kg^{-1}, formation of 100 pmol $CaCO_3$ would reduce the [DIC] by 0.1 unit, and the alkalinity by 0.2 units (i.e. twice as much). This process will move the seawater composition along the long vector through alkalinity-DIC space, away from the previous seawater CO_2 concentration. Therefore, CO_2 equivalent to the short horizontal vector will be released from the seawater, as it re-equilibrates (assuming an open system). Modified from Zondervan et al. (2001).

2100, the average surface ocean pH is expected to have fallen by 0.3 units (Orr et al., 2005). At pH 7.9, total DIC becomes 93.0% HCO_3^-, 5.9% CO_3^{2-} and 1.2% CO_2, highlighting the sensitivity of the carbonate system to pH.

Calcium carbonate ($CaCO_3$) precipitation is dependent primarily on the concentration of the two components, Ca and CO_3. It has therefore been suggested that decreasing CO_3 concentrations with decreasing seawater pH will cause a reduction in marine calcification (e.g. Bijma et al., 2002; Riebesell et al., 2000). The degree of calcification by marine plankton, together with the flux of carbon from the mixed layer, govern the surface water CO_2 storage capacity. The production of $CaCO_3$, from double charged carbonate (CO_3^{2-}) ions requires that bicarbonate (HCO_3^-) dissociates to carbonate to maintain surface ocean total alkalinity (the buffering capacity of the seawater). At any given pH, the relative proportion of the DIC species are fixed (Figure 1), and consequently the formation of $CaCO_3$ is accompanied by the production of CO_2 (Ridgwell and Zeebe, 2005). Thus, a decrease in marine calcification would increase surface ocean alkalinity, allowing increased drawdown of atmospheric CO_2 (see Figure 2 and accompanying description).

Recent evidence suggests that the calcification response of coccolithophores to increasing pCO_2 is significant (Figure 3) (Delille et al., 2005; Langer et al., 2006; Riebesell et al., 2000; Zondervan et al., 2001) but whether the associated CO_2 feedback will be positive or negative remains unclear. Coccolithophore culture studies in which the carbonate system has been modified, at least in part, by the addition of acids/bases, have demonstrated a decreasing calcification with rising pCO_2 in *E. huxleyi* and *Gephyrocapsa oceanica* (Riebesell et al., 2000; Zondervan et al., 2001), a small but statistically significantly increasing calcification in *Coccolithus pelagicus (Langer et al., 2006)* and an increase (to present day pCO_2), followed by a decrease in *Calcidiscus leptoporus* calcification (Figure 3) *(Langer et al., 2006)*. However, a recent experiment in which the carbonate system was modified purely by equilibrating the culture medium with ambient air of different CO_2 partial pressures has shown calcification

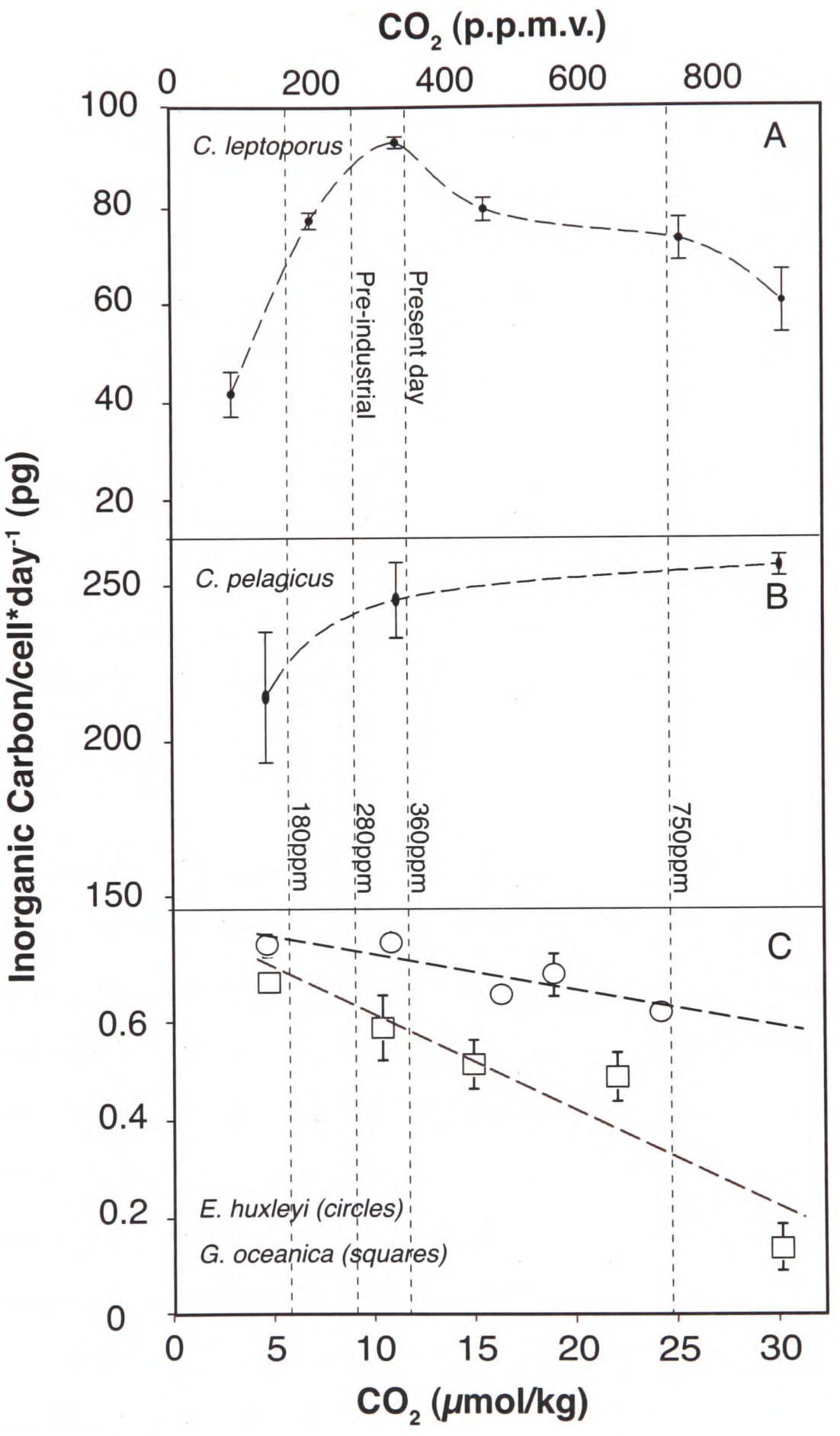

Figure 3. Mass of inorganic carbon produced per coccolith per day for A. *Calcidiscus leptoporus*, B. *Coccolithus pelagicus* and C. *Emiliania huxleyi* and *Gephyrocapsa oceanica*. Modified from Langer et al. (2006) and Riebesell et al. (2000).

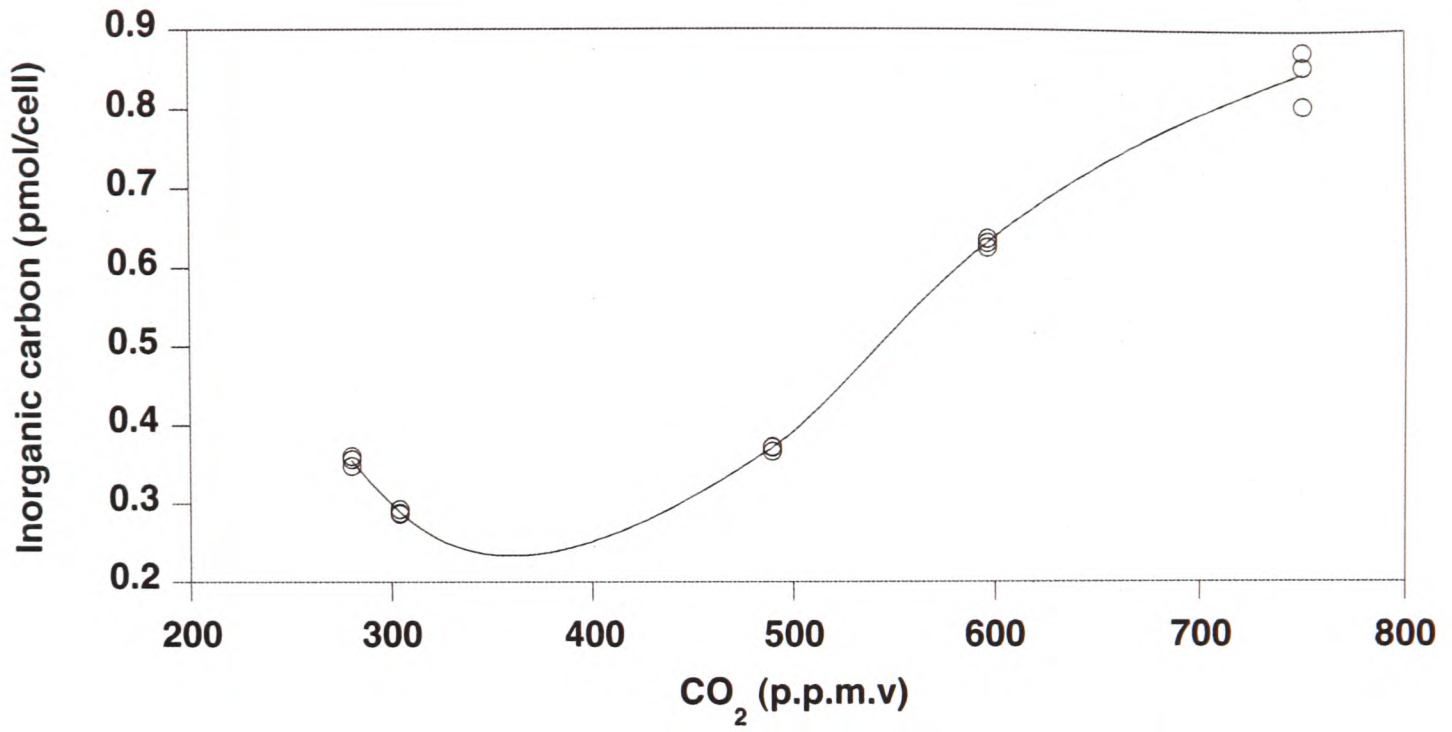

Figure 4. Moles of inorganic carbon produced per coccolith by *E. huxleyi* when the carbonate system is modified by changing the ambient pCO_2. Modified from Iglesias-Rodriguez and Halloran et al., (2008).

by *E. huxleyi* to increase, rather than decrease, under rising pCO_2 (Figure 4). These two experimental setups differ in terms of their carbonate system parameters; in the former, DIC concentration remains constant, but in the latter DIC concentration will increase as CO_2 is absorbed, analogous with contemporary ocean acidification, fully simulating the shift in carbonate saturation state. Between the years 1800 and 2100, seawater pH is likely to fall from 8.2 to 7.8 (Feely et al., 2004). Within this pH range, CO_3^{2-} displays a much greater sensitivity to pH than does HCO_3^-. Whilst the influence of [DIC] over $[CO_3^{2-}]$ is subtle compared to the influence of pH (see Figure 5 for further explanation), DIC concentration is the major factor controlling HCO_3^- concentration. The coccolithophore *E. huxleyi* has been shown to utilise the HCO_3^- rather than the CO_3^{2-} ion when calcifying (Buitenhuis et al., 1999). Furthermore, there is experimental evidence from *E. huxleyi* that coccolithophores calcify more heavily under elevated HCO_3^- concentration (Shiraiwa, 2003). Consequently, manipulating just the culture medium pH to produce CO_3^{2-} concentrations representative of future CO_2 levels as one might to influence inorganic $CaCO_3$ growth, will not necessarily simulate coccolith calcification under high CO_2. A non-unified calcification response

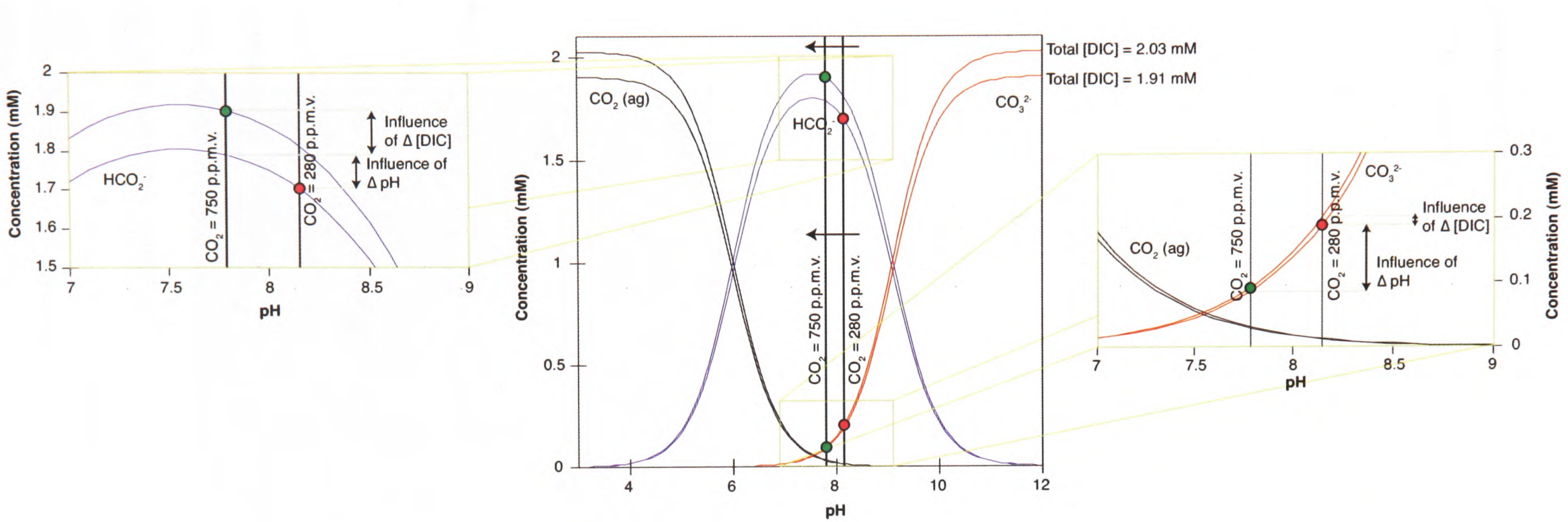

Figure 5. Bjerrum plots calculated from the [total DIC] measurements presented in Iglesias-Rodriguez and Halloran et al. (2008) for CO_2 culture experiments undertaken at pre-indusrial conditions (280 ppmv pCO_2 and 1.91 mM DIC) and values predicted for the year 2100 (750 ppmv pCO_2 and 2.03 mM DIC), lower and upper set of curves respectively. The black, blue and red lines represent the calculated CO_2, HCO_3 and CO_3 concentrations respectively, over a pH range from 3 to 12 units. The two black vertical lines mark pH 8.15 and 7.79, the seawater pH values measured when bubbled with air with 280 ppmv and 750 ppmv pCO_2. The red and green circles therefore mark the 250 ppmv CO_2 and 750 ppmv CO_2 carbonate system composition respectively. As indicated in the sub-Figures situated to the left and right of the main diagram, the increase in HCO_3 (blue lines) is an almost equal response to pH and [DIC] change, whereas the decrease in CO_3 (red lines) is almost entirely in response to pH change. [HCO_3] change is therefore more sensitive to variations in [DIC] than is CO_3 (the concentration of which is more sensitive to pH changes).

between different coccolithophore species is not an unlikely scenario, and may represent a movement towards, or away from, an optimum pCO_2 for individual coccolithophore groups (Henderiks and Rickaby, 2007). The apparent experimental and species dependence of this CO_2 feedback highlights the critical need to consider the problem holistically, on an assemblage-wide level, in the real ocean.

The debate about whether calcification is likely to increase or decrease under elevated atmospheric CO_2 concentrations appears to be limited to coccolithophores, most likely reflecting their unique calcification mechanism. The other major marine calcifiers, corals, foraminifera and shellfish all appear to demonstrate a reduction in calcification under future CO_2 scenarios (Bijma et al., 2002; Gazeau et al., 2007; Langdon and Atkinson, 2005). Although questions remain about the issue of adaptability in such culture experiments, at least for foraminifera, this calcification decrease is consistent with measurements made over the last glacial-interglacial transition, where CO_2 increased by ~100 ppmv and *G. bulloides* decreased in average test weight by 6 μg (Barker and Elderfield, 2002).

2.2 Samples and Methods I - Downcore

We have developed a methodology, which, independent of growth rate effects, can examine how the degree of coccolith calcification, across many coccolithophore taxa, has responded to historical pCO_2 changes in the open ocean. This technique has been applied to material from the box core RAPID 21-12-B (57°27.09' N, 27°54.53' W), situated at 2630 m water depth in the sub-polar North Atlantic (Figure 6). Core RAPID 21-12-B contains unprecedented open-ocean sedimentation rates of 2.3 mm yr^{-1} spanning the time interval from 1770 to 2004 A.D. (Boessenkool et al., 2007), which allow a unique view of coccolith formation over the Anthropocene - the period of anthropogenic CO_2 release.

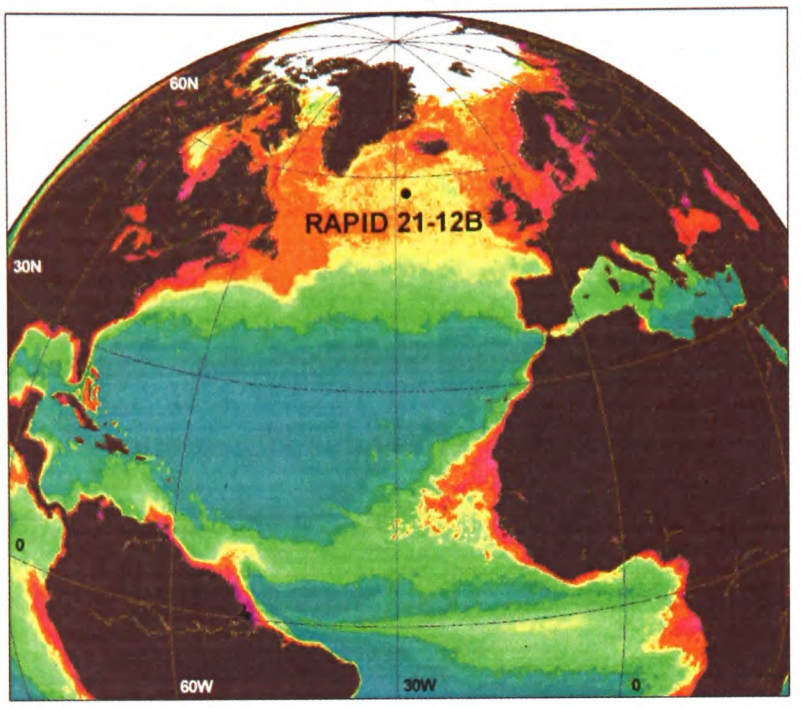

Figure 6. Location of core RAPID 21-12-B at 2630 m water depth, 57°27.09' N, 27°54.53' W in the subpolar North Atlantic. The ocean shading is SeaWiFS ocean colour highlighting the areas of high biomass in bright colours.

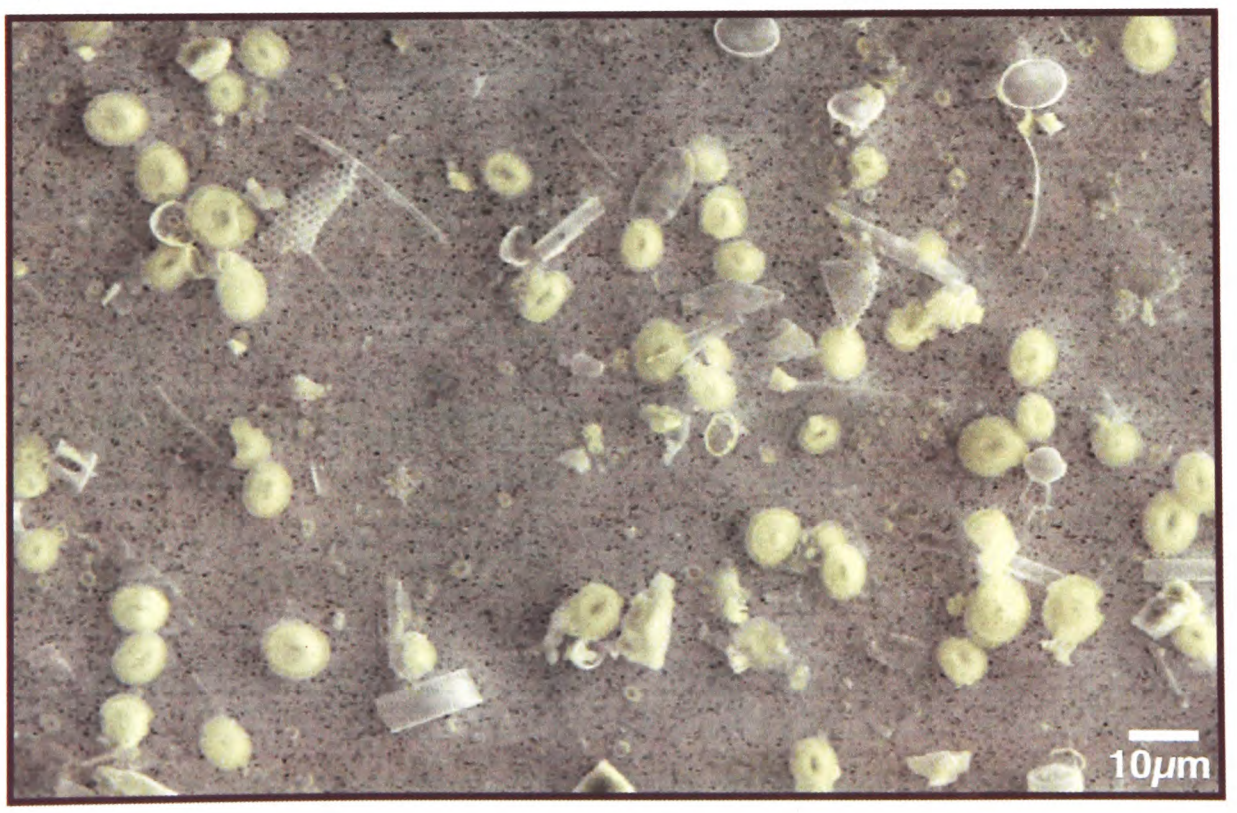

Figure 7. Scanning Electron Micrograph (SEM) image of < 10 μm filtered sediment of RAPID 21-12-B core-top. The image has been overlaid with a Ca map to highlight $CaCO_3$ material. It is evident that coccoliths dominate the $CaCO_3$ material. Note; SEM image taken at filter edge skewing population.

This study examines how the average mass of $CaCO_3$ per coccolith has varied within a static species assemblage over the last two centuries. Sediment was sampled at 5 mm resolution, suspended in buffered H_2O (0.2 μm filtered tap-water, pH 7 and saturated with respect to $CaCO_3$), suspended by bubble agitation, and passed through 10 μm track-etched polycarbonate membranes to obtain the coccolith fraction and exclude larger carbonate grains (Figure 7). The sub-10 μm fraction was subsampled for counting and weighing. 1000 μl of the filtered suspension was pipetted into each of two 1500 μl centrifuge tubes, spun at 16000 rpm and the supernatant removed. Samples were then re-suspended in ethanol, centrifuged and supernatant removed, then dried for 24 hours at 70°C. Dried samples were weighed using a seven-place balance three times, on three separate days, then 500 μl of 10% HNO_3 was added. The samples were again rinsed, dried and weighed. The difference between pre and post-acid weighing is considered to be the $CaCO_3$ mass.

100 μl of the sub-10 μm suspended fraction was pipetted into each of three Beckman Coulter sample beakers and diluted to 100 ml with Isoton II. A Beckman Coulter Multisizer III fitted with a 30 μm aperture was then used to count the number of particles between 0.63 μm and 10 μm (reasonably assumed to be coccoliths (Figure 8) (Frenz et al., 2005; McCave et al., 1995; Wang and McCave, 1990)) three times in each replicate. 500 μl of concentrated HCL was added to the suspension, left to stand, then stirred vigorously for 4 minutes. Replicates were then re-analysed three times, and average counts, pre and post-acid addition, considered to record the number of $CaCO_3$ particles (see Figure 9 for an explanation of the Coulter counter operation). An upper detection limit of 10 μm was critically chosen to focus observations on particles with cohesive behaviour, and avoid sampling the drift component of the sediment (McCave and Hall, 2006). This method excludes coccoliths with a diameter > 10 μm. Only coccoliths of *Coccolithus pelagicus braarudii* were consistently > 10 μm, and were correspondingly excluded from the species counts. Any coccoliths > 10 μm in diameter produced by species other than *C. pelagicus braarudii* would also have been removed, and consequently the measurements represent the lower limit of calcification. This approach

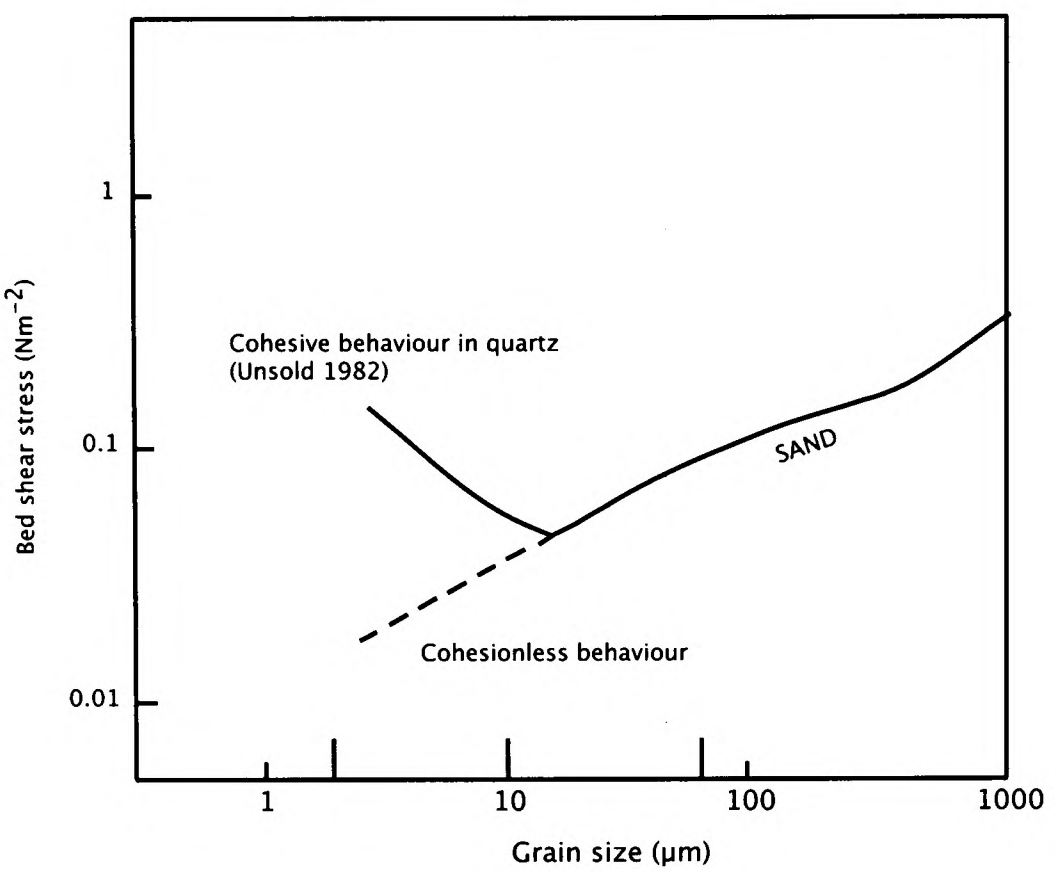

Figure 8. For particles larger than ~12 μm the shear stress required to pick up a particle from the sediment decreases with particle size. However, below 12 μm particles become cohesive, and the shear stress required to take the particles into suspension rapidly rises. For this reason, it is assumed that once deposited, particles smaller than 10 μm are not sorted and transported by currents flowing over the sediment. After McCave et al. (1995).

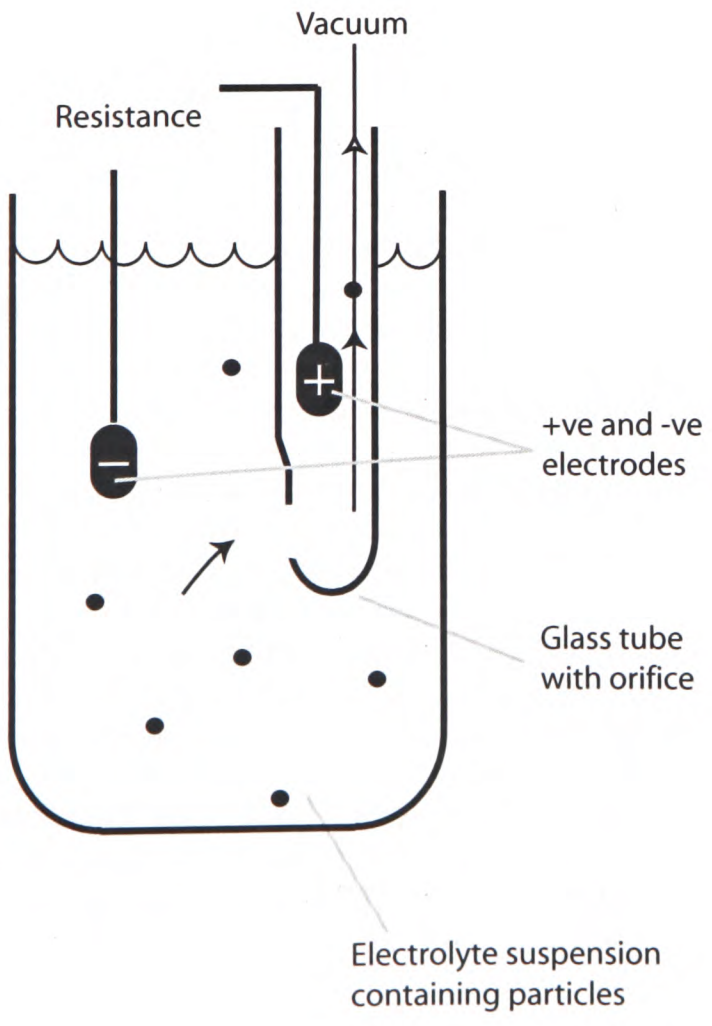

Figure 9. A schematic diagram demonstrating how a Beckman Coulter electrical resistance pulse counter functions. The sample is taken into suspension in a saline electrolyte solution (ISOTON II), then a known volume of that solution is sucked through a small aperture (30 μm) bored into a ruby, and mounted on a glass tube. Either side of the aperture lie an anode and cathode respectively. When a particle (an insulator) passes through the aperture, a certain volume of the electrolyte is displaced. The change in resistance through the aperture is proportional to the volume of the particle, and can be used to count and size the number of particles in suspension.

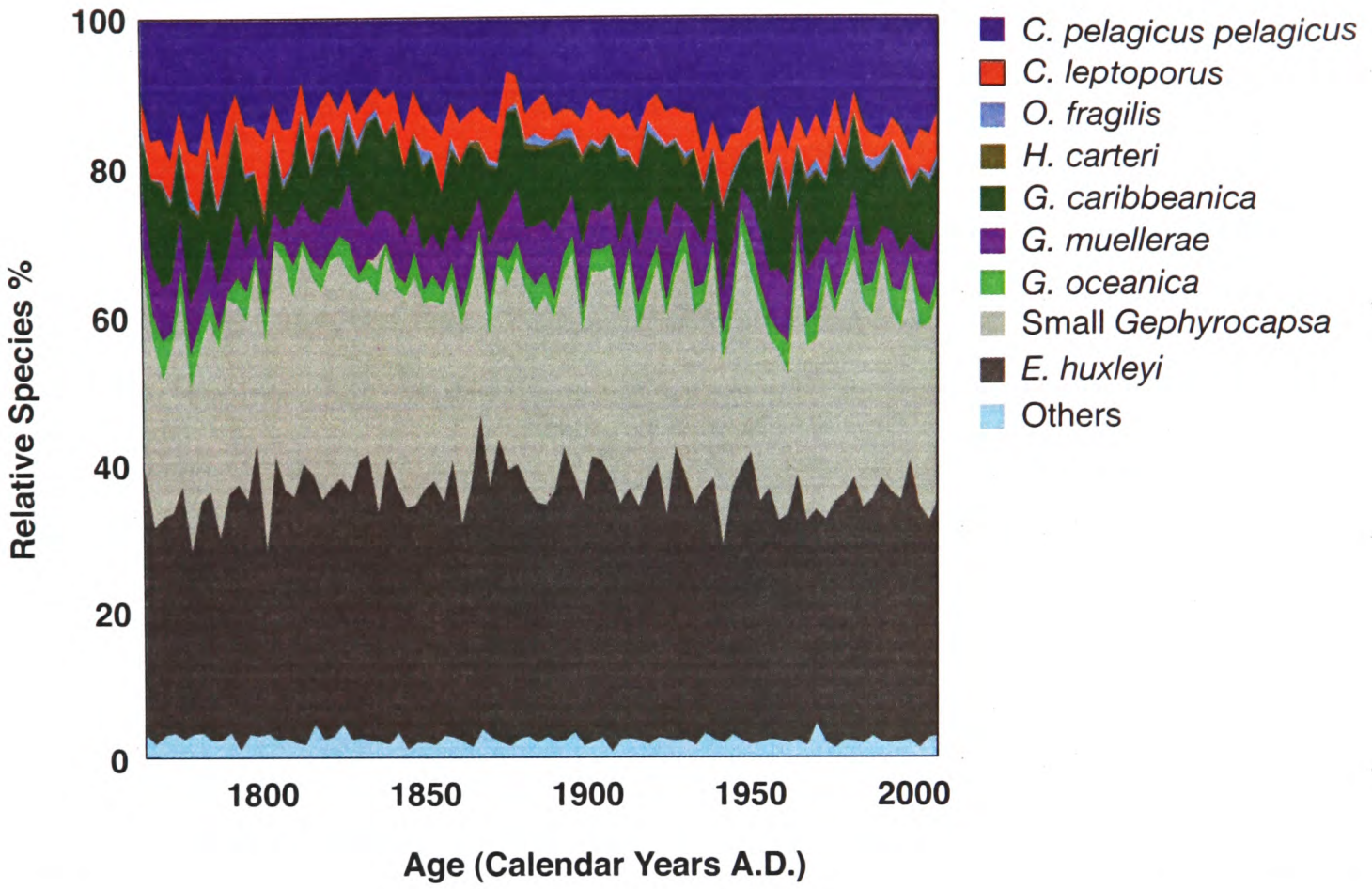

Figure 10. Light microscope coccolith counts displayed as relative percentages of each species. No long-term trend in species composition is observed, indicating little or no species response to anthropogenic forcing. Stasis in the species composition implies the core is unaffected by dissolution (Hill, 1975), confirmed by SEM examination.

measures the average calcification per coccolith, which integrates any change in $CaCO_3$ mass due to variations in the assemblage and due to intra-species shifts in coccolith mass. To examine whether changes in species composition could account for the observed trend, Elena Colmenero-Hidalgo (of Cardiff and Salamanca Universities) counted coccolith assemblages under a light microscope, following standard techniques for preparation by settling (Flores and Sierro, 1997). No significant trend in species composition (Figure 10), or species mass contribution is observed. Dividing particle counts by sediment weight, before and after removal of $CaCO_3$ by dissolution, not only allows examination of a high number of coccoliths quickly (average sample size ~80,000 $CaCO_3$ particles), but is also sensitive to calcification changes in any dimension. By comparison, quantitative assessment of scanning electron microscope images would rely on a very limited number of observations, and be blind to changes in dimensions other than diameter.

2.3 Results and Discussion I - Downcore

The average coccolith mass increased from 1.08 $x10^{-11}$ to 1.55 $x10^{-11}$ g between 1770 and the modern day (Figure 11) (Appendix A), with a statistically significant accelerated increase over recent decades (Figure 12). The absence of any down-core trend in species abundance, inclusive of many dissolution-sensitive taxa, indicates that our observed increase in coccolith mass cannot be accounted for by changing species compositions or dissolution effects (Hill, 1975). This is consistent with scanning electron microscope examination of the coccoliths (Figure 7). Furthermore, evidence is building that coccoliths are more resistant to dissolution than are foraminifera (Beaufort et al., 2007; Frenz and Henrich, 2007) and that they remain pristine when exposed to fluids in the pH range 6-8 (Beaufort et al., 2007; Frenz and Henrich, 2007).

The increase of ~4.5 pg in the average mass of $CaCO_3$ per coccolith since ~1960, correlates with rising atmospheric pCO_2. It is important to note that on average, ~75% of the < 10 μm calcite by mass, at site RAPID 21-12-B constitutes coccoliths of only two taxa, *C. pelagicus pelagicus* and *Calcidiscus leptoporus* (Figure 13). Typical coccoliths of these species are 15 and 7 times the average pre-1950 coccolith mass respectively (Young and Ziveri, 2000), and *C. pelagicus pelagicus* alone would require a < 5% increase in coccolith mass (equivalent to ~0.25 μm diameter increase) to account for the entire observed calcification change, well within present-day variability. As demonstrated, changes in the average coccolith calcification can be dominated by only a small number of heavily calcifying species, therefore it is quite possible that the global calcification response may vary greatly with coccolith assemblage in diverse oceanic regimes. However, the dominance of *C. pelagicus pelagicus* over the sedimentary calcite mass observed in this core is typical within the North Atlantic (Ziveri et al., 2004) and therefore our findings most likely represent the regional response, the response of a basin highly sensitive to anthropogenic CO_2 production (Feely et al., 2004). A more detailed consideration of species-specific response is presented in Figures

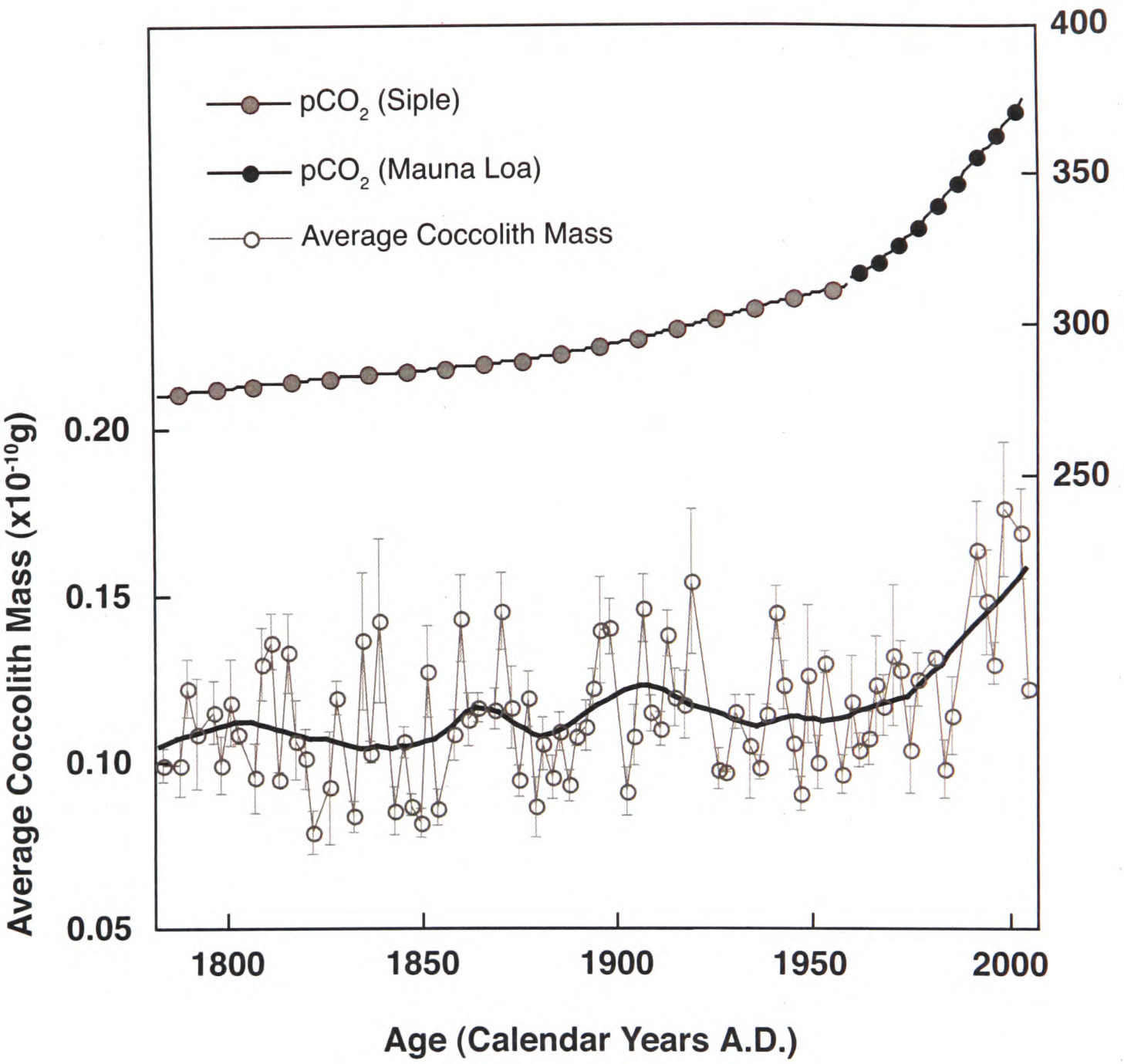

Figure 11. Average mass of $CaCO_3$ per coccolith in core RAPID 21-12-B and atmospheric CO_2. The average mass of $CaCO_3$ per coccolith in core RAPID 21-12-B (○) increased from 1.08 $x10^{-11}$ to 1.55$x10^{-11}$ g between 1780 and the modern day, with an accelerated increase over recent decades. The calcification increase correlates with rising atmospheric CO_2 concentrations as recorded in the Siple ice core (10) (▪) and instrumentally at Mauna Loa (37) (●), every tenth and fifth data point shown respectively. Error bars represent one standard deviation as calculated from replicate analyses. Samples with a standard deviation greater than 0.05 were discarded. The smoothed curve for the average coccolith mass was calculated using a 20% locally weighted least squares error method. See Figure 12 for statistical analysis of this trend.

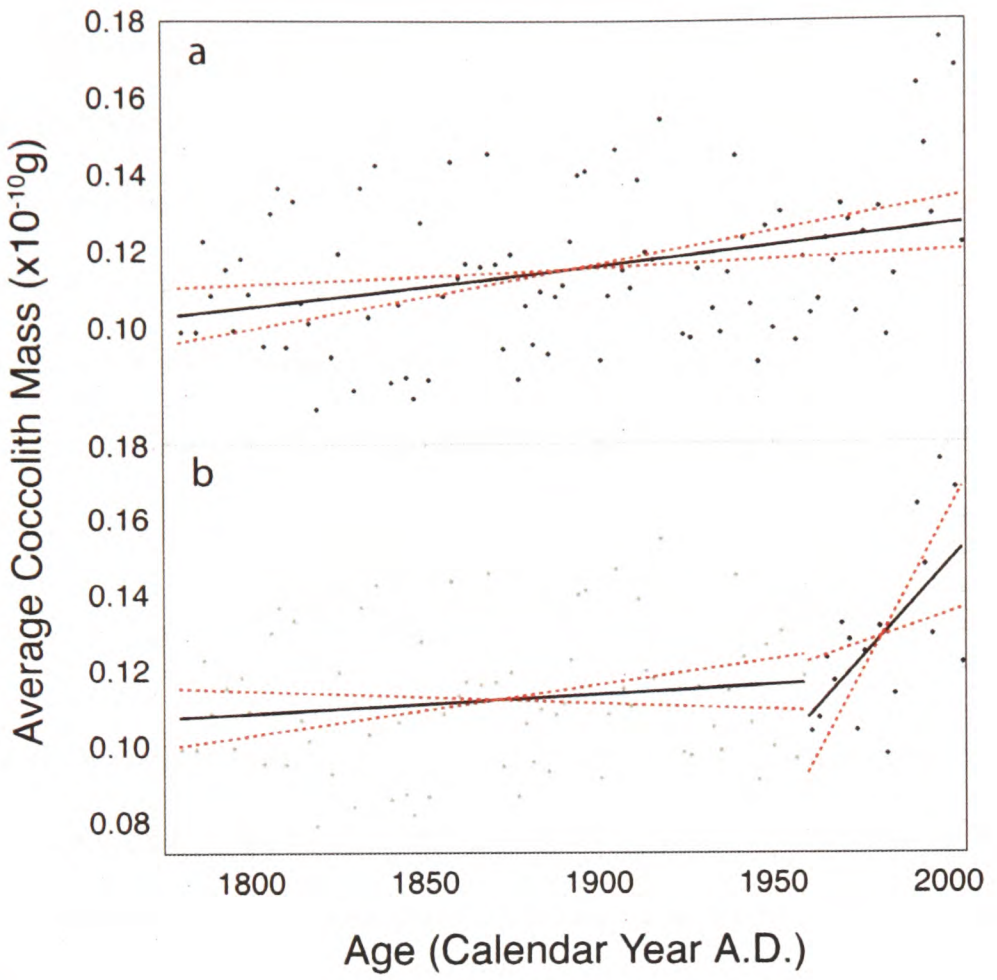

Figure 12. Regression analysis of down-core coccolith mass data. Black lines represent least squares regression lines, and dashed red lines represent the 95% confidence envelope for those regressions. **a**. Assuming a linear change in coccolith mass, an increase of greater than 0.09 x10-10 g over the studied time interval can be observed with a confidence of 95%. This trend exhibits a mean slope of 1.0507 $x10^{-4}$, corresponding to a mean mass increase of 2.3 $x10^{-10}$ g ($N=88$, $R^2=0.11$). **b.** To test the significance of the accelerated rate of change of coccolith mass during the last century as indicated by the smoothed least-squares curve shown in Figure 11, the data have been split into two groups, one containing all data older than 1960, and one containing data younger than 1960. Least-squares regression lines have been fitted to this data (Pre 1960 $N=71$, $R^2=0.02$ Post 1960 $N=17$, $R^2=0.39$), and 95% confidence intervals calculated. The upper limit of the 95% confidence interval of a least squares regression through the data up to 1960 follows a slope of gradient 0.00013, and the lower limit of the 95% confidence interval for data since 1960 follows a slope of gradient 0.00032. We can say with a confidence greater than 95% that the rate of change of coccolith mass since 1960 has been greater than that prior to 1960.

14 and 15 and corresponding text. Temperature, salinity and nutrient supply have also been shown to influence coccolith size and surface ocean $CaCO_3$ production, although where studied, the calcification sensitivity to these factors appears too low to explain the observed trend (Bollmann, 1997; Bollmann and Herrie, 2007; Paasche, 1998; Schmittner et al., 2008; Watabe and K., 1966). A further and potentially significant influence over coccolith mass is primary production (Beaufort et al., 2007). However, if the observed coccolith mass increase occurred in response to a productivity change, we may expect to see an accompanying shift in species composition, which is not observed (Figure 10).

Although the particle-sizing accuracy of the Beckman Coulter Multisizer III, when analysing high concentration samples, is limited by its ability to deconvolve data relating to multiple-particles events (i.e. more than one article passing through the aperture simultaneously), the trends presented in the size data provide an opportunity to investigate the contribution of different species to the measured calcification trend. Figure 14 presents $CaCO_3$ particle (coccolith) frequency data in 256 size bins (where bin-size is defined by particle equivalent spherical diameters - ESD) between 0.63 and 10 μm in Rapid 21-12-B, where data has been normalised by dividing frequencies by the total number of $CaCO_3$ particles in each sample. Above the frequency data, the typical size ranges of the main coccolith species identified in the core have been plotted (Young and Ziveri, 2000) (Table 1). Yellow shades in Figure 14 represent high frequency values and purple shades low frequency values. Assuming a constant species composition (Figure 10), frequency data provides an indication of the species-specific response of the coccolithophores to acidification, with an increase in frequency of larger particles within the size range of one of more species representing an increase in size of one or more of those species. No increase in frequency is observed towards the upper-limit of the size ranges occupied by *E. huxleyi, G. oceanica,* or *G. muellerae* (ESD = 0.84-1.51 μm, 1.60-2.28 μm and 1.39-2.06 μm respectively) indicating no increase in calcification by these species over the period studied. Conversely the size ranges occupied by *H. carteri*, *O. fragilis*, *C. leptoporus* and *C. pelagicus* (ESD = 3.72-5.48 μm, 2.58-4.10 μm,

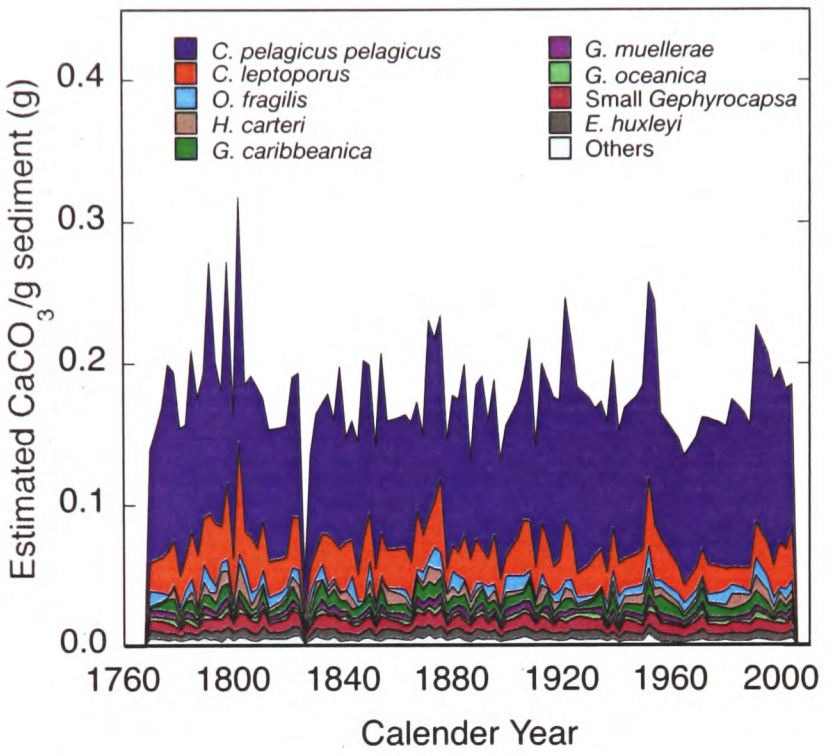

Figure 13. Estimations of $CaCO_3$ mass accumulation based on taxa counts. Areas represent the $CaCO_3$ mass g^{-1} of sediment attributed to each coccolithophore species. Estimates are based on absolute coccolith counts multiplied by the species typical modern coccolith mass (Young and Ziveri, 2000). Coccoliths of *C. pelagicus pelagicus* and *C. leptoporus* constitute ~75% of the total $CaCO_3$ mass throughout the record. We see no long-term trend in $CaCO_3$ accumulation from any single taxa, or across the assemblage. Estimates are calculated using a fixed coccolith mass for each taxon, calibrated to core-top measurements (Young and Ziveri, 2000).

2.67-5.87 μm and 2.92-7.77 μm respectively), including that occupied by *C. pelagicus* alone, record a significant increase in large-particle frequency since ~1960, indicating, certainly in *C. pelagicus* and potentially in the other species, an increased calcification. Presented three-dimensionally, plotting anomalies from the average frequency values, it is clear that the major calcification increase is occurring in the size-region occupied by *C. pelagicus* alone (Figure 15). These observations are consistent with the results of the culture experiments undertaken by Langer et al. (Langer et al., 2006) and Iglesias-Rodriguez and Halloran et al. (2008), in which *C. leptoporus* and *C. pelagicus* display an increasing calcification between pre-industrial and present pCO_2 values (although the statistics are unclear with regard to the level of significance of the change recorded in *C. pelagicus*), and *E. huxleyi* displays a decrease in calcification between pre-industrial and present-day pCO_2 values (Figures 3

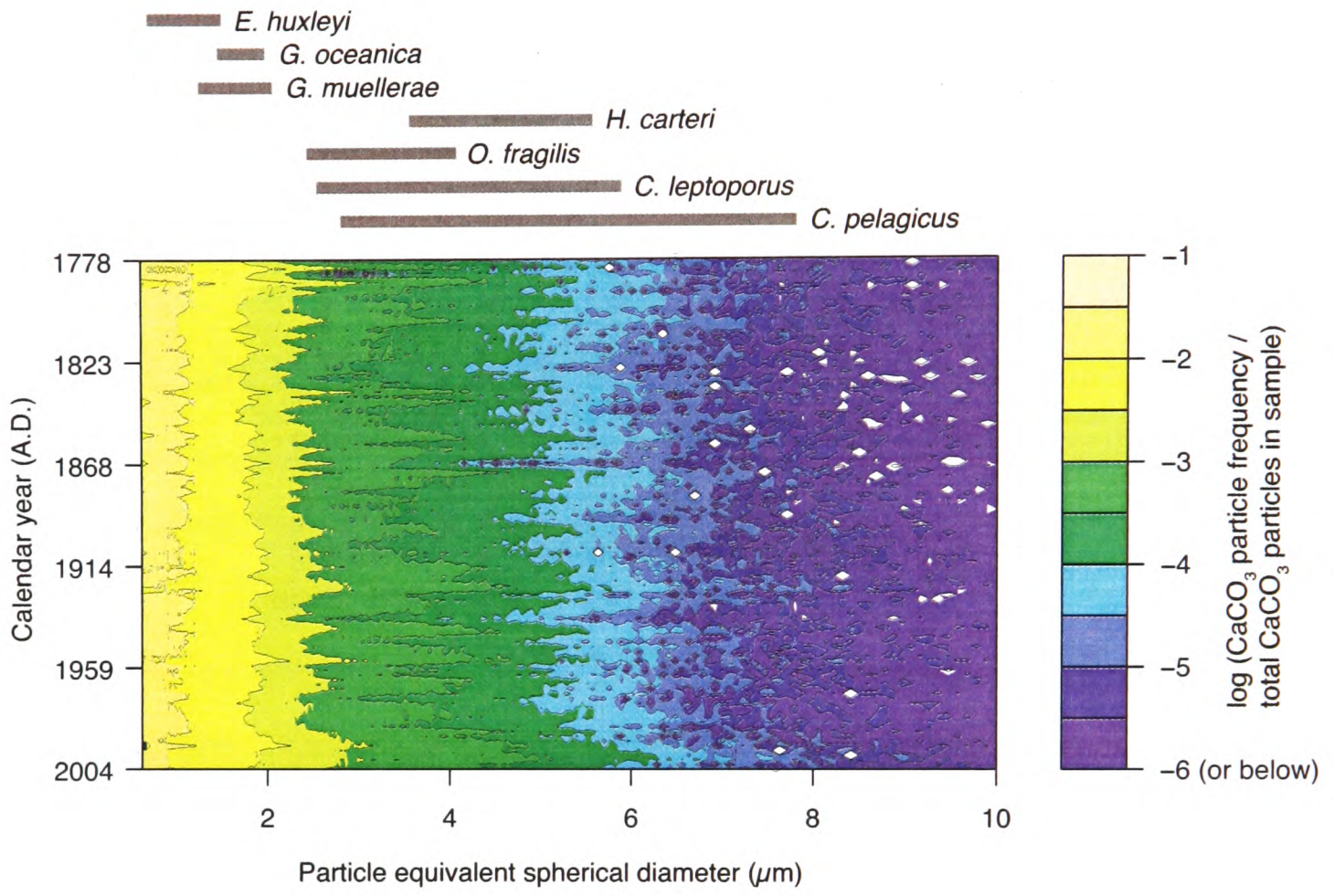

Figure 14. Contour plot showing logged $CaCO_3$ particle (coccolith) frequency data in 256 size bins between 0.63 and 10 μm in sub 10 μm filtered RAPID 21-12-B sediment from 1778 to 2004. Data calculated by subtracting average $CaCO_3$-free sediment size-frequency data (after HNO_3 addition) from average total sediment size-frequency data, then normalising by dividing this by the average total (undissolved) particle count from that sample. The log of this value was then taken to increase the sensitivity of the contour plot to changes within the larger by less numerous fractions towards the right hand side of the figure. Above the main figure-body, highlighted by grey-bars, are the known size ranges for the common species identified in RAPID-21-12-B, where equivalent spherical diameters have been calculated from Young et al. (2000).

and 4). The agreement between laboratory and field data that *C. pelagicus* and possibly *C. leptoporus* are among the first species to respond strongly to ocean acidification lends confidence to the culture experiments. The quality of the Coulter counter size data is highlighted by comparison of $CaCO_3$ to non-$CaCO_3$ particle-count ratios (Figure 16) and the species counts (Figure 10). The highest $CaCO_3$ to non-$CaCO_3$ ratios (greens and yellows in Figure 16) correspond with the size-ranges of *E. huxleyi* and the *Gephyrocapsa* and of *C. pelagicus*, the most populous species in RAPID 21-12-B, as indicated by manual species

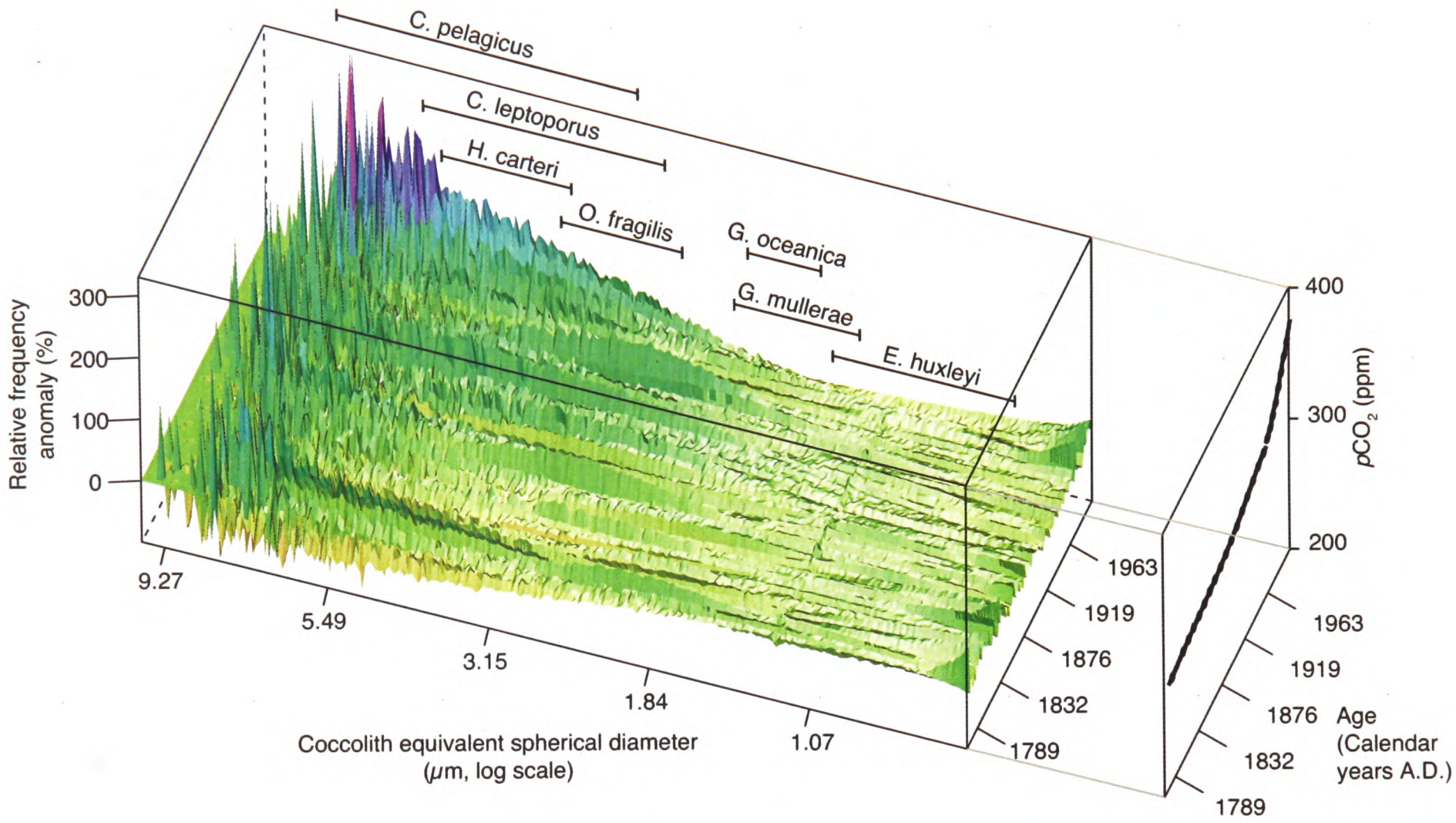

Figure 15. 3-D surface showing the percentage anomaly in frequency data (with respect to the average value for each size-bin) for $CaCO_3$ particles (coccoliths) in samples normalised by dividing the frequency measured in each bin by the total number of $CaCO_3$ counts in each sample. Bars represent the size-ranges occupied by coccoliths of different species, and the curve on the right hand side shows the concomitant increase in atmospheric pCO_2. Because no change in population structure is observed, the increasing frequency anomaly highlighted by dark colours (blues and purples) since ~1960, indicates an increase in size of coccoliths produced by *C. pelagicus* and possibly *C. leptoporus, H. carteri* and *O. fragilis*. No change in frequency anomaly is observed for the species *E. huxleyi, G. oceanica* or *G. mullerae* indicating that these species have not increased their calcification in response to increased pCO_2 over the anthropocene.

counts. Further, Figure 16 shows an increase in the ratio of $CaCO_3$ to non $CaCO_3$ in the 4-6 μm equivalent sperical diameter (ESD) range towards the top of the core, consistent with the observed basin-wide Atlantic change in $CaCO_3$:biogenic-silica as a result of increased $CaCO_3$ ratio since 1980 (Antia et al., 2001; Deuser et al., 1995). Average $CaCO_3$:non-$CaCO_3$ particle data is presented in Figure 17.

2.4 Samples and Methods II – Cultured Coccolithophores

To investigate whether coccolith size was a valid proxy for the mass of $CaCO_3$ produced by each coccolithophore (i.e. the calcification), and examine whether coccolith size changes of the range observed in this data were realistic over the pCO_2 range recorded between 1800 and present, a collaboration was set up with Dr. Iglesias-Rodriguez of Southampton University. Iglesias-Rodriguez et al. were culturing coccolithophores of *E. huxleyi* at different partial pressures of CO_2. As illustrated in Figure 18 and discussed in the next paragraph, the amount of organic carbon produced per cell increased under future CO_2 scenarios. Here we have used the sizing capacity of the Beckman Coulter Multisizer III to measure the average coccolith, and coccosphere volumes.

	Volumes (μm³) From Young and Ziveri (2000)		**Equivalent Spherical Diameters (μm)**	
	Min.	**Max.**	**Min.**	**Max.**
C. pelagicus	13.00	246.00	2.92	7.77
C. leptoporus	10.00	106.00	2.67	5.87
O. fragilis	9.00	36.00	2.58	4.10
H. carteri	27.00	86.00	3.72	5.48
G. muellerae	1.40	4.60	1.39	2.06
G. oceanica	2.14	6.20	1.60	2.28
E. huxleyi	0.31	1.80	0.84	1.51

Table 1. Range of North Atlantic coccolith volumes calculated in Young and Ziveri (2000) and corresponding equivalent spherical diameters (ESD's).

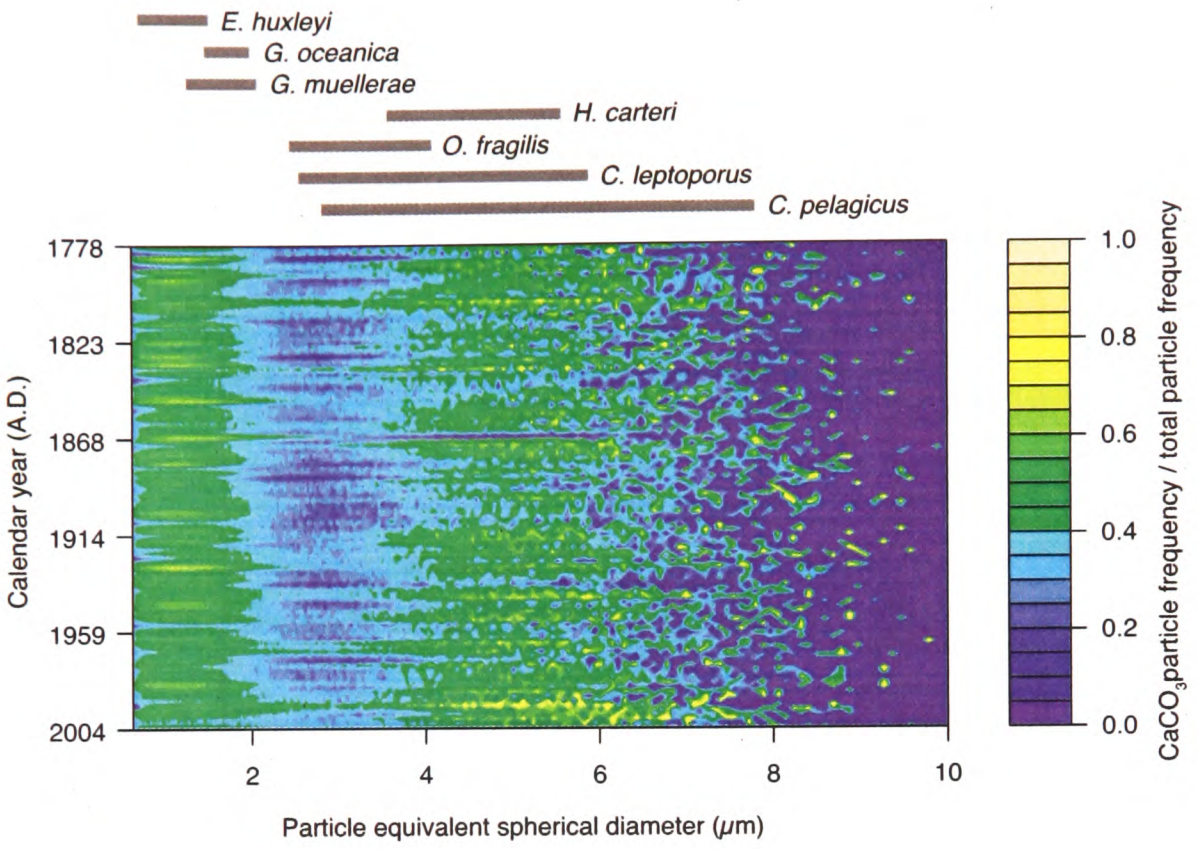

Figure 16. Contour plot showing the ratio of $CaCO_3$ to non-$CaCO_3$ (biogenic silica and clay) particles in 256 size bins between 0.63 and 10 μm in sub 10 μm filtered RAPID 21-12-B sediment from 1778 to 2004. Calculated from the sediment particle counts before and after acid-addition. Above the main Figure-body are the known size ranges for the common species identified in RAPID-21-12-B, where the equivalent spherical diameters have been calculated from Young et al. (2000).

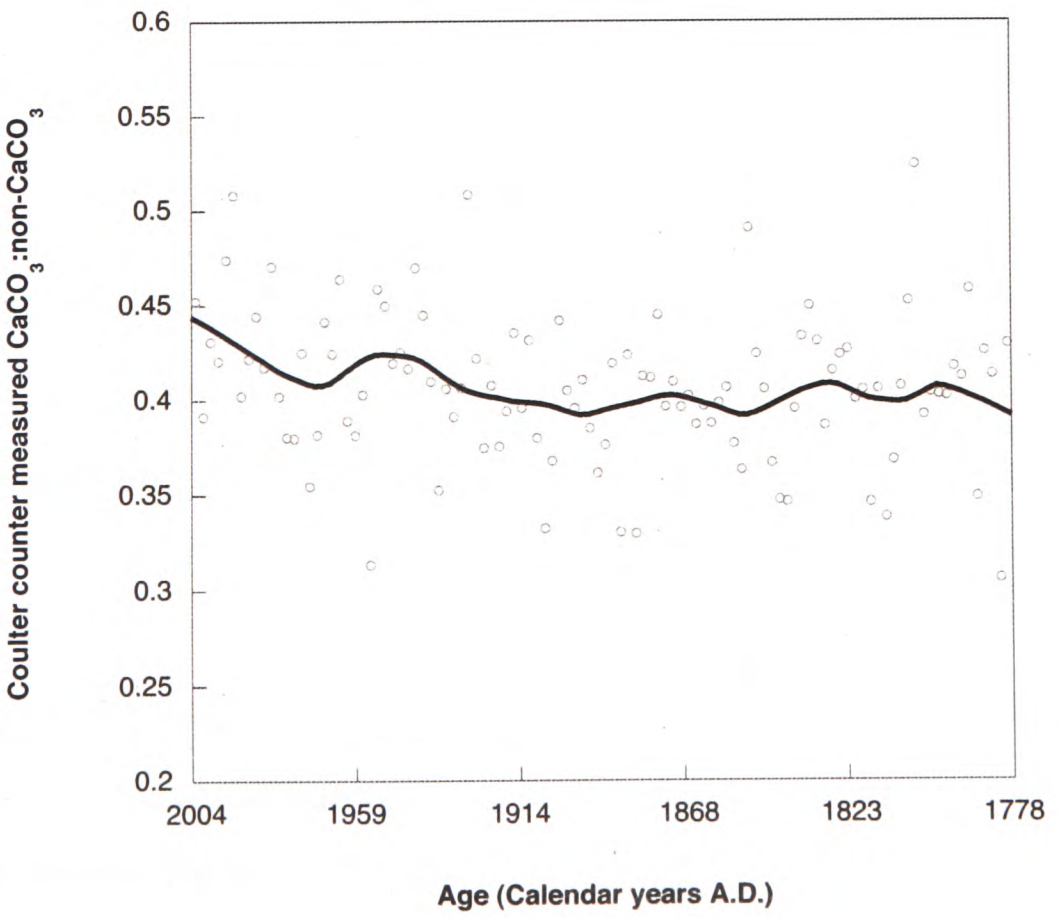

Figure 17. Average $CaCO_3$ to non-$CaCO_3$ particle ratio from Coulter Counter data.

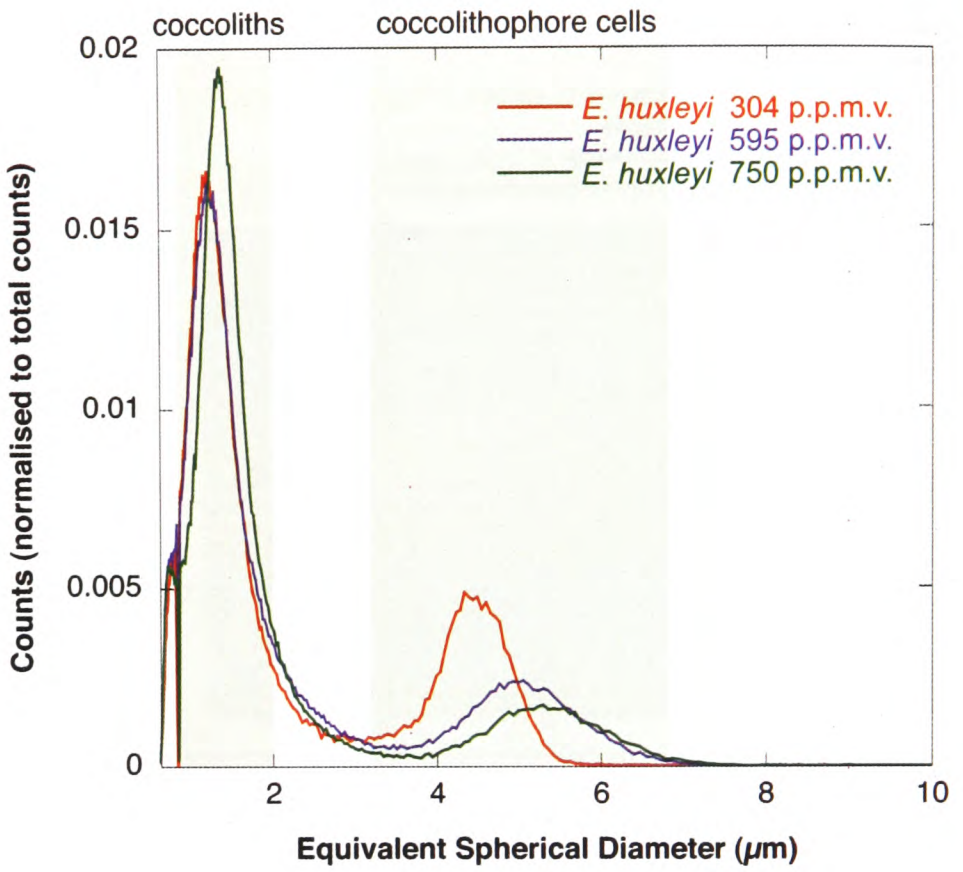

Figure 18. Equivalent spherical diameter (EQD) distributions of *E. huxleyi* coccoliths (< 2 μm) and coccospheres (3-7 μm). Measurements shown are from HgCl preserved samples, which are consistently preserved well. Glutaraldehyde, formaldehyde, sodium borate preservation repeatedly blocked the aperture, and required statistical evaluation of (students t-test) ~10 replicate measurements to obtain mean coccolith and coccosphere EGDs. Moving from coccolithophores grown at 304 ppmv pCO_2 to coccolithophores grown at 750 ppmv (red to green) it can be seen that both the coccoliths (left peak) and cells (right peak) increase in size (i.e. the peaks move to the right).

9 ml aliquots of the culture medium were taken, and preserved with the addition of either 1 ml of a glutaraldehyde, formaldehyde, sodium borate (500 μl of 50% glutaraldehyde to 50 ml of 10% formaldehyde, 100 mM sodium borate) solution or 1 ml of mercury chloride, then frozen until use.

Thawed samples were analysed using the coulter counter using a 20 μm aperture, and measuring equivalent spherical diameters between 0.63 μm and 10 μm. Figure 18 shows the size distribution of the coccoliths and coccospheres grown at different pCO_2, clearly distinguishing the coccolith peak (< 2 μm) and coccolithophore peak (3-7 μm). Mean coccolith and coccosphere volumes were obtained using the students t-test (Table 2).

CO_2 partial pressure	Mean Coccolith volume (μm^3)	Mean Coccosphere volume (μm^3)	PIC (pmol/cell)	POC (pmol/cell)
280.0 ppmv	1.09	55.44	0.36	0.43
303.8 ppmv	0.84	45.95	0.29	0.39
489.2 ppmv	1.11	65.13	0.37	0.49
595.1 ppmv	1.84	55.23	0.63	0.90
750.3 ppmv	1.86	69.33	1.01	1.36

Table 2. Mean coccolith volume, coccosphere volume, PIC and POC as measured in *E. huxleyi* cultures grown by Iglesias-Rodriguez and Halloran et al. (2008)

2.5 Results and Discussion II – Cultured Coccolithophores

Coccolith volume closely follows PIC/cell (Figure 19), indicating that the increase in $CaCO_3$ being produced by each coccolithophore is being accommodated by an increase in coccolith size rather than an increase in number of coccoliths produced. This result validates the use of coccolith volume (or mass) as an indicator of changing calcification. Figure 20 shows a less strong correlation between the mean coccosphere volume and POC/cell with changing pCO_2. It is perhaps not surprising that coccosphere volume and POC show poor agreement. The measurement of the coccosphere volume is a measurement of the coccolith cell volume together with the volume of all of the coccoliths on the cells surface. Differential loss of coccoliths from the cell surface may have occurred during transportation, storage and analysis. An improved method is to decalcify the cells by reducing the pH of the media to < 5 units (to dissolve the $CaCO_3$), then perform a volume measurement only on the cell. Once decalcified, the size distribution no longer shows a peak for loose coccoliths, but also shows a reduction in 'coccosphere' size (Figure 21). This is interpreted as a removal of the coccoliths from the cell surface, and a measurement of actual cell volume. Unfortunately there was not enough material to do this across the range of coccolithophores grown at different CO_2 partial pressures.

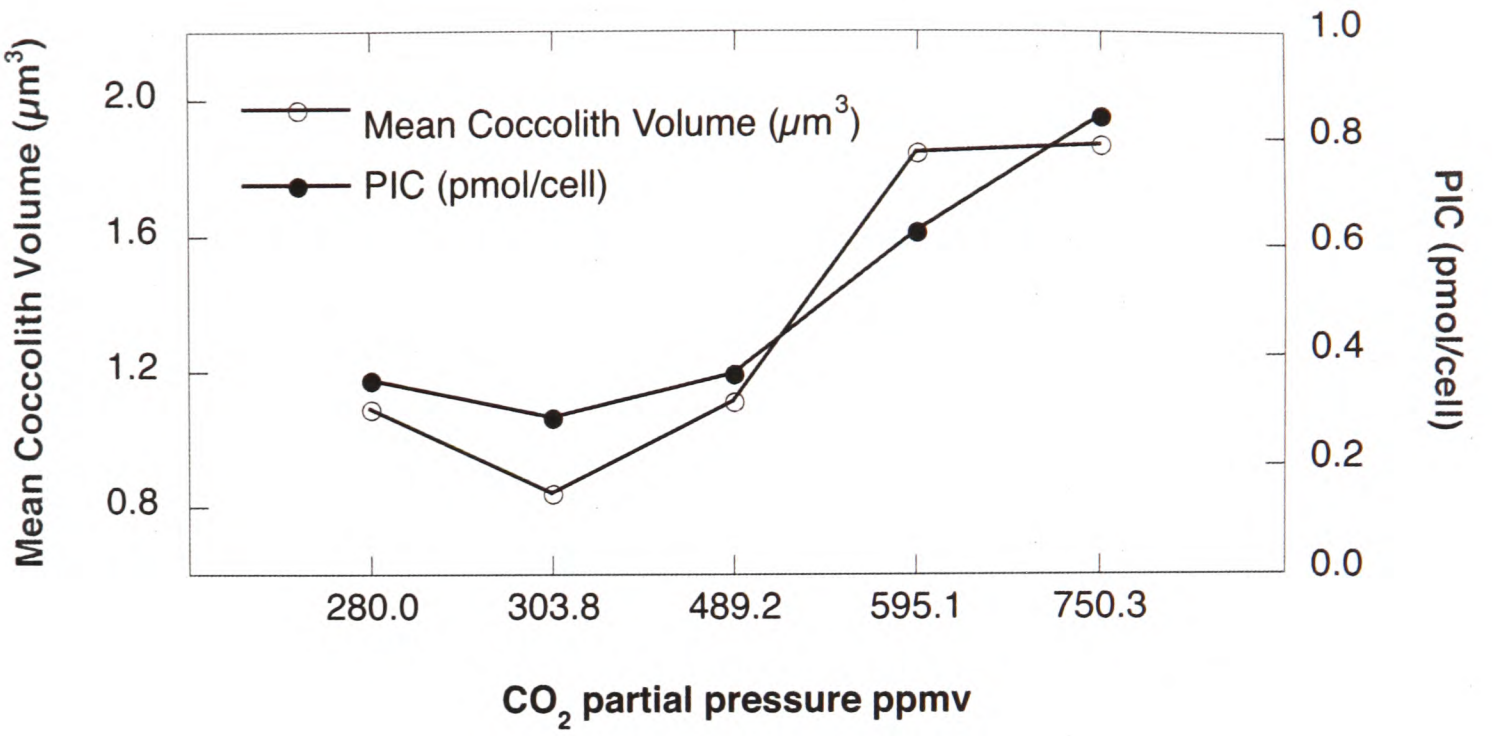

Figure 19. Median coccolith volumes measured using a Beckman Coulter Multisizer III with a 20 μm aperture (open circles), and Particulate Inorganic Carbon (PIC) per cell (closed circles) for *E. huxleyi* cultures at five different CO_2 concentrations. A strong correlation exists between the coccolith volume and PIC indicating that coccolith size provides a good first order indication of coccolithophore calcification.

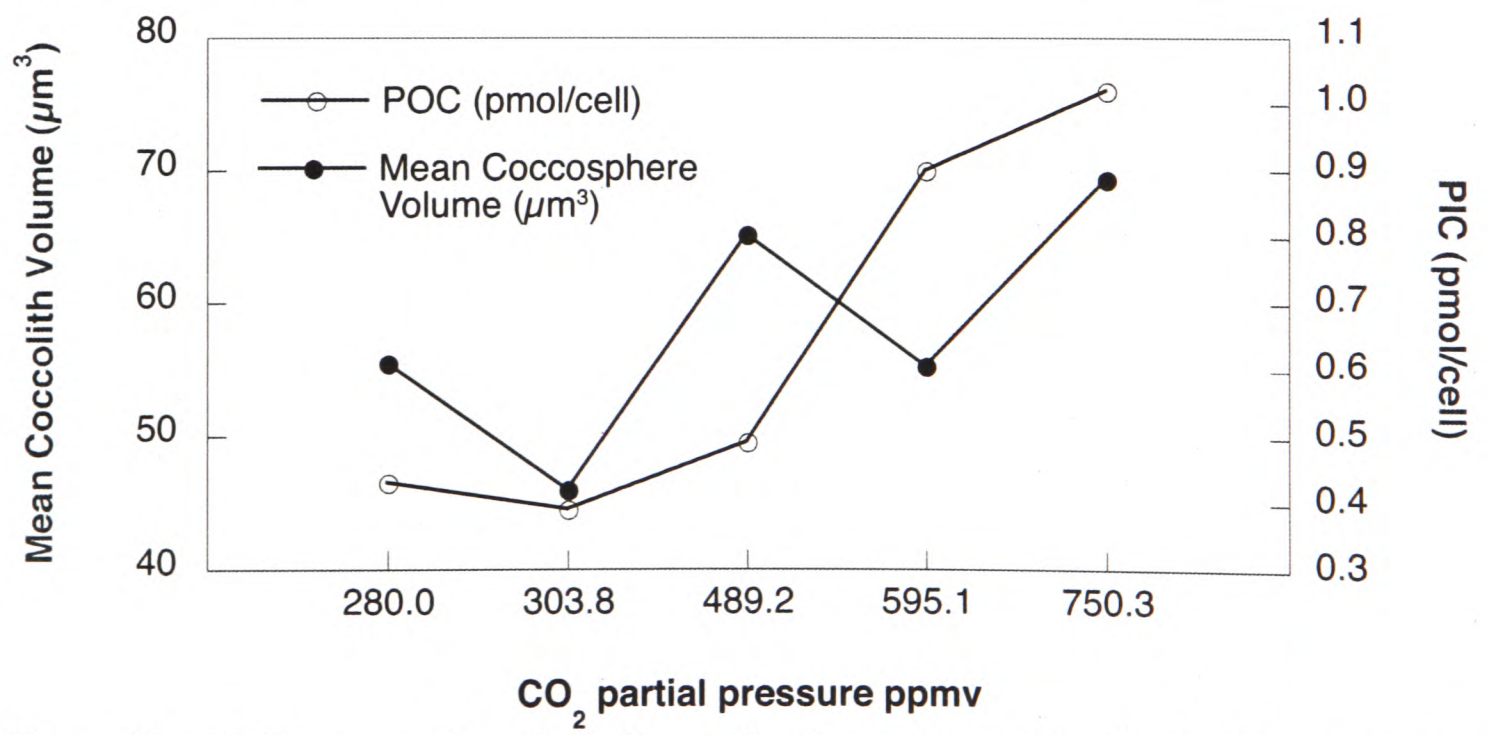

Figure 20. Median coccosphere (including cell) volumes measured using a Beckman Coulter Multisizer III with a 20 μm aperture (open circles), and Particulate Organic Carbon (POC) per cell (closed circles) for *E. huxleyi* cultures at five different CO_2 concentrations. Coccosphere volume measurements were made on calcified cells. A weak correlation exists between the coccosphere volume and the POC. This may reflect the fact that the coccosphere measurement is including the cell volume together with the volume of any coccoliths on the surface, and therefore is not a measurement of pure organic carbon volume. A better test of this correlation would be to measure decalcified cells, unfortunately the amount of material avaliable did not allow these measurements.

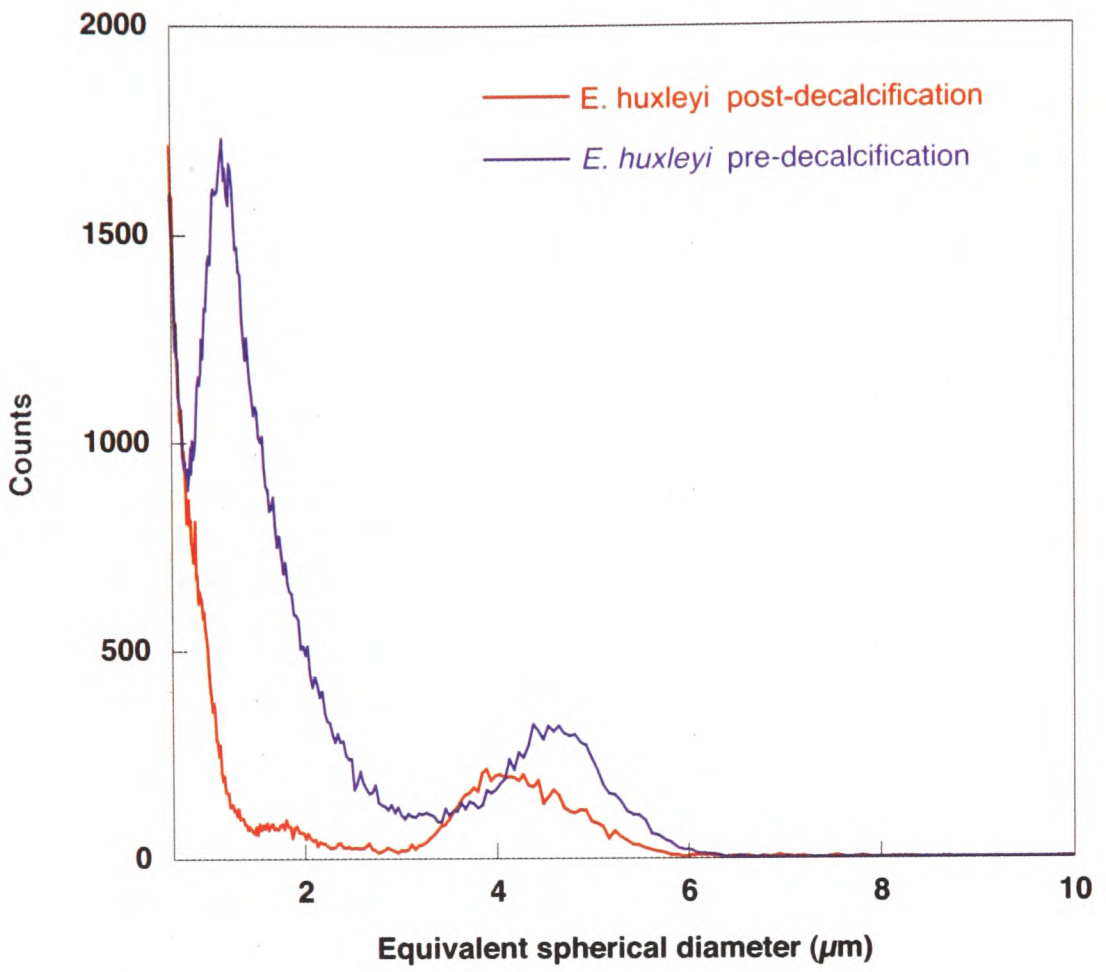

Figure 21. Size distribution of coccoliths and coccospheres before (blue) and after (red) decalcification. Note that coccoliths disappear, and 'coccosphere' size is reduced.

2.6 Discussion and Conclusions

In order to understand the net influence of changing coccolithophore production to pCO_2, it is important not just to investigate the production of $CaCO_3$, but also to understand how organic carbon production in coccolithophores may vary. Unlike the formation and burial of $CaCO_3$ which results in the release of CO_2 from the ocean (over timescales < ocean mixing), the growth of organic carbon consumes CO_2 through photosynthesis (Figure 22). If organic carbon is transported out of the surface waters it acts as a CO_2 sink. It is the balance between removal of particulate inorganic carbon (PIC) and particulate organic carbon (POC), which will ultimately control the influence of phytoplankton on partitioning of CO_2 into surface waters (Archer and Maier-Reimer, 1994). Without a record of total organic carbon production we cannot quantify changes in the PIC/POC ratio at this site.

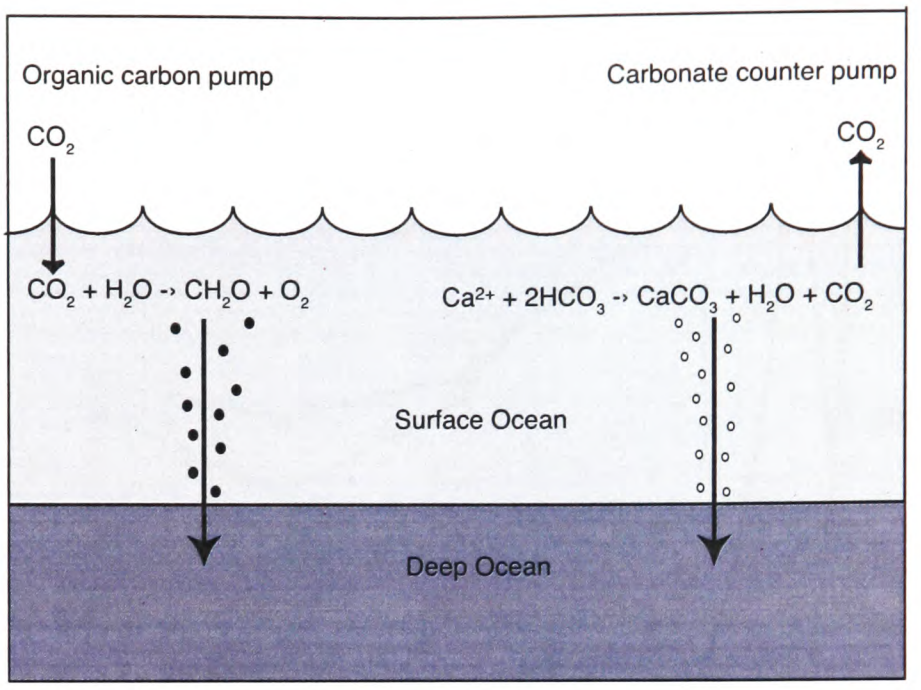

Figure 22. A simple schematic representation of the biological pump.

In addition to changes in the production ratio, another potential consequence of increasing calcification is a greater removal of $CaCO_3$ from the surface waters due to increased ballast effects (Armstrong et al., 2002).

The molar ratio of organic carbon and inorganic carbon (i.e. calcite) being transported to the deep ocean has been termed the rain ratio. The exact method of transport, and factors effecting transport are widely debated. To calculate the settling time of a single coccolith (assuming it to be a spherical particle of 2 μm radius) in a still ocean 4 km deep using Stokes Law gives a settling time of many thousands of years, yet transport in the real ocean operates on a timescale of days. It is clear from sediment traps, and even observations of coccolith in culture, that mechanisms must be acting to accelerate this process. A number of such transportation methods have been proposed and observed, including; particle aggregation (Billett et al., 1983; Passow, 2004), production of transparent exopolymers (TEP) by algal cells which act as particle 'glue' (Engel, 2004), aggregate ballasting (Schiebel, 2002) and faecal pellet production and transport (Elder and Fowler, 1977). All of these mechanisms act to increase the settling object's size, and therefore increase its settling velocity. Other than particle size, the density difference between the particle and the fluid is the second variable

in Stoke's Law. It is therefore important that we understand natural ballast processes. Considering transportation out of a pure coccolithophore bloom, two material-types will be present, cell debris and calcite. Cell debris contains a high level of water, and therefore has a density near 1 kg m^{-3}. In contrast, calcite has a density of 2.7 kg m^{-3}. Assuming an aggregate particle of radius 1 mm, changing the ratio of organic material to calcite from 50:50 to 40:60 will increase the settling velocity by 5%. Therefore, changing the proportion of the ballast material (here $CaCO_3$) can dramatically affect the settling velocity. The rate of settling is a critical variable to understand because it has been shown that significant dissolution occurs during transport through the upper ocean (Milliman et al., 1999). Another very important aspect of the rain ratio is its effect on dissolution once the particles have reached the sediment. Breakdown of organic matter releases CO_2, reducing the saturation state of the surface sediment pore waters and increasing the opportunity for dissolution (Archer and Maier-Reimer, 1994; Emerson and Bender, 1981). Ultimately, the composition of material reaching the sediment is a function of that produced at the surface. A further export flux consideration results from an understanding that whilst coccolithophores contribute around half of the pelagic $CaCO_3$ production, they account for a relatively minor component of the pelagic organic carbon fixation. Therefore, although these experiments demonstrate that there may not be a change in coccolithophore PIC/POC, there could still be a very significant change in total pelagic PIC/POC, if non-coccolithophore species were to follow contrasting carbon fixation responses.

It is not yet conclusive whether increased $CaCO_3$ ballast would favour a relative increase in export and sedimentation of PIC or POC (Barker et al., 2003). Future research is needed to fully constrain productivity changes over the Anthropocene, extend our understanding of calcification change to different latitudes and different ocean basins, and quantify how changing ballast will affect export production. Our findings have demonstrated an assemblage-wide calcification increase since ~1960, of the same order of magnitude as has been predicted experimentally for similar pCO_2 steps moving into a high CO_2 world,

indicating that coccolithophores may already be responding to ocean acidification.

Anthropogenic CO_2 emissions during the 1990s were estimated to be ~8 Gt C yr^{-1} (IPCC, 2001). Over the same period, the ocean was estimated to absorb 1.7 ± 0.5 Gt C yr^{-1}. Pre-industrial CO_2 production by pelagic carbonate has been estimated at ~0.86 Gt C yr^{-1} (Morse and Mackenzie, 1990). Since 1850 a near doubling in the total coccolith assemblage calcification has been demonstrated at a sub-polar North Atlantic site. If it were assumed that organic carbon production remained constant, and consider our findings in the North Atlantic to be representative of a whole ocean response, attributing 75% of the pelagic carbonate production to coccolithophores, our observed change corresponds to an increased coccolithophore CO_2 production of ~0.4 Gt yr^{-1} since 1850. As a worst case scenario, if the coccolithophore calcification response to CO_2 rise continues as shown for the previous 100 ppmv increase, and our results prove to be representative of the global coccolith response, by the year 2100 it is possible that the oceans could stop being a sink for increasing anthropogenic CO_2, and start becoming a source. This positive feedback must be considered carefully when modelling future climate change, in particular because coccolithophore growth rate over this period remains unknown. Alternatively, if POC is increasing at the same rate as PIC, the increasing demand for nutrients may result in vast areas of the ocean becoming nutrient limited. Future research is needed to fully constrain productivity changes over the Anthropocene, and extend our understanding of calcification change to different latitudes and different ocean basins to test these conclusions.

Ultimately, the key to predicting the role of future calcification in climate and ecosystem change will be to develop a physiological understanding of how different species react to elevated pCO_2 under an array of nutrient and temperature regimes. We have demonstrated here that, amongst coccolithophores alone, a complex calcification-CO_2 response exists (Figure 15). Only once a physiological understanding has been gained can we numerically describe that response and apply it to the global ocean within biogeochemical ecosystem-

models. The work presented in this chapter provides a starting point for this exploration, indicating, in agreement with the culture studies published by Langer et al. (Langer et al., 2006) and Iglesias-Rodriguez and Halloran et al. (2008), between pre-industrial and present-day pCO_2 levels, it is the larger species (*C. pelagicus* and *C. leptoporus*), rather than the smaller species (*E. huxleyi* and *G. oceanica*) that undergo a calcification increase. This could perhaps be a consequence of the lower surface area to volume ratio of smaller species, meaning that they can absorb enough CO_2 and HCO_3 that these ions are not limiting. As implied by Henderiks and Rickaby (2007), the complexity of the response may reflect an evolutionary adaptation, in terms of carbon concentration mechanisms, to the ambient pCO_2 at the time of emergence? Hopefully these questions will be answered as new sedimentary, mesocosm and laboratory experiments are performed and considered in a genetic and geochemical context.

2.8. Bibliography

ANTIA, A. N., KOEVE, W., FISCHER, G., BLANZ, T., SCHULZ-BULL, D., SCHOLTEN, J., NEUER, S., KREMLING, K., KUSS, J., PEINERT, R., HEBBELN, D., BATHMANN, U., CONTE, M., FEHNER, U. AND ZEITZSCHEL, B. (2001) Basin-wide particulate carbon flux in the Atlantic Ocean: Regional export patterns and potential for atmospheric CO_2 sequestration. Global Biogeochemical Cycles, 15, 845-862.

ARCHER, D. AND MAIER-REIMER, E. (1994) Effect of deep-sea sedimentary calcite preservation on atmospheric CO_2 concentrations. Nature, 367, 260 - 263.

ARMSTRONG, R. A., LEE, C., HEDGES, J. I., HONJO, S. AND WAKEHAM, S. G. (2002) A new, mechanistic model for organic carbon fluxes in the ocean based on the quantitative association of POC with ballast minerals. Deep-Sea Research Part II-Topical Studies in Oceanography, 49, 219-236.

BARKER, S. AND ELDERFIELD, H. (2002) Foraminiferal calcification response to glacial-interglacial changes in atmospheric CO_2. Science, 297, 833-836.

BARKER, S., HIGGINS, J. A. AND ELDERFIELD, H. (2003) The future of the carbon cycle: review, calcification response, ballast and feedback on atmospheric CO_2. Philos. Trans. R. Soc. London Ser. A, 361, 1977-1998.

BEAUFORT, L., PROBERT, I. AND BUCHET, N. (2007) Effects of acidification and primary production on coccolith weight: Implications for carbonate transfer from the surface to the deep ocean. Geochemistry Geophysics Geosystems, 8, doi:10.1029/2006GC001493.

BIJMA, J., HONISCH, B. AND ZEEBE, R. E. (2002) Impact of the ocean carbonate chemistry on living foraminiferal shell weight: Comment on "Carbonate ion concentration in glacial-age deep waters of the Caribbean Sea" by W. S. Broecker and E. Clark. Geochemistry Geophysics Geosystems, 3, doi:10.1029/2002GC000388.

BILLETT, D. S. M., LAMPITT, R. S., RICE, A. L. AND MANTOURA, R. F. C. (1983) Seasonal sedimentation of phytoplankton to the deep-sea benthos. Nature, 302, 520-522.

BOESSENKOOL, K. P., HALL, I. R., ELDERFIELD, H. AND YASHAYAEV, I. (2007) North Atlantic climate and deep-ocean flow speed changes during the last 230 years. Geophys. Res. Lett., 34, 10.1029/2007GL030285.

BOLLMANN, J. (1997) Morphology and biogeography of *Gephyrocapsa* coccoliths in Holocene sediments. Mar. Micropaleontol., 29, 319-350.

BOLLMANN, J. AND HERRIE, J. O. (2007) Morphological variation of *Emilliana huxleyi* and sea surface salinity. Earth Planet. Sci. Lett., 255, 273-288.

BUITENHUIS, E. T., DE BAAR, H. J. W. AND VELDHUIS, M. J. W. (1999) Photosynthesis

and calcification by *Emiliania huxleyi* (*Prymnesiophyceae*) as a function of inorganic carbon species. J. Phycol., 35, 949-959.

DELILLE, B., HARLAY, J., ZONDERVAN, I., JACQUET, S., CHOU, L., WOLLAST, R., BELLERBY, R. G. J., FRANKIGNOULLE, M., BORGES, A. V., RIEBESELL, U. AND GATTUSO, J.(2005) Response of primary production and calcification to changes of pCO_2 during experimental blooms of the coccolithophorid *Emiliania huxleyi*. Global Biogeochemical Cycles, 19, doi:10.1029/2004GB0023.

DEUSER, W. G., JICKELLS, T. D., KING,AND COMMEAU, J. A. (1995) Decadal and annual changes in biogenic opal and carbonate fluxes to the deep Sargasso Sea. Deep-Sea Research Part I-Oceanographic Research Papers, 42, 1923-1932.

ELDER, D. L. AND FOWLER, S. W. (1977) Polychlorinated Biphenyls - Penetration into Deep Ocean by Zooplankton Fecal Pellet Transport. Science, 197, 459-461.

EMERSON, S. AND BENDER, M. (1981) Carbon Fluxes at the Sediment-Water Interface of the deep-sea - calcium-carbonate preservation. Journal of Marine Research, 39, 139-162.

ENGEL, A. (2004) Distribution of transparent exopolymer particles (TEP) in the northeast Atlantic Ocean and their potential significance for aggregation processes. Deep-Sea Research Part I-Oceanographic Research Papers, 51, 83-92.

FEELY, R. A., SABINE, C. L., LEE, K., BERELSON, W., KLEYPAS, J., FABRY, V. J. AND MILLERO, F. J. (2004) Impact of anthropogenic CO_2 on the $CaCO_3$ system in the oceans. Science, 305, 362-366.

FLORES, J. A. AND SIERRO, F. J. (1997) Revised technique for calculation of calcareous nannofossil accumulation rates. Micropaleontology, 43, 321-324.

FRENZ, M., BAUMANN, K. H., BOECKEL, B., HOPPNER, R. AND HENRICH, R. (2005) Quantification of foraminifer and coccolith carbonate in South Atlantic surface sediments by means of carbonate grain-size distributions. Journal of Sedimentary Research, 75, 464-475.

FRENZ, M. AND HENRICH, R. (2007) Carbonate dissolution revealed by silt grain-size distribution: comparison of Holocene and Last Glacial Maximum sediments from the pelagic South Atlantic. Sedimentology, 54, 391-404.

GAZEAU, F., QUIBLIER, C., JANSEN, J. M., GATTUSO, J. P., MIDDELBURG, J. J. AND HEIP, C. H. R. (2007) Impact of elevated CO_2 on shellfish calcification. Geophysical Research Letters, 34, doi:10.1029/2006GL028554.

HENDERIKS, J. AND RICKABY, R. E. M. (2007) Algal constraints on the Cenozoic history of atmospheric CO_2. Biogeosciences Discussions, 4, 1-11.

HILL, M. E. (1975) Selective Dissolution of Mid-Cretaceous (Cenomanian) Calcareous Nannofossils. Micropaleontology, 21, 227-235.

IGLESIAS-RODRIGUEZ, M. D., HALLORAN, P. R., RICKABY, R. E. M., HALL,

I. R., COLMENERO-HIDALGO, E., GITTINS, J. R., GREEN, D. R. H., TOBY TYRRELL, T., GIBBS, S. J., VON DASSOW, P., REHM, E., ARMBRUST, V. E. AND BOESSENKOOL, K. (2008) Phytoplankton calcification in a high CO_2 world. Science, (accepted Feb, 2008).

IPCC (2001) Climate Change 2001: The Scientific Basis, Cambridge, Cambridge University Press.

LANGDON, C. AND ATKINSON, M. J. (2005) Effect of elevated pCO_2 on photosynthesis and calcification of corals and interactions with seasonal change in temperature/ irradiance and nutrient enrichment. Journal of Geophysical Research-Oceans, 110, -.

LANGER, G., GEISEN, M., BAUMANN, K. H., KLAS, J., RIEBESELL, U., THOMS, S. AND YOUNG, J. R. (2006) Species-specific responses of calcifying algae to changing seawater carbonate chemistry. Geochemistry Geophysics Geosystems, 7, Q09006.

MCCAVE, I. N. AND HALL, I. R. (2006) Size sorting in marine muds: Processes, pitfalls, and prospects for paleoflow-speed proxies. Geochemistry Geophysics Geosystems, 7, Q10N05, doi:10.1029/2006GC001284.

MCCAVE, I. N., MANIGHETTI, B. AND ROBINSON, S. G. (1995) Sortable silt and fine sediment size composition slicing - parameters for paleocurrent speed and paleoceanography. Paleoceanography, 10, 593-610.

MILLIMAN, J. D., TROY,J., BALCH, W. M., ADAMS, A. K., LI, Y. H. AND MACKENZIE, F. T. (1999) Biologically mediated dissolution of calcium carbonate above the chemical lysocline? Deep-Sea Research Part I-Oceanographic Research Papers, 46, 1653-1669.

MORSE, J. W. AND MACKENZIE, F. T. (1990) Geochemistry of sedimentary carbonates, Amsterdam ; Oxford, Elsevier.

ORR, J. C., FABRY, V. J., AUMONT, O., BOPP, L., DONEY, S. C., FEELY, R. A., GNANADESIKAN, A., GRUBER, N., ISHIDA, A., JOOS, F., KEY, R. M., LINDSAY, K., MAIER-REIMER, E., MATEAR, R., MONFRAY, P., MOUCHET, A., NAJJAR, R. G., PLATTNER, G. K., RODGERS, K. B., SABINE, C. L., SARMIENTO, J. L., SCHLITZER, R., SLATER, R. D., TOTTERDELL, I. J., WEIRIG, M. F., YAMANAKA, Y. AND YOOL, A. (2005) Anthropogenic ocean acidification over the twenty-first century and its impact on calcifying organisms. Nature, 437, 681-686.

PAASCHE, E. (1998) Roles of nitrogen and phosphorus in coccolith formation in *Emiliania huxleyi* (*Prymnesiophyceae*). European Journal of Phycology, 33, 33-42.

PASSOW, U. (2004) Switching perspectives: Do mineral fluxes determine particulate organic carbon fluxes or vice versa? Geochemistry Geophysics Geosystems, 5, -.

RIDGWELL, A. AND ZEEBE, R. E. (2005) The role of the global carbonate cycle in the regulation and evolution of the Earth system. Earth Planet. Sci. Lett., 234, 299-315.

RIDGWELL, A., ZONDERVAN, I., HARGREAVES, J. C., BIJMA, J. AND LENTON,

T. M. (2006) Significant long-term increase of fossil fuel CO_2 uptake from reduced marine calcification. Biogeosciences Discussions, 3, 1763-1780.

RIEBESELL, U., ZONDERVAN, I., ROST, B., TORTELL, D., ZEEBE, R. E. AND MOREL, F. M. M. (2000) Reduced calcification of marine plankton in response to increased atmospheric CO_2. Nature, 407, 364-367.

SCHIEBEL, R. (2002) Planktic foraminiferal sedimentation and the marine calcite budget. Global Biogeochemical Cycles, 16,

SCHMITTNER, A., OSCHLIES, A., MATTHEWS, H. D. AND GALBRAITH, E. D. (2008) Future changes in climate, ocean circulation, ecosystems and biogeochemical cycling simulated for a business-as-usual CO_2 emission scenario until year 4000 AD. Global Biogeochemical Cycles, 22, doi:10.1029/2007GB002953

SHIRAIWA, Y. (2003) Physiological regulation of carbon fixation in the photosynthesis and calcification of coccolithophorids. Comp. Biochem. Physiol. B, 136, 775-783.

WANG, H. Z. AND MCCAVE, I. N. (1990) Distinguishing climatic and current effects in Midpleistocene sediments of Hatton and Gardar Drifts, N.E. Atlantic. J. Geol. Soc. London, 147, 373-383.

WATABE, N. AND K., W. (1966) Effects of temperature on growth, calcification, and coccolith form in *Coccolithus huxleyi* (*Coccolithineae*). Limnol. Oceanogr., 11, 567-575.

YOUNG, J. R. AND ZIVERI, P. (2000) Calculation of coccolith volume and its use in calibration of carbonate flux estimates. Deep-Sea Research Part II -Topical Studies in Oceanography, 47, 1679-1700.

ZIVERI, P., BAUMANN, K. H., BOCKEL, B., BOLLMANN, J. AND YOUNG, J. (2004) Biogeography of selected Holocene coccoliths in the Atlantic Ocean, In: Coccolithophores: from molecular processes to global impact, Berlin, Springer.

ZONDERVAN, I., ZEEBE, R. E., ROST, B. AND RIEBESELL, U. (2001) Decreasing marine biogenic calcification: A negative feedback on rising atmospheric pCO_2. Global Biogeochem. Cycles, 15, 507-516.

Sorting Coccoliths from Clays and Unlocking New Palaeoproxies

3

3.1 Introduction

Two major challenges must be addressed before coccolith geochemistry can begin to provide detailed and accurate palaeo-environmental data; separation of individual coccolith species and measurement of coccolith chemistry without interference from clay-bound trace elements. The ideal solution to these challenges would be to develop a highly sensitive separation technique, which could distinguish between coccoliths and clays, and between individual coccolith species. Unfortunately the size ranges of different coccolith species overlap, as do their Stoke's Law parameters (i.e. the size ranges, densities, and broad morphologies) with those of clay grains. This prevents separating by sieving and settling. A novel approach to the problem of separation is therefore required. This chapter presents a technique which automatically inspects each individual particle in a suspended sediment sample, identifies the coccoliths and physically separates them from the remainder of the sediment, producing high-purity calcium carbonate samples for geochemical analysis.

3.2 Background

Understanding the importance of silicate (i.e. clay) removal from sedimentary foraminiferal samples allowed Boyle (1981) to make the first measurements of benthic foraminiferal Cd/Ca, spawning much of the field of foraminiferal trace-element analysis. Work by Emiliani (1955), and now many others (e.g. Barker et al., 2003; Lea et al., 2005) indicates that contamination by clays also influences measurement of Mg/Ca, the widely utilised temperature proxy, but not of Sr/Ca, the coccolithophore growth-rate proxy (Figure 1). This conclusion follows logically from an understanding of the Mg and Sr content of the major marine clay-minerals [on average constituting 1-10 and ~ 0 weight percent Mg and Sr respectively (Deer et al., 1992)]. The observation that Sr/Ca measurements are not significantly influenced by the

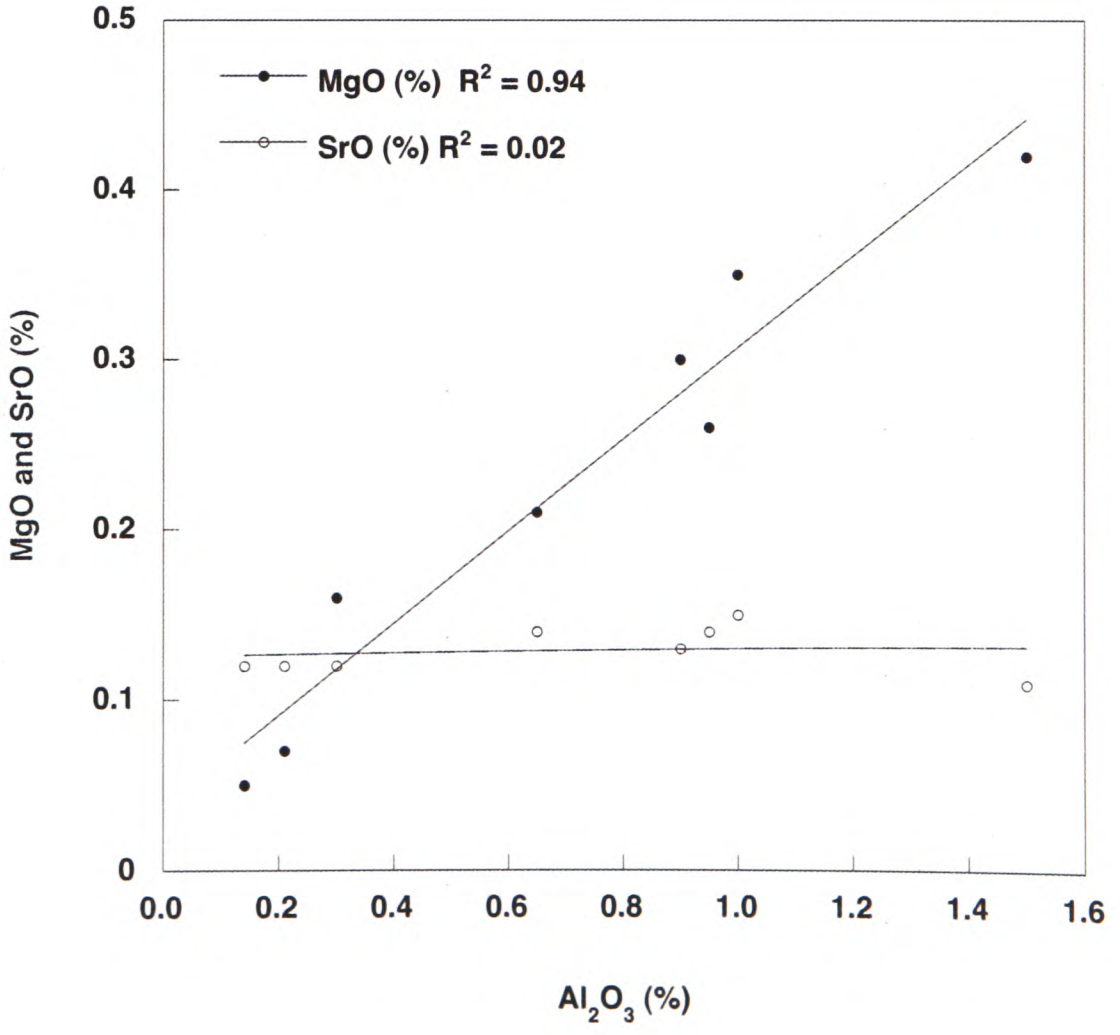

Figure 1. MgO and SrO percentages against Al_2O_3 percentages measured in eight foraminiferal samples containing greater than 1% $MgCO_3$ and $SrCO_3$ from six globally distributed cores. Data from Emiliani (1955).

presence of clay grains explains how, despite presently being unable to clay-clean coccolith-rich sediment samples, interesting and valuable down-core coccolith Sr/Ca records have been produced (e.g. Stoll and Bains, 2003; Stoll et al., 2007). In addition to Mg, Al and Fe, Mn is the only other element measured routinely in foraminiferal samples with significant presence in clay minerals [~ 0.003 wt % (Deer et al., 1992)]. For this reason, we would expect measurements of sedimentary carbonate Mn/Ca to be sensitive to the degree of clay contamination. Clay does not only contain contaminants within its structure, but also allows sorption of many different contaminant elements to its large, highly charged, external surface area. Cleaning samples for clay contamination is therefore a fundamental step in nektonic carbonate trace-element analyses.

3.3 Separation Techniques

Many microseparation techniques exist within the physical and biological sciences. Of these, flow cytometry is perhaps the most flexible, and the function for which it is designed (cell sorting) most similar in nature to the problem of coccolith-clay separation. Flow cytometry is a technique whereby a suspension of micron-sized particles is hydrodynamically focused into a narrow linear stream of fluid by a sheath of flowing saline liquid (Figure 2). The sheath fluid focuses the sample stream through a laser beam such that the particles held in suspension intersect the beam one at a time. Opposite the laser lies a series of charged couple devices or photo-multiplier tubes, which have the potential to detect the degree of radial scatter of light incident on the particle in a number of wavelength bands. In addition to the light sensors facing the laser and collecting forward scattered light, lie a set of detectors measuring side scattered light (perpendicular to the laser beam). The signals produced by the detectors are sent to a computer where they are queried against a set of predefined criteria. If the criteria are found to be satisfied, a sort occurs. To facilitate the sort, the nozzle of the chamber from which the stream exits, is vibrated at a high frequency (Hz to kHz),

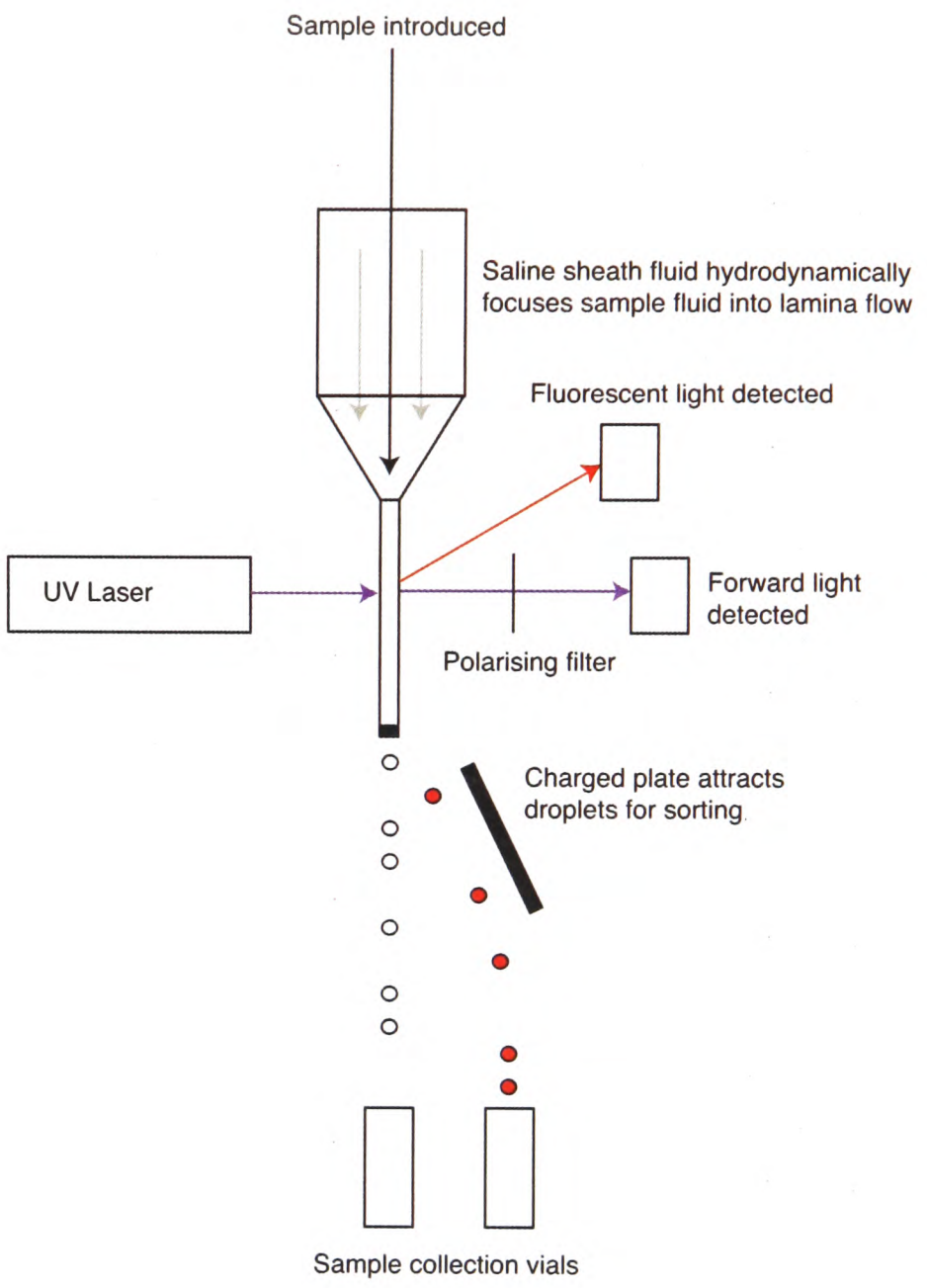

Figure 2. Schematic diagram of a flowcytometer. Particles are held in suspension then drawn through an inlet tube into the flowcytometer by a sheath of saline fluid passing over the internal end of the tube (as explained by the Bernoulli principle). The flow of the sheath fluid hydrodynamically focuses the incoming suspension into a fine laminar stream such that particles fall in a single dimension. A laser beam is focused through the laminar flow to be incident on a single particle. By detecting the modification (with respect to displacement, wavelength and in this case polarisation) of this beam in the forward and sideways direction as a result of the particle passing into the beam, the optical properties of the particle can be examined. The optical characteristics will be compared to a pre-defined set of criteria, and if in agreement, the particle will be collected. Particle collection is made possible by passing the laminar flow through a vibrating nozzle and breaking the flow into a series of droplets. Immediately prior to leaving the nozzle the droplets will be passed a charge (depending on the flowcytometer, potentially; strong positive, weak positive, strong negative, weak negative or neutral). Charged plates placed below and offset from the nozzle will provide an electromagnetic force tuned to divert the droplets into one of up to five different vials for collection and subsequent analysis.

causing the stream to break into droplets. If a droplet is known to contain a particle fitting the selection criteria, a positive or negative charge is passed to the droplet as it leaves the nozzle, allowing it to be pulled by charged plates into one of a number of collection vessels. Scrutiny of light scattered onto two, two-dimensional planes, and in a number of wavelength bands allows for a more comprehensive sorting than can be achieved by settling or filtration, facilitating sorting based on optical as well as physical characteristics. Flow cytometry is well established in the bio-medical sciences as a cell sorting technique. Coccoliths are of similar size and shape to many living cells, and as such flow-cytometry provides a powerful and ideally suited solution to the coccolith-sorting problem.

3.3 Flowcytometry: Method

Separating coccoliths from clays using flow cytometry required either that the two particle types scattered the incoming light in a characteristic and contrasting way, or that the particle types could be distinguished by their non-morphologically mediated optical characteristics. At present flowcytometers typically distinguish particles based either on the intensity and angle of light scatter from the particle, or the wavelength and intensity of fluorescence emitted from a particle. As a result of the necessary speed of the feedback loop (modern machines are designed to sort ~10,000 particles a second), production flowcytometers cannot yet distinguish particles using pattern or image recognition, although new neural network devices have been proposed to tackle this limitation. Initial investigations demonstrated that light scatter alone does not allow distinction between coccolith and clay particles. Subsequently it was necessary to identify distinctive optical characteristics to which the flowcytometer could be made sensitive.

Two optical characteristics with the potential to allow distinction between these particle types are fluorescence and birefringence. Calcite is naturally fluorescent in the red-wavelength

band when stimulated with an UV light source. This fluorescence results from energy transferred to, and emitted from, Mn cations substituted into the calcite lattice (Aguilar and Osendi, 1982). Although coccolith [Mn] is very low (see Chapter 5) there does not appear to be a lower limit to the [Mn] necessary for fluorescent emission (Figure 3) (Habermann et al., 1998). Measurements were made to assess the natural fluorescence of coccolith calcite and clay (Figure 4). Figure 4 indicates that although both clays and coccoliths exhibit fluorescence in the red band, the shapes of the curves are very different. This allowed us to use a dichroic mirror to split the light above and below 580 nm, and analyse the relative intensity of these two signals. Theoretically, coccoliths should show a lower < 580 nm / > 580 nm ratio than clay grains when stimulated by UV light. The data presented in Figure 4 were obtained from a particle suspension held in a fluorometer. Because this technique is highly dependent on the concentration of the sample in suspension, and the measurement of fluorescence in flow-cytometry is dependent on the size of particle examined and the

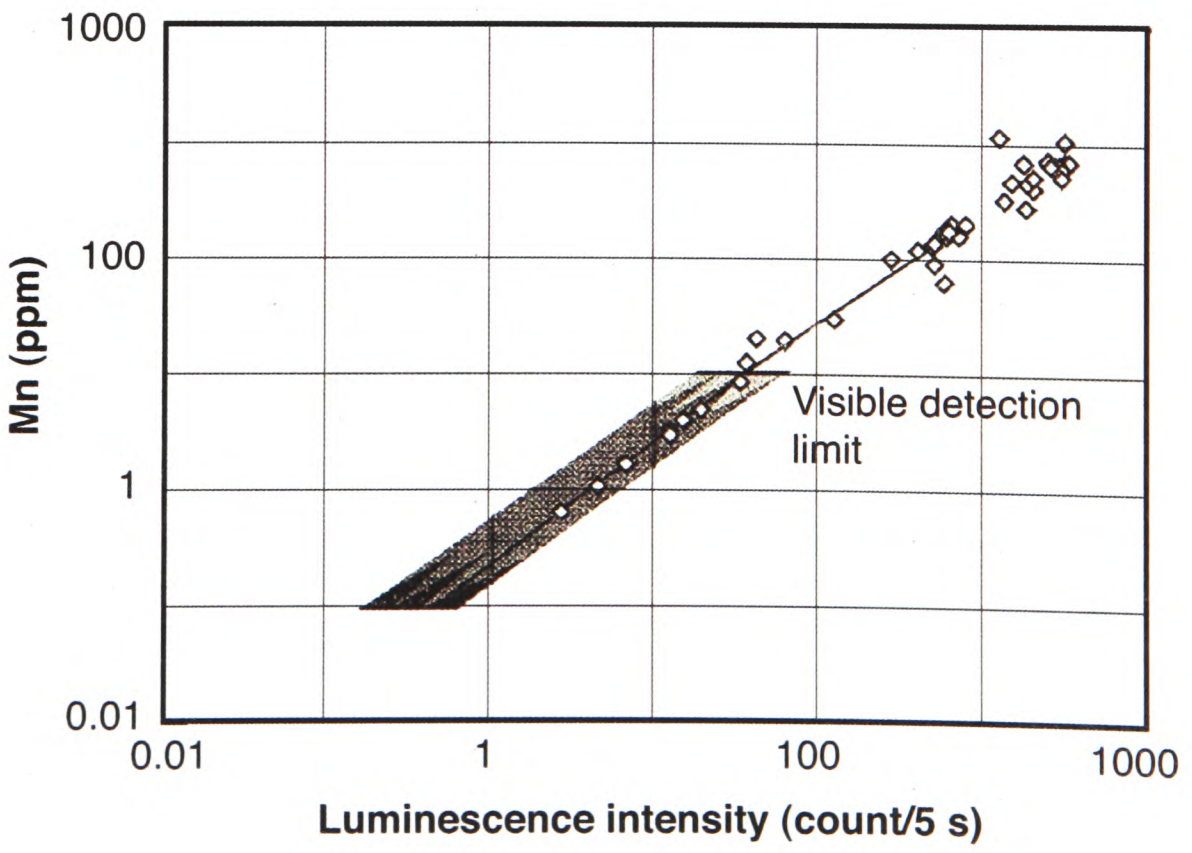

Figure 3. Manganese concentration in $CaCO_3$ versus luminescence intensity. The linear relationship appears to only be limited by the sensitivity of the detection equipment. Modified from Habermann et al. (1998).

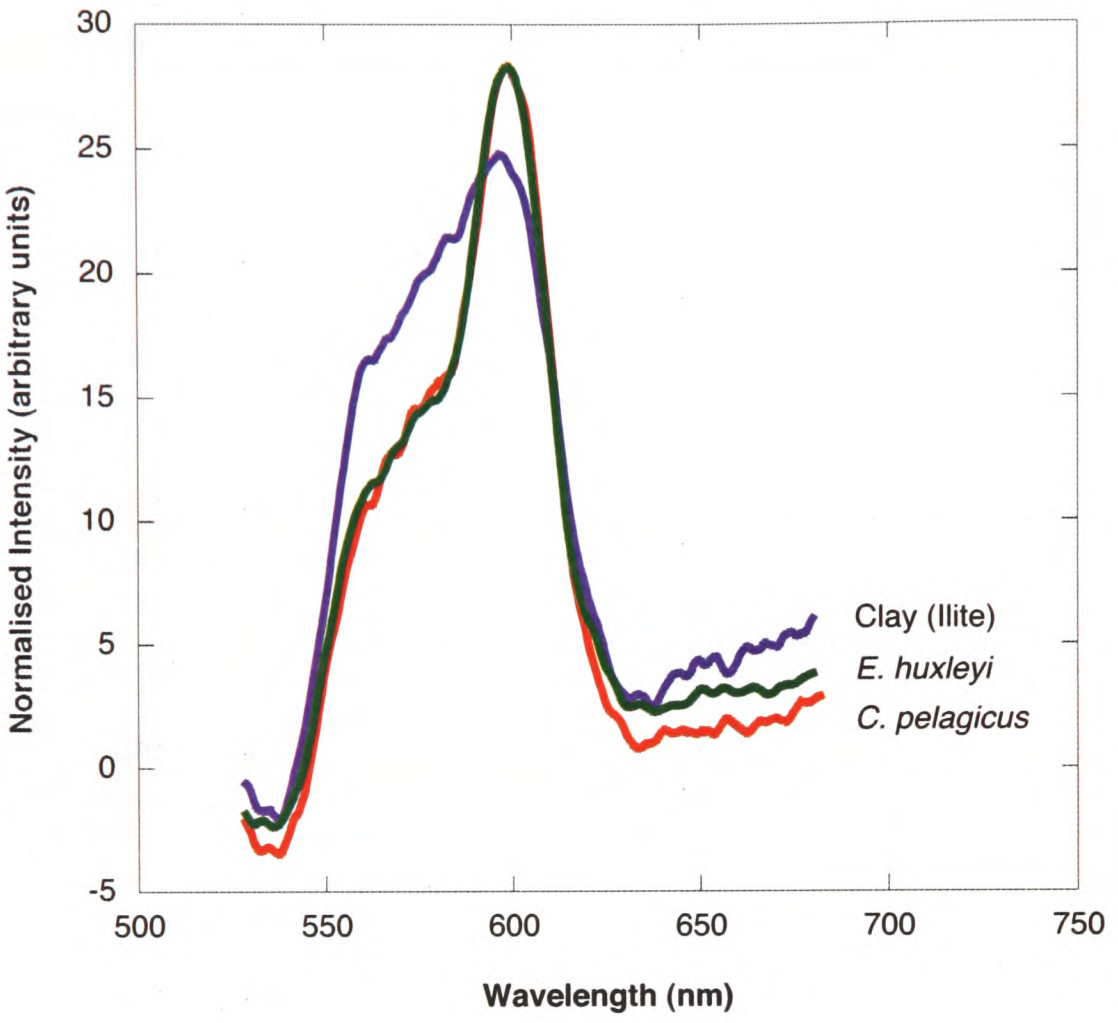

Figure 4. Clay (blue), *E. huxleyi* (green) *C. pelagicus* (red) fluorescence intensity in wavelengths between 530 and 680 nm when stimulated with a 400 nm light-source. Measurements were made using a fluorometer, and therefore fluorescence intensity is a function of the particles fluorescence and the particle concentration. For this reason the intensity has been normalised to a mean value. Despite the values being normalised the coccoliths and clays can be separated based on the shape of the emitted wavelength-intensity curve. Many thanks to Mark Wallace in the Oxford University Department of Chemistry for allowing me to carry out this work, and assisting me in the fluorometer operation.

particle's orientation with respect to the incident laser beam, the relative fluorescence in different wavelength bands, rather than absolute fluorescence intensities have been used to facilitate sorting.

The second criterion for selection is birefringence. Figure 5 shows that, assuming equal thickness, the retardation of the slow-ray in calcite is almost two orders of magnitude higher

than that in kaolinite or chlorite clay. To utilise the difference in birefringent properties when examining samples using the flowcytometer, the laser beam was split after the sample stream and before the detectors; one beam passed though a 45° (clockwise from vertical) orientated polarizing filter, and the other passed through a 315° (clockwise from vertical) orientated filter. The ratio between the signal strengths produced by the detectors in-line with the two filters gives a first order indication of the degree of birefringence of the particle. Because lasers produce polarized light, when the laser beam enters the anisotropic crystal (calcite or clay) two orthogonal rays are produced, vibrating parallel to the crystallographic axes (Figure 6). Upon exiting the crystal, the rays will recombine through superposition to produce a ray of orientation equal to the vector sum on the two components. Splitting the beam and measuring the signal intensity after passing through two orthogonal polarizing filters will indicate the orientation of the ray by measuring the proportion of the ray made up by each of two orthogonal components. The low birefringence of clay will result in very limited rotation of the ray orientation, so where the polarizing filters are both organised at ± 45 degrees to the incident beam, both detectors will measure similar intensities. Calcite however displays a strong birefringence, so the orientation of the beam will rotate significantly, meaning that the two polarized detectors will measure contrasting signals.

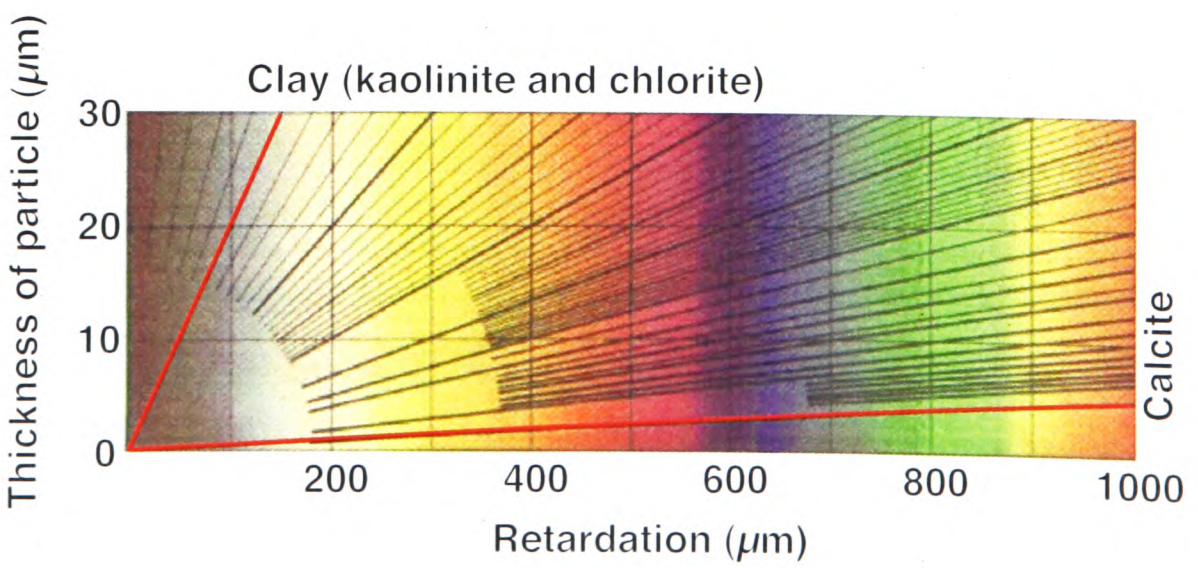

Figure 5. Birefringence colour chart illustrating the relative retardation of the ordinary/extraordinary beam, and the colour subsequently observed under a cross polarised microscope, in relation to the particles thickness in the beam direction for clay and calcite. Modified from Nesse (2000).

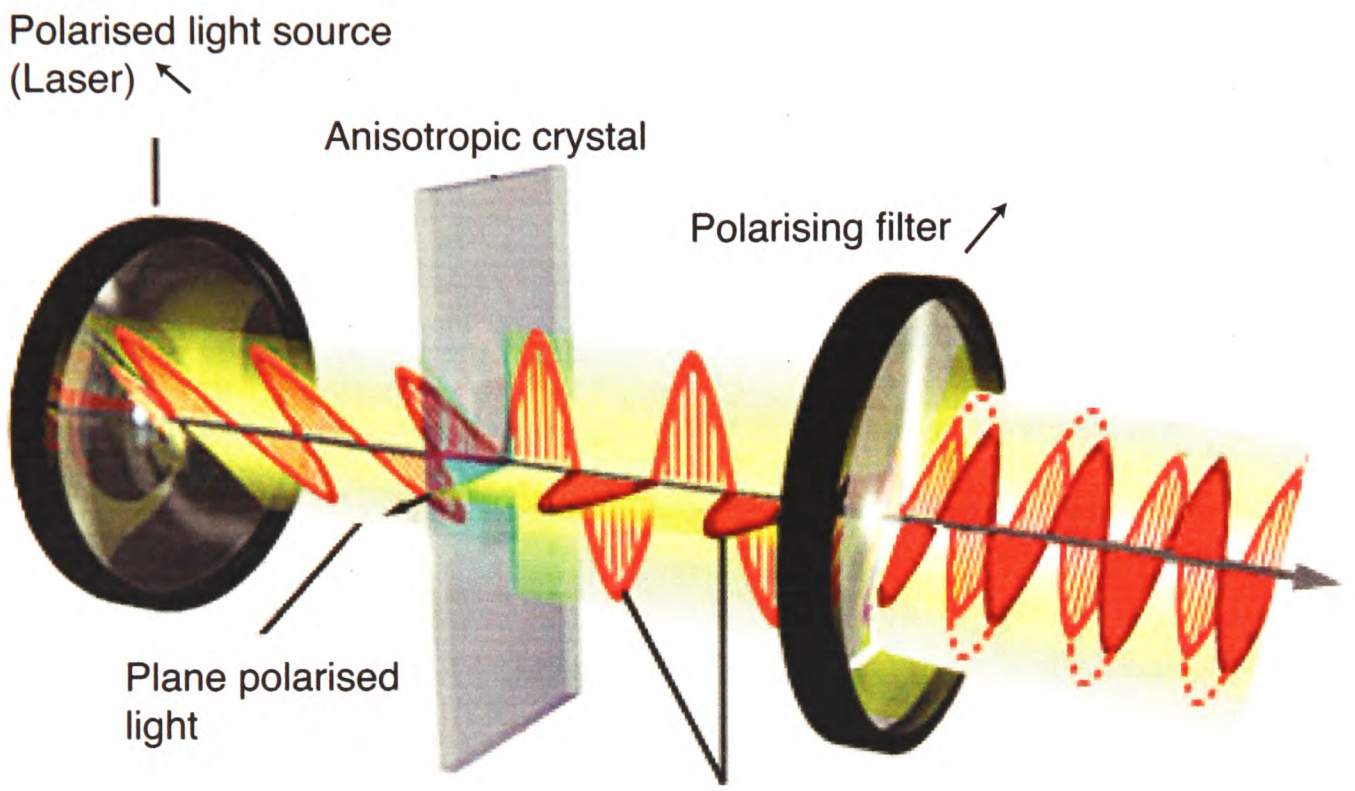

Figure 6. A diagrammatic representation of birefringence as produced by an incident polarised light beam on an anisotropic crystal. Because light can be considered to travel as an electromagnetic wave, electrons within the crystal interact with the propagation of the light. In an anisotropic crystal the electron density field is not homogeneous and the incoming light is split into two components, one parallel and one perpendicular to the crystallographic axis. Upon exiting the crystal these two components will be combined through superposition, but the relative retardation of the components will have been different as a result of the different number of electrons with which they interacted in the crystal, and subsequently superposition will combine the two components to produce a wave with a modified angle of polarisation. To inspect the orientation of polarisation in this resulting wave a polarising filter can be introduced, which will allow only the component of that ray parallel with the polarising filter's structure to pass through. The closer the angle of the filter to that of the ray, the greater the intensity of light passing through the filter. Modified from www.molecularexpressions.com.

Figure 7 shows the intensities recorded by the flow cytometer at the detectors in-line with the two polarizing filters, for a clay and a cultured coccolith sample (each point represents measurements made on a single particle). As described theoretically, the low birefringence of the clay particles results in an approximately equal light intensity measured by the detectors following the two polarizing filters, whereas the coccolith sample measures a range of responses, from approximately equal, to strongly skewed. When examining bulk sediment, particles recording intensities falling in the region above the black line are therefore considered to be calcite. Data measured from particles satisfying this criterion are then scrutinised with respect to their fluorescence characteristics.

Fluorescence analysis examines the ratio of intensities of visible light, perpendicular to the incident UV laser, above and below 580 nm. The main section of Figure 8 shows the measured fluorescence intensities of particles from a < 8 μm filtered sediment (particles which have

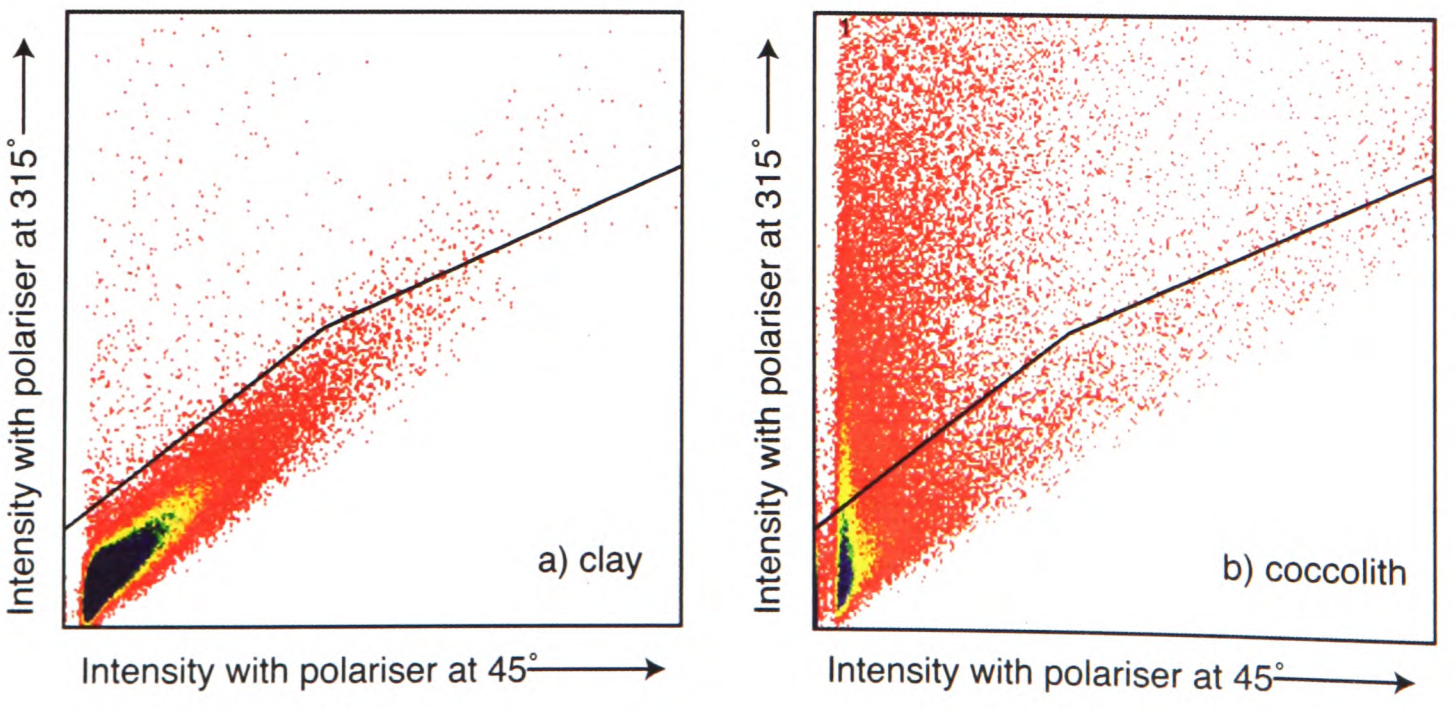

Figure 7. Flow-cytometry intensity plots representing the degree of birefringence produced by each clay **(a)** and cultured *E. huxleyi* **(b)** particle. The x and y-axes record the intensity of light passing through the polarising filters arranged at 45° and 315° to the polarisation of the incident laser beam.

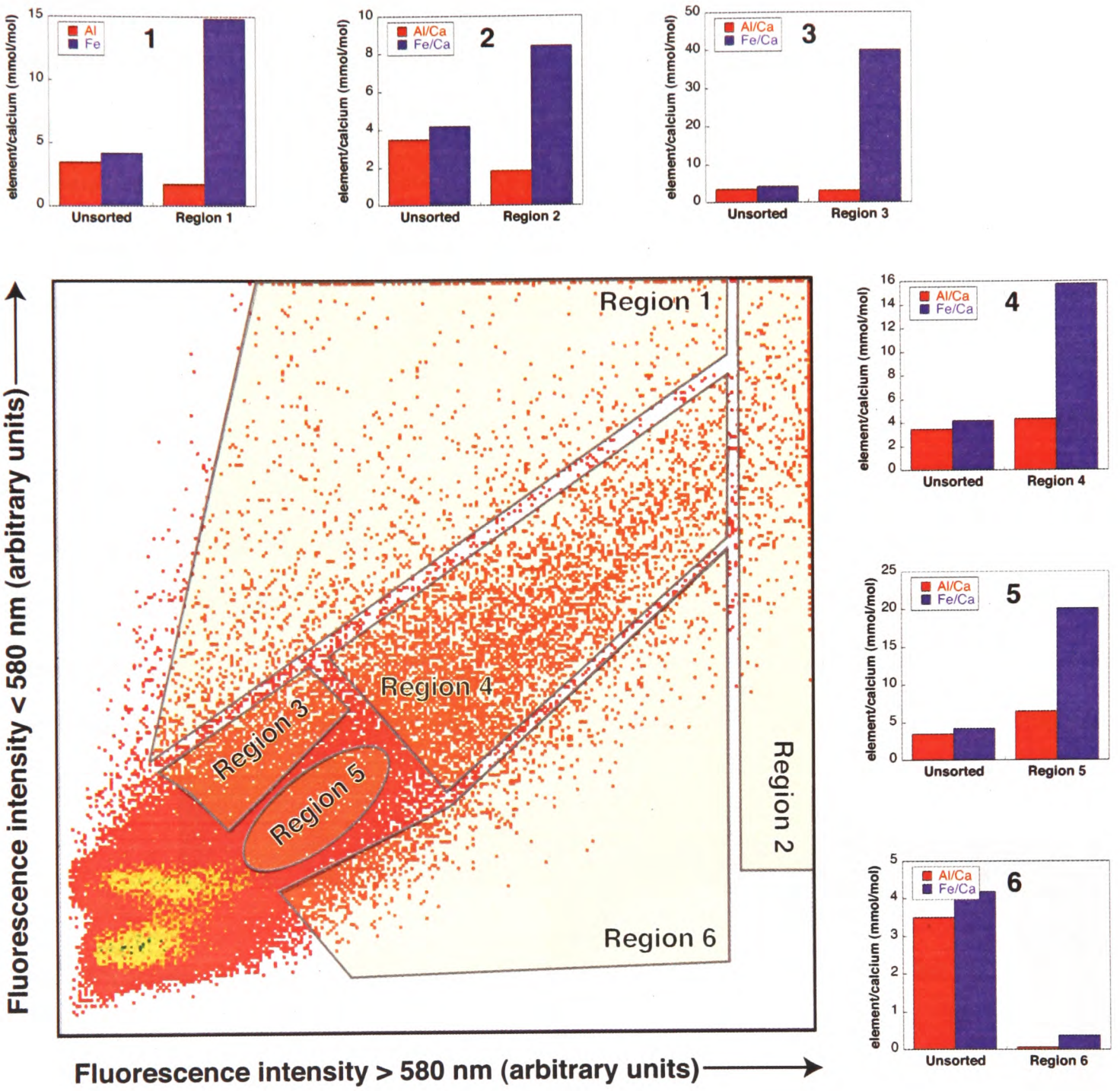

Figure 8. A graphical representation of the degree of clay reduction associated with different regions of a flow-cytometry fluorescence-intensity plot. Main body: each coloured pixel represents the relative intensity of fluorescence above and below 580 nm produced by a particle. The boxed regions describe the particle criteria selected for sorting in areas of fluorescence-space in which coccoliths were optically recognised. Bar-charts surrounding the fluorescence plot show the Al/Ca (red) and Fe/Ca (Blue) measurements made on the original unsorted sample (left) and sorted samples (right) corresponding to the regions one to six on the fluorescence intensity plot. In agreement with theoretical predictions, particles sorted from region six display the lowest Al/Ca and Fe/Ca ratios of any sorts, and are considerably reduced from the values associated with the unsorted sample. It can be inferred that the criteria described by region six produce highly clay-clean samples.

already passed the polarizing criteria). Theoretically the region with higher fluorescence > 580 nm relative to fluorescence < 580 nm should contain calcite particles. However, when examining sorted samples using a polarizing light microscope, all the labelled regions contained coccoliths. To test which regions produced the 'cleanest' coccolith samples (i.e. least clays), sorts were made from all of the labelled regions, and their chemistries analysed. The six charts surrounding the flow-cytometry plot (Figure 8) each show the Al/Ca and Fe/Ca ratios for the unsorted sample and the sample sorted from the correspondingly numbered region (red and blue respectively). Al and Fe are considered to be sensitive indicators of the presence of clay contamination (Barker et al., 2003). As predicted from theory, region six, the region representing particles with a low < 580 / > 580 nm wavelength ratio is the region producing samples with the lowest Al/Ca and Fe/Ca ratios. Al/Ca and Fe/Ca are 0.1 and 0.4 mmol/mol respectively, comparable with a clay-cleaned foraminiferal sample (Barker et al., 2003). To further validate this, the samples have been analysed optically (Figure 9) and using SEM (Figure 10).

Figure 9. Photograph showing the colour change [i.e. increased purity of (light coloured) calcite particles] of < 8 μm filtered sedimentary material after flow-cytometry sorting. Unsorted (a) and sorted (b) samples are displayed in 1.5 ml tubes after centrifugation.

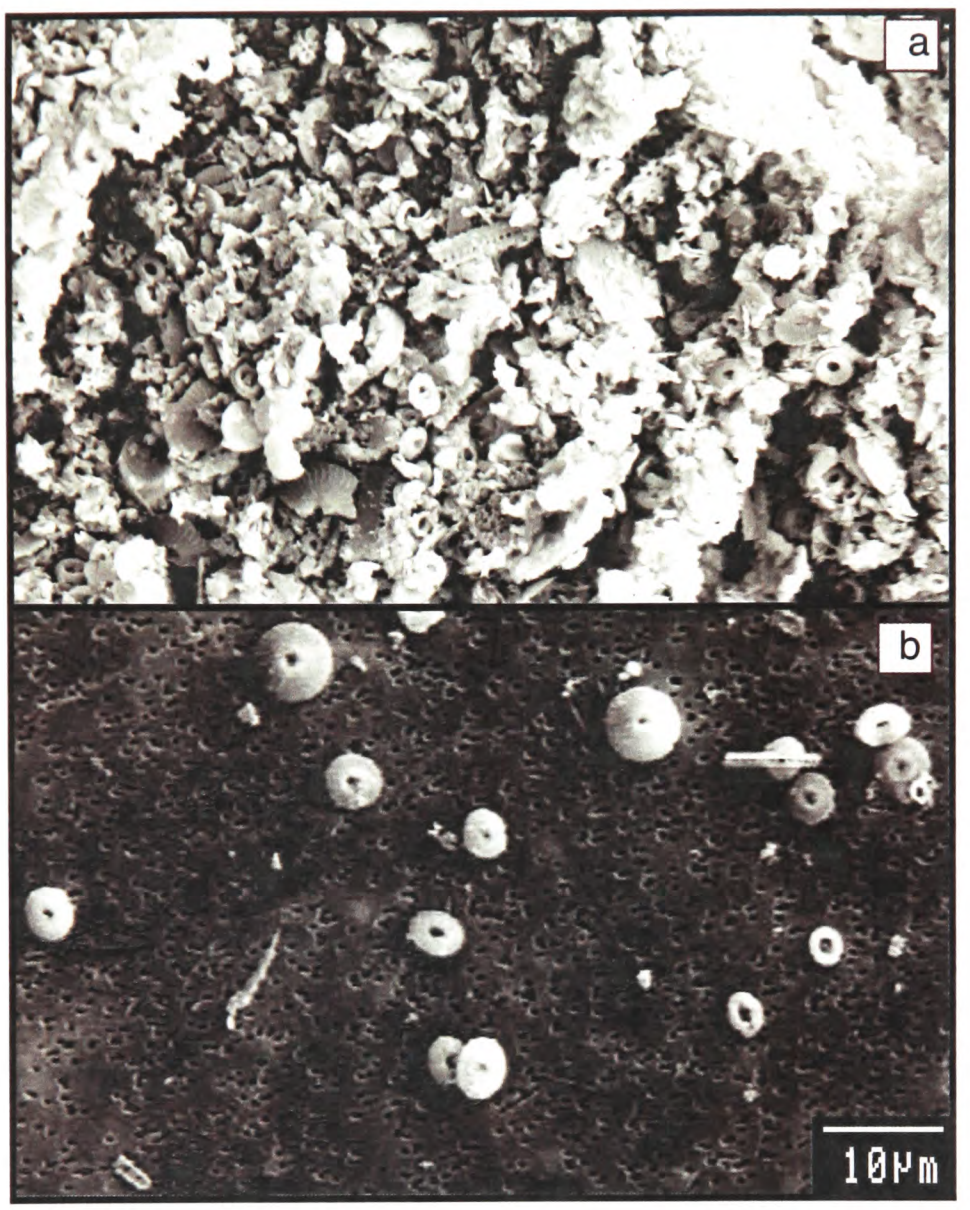

Figure 10. Scanning electron micrographs of unsorted **(a)** and flow-cytometry sorted **(b)** sediments. The sorted sample demonstrated a greatly increased coccolith purity.

3.4 Method and Validation

Careful validation of this technique has been carried out using samples from the North Atlantic core MD04-2829CQ. Samples were suspended in buffered H_2O and filtered through an 8 µm laser etched polycarbonate membrane using bubble agitation. The < 8 µm fraction was then examined by a Cytomation MoFlow flowcytometer, using both a 488 nm and a UV, coherent I90 (water-cooled three-phase powered) laser. Simple forward scatter from the 488 nm source was detected on a photodiode, and forward scatter split through two orthogonal

polarising filters and detected on photomultiplier tubes. Sidescatter from the 488 nm laser was recorded, and sidescatter from the UV laser examined for fluorescence. Fluorescence was scrutinised by splitting the sidescatter signal at a 580 nm long-pass dichroic mirror, and detecting the > 580 nm fluorescence, and 565±20 nm fluorescence at photodiodes. Pulse-width was gated to eliminate doublets. The flowcytometer used for these sorts is housed in the Oxford University Department of Physiology, and run by Nigel Rust.

As described in section 3.1 the presence of moderate-to-high concentrations of Fe and Al in a sample is indicative of clay contamination. To test the purity of sorted samples, 15 down-core < 8 μm filtered samples from MD04-2829CQ were analysed, and the significance of the correlation between their Mg/Ca, Mn/Ca and Fe/Ca chemistry examined (Figure 11). It was clear that prior to sorting, a highly statistically significant correlation existed between Mg/Ca and Fe/Ca and Mg/Ca and Al/Ca (p-values = 1.82×10^{-7} and 6.95×10^{-4}), and that this correlation no longer existed post-sorting (p-values = 7.55×10^{-2} and 6.53×10^{-2}) (Table 1). A similar break-down of correlation was observed between Mn/Ca:Fe/Ca and Mn/Ca:Al/Ca (Figure 11), consistent with the presence of Mn in high concentrations in clay minerals (Deer et al., 1992). The described correlations break down further if the three samples with Fe/Ca or Al/Ca > 5 mmol/mol are removed (Mg/Ca:Fe/Ca p-value = 0.026, Mn/Ca:Fe/Ca p-value = 0.14, Mg/Ca:Al/Ca p-value = 0.27, Mn/Ca:Al/Ca p-value = 0.26).

Figure 11. On next page. Unsorted < 8 μm filtered sedimentary material (red circles) from the top 3 m of core MD04-2829CQ exhibit a strong correlation (R^2 = 0.88 and 0.91 respectively) between **a.** Mg/Ca and Fe/Ca, and **b.** Mn/Ca and Fe/Ca, where the red-dashed lines represent the 95% confidence intervals of the least-squares linear fit (black line), n = 15 and 15, and the p-values = 1.82×10^{-7} and 4.10×10^{-8}. The strong correlation indicates a significant Mg and Mn contribution from clay contaminants. After sorting the average Mg/Ca and Mn/Ca drops by up to an order of magnitude, and the significance of the correlations between Mg/Ca and Fe/Ca and Mn/Ca and Fe/Ca decreases, with R^2 = 0.26 and 0.32, n's = 13 and p-values = 0.075 and 0.044 respectively. Taking p=0.01 (i.e. a 1 in 100 chance of obtaining the result by chance) as statistical significance, we can say that the correlations between Mg/Ca and Fe/Ca and Mn/Ca and Fe/Ca after sorting are not significant. This indicates that the samples have been adequately cleaned for clay contamination.

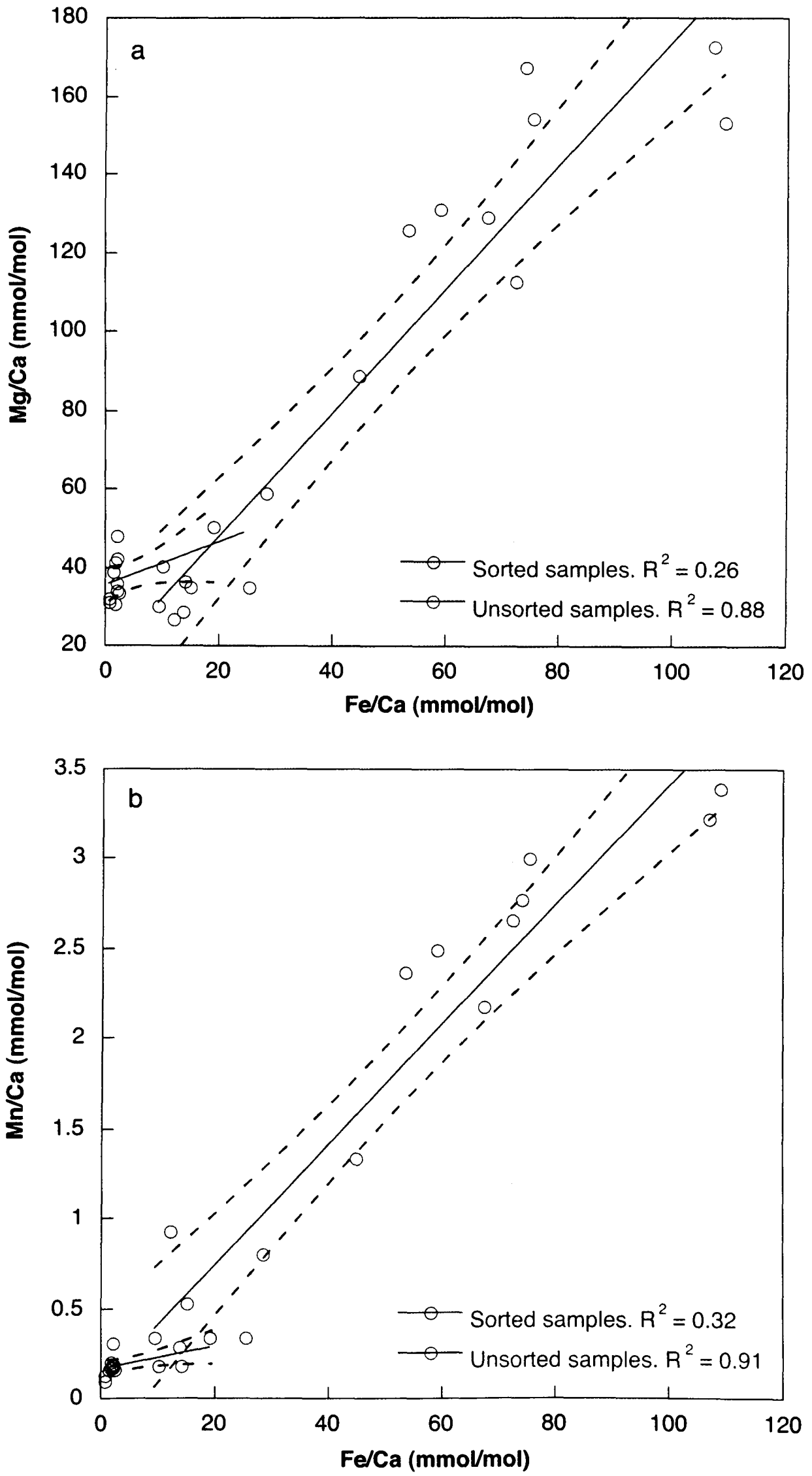
a
Mg/Ca (mmol/mol)
180
160
140
120
100
80
60
40
20
0
20
40
60
80
100
120
Sorted samples. R 2 = 0.26
Unsorted samples. R 2 = 0.88
Fe/Ca (mmol/mol)
b
Mn/Ca (mmol/mol)
3.5
3
2.5
2
1.5
1
0.5
0
0
20
40
60
80
100
120
Sorted samples. R 2 = 0.32
Unsorted samples. R 2 = 0.91
Fe/Ca (mmol/mol)

Table 1 presents p-values calculated for the correlations between sorted and unsorted element/Ca values and Fe/Ca and Al/Ca. P-values calculated for unsorted samples indicate that Cd/Ca, Ba/Ca, Zn/Ca and potentially U/Ca are not affected by clay-contamination and therefore that, assuming no further contamination, these element/Ca ratios can be measured with confidence in clay-rich samples. These data also indicate a strong correlation between Sr/Ca and Fe/Ca in these samples; however because these are samples taken from a core spanning the glacial-Holocene transition, this correlation can be attributed to both coccolith Sr/Ca and the sample's clay proportion being affected by the same forcing. Coccolith Sr/Ca will respond to species, temperature and productivity changes, and Fe/Ca will be affected by the clay content of samples moving from the glacial into the Holocene. The final, and perhaps most surprising result highlighted in Table 1 is that after sorting, a highly statistically

	v. Fe/Ca p-value	v. Al/Ca p-value
Unsorted		
Mg/Ca	1.82×10^{-7}	6.95×10^{-4}
Sr/Ca	5.37×10^{-5}	1.82×10^{-2}
Cd/Ca	2.73×10^{-1}	7.65×10^{-1}
Ba/Ca	2.80×10^{-1}	1.84×10^{-1}
Mn/Ca	4.10×10^{-8}	5.02×10^{-4}
Zn/Ca	1.82×10^{-1}	8.99×10^{-1}
U/Ca	7.63×10^{-2}	1.54×10^{-2}
Sorted		
Mg/Ca	7.55×10^{-2}	6.53×10^{-2}
Sr/Ca	4.46×10^{-1}	4.16×10^{-1}
Cd/Ca	6.46×10^{-1}	7.33×10^{-1}
Ba/Ca	1.76×10^{-1}	2.05×10^{-1}
Mn/Ca	4.38×10^{-2}	3.45×10^{-2}
Zn/Ca	8.60×10^{-1}	7.78×10^{-1}
U/Ca	1.59×10^{-7}	3.91×10^{-7}

Table 1. P-values testing the statistical strength of a linear correlation between element/Ca ratios and Fe/Ca and Al/Ca. Blue text highlights correlations with a moderate degree of significance (< 1:20 chance of occurring by chance) and red text highlights correlations with an extremely high degree of significance (< 1:1000 chance of occurring by chance)

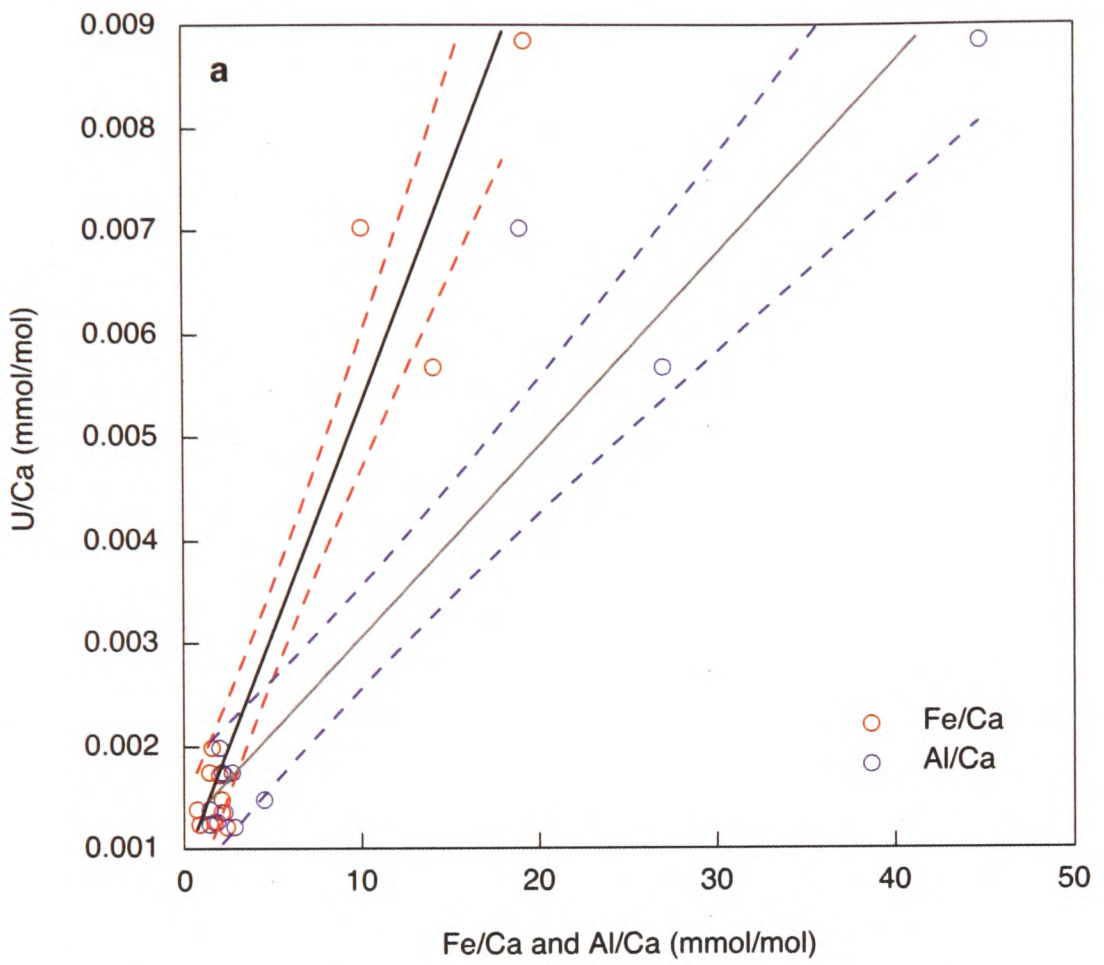

Figure 12. < 8 μm U/Ca plotted against Fe/Ca and Al/Ca. Upper panel shows all sorted data, and lower panel, data with the three Fe/Ca and Al/Ca ratios > 5 mmol/mol removed. Dashed lines represents the 95% confidence intervals on the linear regressions through data. P-values before and after removal of the three high values are Fe/Ca =1.59 $x10^{-7}$, Al/Ca =3.91 $x10^{-7}$ and Fe/Ca =0.82, Al/Ca =0.86 respectively.

robust correlation appears between U/Ca and Fe and Al/Ca. The strength of this correlation results from the high U/Ca of the three sorts which fail to bring Fe/Ca and Al/Ca below 5 mmol/mol (Figure 12). These samples are therefore considered to still contain a significant degree of clay contamination. Samples with Fe/Ca or Al/Ca > 5 mmol/mol should therefore not be considered clay clean.

3.5 Conclusions

The methods described and the results presented in this chapter represent the first step towards unlocking new trace-element proxies in coccolith calcite. A technique has been developed and demonstrated which can separate, simply and reliably, sedimentary coccoliths from contaminant clays, and begin to provide accurate and exciting coccolith trace-element data. Future developments are required to assess the cleanliness of the samples with respect to non-clay contaminants, and apply traditional chemical cleaning steps as required to remove these contaminants. Combined with a technique to separate single coccolith species from the sorted samples, calibration studies can begin to examine and exploit the palaeoceanographic and climatic-information recorded within coccolithophore calcite.

3.6 Bibliography

AGUILAR, G.M., AND OSENDI, M.I., 1982, Fluorescence of Mn^{2+} in $CaCO_3$: Journal of Luminescence, v. 27,365-375.

ANDERSON, T.F., AND STEINMETZ, J.C., 1981, Isotopic and biostratigraphical records of calcareous nannofossils in a Pleistocene core: Nature, v. 294,741-744.

BARKER, S., GREAVES, M., AND ELDERFIELD, H., 2003, A study of cleaning procedures used for foraminiferal Mg/Ca paleothermometry: Geochemistry Geophysics Geosystems, v. 4,. doi:10.1029/2003GC000559.

BOYLE, E.A., 1981, Cadmium, zinc, copper, and barium in foraminifera tests: Earth and Planetary Science Letters, v. 53,11-35.

COLMENERO-HIDALGO, E., FLORES, J.A., SIERRO, F.J., BARCENA, M.A., LOWEMARK, L., SCHONFELD, J., AND GRIMALT, J.O., 2004, Ocean surface water response to short-term climate changes revealed by coccolithophores from the Gulf of Cadiz (NE Atlantic) and Alboran Sea (W Mediterranean): Palaeogeography Palaeoclimatology Palaeoecology, v. 205,317-336.

DEER, W.A., HOWIE, R.A., AND ZUSSMAN, J., 1992, An introduction to the rock-forming minerals: Harlow, Longman Scientific AND Technical ; Pearson, xvi, 696p.

DUDLEY, W.C., BLACKWELDER, P., BRAND, L., AND DUPLESSY, J.C., 1986, Stable isotopic composition of coccoliths: Mar. Micropaleontol, v. 10,1-8.

EMILIANI, C., 1955, Mineralogical and chemical composition of the tests of certain pelagic foraminifera: Micropaleontology, v. 1,377.

FRENZ, M., AND HENRICH, R., 2007, Carbonate dissolution revealed by silt grain-size distribution: comparison of Holocene and Last Glacial Maximum sediments from the pelagic South Atlantic: Sedimentology, v. 54,391-404.

HABERMANN, D., NEWER, R., AND RICHTER, D., 1998, Low limit of Mn^{2+} -activated cathodoluminescence of calcite: state of the art: Sedimentary Geology, v. 116,13-24.

HARDING, D., 2007, Quick corruption of conveyour circulation: a geochemical approach: Oxford, Oxford University.

HARDING, D.J., ARDEN, J.W., AND RICKABY, R.E.M., 2006, A method for precise analysis of trace element/calcium ratios in carbonate samples using quadrupole inductively coupled plasma mass spectrometry: Geochemistry Geophysics Geosystems, v. 7, doi:10.1029/2005GC001093.

HARDING, D.J., AND RICKABY, R.E.M., 2006, Reconstructing North Atlantic deglacial ocean circulation: A high resolution trace metal and stable isotope record: Geochimica Et Cosmochimica Acta, v. 70,A229-A229.

HUYBERS, P., AND EISENMAN, I., 2006, Integrated summer insolation calculations: IGBP PAGES/World Data Center for Paleoclimatology NOAA/NGDC, v. Data Contribution Series # 2006-079.

KNUTZ, P.C., HALL, I.R., ZAHN, R., RASMUSSEN, T.L., KUIJPERS, A., MOROS, M., AND SHACKLETON, N.J., 2002, Multidecadal ocean variability and NW European ice sheet surges during the last deglaciation: Geochemistry Geophysics Geosystems, v. 3, 7 ISSN 1525-2027.

KNUTZ, P.C., ZAHN, R., AND HALL, I.R., 2007, Centennial-scale variability of the British Ice Sheet: Implications for climate forcing and Atlantic meridional overturning circulation during the last deglaciation: Paleoceanography, v. 22,doi:10.1029/2006PA001298,.

LEA, D.W., PAK, D.K., AND PARADIS, G., 2005, Influence of volcanic shards on foraminiferal Mg/Ca in a core from the Galapagos region: Geochemistry Geophysics Geosystems, v. 6, doi:10.1029/2005GC000970.

LISIECKI, L.E., AND RAYMO, M.E., 2005, A Pliocene-Pleistocene stack of 57 globally distributed benthic delta O-18 records: Paleoceanography, v. 20, doi:10.1029/2004PA001071.

SPERO, H.J., AND LEA, D.W., 2002, The cause of carbon isotope minimum events on glacial terminations: Science, v. 296,522-525.

STOLL, H.M., AND BAINS, S., 2003, Coccolith Sr/Ca records of productivity during the Paleocene-Eocene thermal maximum from the Weddell Sea: Paleoceanography, v. 18, doi:10.1029/2002PA000875.

STOLL, H.M., KLAAS, C.M., PROBERT, I., ENCINAR, J.R., AND ALONSO, J.I.G., 2002a, Calcification rate and temperature effects on Sr partitioning in coccoliths of multiple species of coccolithophorids in culture: Global and Planetary Change, v. 34,153-171.

STOLL, H.M., SHIMIZU, N., ARCHER, D., AND ZIVERI, P., 2007, Coccolithophore productivity response to greenhouse event of the Paleocene-Eocene Thermal Maximum: Earth and Planetary Science Letters, v. 258,192-206.

STOLL, H.M., ZIVERI, P., GEISEN, M., PROBERT, I., AND YOUNG, J.R., 2002b, Potential and limitations of Sr/Ca ratios in coccolith carbonate: new perspectives from cultures and monospecific samples from sediments: Philosophical Transactions of the Royal Society of London Series a-Mathematical Physical and Engineering Sciences, v. 360,719-747.

ZIVERI, P., STOLL, H., PROBERT, I., KLASS, C., GEISEN, M., GANSSEN, G., AND YOUNG, J., 2003, Stable isotope vital effects in coccolith calcite: Earth and Planetary Science Letters, v. 210,137-149.

Flowcytometry: Down-core Application

4

Chapter 3 describes and demonstrates a new technique, the application of which allows down-core, clay-clean coccolith samples to be produced. Here, this new procedure has been applied to core-material spanning the last 20 kyr from the North East Atlantic, allowing an exploration of variations in coccolith chemistry in the context of glacial-interglacial environmental change. High sedimentation rate, high coccolithophore productivity and excellent preservation in the sediment-core MD04-2829CQ, provide ideal conditions for examining and exploring changes in coccolith trace-element chemistry over this interval.

4.1 Material

Core MD04-2829CQ (58 56.93' N, 9 34.30' W) is situated at a depth of 1743 m below sea-level, immediately northwest of the Scottish continental margin (Figure 1). The present sea-surface is warmed by the North Atlantic Drift, with summer sea surface temperatures (SSTs) of 12-13°C (Knutz et al., 2007). During the last glacial period, this site was believed to have been within ~200 km of the continental ice sheet, where SSTs were below 5°C (Knutz et al., 2002). Preliminary work on the geochemistry of foraminifera in this core, indicated a complex environmental evolution over the glacial-interglacial transition at this site (Harding, 2007).

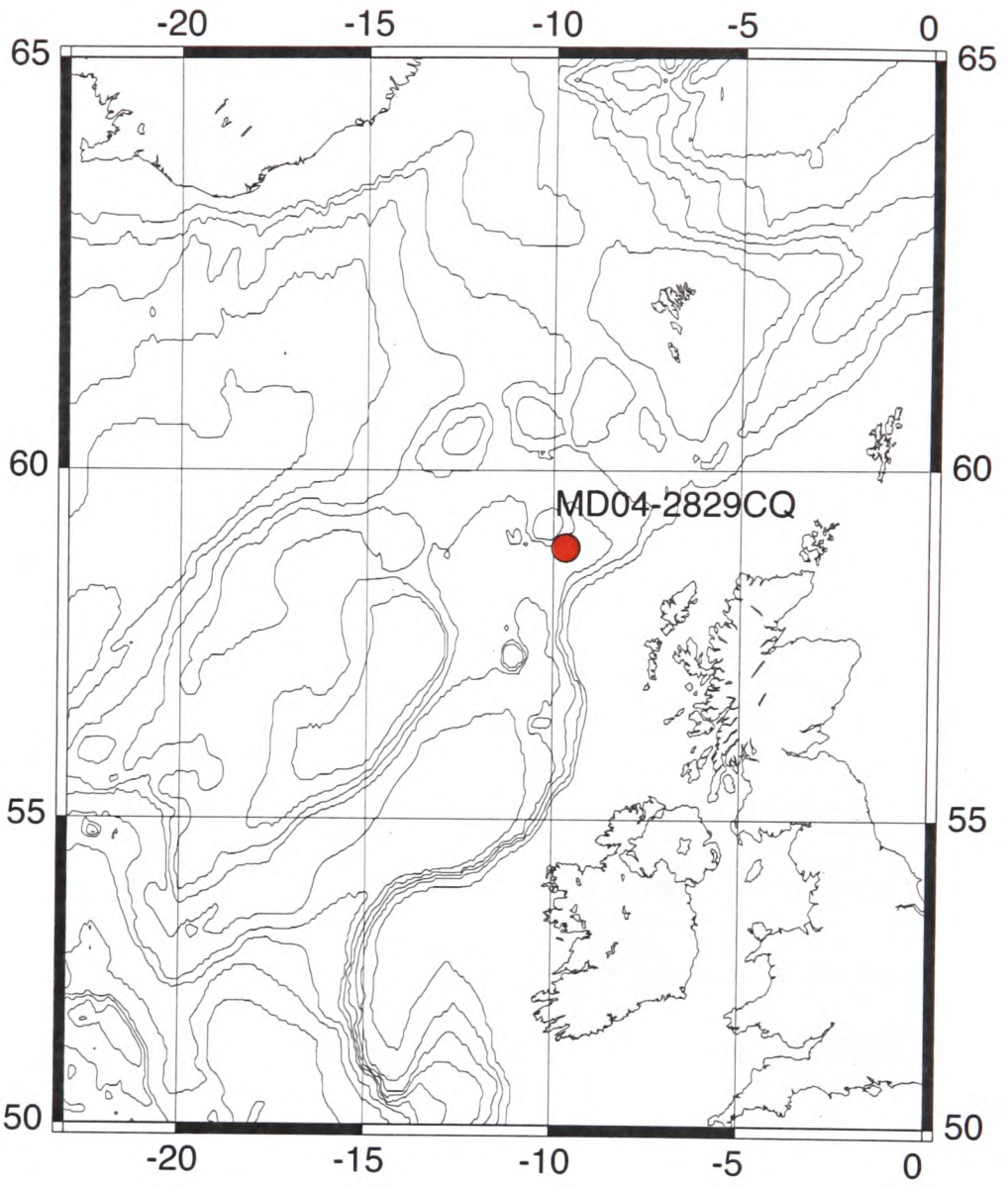

Figure 1. Location of Core MD04-2829CQ, in the North East Atlantic (58 56.93'N, 9 34.30'W, in 1743 m water depth). Collected in 2004 by the French research vessel the RV Marion Dufresne. Map produced using the GMT OMC tool.

4.2 MD04-2829CQ Age Model

MD04-2829CQ is a re-core of DAPC2, and as such the ^{14}C dates obtained from DAPC2 (Knutz et al., 2002) have previously been used to provide an age-model of this core (Harding and Rickaby, 2006, Harding, 2007) (Table 1). When considering our new data in the context of published records, the DAPC2 timescale has been adopted.

DAPC2 Depth (m.b.s.f)	^{14}C Age	CALIB Age
10	3740±55	3672
42	8590±90	9238
78	10830±90	12336
96	11380±110	12931
138	13410±75	15367
154	14400±110	16679
160	14900±110	17424
171	15330±100	17673
178	15390±130	17832
199	15400±170	18307
209	15560±140	18524
269	16430±150	19203
352	17310±170	20042
387	17870±200	20672

Table 1. Carbon-14 ages from DAPC2 and Carbon-14 ages calibrated to include the carbon-isotope marine reservoir age.

4.3 Sample Preparation

100 samples were filtered at < 63 μm, treated with H_2O_2 to remove organic material, then analysed for $\delta^{18}O$ and $\delta^{13}C$ to provide a chemical framework for this study (Figure 2). 15 samples (Table 2) were then filtered further in buffered H_2O (tap-water passed through a 0.2 μm filter, and naturally $CaCO_3$ and pH-buffered) through an 8 μm pore-size polycarbonate track-etched membrane, using bubble agitation to keep pores clear. These samples were cleaned for organic material by heating for 1 hour in a 50:50 solution of H_2O_2 and NaOH, then left to cool in this solution overnight. Samples were then centrifuged for 10 minutes at 6000 r.p.m., supernatant removed by pipetting, then rinsed three times in buffered H_2O, separated by centrifugation and pipetting stages, to remove residual H_2O_2 and prevent contamination of the flow-cytometer. The flowcytometry prepared samples were then analysed for; $\delta^{18}O$, $\delta^{13}C$, Mg/Ca, Sr/Ca, Cd/Ca, Ba/Ca, Mn/Ca, Zn/Ca, U/Ca, Fe/Ca and Al/Ca before sorting, and for the trace-elements and calcium only, after sorting (unfortunately post-sorting sample volume was too low to allow isotope analysis in addition to trace-element analysis on these samples).

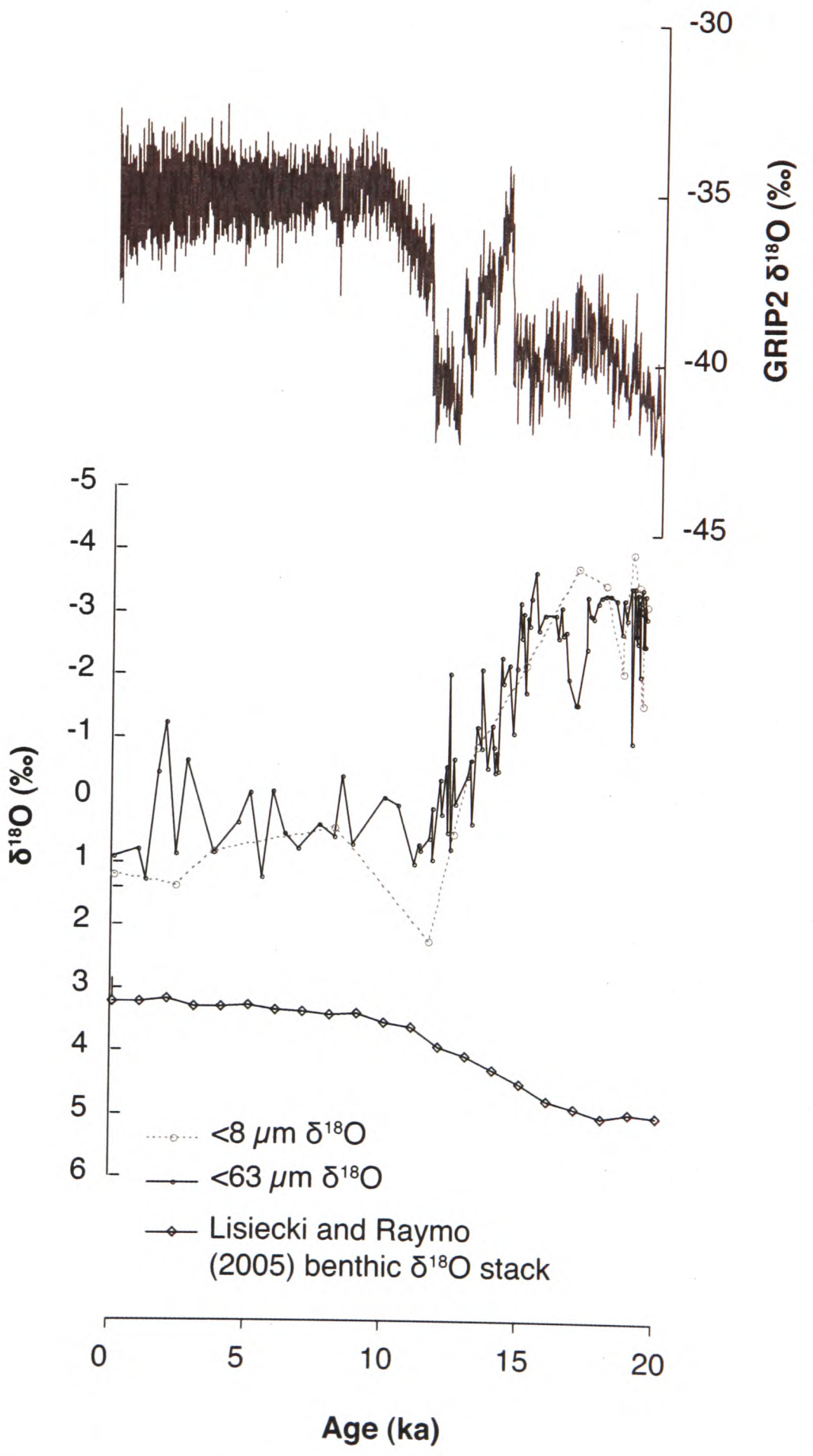

Figure 2. NGRIP $\delta^{18}O$ using original age model (upper panel). MD04-2829CQ < 63 μm (black circles) and < 8 μm (grey circles) carbonate $\delta^{18}O$ using DAPC2 timescale. Globally stacked benthic foraminiferal $\delta^{18}O$ (black diamonds) from Lisiecki and Raymo (2005).

Sample (Depth in cm)	$\delta^{18}O$ and $\delta^{18}C$ analysis (pre-sorting)	Trace-element analysis (post-sorting)
0	x	x
6	x	Dissolved during cleaning
11	x	x
36	x	x
70	x	x
86	x	x
103	x	x
133	x	x
161	x	x
188	x	x
224	x	x
251	x	x
270	x	x
285	x	Dissolved during cleaning
299	x	x

Table 2. < 8 μm samples analysed for oxygen and carbon isotope and trace element composition. Sample analyses are marked with a cross (x). All 15 samples were analysed for their trace-element composition pre-sorting.

4.4 MD04-2829CQ Flow Cytometry and Mass Spectrometry

Samples were brought into suspension in buffered H_2O and processed using the technique described in Chapter 3. 250,000 positive sorts (coccoliths) were collected from each sample into vials pre-filled with buffered H_2O [to prevent post-sorting corrosion during contact with the undersaturated (with respect to $CaCO_3$) sheath fluid]. The number of positive sorts, as a percentage of the total number of particles analysed, ranged from 0.06 – 0.39%, indicating that the procedure selects only a small sub-population of the total processed coccolith number. After sorting, samples were centrifuged at 13,000 r.p.m. and rinsed with quartz-distilled Aristar-grade propanol, transferred to new acid cleaned tubes, centrifuged and rinsed in propanol three further times, then given a short (< 10 s) rinse in 18 MΩ H_2O, centrifuged, supernatant removed, and dissolved in 0.5 ml Aristar-grade 2% HNO_3.

20 µl of each dissolved sample was taken, spiked with 20 µl of 500 p.p.b. In and diluted to 1 ml with 2% HNO_3. Sample Ca concentrations were then calculated from Ca and In measurements performed on samples and standards using a Thermo-Scientific Element ICP-MS. Samples were then diluted to 10 or 2 p.p.m. Ca depending on their initial concentration (i.e. down to 10 p.p.m. if initially above 10 p.p.m. and down to 2 p.p.m. if initially below 10 p.p.m.), to allow sample Ca concentrations to match standard Ca concentrations and minimise errors associated with mismatched element matrices within the ICP-MS plasma. Mg, Sr, Cd, Ba, Mn, Zn, U, Fe and Al/Ca analyses were then performed by measuring element intensities in sorted samples, synthetic foraminiferal standards containing Ca, Mg, Sr, Cd, Ba, Mn, Zn, U (Harding et al., 2006) and multi-element standards containing Ca, Fe and Al at 1, 0.1 and 0.1 p.p.m. respectively.

4.5 MD04-2829CQ Results

In light of the observation described in Chapter 3, that clay-contamination of samples does not influence all of the analysed elements, we will first consider the data produced from the unsorted < 63 and < 8 µm fractions and consider the implications for the past oceanography and climatology of the North-East Atlantic.

Before considering the chemistry of the unsorted and sorted samples, it is important to characterise changes in coccolithophore species composition over the examined interval. Elena Colmenero-Hidalgo of Salamanca University in Spain kindly provided the following species analysis from two glacial, and two Holocene samples filtered to < 8 µm:

Sample from 299-300 cm (19.5 ka): assemblage dominated by large coccoliths. Mainly large (> 4 µm) *E. huxleyi* with some *G. muellerae* and *G. caribbeanica*. Also contains some *Syracosphaera* spp., small *Gephyrocapsa*, and *C. pelagicus*. Reworked nannofossils

are reasonably common. Preservation is good, with no clear signs of dissolution.

Sample from 285-286 cm (19.4 ka): Similar assemblage to 299-300 cm. Good preservation, no dissolution.

Sample from 6-7 cm (2.3 ka): dominated by small placoliths, mostly small *Gephyrocapsa,* but also *E. huxleyi*. Abundant *C. pelagicus*, *C. leptoporus* and *Syracosphaera* spp. Less abundant coccoliths include *H. carteri* and *Oolithotus* spp. Large (> 4 μm) *E. huxleyi*, and *Calciosolenia* are present in small quantities. Good preservation, no dissolution. No re-worked specimens.

Sample from 0-1 cm (recent): same as above 6-7 cm. Good preservation, no dissolution.

The overall trend through time is therefore of a decrease in size of the common species, *Gephyrocapsa,* and *E. huxleyi*. An increase in abundance of *C. pelagicus*, *C. leptoporus, Syracosphaer, H. carteri, Oolithotus* spp and *Calciosolenia* and a decrease in abundance of *G. muellerae* and *G. caribbeanica*. These changes are consistent with those observed by Colmenero-Hidalgo et al. (2004), where the change from large to small *E. huxleyi* and the increase in small placoliths was interpreted to record a decrease in temperature and increase in productivity.

4.5.1 $\delta^{18}O$ < 63 and < 8 μm Unsorted Samples

Between the last glacial maximum (~20 ka) and the Holocene, the MD04-2829CQ < 63 μm and < 8 μm carbonate $\delta^{18}O$ increases from -3.0 to 0.5‰, following a smooth transition from the start of the Bolling-Allerod (14.5 ka) to the start of the Holocene (11.5 ka) (Figure 2). The < 63 μm fraction carbonate will be composed of both coccolithophores and foraminifera

fragments (Frenz and Henrich, 2007), however, because similar values and trends are recorded in the < 8 μm and < 63 μm fractions (although at different resolutions), we can be confident in interpreting both signals as being controlled by coccolith $\delta^{18}O$. Coccolith $\delta^{18}O$ is known to respond to three variables; seawater $\delta^{18}O$, temperature and species composition (Ziveri et al., 2003, Anderson and Steinmetz, 1981, Dudley et al., 1986). Over the last 20 ka, benthic foraminiferal $\delta^{18}O$ show seawater $\delta^{18}O$ to have decreased by at most (i.e. assuming no temperature influence) 1.8‰ (Lisiecki and Raymo, 2005) (Figure 2). This change is contemporaneous with, but of opposite magnitude to, that which we measure in the coccoliths (Figure 2). Culture studies with nine species of coccolithophore, show coccolith $\delta^{18}O$ to change by between +0.12 and +0.28‰ per positive degree temperature increase (Dudley et al., 1986, Ziveri et al., 2003). The positive summer surface water temperature change above site MD04-2829CQ of 7-13˚C (Knutz et al., 2002, Knutz et al., 2007) over the last 20 ka, if temperature were the only variable operating to affect $\delta^{18}O$, would therefore produce a positive 0.84 to 3.64‰ shift in coccolith $\delta^{18}O$. This change would probably follow a similar structure (i.e. relatively stable in the glacial and Holocene, undergoing a rapid change between the two intervals) to that recorded in < 63 μm $\delta^{18}O$, but of the opposite magnitude. It therefore follows that the MD04-2829CQ < 63 μm and < 8 μm $\delta^{18}O$ curves presented in Figure 2 predominantly record the change in species composition at this site, which results in a positive $\delta^{18}O$ change, greater in magnitude than the negative $\delta^{18}O$ response to temperature and changing seawater $\delta^{18}O$. A modification of coccolithophore assemblage, driven by the changing surface water conditions over the Marine Isotope Stage (MIS) 4 to MIS 1 transitions, has been widely documented (e.g. Colmenero-Hidalgo et al., 2004).

It is not possible to allocate $\delta^{18}O$ values to different species from the data we have avaliable, but it is clear that some or all of small *Gephyrocapsa* and *E. huxleyi* and *C. pelagicus*, *C. leptoporus, Syracosphaer, H. carteri, Oolithotus* spp and *Calciosolenia* have high $\delta^{18}O$ values in comparison to large *Gephyrocapsa* and *E. huxleyi,* and *G. muellerae* and *G. caribbeanica.*

4.5.2 $\delta^{13}C$ < 63 and < 8 µm Sorted Samples

Coccolith $\delta^{13}C$ values will vary in response to changes in nutrient supply, nutrient utilisation, and potentially species change. The elevated $\delta^{13}C$ values measured during the glacial termination presented in Figure 3, could therefore indicate a reduction in the supply of nutrient and ^{12}C-rich water, an increase in the utilisation of the available carbon, through rising productivity, or a combination of these and a change between glacial and Holocene coccolithophore assemblage. It is widely believed that the termination of the last glacial interval corresponds to a re-invigoration of circulation and the upward-mixing of ^{12}C and CO_2-rich waters. Evidence for this comes from records of tropical to high southern-latitude foraminiferal $\delta^{13}C$ (Spero and Lea, 2002 and references there-in). The authors do not explain why the event is not seen at high northern latitudes, but if we believe their interpretation, it seems unlikely that a reduction in supply of ^{12}C-rich water could account for the observed $\delta^{13}C$ elevation. Furthermore, in light of our observation that the < 8 and < 63 µm carbonate $\delta^{18}O$ curves are reflecting species change, and therefore that the species composition remained relatively stable within the Holocene and within the glacial period, it seems unlikely that the full $\delta^{13}C$ signal can be explained by species change. It therefore appears that the $\delta^{13}C$ curve presented in Figure 3 represents an increase in nutrient utilisation leading up to, and over the glacial termination, followed by a decrease and lower nutrient utilisation during the first 8 kyr of the Holocene, rising again over the last two kyr. It is possible that this response is caused by changes in coccolithophore productivity following changes in the duration and intensity of northern hemisphere summer insolation (Huybers and Eisenman, 2006) (Figure 4). Considering the data presented here in the context of culture studies by Ziveri et al. (2003) it is evident that the range of $\delta^{13}C$ values recorded in these samples (0.6 – 1.7‰) is within the range of inter-species coccolith $\delta^{13}C$ values. It is therefore possible (although unlikely for the aforementioned reasons) that the < 63 and <8 µm $\delta^{13}C$ data reflect changes in species composition, but changes between species with similar $\delta^{18}O$. The similarity of trend despite a 0.5 ‰ offset between the < 8 and < 63 µm size fraction $\delta^{13}C$ records, indicates that the

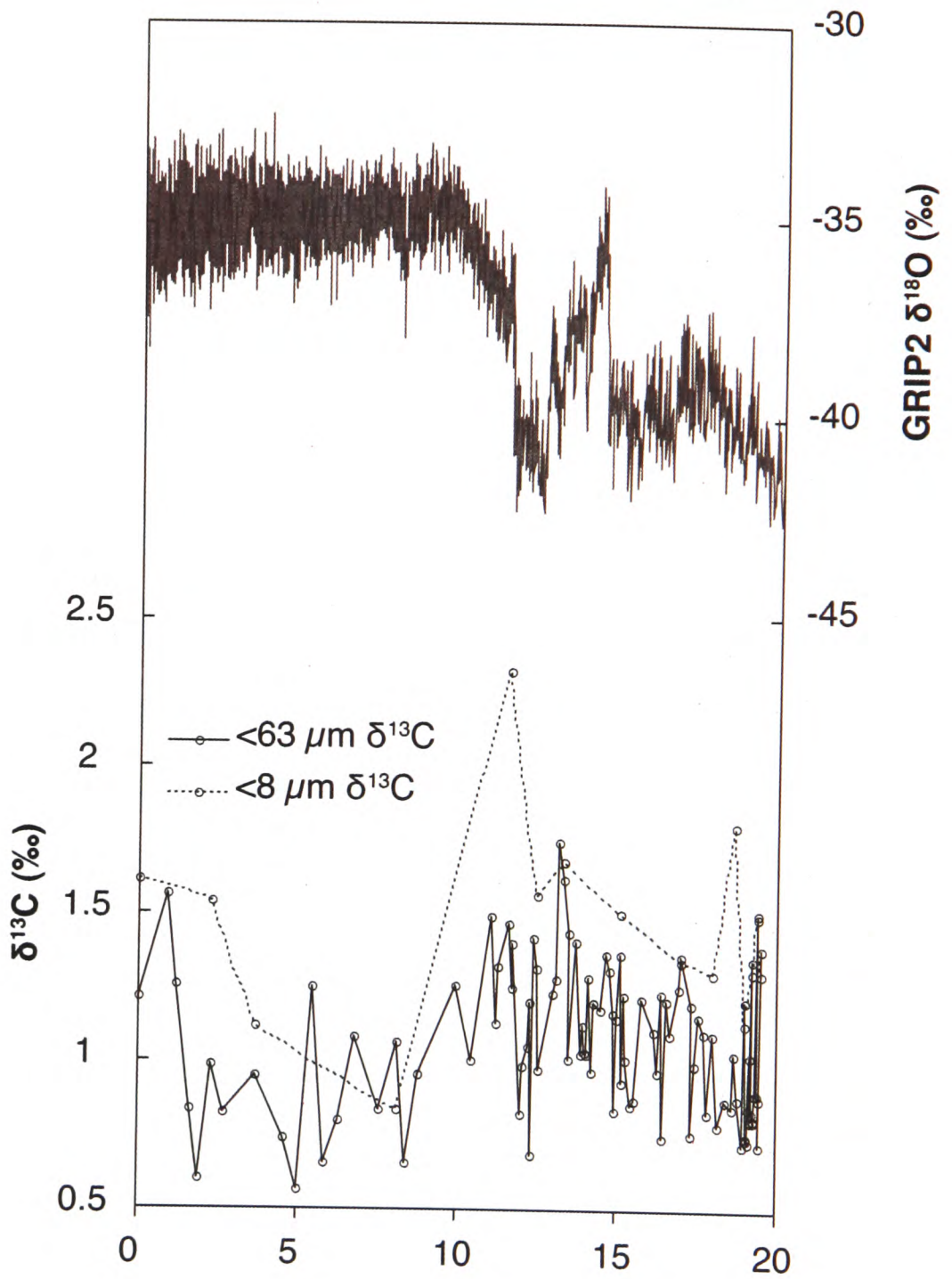

Figure 3. NGRIP $\delta^{18}O$ (North Greenland Ice Core Project Members, 2004) and < 8 and < 63 μm carbonate $\delta^{13}C$.

coccoliths have a higher $\delta^{13}C$ value than the foraminifera fragments, and that the relative production of coccoliths and foraminiferal fragments has remained relatively constant over this interval.

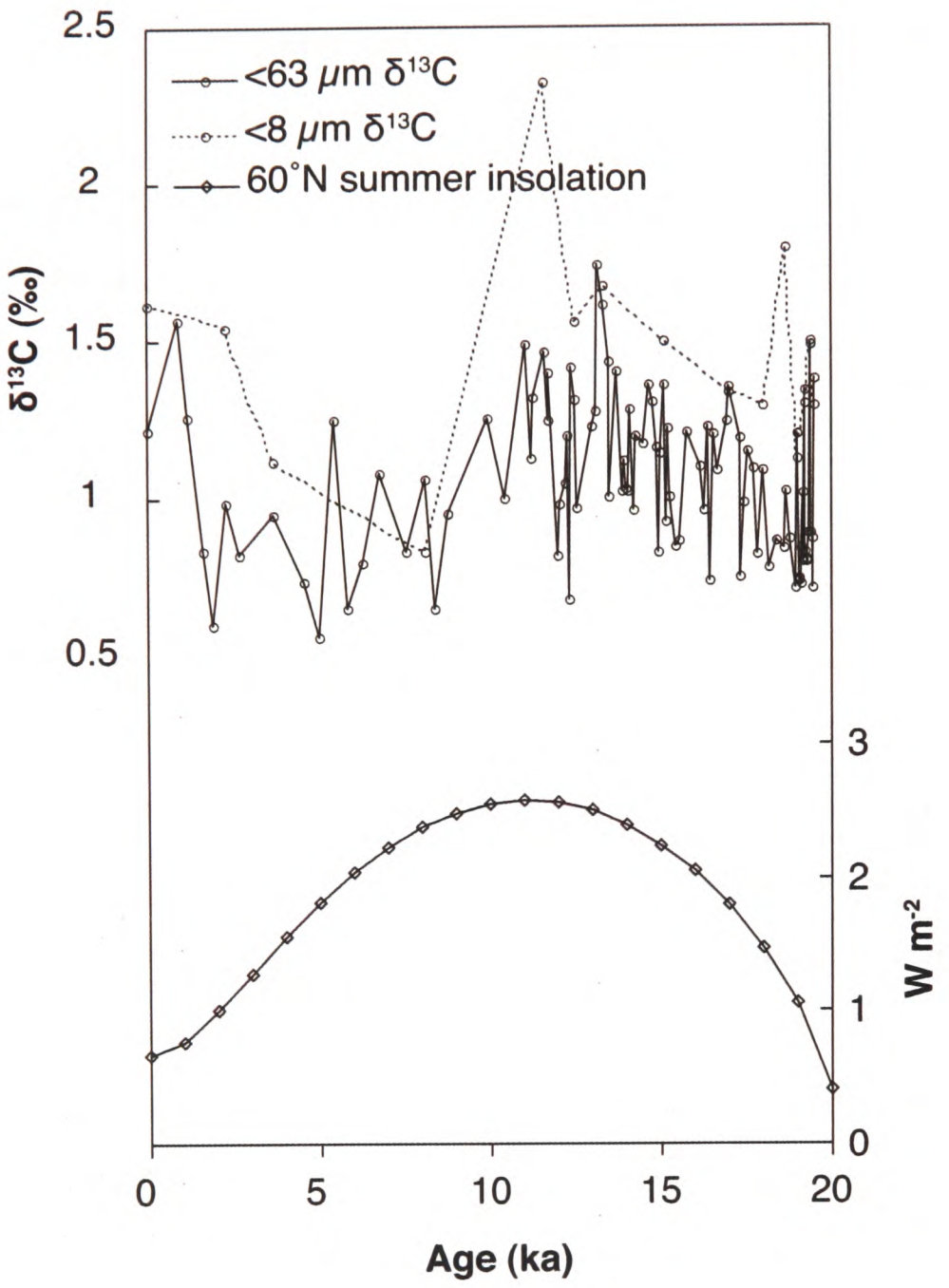

Figure 4. < 8 and < 63 μm $\delta^{13}C$ and 60°N summer insolation, as a sum of the diurnal average insolation (Wm^{-1}) in excess of 475 Wm^{-2}, on days in which the average insolation exceeds 475 Wm^{-1} (Huybers and Eisenman, 2006).

4.5.3 Sr/Ca < 8 µm Unsorted Samples

A highly significant inverse correlation exists between Sr/Ca and $\delta^{18}O$ in the unsorted samples (p-value = 2.20 $x1^{0-16}$ for a linear model correlating 100-point interpolated curves through the Sr/Ca and < 63 µm $\delta^{18}O$ data) (Figure 5). The strength of this correlation suggests that, to a large degree, the two signals share a common source. It was concluded that the < 63 µm and <8 µm MD04-2829CQ $\delta^{18}O$ curves follow a systematic change in species composition. It therefore seems likely that the exact combination of species present in each sample exerts a primary control over coccolith Sr/Ca in this location. Stoll et al. (2002b) highlighted that the $Sr/Ca_{coccolith}$ between different coccolithophore species varies by up to 1 mmol/mol when cultured under the same temperature and light-intensity conditions. The Sr/Ca variability associated with changes in species composition alone could, in theory, be large enough to explain the Sr/Ca dataset presented in Figure 5. In addition to species change, both the glacial-Holocene temperature increase, and the variations in productivity indicated by the MD04-2829CQ $\delta^{13}C$ data, might be expected to influence coccolith Sr/Ca (e.g. Stoll et al., 2002a). However, the temperature increase after MIS 4 should theoretically decrease coccolith $\delta^{18}O$ values, whilst increasing coccolith Sr/Ca values. If temperature had a significant influence over either of these two records, we would expect the strength of their correlation to be considerably reduced.

4.5.4 Cd/Ca, Ba/Ca and Zn/Ca < 8 µm Unsorted Samples

Data presented in Chapter 3, Table 1, demonstrate that no significant correlation exists between unsorted Cd, Ba, Zn and possibly U/Ca and Fe/Ca or Al/Ca. This result indicates that the measurement of these elements as a ratio with Ca would not be compromised by the presence of clays. The unsorted sample element/Ca ratios are presented in Figure 6, however our lack of knowledge about species-specific trace-element chemistry prevents further useful interpretation of these results at this time.

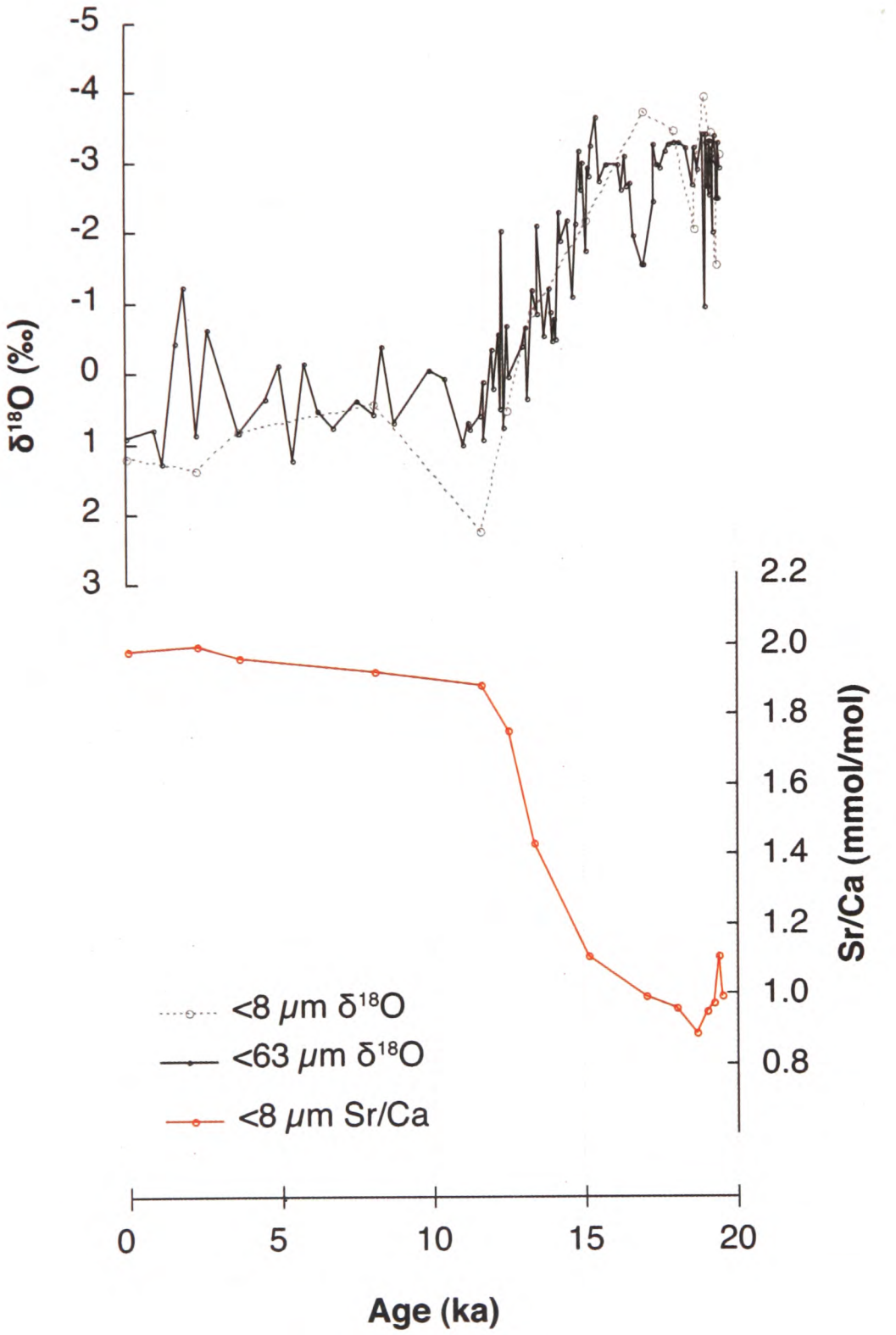

Figure 5. MD04-2829CQ < 63 and < 8 μm carbonate $\delta^{18}O$ and < 8 μm Sr/Ca.

4.6 < 8 μm Flowcytometry Sorted Samples

Figure 6 illustrates the change in chemistry between unsorted and sorted samples. The sorted data with Fe/Ca below 2.5 mmol/mol (considered to be clay-clean) is reproduced without unsorted data in Figure 7. The contrast between sorted and unsorted data is of particular value. Theoretically, it is expected that two things would occur; firstly a reduction in the element/Ca ratio of any cation present in high concentrations in clays, secondly the preferential selection of large coccoliths by the flowcytometry sorting step (as a result of their stronger birefringence and more intense fluorescence). Therefore, in the sorted samples, one should observe a decreased species-control over bulk sample coccolith chemistry in comparison with that inferred to exist within the unsorted samples. Consequently, as previously discussed, Mg/Ca and Mn/Ca signals are reduced significantly by sorting, as do Holocene and transition Sr/Ca values. However, the glacial Sr/Ca records from both the unsorted and sorted samples display similar values. There is good reason to believe that the change in Sr/Ca does not reflect clay-removal (Barker et al., 2003, Emiliani, 1955), therefore the similarity of unsorted glacial Sr/Ca to sorted glacial Sr/Ca, and the lack of a step-change in sorted Sr/Ca over the glacial-Holocene transition, may indicate that the flowcytometry procedure preferentially selects coccoliths of the species which dominate the Sr/Ca chemistry of the glacial assemblage. This result agrees with the theoretical predictions, because the glacial assemblage was dominated by larger coccoliths. Unfortunately, as a result of limited access to the flow-cytometer it was not possible to sort samples for assemblage analysis as well as chemical analysis. If one is to assume that sorted coccolith populations remain stable over the past 20 ka, one would expect Sr/Ca to increase slightly in response to temperature, and one might expect an elevated Sr/Ca over the glacial-Holocene transition in response to a productivity increase, postulated in reference to the $\delta^{13}C$ data (Figure 4). The first expectation, an elevated Sr/Ca with temperature is consistent with the 0.2-0.5 mmol/mol Sr/Ca increase from the glacial values to Holocene values, however no Sr/Ca peak is observed during the transition. The absence of a Sr/Ca peak over the glacial-Holocene transition

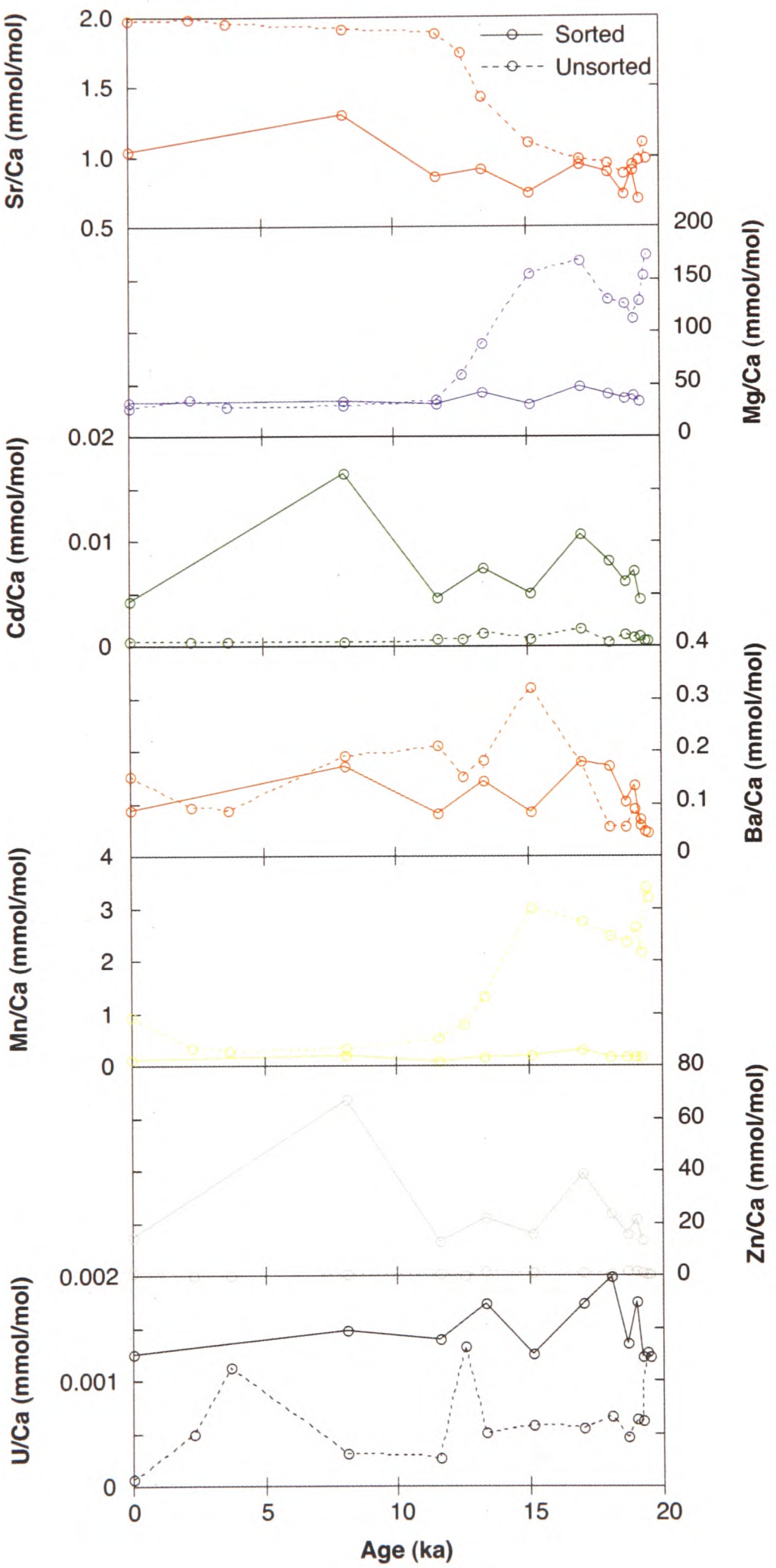

Figure 6. < 8 μm unsorted (dashed lines) and flowcytometry sorted (solid lines) data for Sr, Mg, Ca, Ba, Mn, Zn and U ratioed to Ca. Sorted data presented where Fe/Ca < 2.5 mmol/mol.

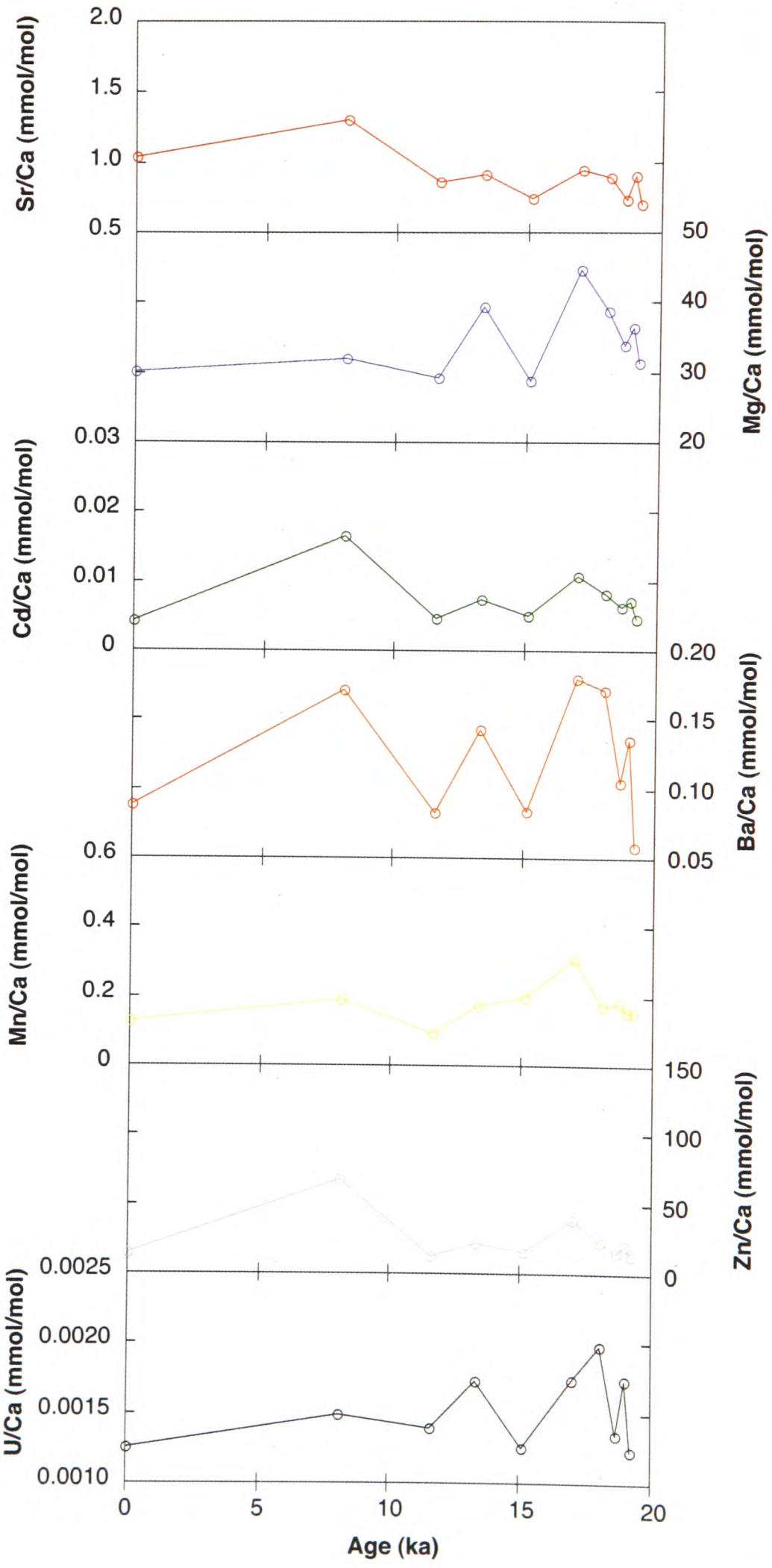

Figure 7. < 8 μm flowcytometry sorted data for Sr, Mg, Ca, Ba, Mn, Zn and U ratioed to Ca. Where Fe/Ca < 2.5 mmol/mol.

may provide further evidence that the $\delta^{13}C$ peak, interpreted as an elevation in productivity, is insolation driven. This interpretation is consistent with evidence that coccolith-Sr/Ca responds only to growth-rate changes driven by changing nutrient availability, not changes in light intensity (Stoll et al., 2002b).

Examination of the direction of change from each data point relative to the next data point for each element/Ca ratio other than Mn/Ca, as presented in Figure 7 highlights that the broad shapes of the sorted element/Ca curves share a common pattern, yet the relative magnitude of change is rarely the same between different elements. Table 3 quantifies the strength of these correlations, with blue text highlighting correlations with a < 1 in 20 probability of occurring by chance, red text highlighting correlations with a < 1 in 100 probability of occurring by chance, and yellow highlighting correlations with a less than 1 in 1000 probability of occurring by chance.

p-values	Mg/Ca	Sr/Ca	Cd/Ca	Ba/Ca	Mn/Ca	Zn/Ca	U/Ca
Mg/Ca		0.84	0.30	9.58×10^{-3}	2.55×10^{-2}	0.45	4.32×10^{-3}
Sr/Ca	0.84		8.42×10^{-3}	8.02×10^{-2}	0.83	3.29×10^{-3}	0.56
Cd/Ca	0.30	8.42×10^{-3}		5.66×10^{-3}	0.14		0.25
Ba/Ca	9.58×10^{-3}	8.02×10^{-2}	5.66×10^{-3}		7.68×10^{-2}	1.89×10^{-2}	2.76×10^{-3}
Mn/Ca	2.55×10^{-2}	0.83	0.14	7.68×10^{-2}		0.17	0.36
Zn/Ca	0.45	3.29×10^{-3}		1.89×10^{-2}	0.17		0.43
U/Ca	4.32×10^{-3}	0.56	0.25	2.76×10^{-3}	0.36	0.43	

Table 3. p-values for linear models correlating every sorted element/Ca ratio (with Fe/Ca < 2.5) against every other element/Ca ratio. Blue text highlights correlations with a < 1 in 20 probability of occurring by chance, red text highlights correlations with a < 1 in 100 probability of occurring by chance, and yellow highlights correlations with a less than 1 in 1000 probability of occurring by chance.

The high degree of correlations between the different element/Ca measurements in the clay-cleaned samples, provides some clues as to the origin of the chemistry. Below are a number of possible explanations for why these strong correlations exists:

- All elements measured react the same way to environmental stimulus i.e. (at least) follow growth-rate and temperature control as demonstrated for Sr/Ca (Stoll et al., 2002b), and the controlling factor(s) are have increased and decreased a number of times at this location over the past 20 ka.
- Species have distinct chemistries where coccoliths are either enriched or depleted in all the measured elements to a similar degree, and species composition varies in the samples over the past 20 ka.
- A contaminant which contains all of the measured elements, is present in samples in varying quantities, at concentrations comparable to, or higher than, those in the coccoliths.
- A measurement artifact exists, meaning that some component of the sample affects all element measurements similarly. Such an artifact can occur if sample [Ca] was not constant between each sample, or between samples and standards. If Ca concentrations vary between samples, disparities in the concentration of elements present in the ICP-MS's plasma can cause changes in the sensitivity of measurement of other elements. However this artifact can be ruled out because all samples were diluted to the same Ca concentration as the standard from which their element/Ca were calculated, and no significant correlation is observed between exact Ca intensities measured during ICP-MS analysis and element/Ca intensity ratios (p-values for correlation between Ca intensities and element/Ca intensity ratios: Mg/Ca = 0.12, Sr/Ca = 0.34, Cd/Ca = 0.05, Ba/Ca = 0.06, Mn/Ca = 0.04, Zn/Ca = 0.05, U/Ca = 0.02).

Two important observations can be made from the data presented in Figures 6 and 7, in the context of which we can consider the validity of the explanations postulated above:

- The high concentration of Sr in coccoliths, and the low concentration in common contaminant phases means that coccolith Sr/Ca is generally considered to be a robust indicator of either growth-rate, temperature or species change within the coccolithophores (Stoll et al., 2002b). Our sorted sample Sr/Ca record varies by up to 0.6 mmol/mol in the sorted samples over the last 20 ka. It is hard to explain how this could result from anything but a change in average coccolith chemistry (i.e. the average chemistry of coccoliths produced by all species), and therefore, because measurements of other elements parallel changes in Sr/Ca, it seems likely that these element/Ca signals also reflect changes in average coccolith chemistry.
- In comparing element/Ca ratios before and after sorting (Figure 6) some ratios decrease (e.g. Sr/Ca, Mg/Ca), whilst others increase (e.g. Cd/Ca, U/Ca). To cause a decrease in ratios, it is necessary to remove a phase with element/Ca higher than that in coccolith calcite, or add a phase with element/Ca lower than that in coccolith calcite (i.e. Ca-rich). To increase the element/Ca ratio, the opposite is true, either remove a phase with element/Ca lower than that in coccolith calcite or add a phase with element/Ca higher than that in coccolith calcite. This is inconsistent with invoking contamination alone to explain the post-sorting element/Ca values because element/Ca ratios in the sorted samples co-vary, increasing and decreasing their ratios in parallel. Therefore, to explain these results by contamination would require that the contaminant is enriched in all of the measured elements relative to their concentrations in coccolith calcite. The addition of a contaminant, enriched in all elements measured in this study, could not result in a decrease in element/Ca ratios after sorting, and therefore cannot explain the total unsorted sample to sorted sample chemical changes.

It is therefore reasonable to assume that the coccolith element/Ca data we present here accurately reports the bulk coccolith chemistry of the samples. However, at this stage, it is not possible to rule out whether or not there is a secondary component of contamination

masking the exact coccolith chemistry. It would be of great benefit now to sort samples large enough to allow application of the full foraminiferal cleaning procedure (but leaving out the clay-cleaning stage) as described by Boyle (1981), and analyse the coccolith chemistry at different stages throughout the cleaning process, to assess the degree of further chemical contamination. Using the current technique, to produce the volume of sediment required to perform analysis of the required chemical cleaning, without risking large-scale dissolution through reaction with reagents used in the process, would require long flowcytometry sorts, of the order of five to ten hours per sample. Consequently, either the methodology must be refined to increase the coccolith yield, or additional funds must be appropriated to allow large sorts to be made using the current protocol. In addition to an analysis of the cleaning protocol, material must be set aside for analysis of sample species-composition and ultimately to allow single-species analysis.

4.7 Conclusions

This chapter has demonstrated that the flowcytometry clay-cleaning protocol for coccolith samples can successfully be applied in a down-core situation. Similarity between all element/Ca ratios (other than Mn/Ca) and data from the apparently robust Sr/Ca (e.g. Stoll et al., 2007) proxy suggest that after sorting, coccolith trace-element compositions have been accurately obtained. However, as a result of variations in post-sorting species composition between samples (although believed to be significantly reduced in comparison with pre-sorting species variance), it is not possible to make definitive conclusions about the controls over coccolith of trace-element variability. In addition to uncertainty regarding the samples' species composition, to confidently interpret our measurements as useful geochemical proxy data, we must first assess the degree of non-clay chemical contamination present in the samples, by applying traditional foraminiferal cleaning procedures to large sorted coccolith samples.

4.8 Bibliography

ANDERSON, T. F. AND STEINMETZ, J. C. (1981) Isotopic and biostratigraphical records of calcareous nannofossils in a Pleistocene core. Nature, 294, 741-744.

BARKER, S., GREAVES, M. AND ELDERFIELD, H. (2003) A study of cleaning procedures used for foraminiferal Mg/Ca paleothermometry. Geochemistry Geophysics Geosystems, 4, doi:10.1029/2003GC000559.

BEAUFORT, L. (2005) Weight estimates of coccoliths using the optical properties (birefringence) of calcite. Micropaleontology, 51, 289-297.

BOYLE, E. A. (1981) Cadmium, Zinc, Copper, and Barium in Foraminifera Tests. Earth and Planetary Science Letters, 53, 11-35.

COLMENERO-HIDALGO, E., FLORES, J. A., SIERRO, F. J., BARCENA, M. A., LOWEMARK, L., SCHONFELD, J. AND GRIMALT, J. O. (2004) Ocean surface water response to short-term climate changes revealed by coccolithophores from the Gulf of Cadiz (NE Atlantic) and Alboran Sea (W Mediterranean). Palaeogeography Palaeoclimatology Palaeoecology, 205, 317-336.

DUDLEY, W. C., BLACKWELDER, P., BRAND, L. AND DUPLESSY, J. C. (1986) Stable isotopic composition of coccoliths. Mar. Micropaleontol, 10, 1-8.

EMILIANI, C. (1955) Mineralogical and chemical composition of the tests of certain pelagic foraminifera. Micropaleontology, 1, 377.

FRENZ, M. AND HENRICH, R. (2007) Carbonate dissolution revealed by silt grain-size distribution: comparison of Holocene and Last Glacial Maximum sediments from the pelagic South Atlantic. Sedimentology, 54, 391-404.

HARDING, D. (2007) Quick corruption of conveyour circulation: a geochemical approach. Departent of Earth Sciences. Oxford, Oxford University.

HARDING, D. J., ARDEN, J. W. AND RICKABY, R. E. M. (2006) A method for precise analysis of trace element/calcium ratios in carbonate samples using quadrupole inductively coupled plasma mass spectrometry. Geochemistry Geophysics Geosystems, 7, doi:10.1029/2005GC001093.

HARDING, D. J. AND RICKABY, R. E. M. (2006) Reconstructing North Atlantic deglacial ocean circulation: A high resolution trace metal and stable isotope record. Geochimica Et Cosmochimica Acta, 70, A229-A229.

HUYBERS, AND EISENMAN, I. (2006) Integrated summer insolation calculations. IGBP PAGES/World Data Center for Paleoclimatology NOAA/NGDC, Data Contribution Series # 2006-079.

KNUTZ,C., HALL, I. R., ZAHN, R., RASMUSSEN, T. L., KUIJPERS, A., MOROS, M.

AND SHACKLETON, N. J. (2002) Multidecadal ocean variability and NW European ice sheet surges during the last deglaciation. Geochemistry Geophysics Geosystems, 3, 077 ISSN 1525-2027 .

KNUTZ,C., ZAHN, R. AND HALL, I. R. (2007) Centennial-scale variability of the British Ice Sheet: Implications for climate forcing and Atlantic meridional overturning circulation during the last deglaciation. Paleoceanography, 22, doi:10.1029/2006PA001298.

LISIECKI, L. E. AND RAYMO, M. E. (2005) A Pliocene-Pleistocene stack of 57 globally distributed benthic delta O-18 records. Paleoceanography, 20, doi:10.1029/ 2004PA001071.

SPERO, H. J. AND LEA, D. W. (2002) The cause of carbon isotope minimum events on glacial terminations. Science, 296, 522-525.

STOLL, H. M., KLAAS, C. M., PROBERT, I., ENCINAR, J. R. AND ALONSO, J. I. G. (2002a) Calcification rate and temperature effects on Sr partitioning in coccoliths of multiple species of coccolithophorids in culture. Global and Planetary Change, 34, 153-171.

STOLL, H. M., SHIMIZU, N., ARCHER, D. AND ZIVERI,(2007) Coccolithophore productivity response to greenhouse event of the Paleocene-Eocene Thermal Maximum. Earth and Planetary Science Letters, 258, 192-206.

STOLL, H. M., ZIVERI, P., GEISEN, M., PROBERT, I. AND YOUNG, J. R. (2002b) Potential and limitations of Sr/Ca ratios in coccolith carbonate: new perspectives from cultures and monospecific samples from sediments. Philosophical Transactions of the Royal Society of London Series a-Mathematical Physical and Engineering Sciences, 360, 719-747.

ZIVERI, P., STOLL, H., PROBERT, I., KLASS, C., GEISEN, M., GANSSEN, G. AND YOUNG, J. (2003) Stable isotope vital effects in coccolith calcite. Earth and Planetary Science Letters, 210, 137-149.

Exploring Coccolith Geochemistry Using Flow-through Time Resolved Analysis

5

Flow-through Time Resolved Analysis (FT-TRA) was initially developed by Haley and Klinkhammer (2002) as a cleaning and dissolution tool for rare-Earth element foraminiferal analysis. The system makes use of a High Precision Liquid Chromatography (HPLC) pump which can be programmed to draw fluid from up to four inlet reservoirs, mix them in pre-specified programmable proportions, and pass the mixture at variable flow rates over a sample. The solution can then be collected in fractions, or directly fed into a mass spectrometer for online analysis (Figure 1). Initial application of this technique used the different inlet reservoirs to hold different cleaning/dissolution solutions, and the valve on the pump to select discretely between these reservoirs. Subsequently it was discovered that by changing the mixing ratio between the acid and water inputs during analysis, an acid strength gradient could be produced to further control the dissolution (Klinkhammer et al., 2004). Results published by Klinkhammer et al. (2004) indicated that the cations leached from the clay and liberated from calcite could be isolated to different stages of the sample dissolution (Figure 2).

The results of Klinkhammer et al. (2004) indicated that FT-TRA may allow the measurement of trace-element/Ca data, from coccoliths, without releasing contaminant elements from sedimentary clays, negating the need for physical coccolith-clay separation (as discussed in

Chapter 3) before analysis. This idea is explored, but found to be compromised by subtle issues associated with the function of the equipment. However, the data obtained during the initial testing indicates that rather than separating the coccolith and clay chemical signals, the results may be indicating the presence of chemical inhomogeneities in the substituted-element distribution within coccoliths. The possibility of non-uniform chemical organisation is examined using a number of techniques, including electron microprobe analysis and atomic force microscopy. The dissolution and chemical data is considered in the context of possible biomineralisation models.

5.1 Background

FT-TRA was conceived as a technique to monitor the cleaning of contaminant phases from the foraminiferal tests, allowing the rare Earth elements (REEs) present in these phases to be held in solution by the flowing acid and moved down-stream from the calcite, preventing re-adsorption and allowing subsequent measurement of the primary foraminiferal REE

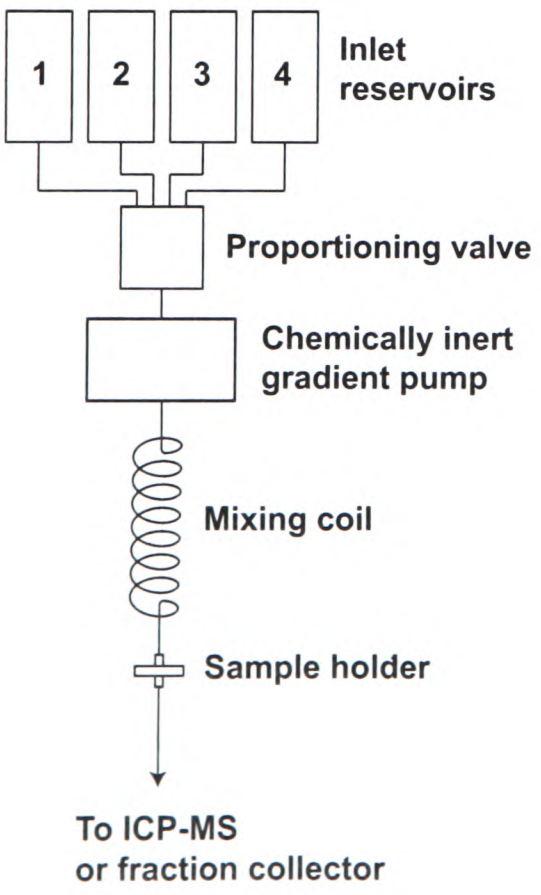

Figure 1. Diagrammatic representation of the flow-through system. The system is designed around a Quaternary Gradient High Pressure Liquid Chromatography Pump, which is able to control the composition and flow-rate of an outgoing fluid between four end-member composition and 0-10 ml/min. The systems is sealed, so the chosen fluid passes through the sample holder (a leuer-locked syringe filter housing containing a 0.1 μm syringe filter) and into the ICP-MS without risk of external contamination.

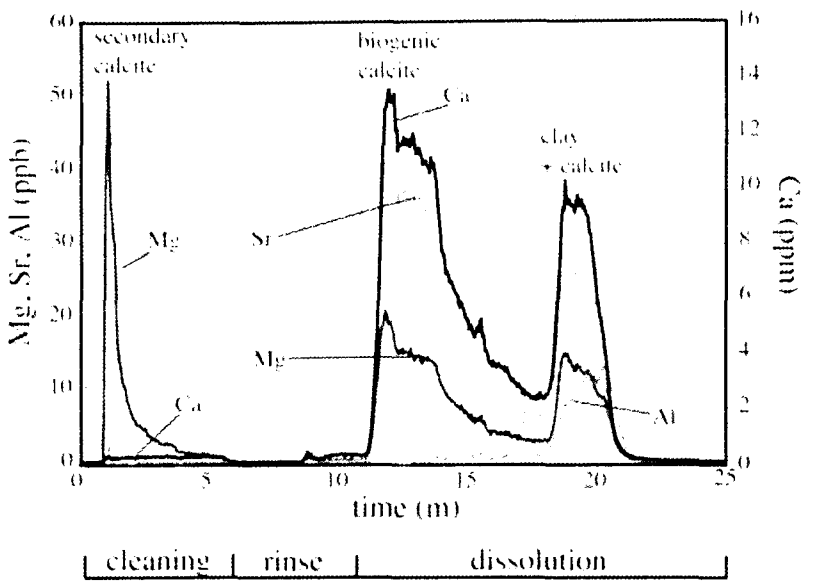

Figure 2. Mg, Sr, Al and Ca concentrations plotted against time during the dissolution of an uncleaned foraminiferal sample. Peaks were interpreted as representing the dissolution of secondary calcite, biogenic (primary calcite) and the leaching of contaminants from clay. From Klinkhammer et al. (2004).

composition (Haley and Klinkhammer, 2002). Subsequently Benway et al. (2003) applied the technique to Mg/Ca palaeotemperature reconstruction, cleaning the foraminifera first for clays as described in the Boyle procedure (Boyle, 1981), then loading the samples into the FT-TRA system and chemically cleaning whilst online using hydroxylamine HCl (pH > 9). The samples were then dissolved in a 0.01 N HNO_3 and the eluent continuously analysed using Inductively Coupled Plasma – Atomic Emission Spectroscopy (ICP-AES). Typical results from these experiments are presented in Benway et al. (2003) and an example given in Figure 3. Figure 3 shows results from a foraminiferal-sample dissolution taking place over ~7 minutes. Dissolution begins with a rapid increase in Ca concentration, relating to a flushing of deionised water from the dissolution chamber and a reduction in pH, followed by a slower decrease in Ca concentration as the foraminifera tests dissolve and the surface area of calcite available for dissolution decreases. Over this period [Mg] initially rises rapidly, then after peaking decreases proportionally faster than [Ca]. The 'early ramp-up' of Mg/Ca occurring at the beginning of dissolution is said to be 'characteristic of a continuous flow system, and reflects diffusive mixing in the regent stream, not a true change in shell Mg/Ca' (Benway et al., 2003). The gradual decrease in Mg/Ca is then thought to reflect a move from

dissolution of the Mg-rich calcite, believed to have formed in warm, near surface waters, to lower-Mg calcite reflecting calcification in cooler, deeper waters. The authors suggest that the most Mg-rich calcite reflects the near-surface water temperature, and choose to select the Mg/Ca associated with the peak [Ca] for future temperature reconstructions. However, a temperature calibration for this Mg/Ca data is yet to be produced.

Klinkhammer et al. (2004) further developed the Mg/Ca FT-TRA method by moving from dissolution using a constant pH acid, to dissolution using an acid gradient mixed from 0 N HNO_3 (i.e. 100% deionised H_2O), to 1 N HNO_3 (the concentration is represented by the upper surface of the grey shaded area in Figure 4). Using this methodology, the authors claim to be able to separate temporally the dissolution of primary calcite and secondary calcite overgrowths, the different phases of biogenic calcite and the trace metal signal associated with the clay phase. Assuming that the interpretation by Klinkhammer et al. (2004) is correct, this provides a very valuable tool, because without undertaking the traditional pre-analysis cleaning of foraminifera it remains possible to pick out the primary biogenic calcite signal. Avoiding the pre-analysis cleaning has many potential advantages. As Klinkhammer et al. (2004) highlight, the full cleaning procedure as described by Boyle et al. (1981) dissolves a considerable amount of calcite at each stage. This calcite is presumably dissolved based in part on its chemically mediated solubility, thereby preferentially removing the most Mg-rich component [Mg substitution increases the solubility of calcite (Morse and Mackenzie, 1990)] of the foraminifera and biasing subsequent batch Mg/Ca measurement to artificially low values.

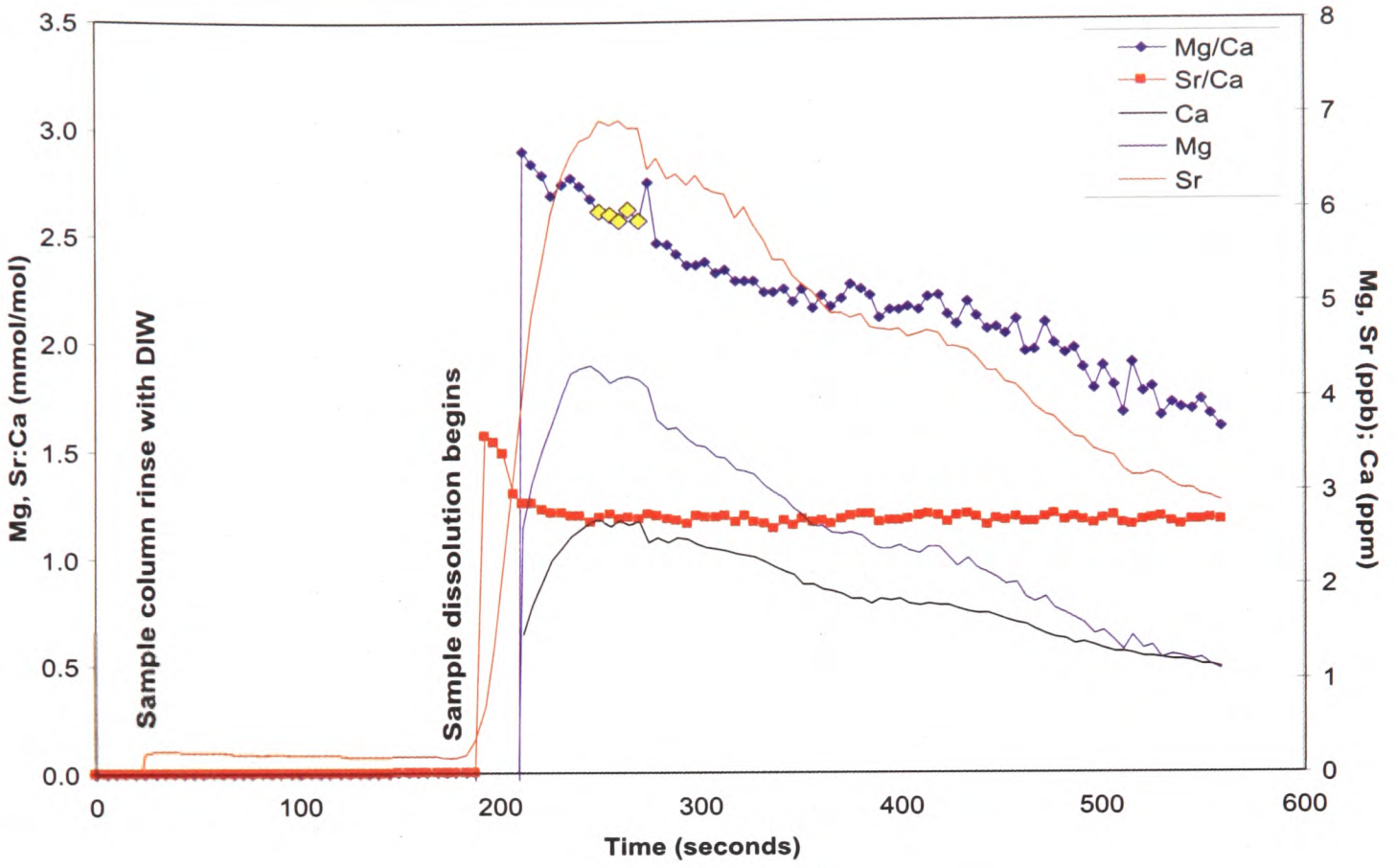

Figure 3. Mg and Sr/Ca ratios, and Mg, Sr and Ca concentrations measured during the dissolution of a clay-cleaned foraminiferal sample. From Benway et al. (2003).

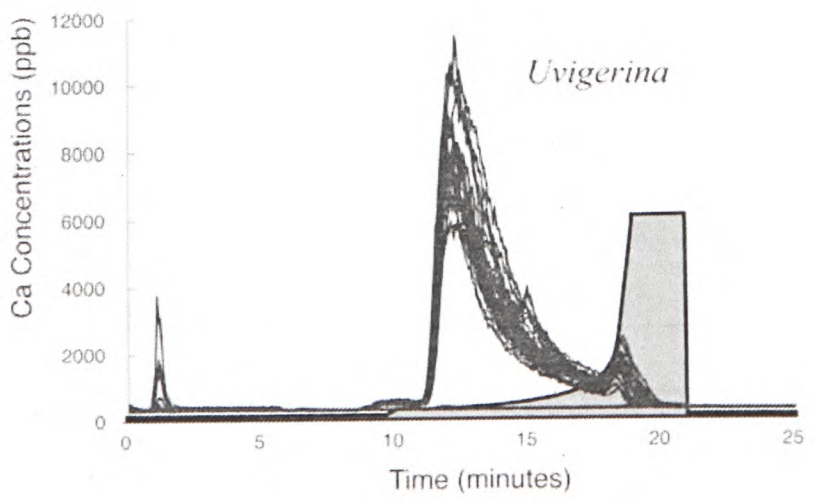

Figure 4. Ca concentrations plotted against time for multiple foraminiferal samples. The gradient of grey shaded area's upper surface represents the rate of change of composition of the dissolution fluid. From Klinkhammer et al. (2004).

5.2 FT-TRA Equipment Setup

The FT-TRA system developed for this study has been set up in such a way that the entire flow-path is constructed from chemically inert plastics (predominantly Polytetrafluoroethylene - PTFE). Inlet reservoirs are 2 L PTFE bottles, into the lids of which holes have been drilled allowing the insertion of PTFE inlet tubing. The inlet tubing connects to the proportioning valve. The proportioning valve and pump are part of a Waters 626 quaternary gradient pump unit, the flow-path of which is entirely PTFE. The outlet from the gradient pump feeds into a 14-position *ChemInert* stream selector valve, and out to a two piece *Savillex* 13 mm filter holder containing a 0.1 μm pore size PTFE filter membrane. From here acid is either fed straight into the Quadrapole ICP-MS or into a series of acid cleaned centrifuge tubes for later analysis.

5.3 System Capabilities

The Waters 626 quaternary gradient pump provides significant flexibility with regard to eluent mixing and flow-rate. The user can specify which of 11 mixing gradients the analysis should follow, ranging from a discrete step between two fluid compositions at the beginning or end of a specified interval, through eight different power curves and a simple linear mixing. These mixing gradients can be programmed to progress over any required period of time up to 100 minutes, and between any two fluid compositions. The flow-rate can be controlled from 0 to 10 ml min^{-1} in steps of 0.01 ml min^{-1}. Importantly for our application, at low flow-rates the speed of the two pump heads can be precisely controlled in response to continuous monitoring of the back-pressure in the system to maintain a constant flow speed.

5.4 FT-TRA Methodology

Initially the FT-TRA system utilised in this study was set up following a similar dissolution sequence to that described by Klinkhammer et al. (2004), mixing from 18 MΩ H_2O to 10% HNO_3 following a cubic power curve (curve 6 on the Waters 626 quaternary gradient pump) over time periods between 10 minutes and 1 hour. The greatest difference between our set-up and that of Klinkhammer et al. is in the application of standards. Klinkhammer et al. add multiple internal standards to their eluent before measuring the dissolving sample using ICP-AES, whereas using a method modified for the Oxford Biogeochemistry Group's Quadrapole ICP-MS, a known 'synthetic calcite' standard is measured before and after each sample is run, and the values extrapolate between these measurements to correct the sample for analytical drift (Harding et al., 2006).

5.5 Standard Application and Data Processing

During a typical batch foraminiferal analysis the concentration of the sample will be diluted to match that of the standard. This means that the concentration of elements in the plasma will be similar when the sample is analysed and when the standards are analysed. In the plasma, the elements interact with each other and consequently significant errors can be introduced by analysing samples at a concentration different to that of the standard (Harding et al., 2006). However, when using FT-TRA an inherent problem is that the sample concentration changes through time. To avoid the introduction of error associated with mismatched sample and standard concentrations, three standards are analysed before and after the sample, at three different concentrations (50, 75 and 100 ppm Ca). Assuming that the machine drift occurs linearly, by extrapolating between these standards allows calculation of planes in intensity-concentration space describing the pulse-count intensities expected from the standard at any given time during the analysis (Figure 5). The data produced by the ICP-MS is recorded as

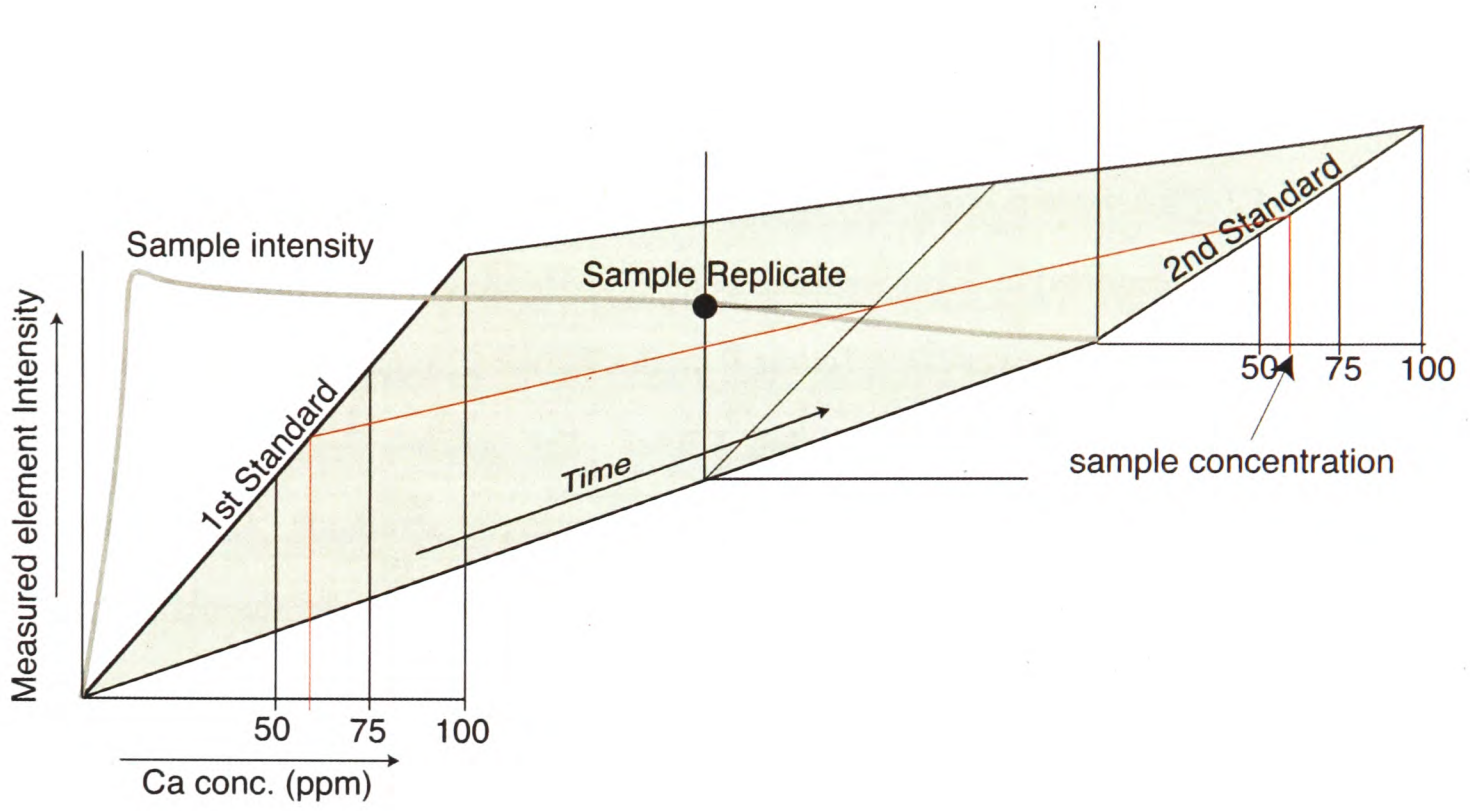

Figure 5. Diagrammatic representation of the FT-TRA standard-correction procedure. Three standards of concentrations 50, 75 and 100 ppm Ca are measured before and after the sample is analysed. A 2-D plane can then be described from the average pulse intensities measured for these standards, with vectors representing the expected intensities of the standard solutions, assuming linear machine drift, throughout the sample analysis time. The element intensities recorded for the sample at any time during the dissolution can then be converted into element concentrations by iteratively matching them with the standard plane. Once this has been done for every replicate and element, data is produced recording the elemental concentrations throughout the experiment.

counts per second averaged over ten-second intervals. At any known time through the run, the data processing software written in Visual Basic for Applications (see appendix B), can iteratively match the intensity recorded for each element with the corresponding element concentration as described by the plane calculated from the analysed standards (Figure 5). This process can be repeated for each replicate throughout the sample analysis and standard-corrected plots of trace-element/Ca ratios can be produced from the calculated element concentrations.

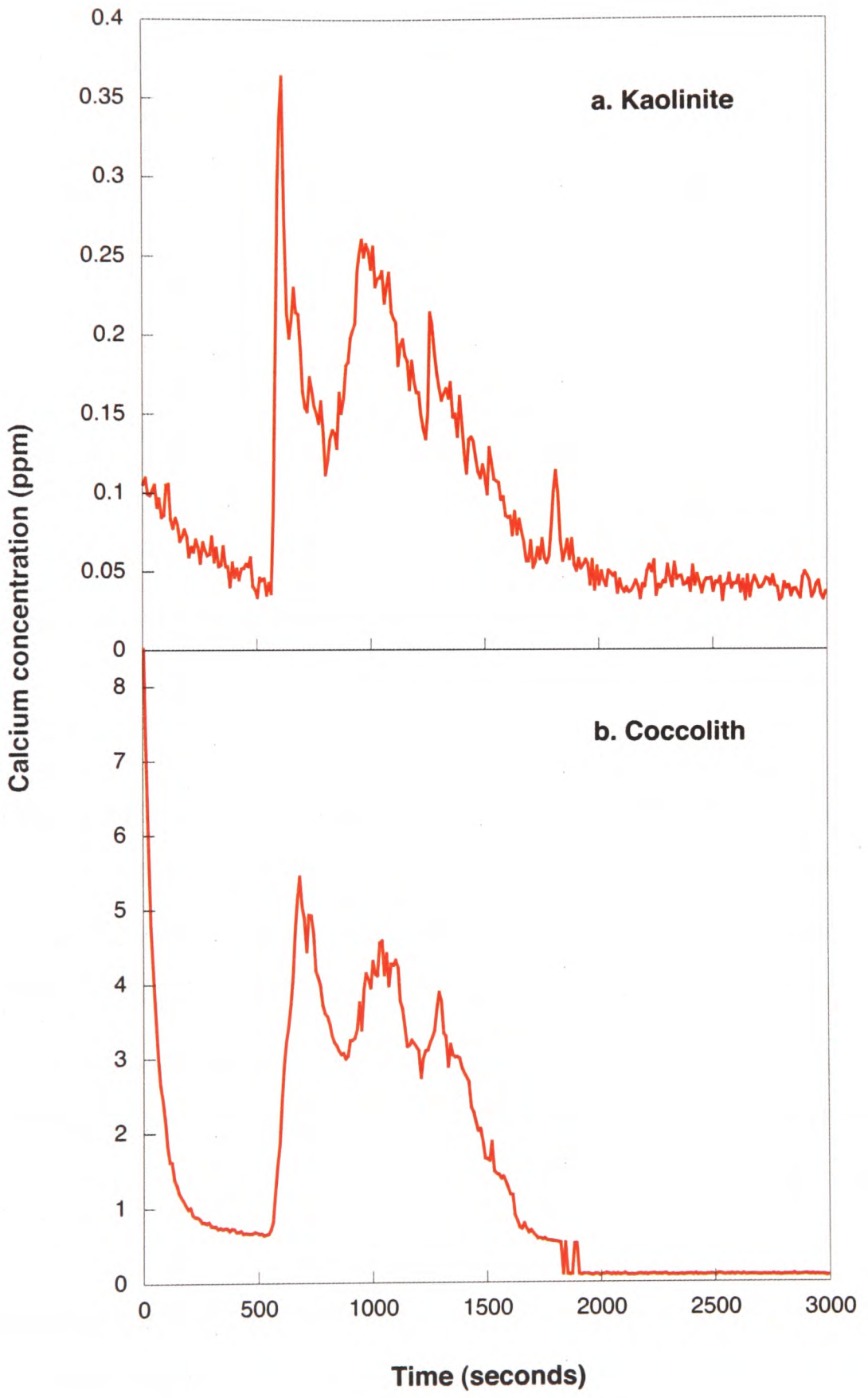

Figure 6. Calcium concentration curves measured during the flow-through analysis of **a.** pure kaolinite and **b.** cultured coccoliths from the species *E. huxleyi.*

5.6 Initial Validation

The reason for applying this technique to the analysis of coccolith-rich sediment was that the method described by Klinkhammer et al. (2004) appeared to separate out the biogenic calcite signal from the clay signal. To validate the technique for this purpose it was first necessary to examine two questions:

- What does a pure clay sample look like using FT-TRA?
- What does a cultured single species coccolith sample look like using FT-TRA?

Using these two analyses it should be possible to confirm whether the FT-TRA system would allow us to separate the trace-element signals associated with coccolith and clay dissolution.

Figure 6 shows the Ca concentrations measured during two FT-TRA experiments, one with pure kaolinite clay (a), and one analysing pure cultured coccoliths of the species *E. huxleyi* (b). It is immediately evident that the peak signals from the coccolith and clay samples are not separated temporally. Comparison of these curves with those obtained by Klinkhammer et al. (2004) shows that the signals are very similar, implying that these multi-peak curves are not necessarily a result of the dissolution of multiple phases of calcite and clays, but in fact a signal inherent to FT-TRA under these condition.

Despite the clear evidence that such a methodology will not allow the separation of the chemistries associated with coccoliths and clays during continuous dissolution, the source of these multiple peaks was of interest.

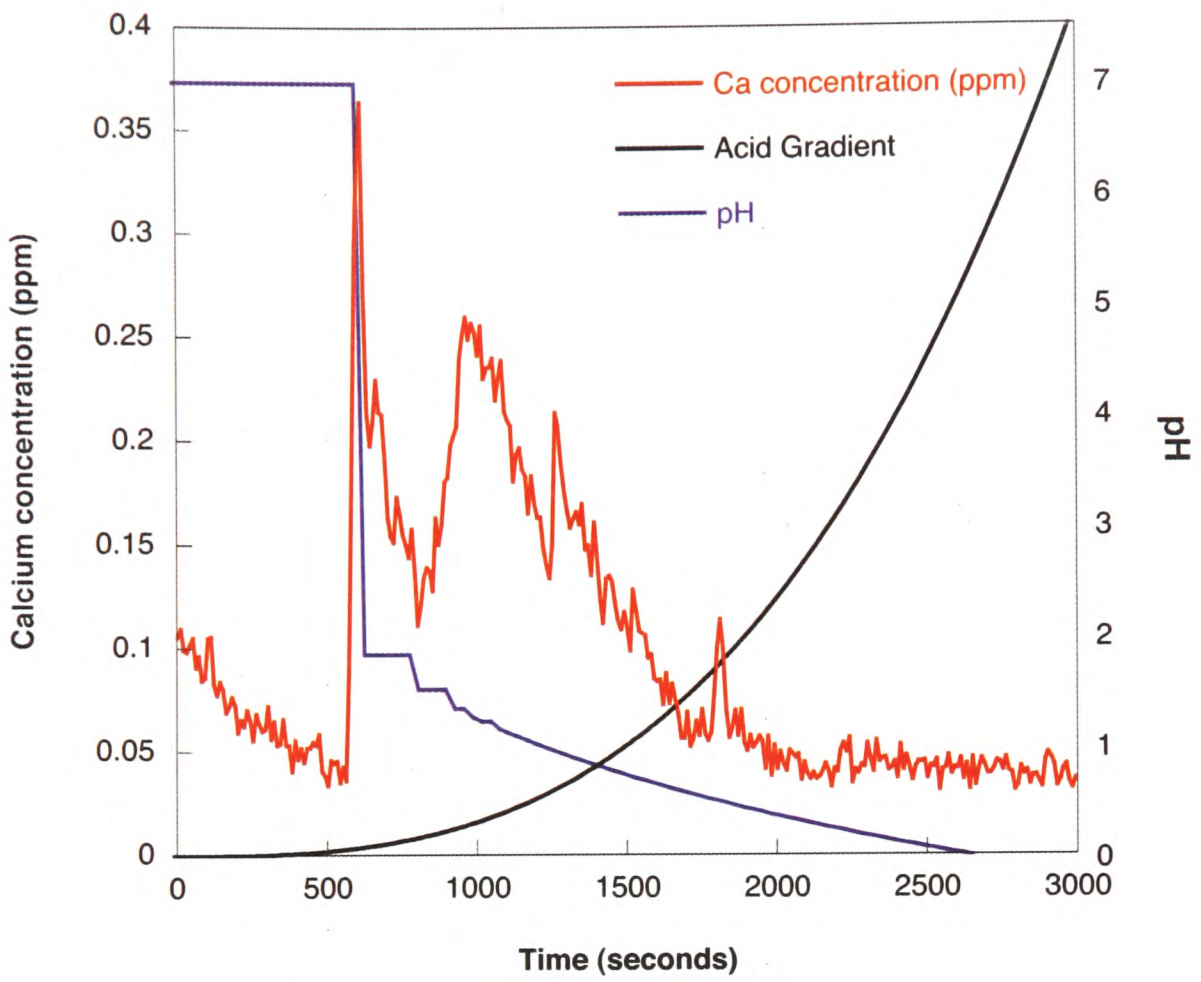

Figure 7. Plot showing the correlation between pH jumps resulting from the step-wise mixing in the gradient pump, and peaks in the sample dissolution. Sample dissolution is recorded by the Ca concentration in red, pH in blue and the curve describing the acid mixing gradient in black.

5.7 Understanding the Intricacies of FT-TRA

Examination of the FT-TRA system revealed that the source of the multiple peaks observed during FT-TRA dissolution was not a reflection of the sample composition, but an artefact of the gradient pump operation. As indicated by the audible switching of the proportioning value during mixing, the valve does not continuously (i.e. linearly) change the relative proportion of the incoming fluids, but is rather a discrete stream-selector valve which dwells for varying lengths of time on each inlet to produce the required final fluid composition. When following a mixing curve the gradient pump's software splits the curve into 100 discrete integer steps from 0% of the final fluid composition to 100% of the final fluid composition. It is only when the mixing curve reaches one of these integer steps that a change in the dwell times

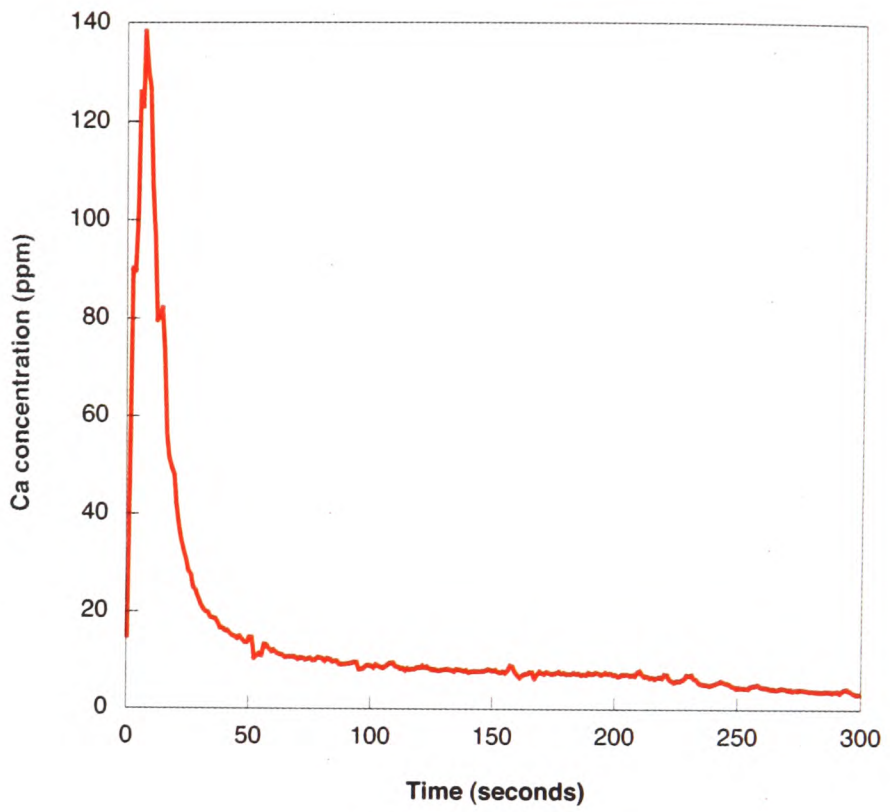

Figure 8. Ca concentration measured over the first 300 seconds of dissolution of a powdered synthetic $CaCO_3$ dissolved at a constant pH.

takes place. The result is that when the user has specified a curve that initially follows a low gradient (as has been done by Klinkhammer et al. (2004) and initially in this study), the gradient pump will begin supplying the initial fluid composition (i.e. 0% of the final acid strength), and continue to do this until the prescribed curve reaches 1% of the final composition. At this point the pump will start dwelling for a short period of time at the inlet from the second fluid. When the initial mixing gradient is low, it may take up to 10% of the estimated dissolution time before this situation is reached. Furthermore, when the final acid strength is high (as it is in Klinkhammer et al. (2004) and this study), this first step causes a very significant stepwise decrease in pH. Figure 7 shows in blue the calculated pH produced when moving from a pH 7 H_2O to a 10% HNO_3 following the gradient pump's mixing procedure. The pH steps can be seen to correlate with the start of dissolution peaks. To test whether these pH steps would cause the observed dissolution curves, experiments were undertaken in which a number of steps were artificially produced at known times, confirming the interpretation that the multiple peak curves are simply an artefact of the gradient pump's mixing protocol. Without knowledge of the mixing curves and timing used

by Klinkhammer et al. (2004), it is not possible to determine definitively if the same logic can be used to explain the peaks in the data they publish, however, the mechanical operation of the pump they use (manufactured by Dionex) is identical to that of the Waters quaternary gradient pump used in this study.

5.8 Further Methodological Development

As discussed in section 4.7, changing the pH of the dissolution acid though the run using a quaternary gradient pump, although initially appealing, produced undesirable results. To avoid peak artefacts the experimental setup was modified to use a constant pH acid throughout dissolution. Using this set-up, multiple peaks in Ca concentration are no longer observed, which further validates our previous interpretation of these features as artifacts (Figure 8).

Sample dissolution at a constant pH requires the consideration of two competing issues. Firstly it is desirable to use a weak acid to allow a slow dissolution, and the chemical signatures relating to different calcite phases to be temporally separated. Secondly, the pH needs to be low enough so that elements released during the dissolution are not re-adsorbed to the sample and walls of the sample delivery system. Although PTFE is highly inert, interaction still occurs between the elements and the various surfaces. This interaction varies between elements, resulting in different mobilities for different elements along the flow-path. In very weak acid solutions, the differential mobility of the elements will mean that even when dissolving a homogenous solid, the concentrations of the various elements dissolved from that solid, as measured as they pass to the ICP-MS, will peak at different times. If one were to then produce element/element ratios from such data, despite the initial solid being chemically homogenous, the ratios would not remain constant. Experiments were carried out to examine the optimal pH for coccolith FT-TRA dissolution by pumping a synthetic

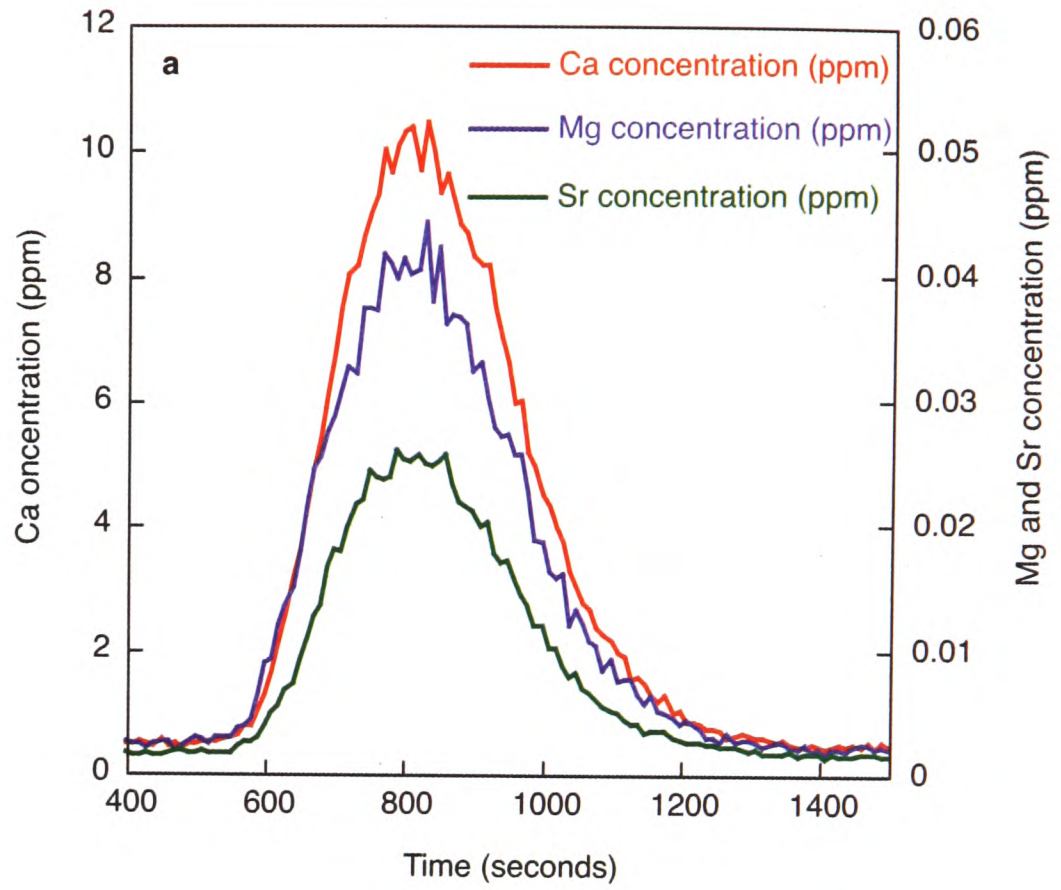

Figure 9. a. Ca, Mg and Sr concentrations measured during the rinsing of the flow-through system with a pH 2.5 HNO_3 after intentionally being contaminated with a synthetic standard. The synchronicity of the element peaks indicates equal mobility between the different elements. **b.** Mg/Ca and Sr/Ca ratios over the same interval. Constant element/Ca during the Ca peak confirms the similar mobility of these elements. Either side of the Ca peak ratios are elevated - this results from large errors associated with numerators and denominators of the ratios being very low.

standard (with a composition similar to that expected to be measured in the coccoliths) through the system, washing the fluid out with deionised water, then pumping acid with various pHs through to mobilise the surface sorbed ions. Figure 9 shows the results of this experiment when undertaken at pH 2.5. The synchronicity of the peaks of Ca, Mg and Sr and the stability of element/Ca ratios, when flushed through the FT-TRA system at pH 2.5 indicate equally mobile. For this reason all future dissolution experiments should be carried out at or below pH 2.5.

The results and discussion presented so far in the chapter add significantly to our understanding of FT-TRA, and its application to the analysis of coccolith samples. It appears that the major obstacle to understanding the results of previous analyses has been a misunderstanding of operation of the proportioning valve. Future FT-TRA experiments using a quaternary gradient pump should therefore be undertaken at a constant pH, where the pH is 2.5 or lower. In light of these new developments, experiments have been designed to examine the chemistry of cultured coccolith samples to provide new information about the incorporation of trace-elements into the $CaCO_3$ structure.

Figure 10 presents a set of trace-element dissolution analyses obtained from two sub-samples from a single culture of *C. pelagicus* in which the organic material has been removed. The organic removal process involves ultrasonically treating, then heating the sample at 70°C in NaOH buffered H_2O_2 for one hour, then leaving the sample in this solution overnight. The samples were then centrifuged at 13,000 rpm, rinsed with Aristar grade ethanol, transferred to new acid cleaned centrifuge tubes, ultrasonically treated for one minute then rinsed a further four times with ethanol. The dissolution took place over one hour at pH 2.5 with a flow rate of 0.1 ml min^{-1}. It should be noted that element calcium ratios obtained using FT-TRA are inherently noisy because each point represents only five seconds of analysis, ~30 times shorter than a typical batch analysis, and therefore represents a mean value with large variance. Furthermore much of the analysis occurs at low elemental concentrations where errors will be greatly amplified when the elements are expressed as ratios.

5.9 Coccolith Dissolution at Constant pH: Results and Discussion

The results presented in Figure 10 display the evolution of trace-element/Ca ratios during dissolution of two separate coccolith sub-samples (*C. pelagicus* grown at 15 °C). Obtaining such data requires that the machine drift in the ICP-MS remains minimal and predictable. The difficulties in obtaining 'good' data are discussed in sections 5.5 and 5.6, however here the discussion will focus on the implications of these results for our understanding of the trace-element composition of *C. pelagicus* coccoliths.

The primary features to note in Figure 10 are:

- Steady and reproducible Sr/Ca measurements at ~3.5 mmol/mol throughout the dissolution.
- Repeatable Mg/Ca, Ba/Ca and Mn/Ca rapidly decreasing from a high initial value, tending towards a value within analytical error of 0 μmol/mol.
- A repeatable decrease in Cd/Ca from ~3.5 to ~2 μmol/mol during the first half of the dissolution, followed by a plateau at ~2 μmol/mol for the remainder of the dissolution experiment.
- Poorly reproducible Zn/Ca decreasing from ~700 to ~400 μmol/mol over the period of dissolution, with an initial rise in Zn/Ca recorded in Sample A.

Figure 10. (on adjacent page) Sr/Ca, Mg/Ca, Ba/Ca, Mn/Ca, Cd/Ca and Zn,Ca ratios measured throughout 3500 seconds of dissolution in two individually cleaned sub-samples of a cultured *C. pelagicus* sample. Samples were recovered from the culture medium by filtration, then treated ultrasonically for 10 minutes and left overnight in 70°C in a mixture of 50:50 H_2O_2:NaOH. Samples were centrifuged at 13000 rpm, liquid pipetted from the tubes and rinsed five times with Aristar grade C_2H_5OH and twice with 18 MΩ H_2O.

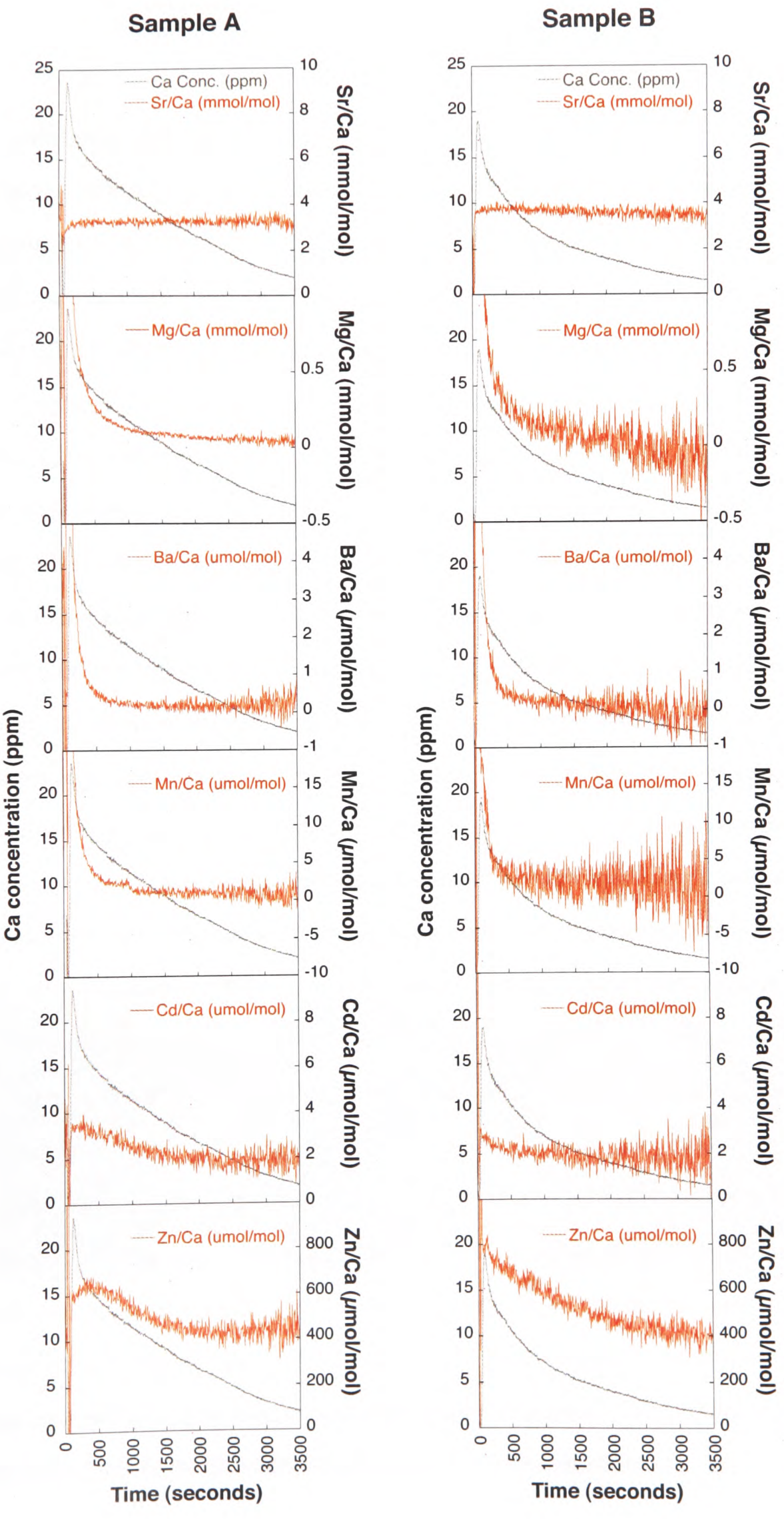
Sample A
Sample B
Ca Conc. (ppm)
Sr/Ca (mmol/mol)
Mg/Ca (mmol/mol)
Ba/Ca (umol/mol)
Mn/Ca (umol/mol)
Cd/Ca (umol/mol)
Zn/Ca (umol/mol)
Ca concentration (ppm)
Sr/Ca (mmol/mol)
Mg/Ca (mmol/mol)
Ba/Ca (µmol/mol)
Mn/Ca (µmol/mol)
Cd/Ca (µmol/mol)
Zn/Ca (µmol/mol)
Time (seconds)

5.9.1 Sr/Ca

The FT-TRA Sr/Ca signal will be considered first (Figure 11). Sr/Ca is the only trace-element to have previously received significant attention in coccolithophore calcite. A background to coccolith Sr/Ca as a palaeoproxy is provided in Chapter 1. The value of ~3.5 mmol/mol for *C. pelagicus* Sr/Ca is consistent with previously published data (for a culture maintained at 17°C Stoll et al. (2002c) measured a *C pelagicus* Sr/Ca of 2.9 mmol/mol), however the spatial distribution of this Sr in the coccolith has not previously been explored. Analogy with foraminiferal calcite might suggest an inhomogeneity in coccolith Sr/Ca. Figure 12, modified from Kunioka et al. (2006) shows a NanoSIMS image of a cross section through part of a foraminiferal chamber. The first two panels from the left show the Mg and Sr distribution respectively considered as ratios with Ca. The right hand panel displays an electron backscatter image of the same cross-section. It can be seen that both the Mg and the Sr are enriched along layers within the test, and in regions towards the inside of the test. Kunioka et al. (2006) interpret these trace-element rich layers as being associated with organic membranes which have been incorporated into the test during growth, however, recent work by Eggins et al. (2007) suggests otherwise. Eggins et al. (2007) have used laser ablation mass spectrometry to bore through foraminifera tests [although the tests belong to different species than those examined by Kunioka et al. (2006)], measuring the elemental composition at progressively greater depths. To test the source of these high Mg layers, the authors performed experiments to ascertain during which stage of the life cycle they were precipitated. To do this, the authors moved cultures between a low [Ba] culture medium during the day, and a high [Ba] culture medium at night. Previously Ba had been constant throughout the test, but now, the Ba and Mg varied together. The authors conclusion was that these element rich layers are precipitated at night when the symbionts have been drawn into the test and consequently the environment of calcification altered (perhaps by altering the ambient pH). Irrespective of the mechanism, it is clear that there are significant inhomogeneities in foraminiferal trace-element distribution. Figure 11 indicates that a more

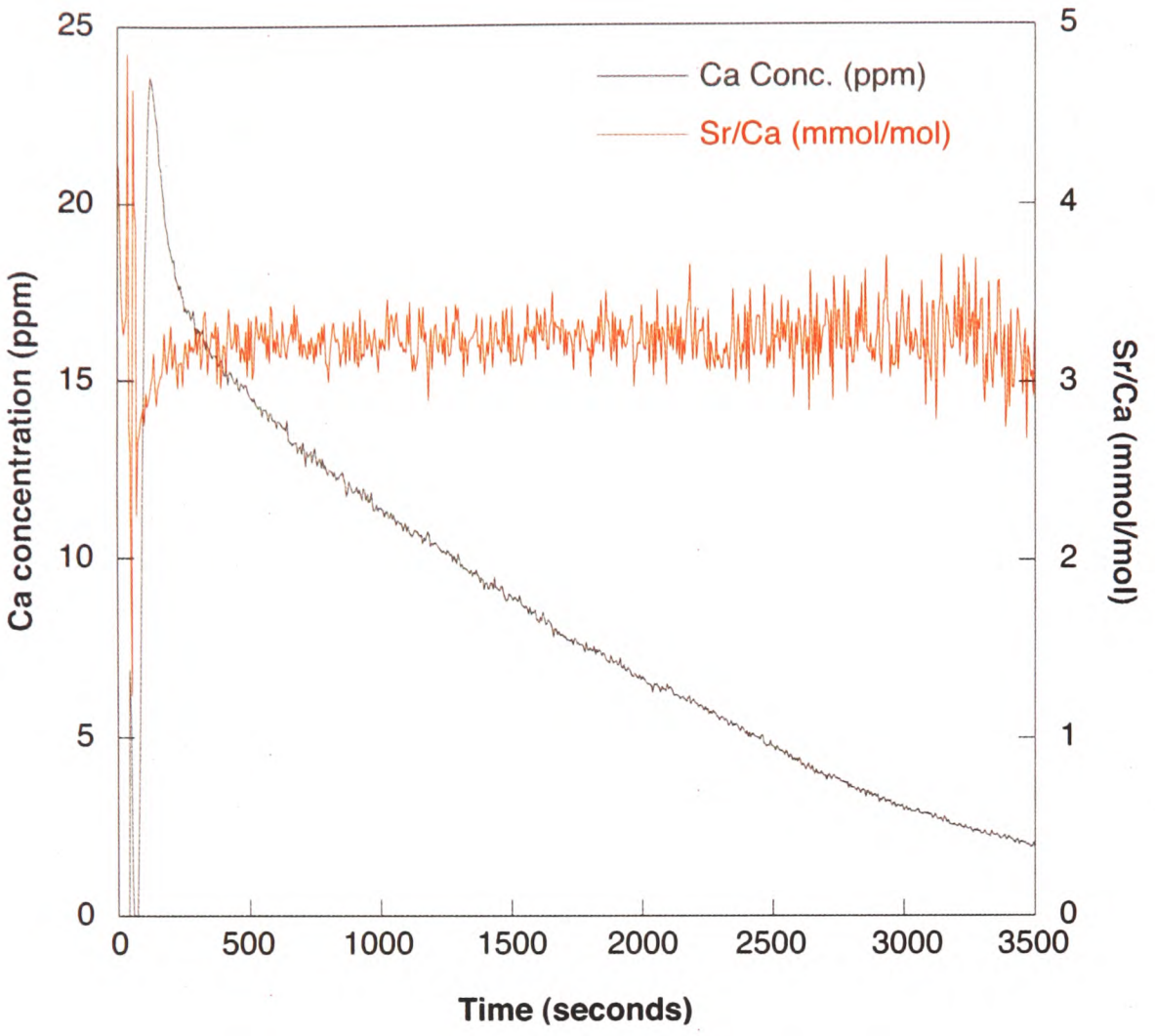

Figure 11. Sr/Ca ratios (mmol/mol) and Ca concentrations (ppm) measured during the dissolution of Sample A (*C. pelagicus*).

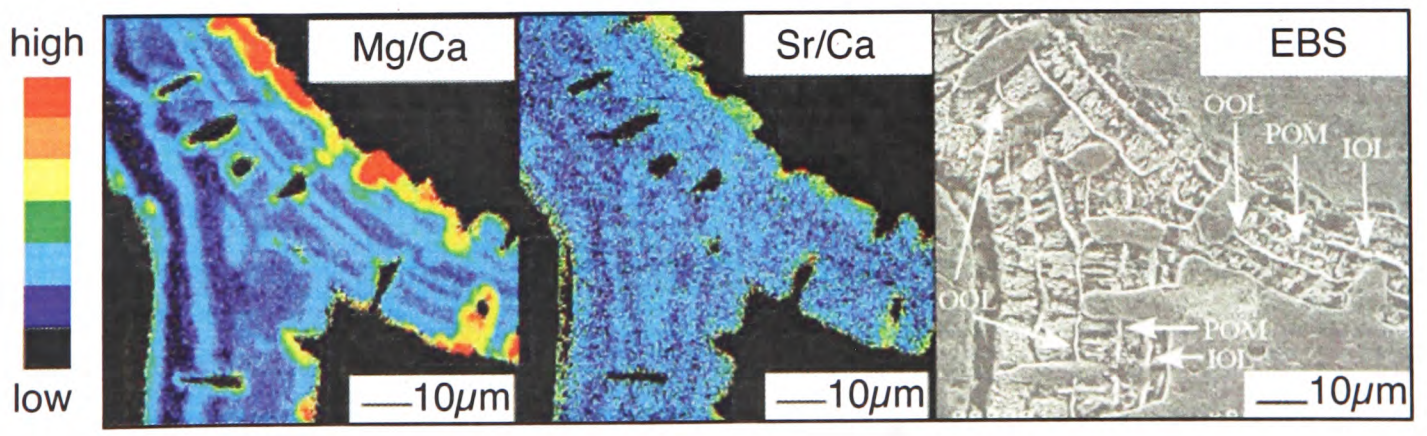

Figure 12. NanoSIMS Mg/Ca, Sr/Ca and electron backscatter images looking at a section through a foraminifera test. In the element maps, bright colours show high Mg or Sr concentrations (relative to Ca), and in the backscatter image, light shades show high electron density.

simple picture is observed in coccolithophore Sr/Ca. The dissolution data from cultured *C. pelagicus* show an initial increase in Sr/Ca of ~0.4 mmol/mol over the first ~100 seconds, followed by a plateau at ~3.2 mmol/mol. The constant Sr/Ca ratio over the majority (latter ~3300 seconds) of dissolution likely indicates that the bulk of the coccolith calcite has a constant Sr/Ca ratio. The initial increase in Sr/Ca is interesting, and potentially indicates a slightly lower Sr phase making up part of the coccolith. The possibility of multiple calcite phases within the coccolith will be explored in section 5.11 following preliminary discussion of the remaining measured elements.

5.9.2 Mg/Ca, Ba/Ca and Mn/Ca

Figure 13 illustrates *C. pelagicus* Mg/Ca Ba/Ca and Mn/Ca flow-through data. These three elements have been grouped together in the discussion due to the similarity in their dissolution curves. All display a trace-element/calcium ratio which rapidly decreases from the start of dissolution and appears to be tending towards zero (within the error of FT-TRA analysis). These curves could be explained by two phenomena:

- The washing out of contaminants sorbed to the surface of the sample
- Mixing between dissolution of a highly soluble trace-element rich phase and a less soluble trace-element poor phase

If the first phenomena was being recorded, a washing out of surface contamination, analogy with our pH experiments would indicate that contaminants should be removed within about 600 seconds of the start of dissolution (Figure 9). However two factors could potentially retard this process. Firstly, in the experiment illustrated by Figure 9, elements must have been sorbed to the various outer surfaces in the filter housing and tubing (because no other surface is avaliable). Therefore, when acid was introduced, all these surfaces would have immediately been in contact with the acid. When considering a coccolith sample, it is

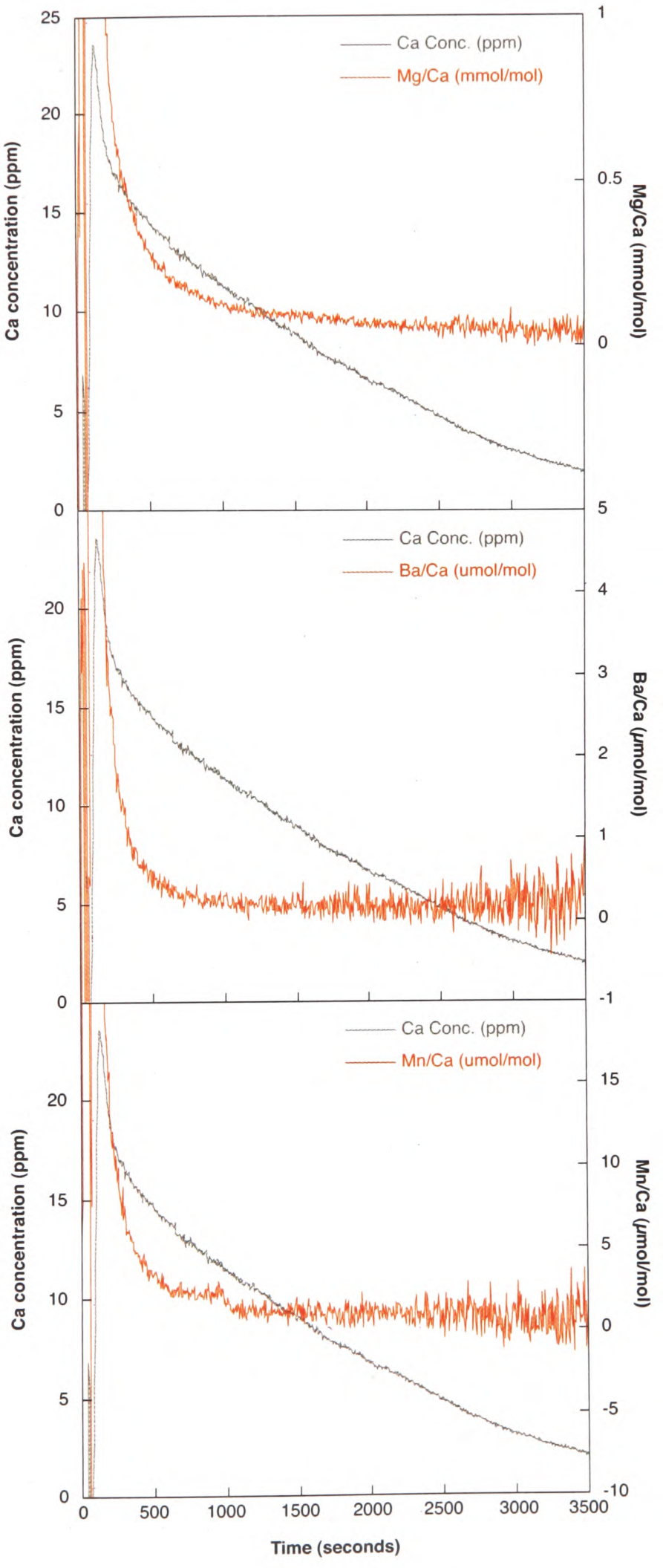

Figure 13. Mg/Ca, Ba/Ca and Mn/Ca data from *C. pelagicus* Sample A.

possible that not all surfaces are initially exposed. Secondly, it was ascertained that pH 2.5 was suitable for these experiments to be undertaken because at this pH the elements appeared to be equally mobile. However, during a coccolith FT-TRA experiment the dissolution of the coccoliths will cause the pH in the sample chamber to rise and potentially result in a reduced mobility of the measured elements.

The second possible explanation for the rapid decay in Mg, Ba and Mn/Ca ratios through the dissolution experiment is that the curves represent mixing between dissolution of a highly soluble trace-element rich phase and a less soluble trace-element poor phase. To explore this option we must consider the potential origin of these two phases. The three most likely explanations for the existence of two phases are listed below:

- A trace-element rich contaminant phase precipitated during cleaning and a low trace-element coccolith phase
- Two phases of calcite precipitated by the coccolith, each with different trace-metal concentrations
- A primary coccolith phase and a secondary altered coccolith phase

To consider which of the above explanations may account for the observed trace-element/Ca curves it is valuable to consider the initial trace-element/Ca ratio at which the dissolution curves begin (Figure 14). Figure 14 presents the Mg/Ca, Ba/Ca and Mn/Ca data for the first 125 and 175 seconds of dissolution of Sample A (red) and Sample B (blue) respectively. Note that the lag between Sample B and A peak values relates to the manual lag between starting the analysis on the ICP-MS, and starting the gradient pump. Sample B peaks at higher values than Sample A, initially suggesting that, if the curves represent dissolution of a two component system, the contaminant phases in the two sub-samples have different chemical compositions, which is unlikely considering their common source. It is possible that the difference in peak height is the consequence of a sampling bias resulting from having

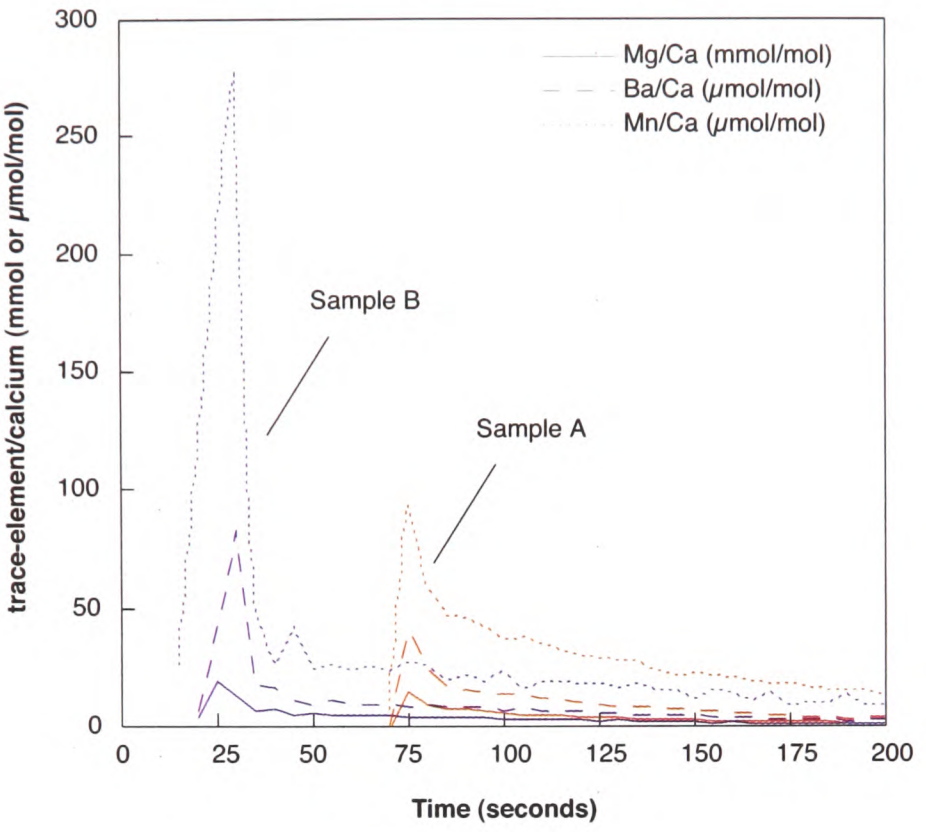

Figure 14. Trace-element/Ca ratios from samples A and B over the first 125 and 175 seconds of dissolution respectively. The temporal lag between peak values results from variability in the manual lag between beginning analysis on the ICP-MS and beginning the dissolution experiment.

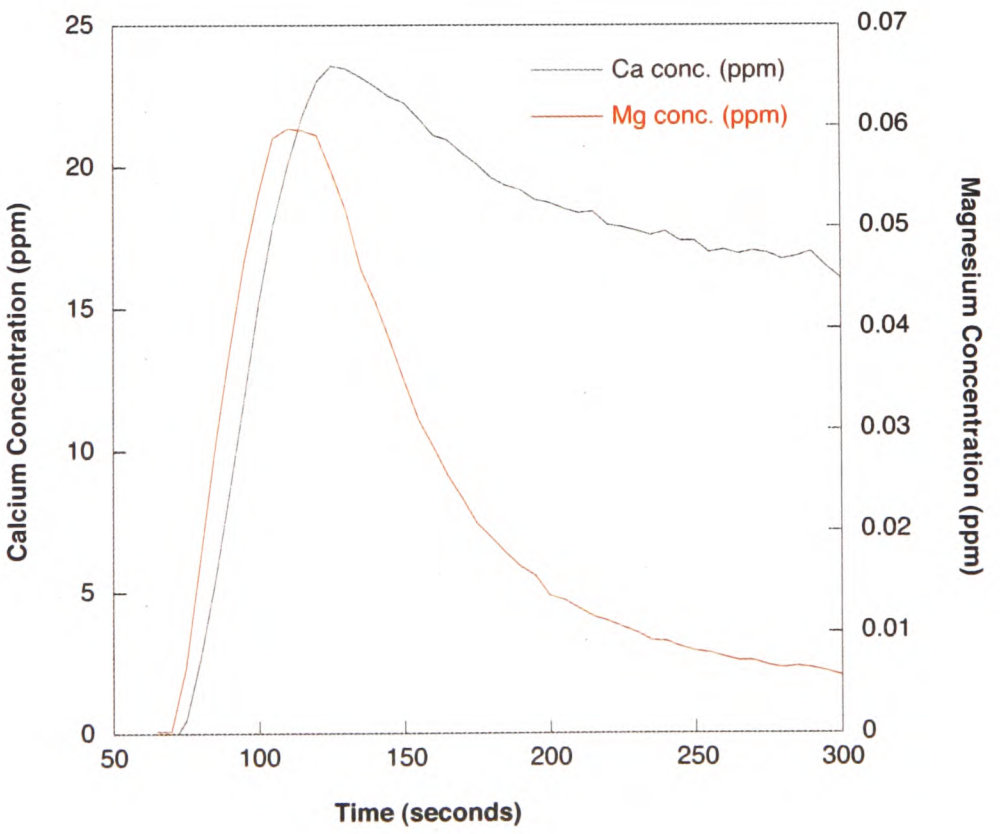

Figure 15. Mg and Ca concentrations measured in *C. pelagicus* Sample A over the first 300 seconds of dissolution. The peaks are not synchronous, indicating that Mg is a contaminant phase and not associated with the $CaCO_3$ lattice.

only a five-second analysis resolution, however Figure 15 shows that the Mg concentration rises and peaks before the Ca concentration, indicating that the Mg is not associated with the Ca, and therefore is not being released from the $CaCO_3$ lattice, instead representing contamination.

A further useful observation is that beyond the peak in element composition, the decreasing value of [Mg], [Ba] and [Mn] closely approximate power curves (Figure 16). The approximation to power curves tells us two things. Firstly, assuming that we are correct in interpreting the signal as contamination, there is no significant Mg, Ba or Mn release from the calcite at any stage in the experiment. This can be inferred because, unless a secondary element source was releasing cations at exactly the same rate as the primary source (contamination), then the curve would be modified in shape. Secondly, the contaminant must interact significantly with the sample surface. If the contaminant was only loosely associated with the sample, we would expect to see an exponential decline in concentrations

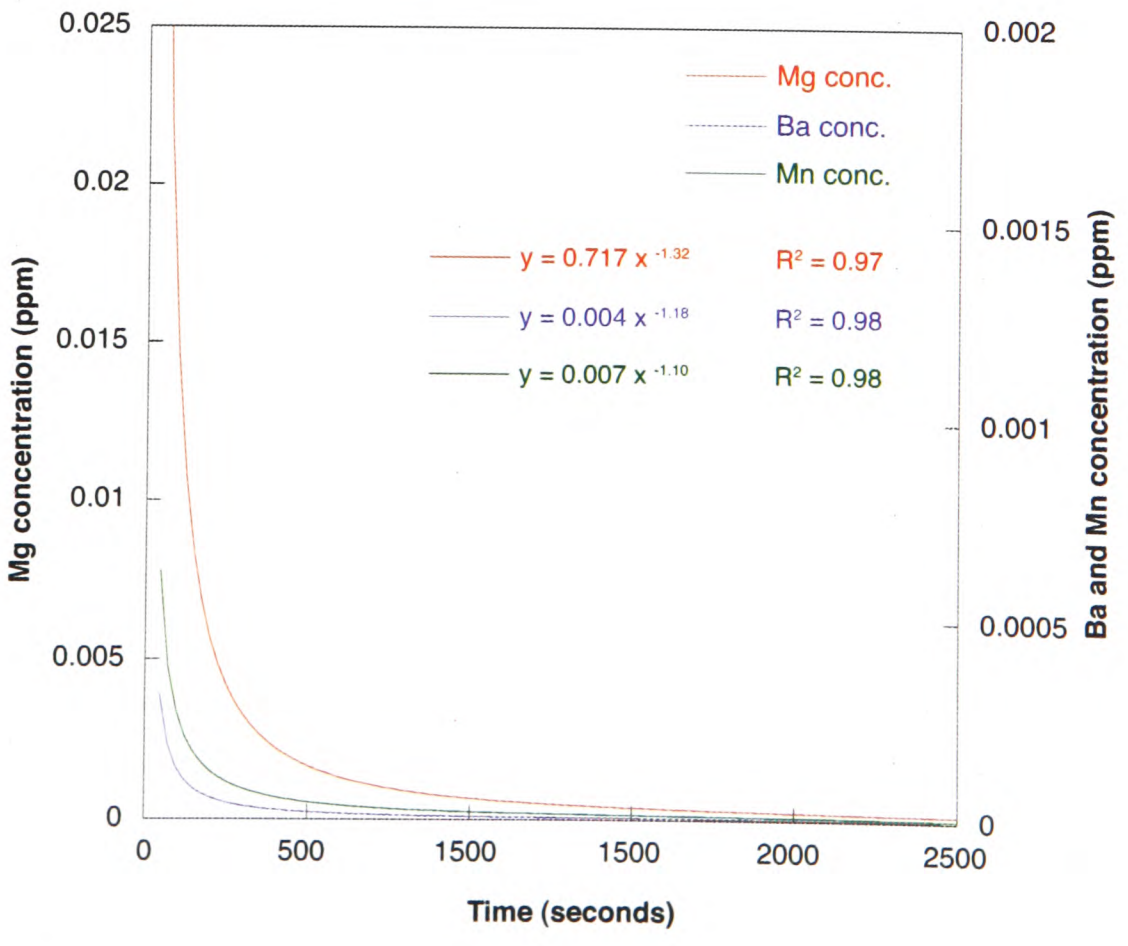

Figure 16. Mg, Ba and Mn concentrations measured in Sample A over 1500 seconds of dissolution, together with fitted power-law curves.

as the contaminant is removed by dilution. In conclusion, we can say that *C. pelagicus* Mg/Ca, Ba/Ca and Mn/Ca values are, within the error associated with FT-TRA, zero.

5.9.3 Cd/Ca

Figure 17 illustrates the evolution of the Cd/Ca curve through the dissolution experiment, starting from a high of ~3.4 μmol/mol and decreasing to a plateau at ~2.9 μmol/mol by half way through the experiment. It might be considered that the described curve represents initial contamination as observed in Mg/Ca, Ba/Ca and Mn/Ca, however, examination of the peak in concentration values (Figure 18) suggests otherwise. The tight temporal correlation between the peak [Cd] and peak [Ca] values shown in Figure 18, unlike those observed in [Mg] and [Ca] (Figure 15), suggests that the measured Cd is released with Ca from the $CaCO_3$ structure. The curve therefore represents either a primary Cd inhomogeneity within the coccolith, or contamination which has entered the surface of the calcite lattice (Stipp et al., 1992). The latter may occur by diffusion if the calcite is held in a Cd-rich solution. Stipp et al. (1992) examined calcite crystals which had been exposed to a Cd-rich solution for between 1 and 100 minutes using x-ray photoelectron spectroscopy. The authors found that Cd could penetrate up to 3 nm into the calcite lattice. Assuming a typical *C. pelagicus* shield has an average thickness of ~500 nm, this would equate to a Cd-enriched rim of thickness less than 1% of the shield thickness. A rough estimation of *C. pelagicus* surface area to volume ratio is 1.9 (appendix C), and therefore assuming a 1% penetration of Cd into the surface, we would expect less than 2% of the coccolith volume to have an elevated Cd concentration. Unless the Cd penetration depth for our samples is considerably larger that shown by Stipp et al. (1992) as a result of longer exposure times to Cd, it is unlikely that lattice penetration of Cd can explain the observed curve. It is therefore possible that the curve is explained by the existence of two chemically distinct primary calcite phases within the coccolith. This will be explored in section 5.10.

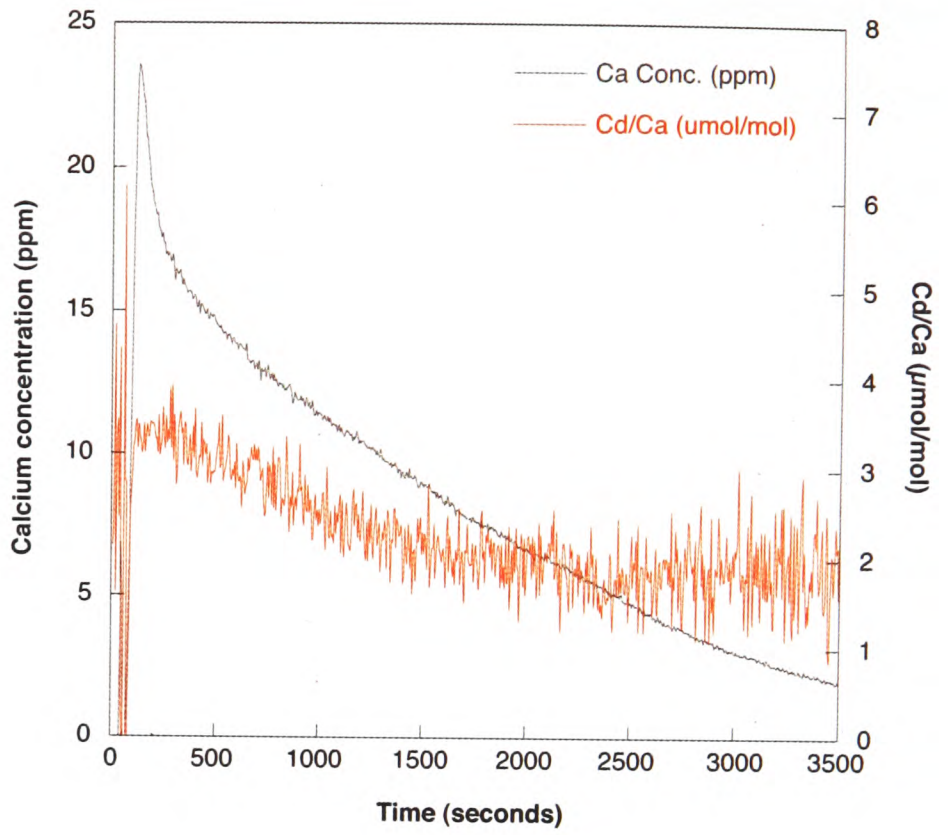

Figure 17. Ca concentrations and Cd/Ca ratios from *C. pelagicus* Sample A.

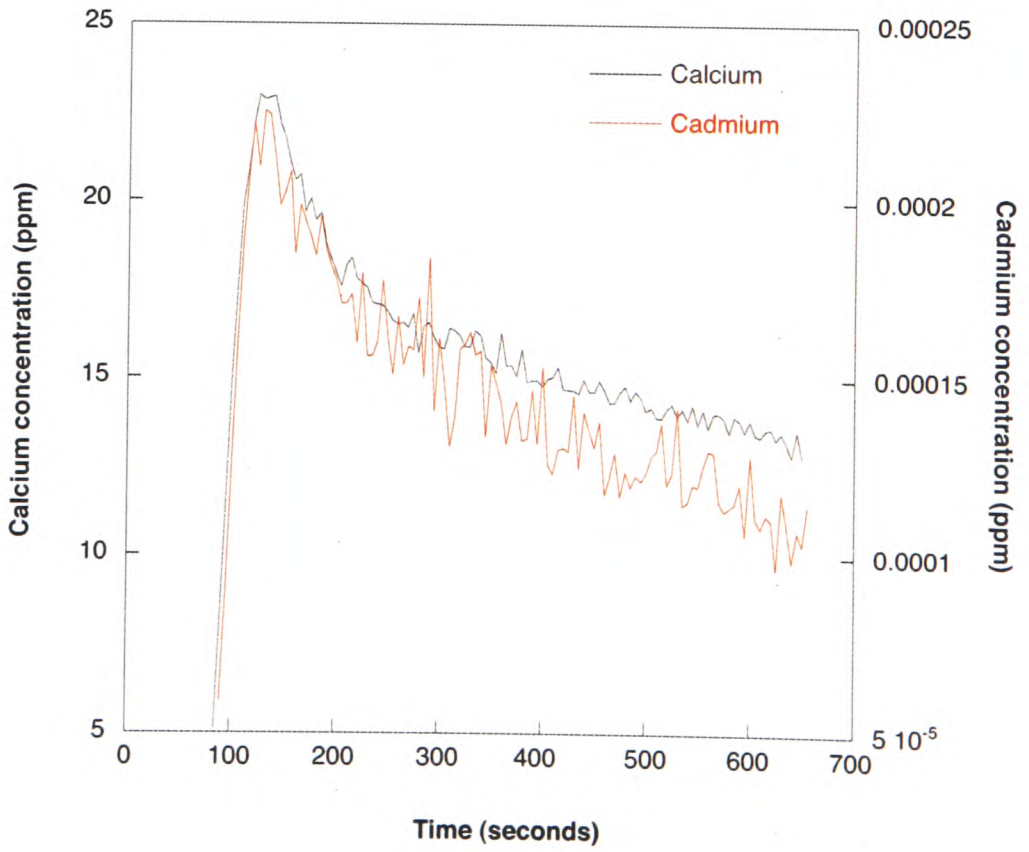

Figure 18. Ca and Cd concentrations measured from the first 700 seconds of dissolution of *C. pelagicus* Sample A. The tight temporal correlation of the peaks indicates the Cd is being released from the $CaCO_3$ structure.

5.9.4 Zn/Ca

The final trace-element/Ca data presented is that measured for Zn/Ca (Figure 19). As stated earlier in this section, the results for Zn/Ca, show poor reproducibility. Sample A begins with a rising Zn/Ca peaking at 650 μmol/mol, falling to a plateau at ~425 μmol/mol by ~1500 seconds. Contrastingly, Sample B shows no initial increase, instead decreasing throughout the dissolution from a ratio of ~800 μmol/mol to a ratio of ~400 μmol/mol. It is tempting to assume the two datasets do not agree because the samples contain Zn contamination, however the [Zn] peaks correspond with the [Ca] peaks, unlike for the contaminated Mg (Figure 14) suggesting that the Zn is being released from the calcite. A further indication of contamination might be the high values of Zn/Ca [a factor of 100 greater than a typical foraminiferal Zn/Ca (Marchitto et al., 2000)], however this is likely to reflect the high Zn/Ca of the medium in which the coccolithophores were cultured (Appendix D). A further indication that the signal measured in Sample A does not represent contamination is the increasing feature during the early stage of dissolution. Unless the contamination is in the form of an inhomogeneous precipitate, one would not expect a contaminant signal to increase with time during the dissolution. It is possible that the measured Zn/Ca signal from Sample A represents the dissolution of a three phase coccolith calcite, where initially a low-Zn phase is dissolved, followed by a higher Zn phase and finally a less Zn-rich phase with Zn/Ca ~400 mmol/mol. This interpretation could be consistent with the dissolution of Sample B if a limited amount of contaminant were initially removed from the sample, masking the initial Zn/Ca increase. A further explanation of this data would be the non-linear machine drift of Zn measurements as will be discussed in section 5.12.

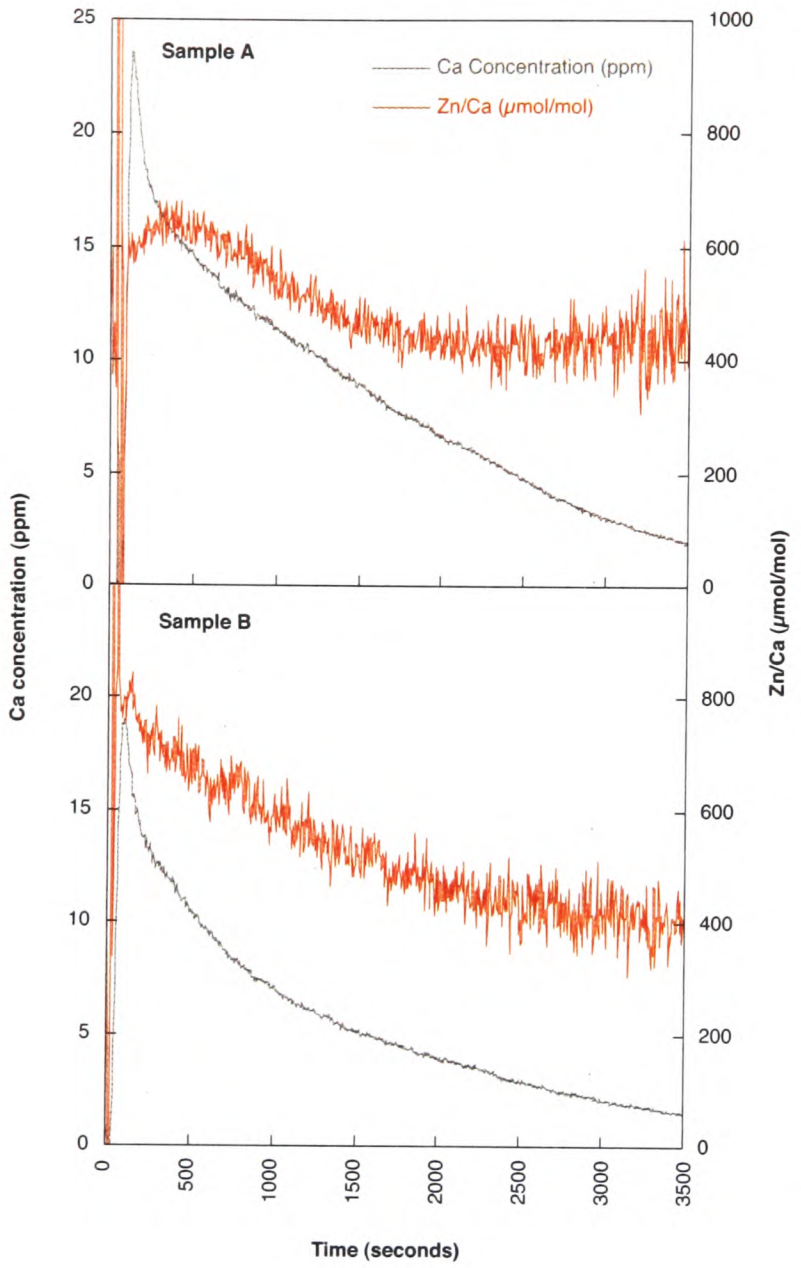

Figure 19. Zn/Ca (µmol/mol) measured during the dissolution of cultured *C. pelagicus* coccoliths from Samples A and B, individually cleaned subsamples from a common culture.

5.10 A Crystallographic Control over Coccolith Calcite Trace-element Incorporation and Distribution?

Heterococcoliths provide an elegant test-case for models of biomineralisation, as a result of their simple crystallography. These coccoliths are constructed from a number of single crystals growing from an initial ring of alternating vertically and radially oriented nucleation sites, with respect to the crystal's optical axis (Figure 20) (Young et al., 1992). Different coccolith species can be distinguished by their appearance in cross polarised light, a consequence of their differing crystallographies. This feature of coccoliths has allowed simple recognition and extensive study despite their small size.

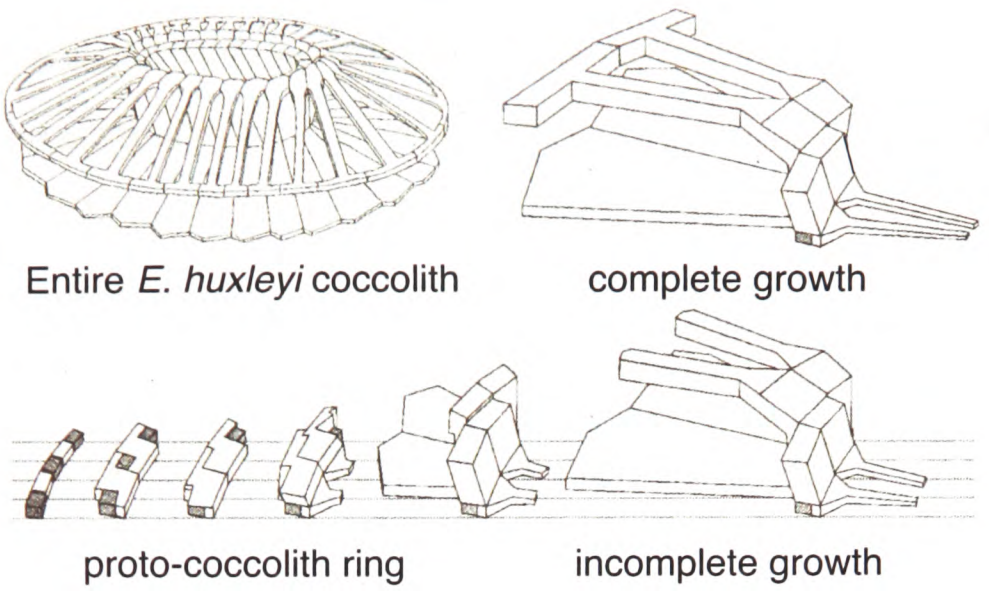

Figure 20. Crystallographic formation steps of *E. huxleyi* coccoliths. Initially a proto-coccolith ring of alternating V and R crystals (crystals with their optical axis vertically 'V' and radially 'R' aligned to the plain of the coccolith) is precipitated from the vesicle fluid. In the case of *E. huxleyi* the R-crystals then grow upwards and outwards to produce the final complex coccolith morphology, and the V-crystals undergo no further growth. In different species the relative growth of V or R-units varies. From Young et al. (1992).

Meticulous light and scanning-electron microscope observations by Young and co-workers (Henriksen et al., 2004c, Marsh, 1999, Young et al., 1999, Didymus et al., 1994) have distinguished the different units and growth stages of coccoliths belonging to a number species. Here the possibility that crystal structure and growth exert a primary control over trace-element incorporation into biominerals, as suggested by Paquette and Reeder (1995) is examined. Paquette and Reeder (1995) measured trace-element concentrations in transects across neighbouring calcite growth faces, demonstrating that different site geometries on different calcite faces result in different trace metal incorporation, and consequently growth rates. New growth progresses across a crystal surface at the front of a step which divides the newly formed slab and the previously precipitated layer. In a typical calcite rhombohedron, these steps contact the lower surface at an angle of either 102°, an obtuse step, or 78°, an acute step. Initial work suggested that at the obtuse growth front, divalent cations larger than Ca^{2+} were incorporated in preference to divalent cations smaller than Ca^{2+} (Paquette and Reeder, 1995). However this rule breaks down in the case of Zn^{2+} (Reeder, 1996), indicating that there are factors other than geometry, controlling the incorporation.

Work by Young and others (Henriksen et al., 2004c, Marsh, 1999, Young et al., 1999, Didymus et al., 1994) suggests that many, if not all, coccoliths share a common mode of growth and fundamental structure. Both Didymus et al. (1994) and Marsh et al. (1999) document the formation of a protococcolith ring comprising rhombic calcite crystals in alternating vertical (V-units) and radial (R-units) crystallographic orientations, associated with some kind of organic base plate. Arranged into numerous structures by so far poorly understood processes, these crystals grow to produce the many diverse duel-disk layer forms observed in different species, and maintain their optical orientations during growth. It has been argued by Rickaby et al. (2006) that because both the V and R units of the protococcolith ring must grow in a common planar orientation, they must primarily grow on different crystallographic faces, and probably through different growth steps. It has therefore been suggested that through the mechanism proposed by Paquette and Reeder (1995) the V and R units of coccoliths could record different trace-element chemistries (Rickaby et al., 2006). To test this theory a *C. pelagicus* sample, was cleaned for organic material, mounted the sample in resin and the surface polished for examination using an electron microprobe. The resulting images show what appears to be a crystallographically organised inhomogeneity (Figure 21), with a low Mg concentration in the V-units (highlighted by grey areas in the upper part of the diagram) and a higher concentration in the R-units (shown in white). Unfortunately, electron microprobe analysis neither has the sensitivity to measure the elemental concentrations we would predict to see from our flow-through analysis, nor has the resolution to accurately determine elemental composition on a sub-micron scale as required in this situation. Because the electron excitation volume of the element is larger than the point resolution of the microprobe, near the edge of a structure, 'edge-effects' may be observed. These 'edge-effects' could potentially explain the high-Mg rims around coccoliths observed in the microprobe images, and mean that low-Mg measurements are recorded only in areas away from a crystal edge, irrespective of sample chemistry.

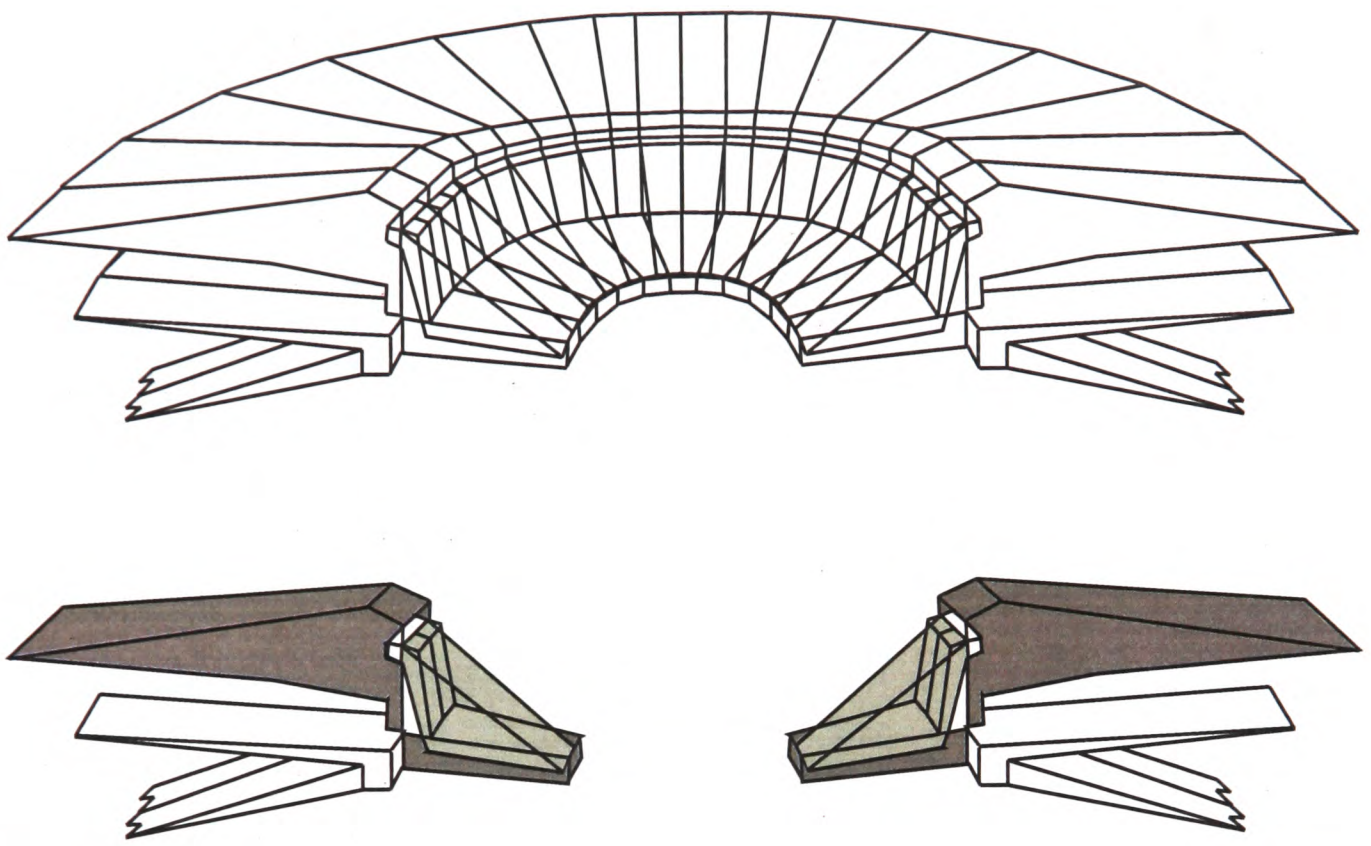

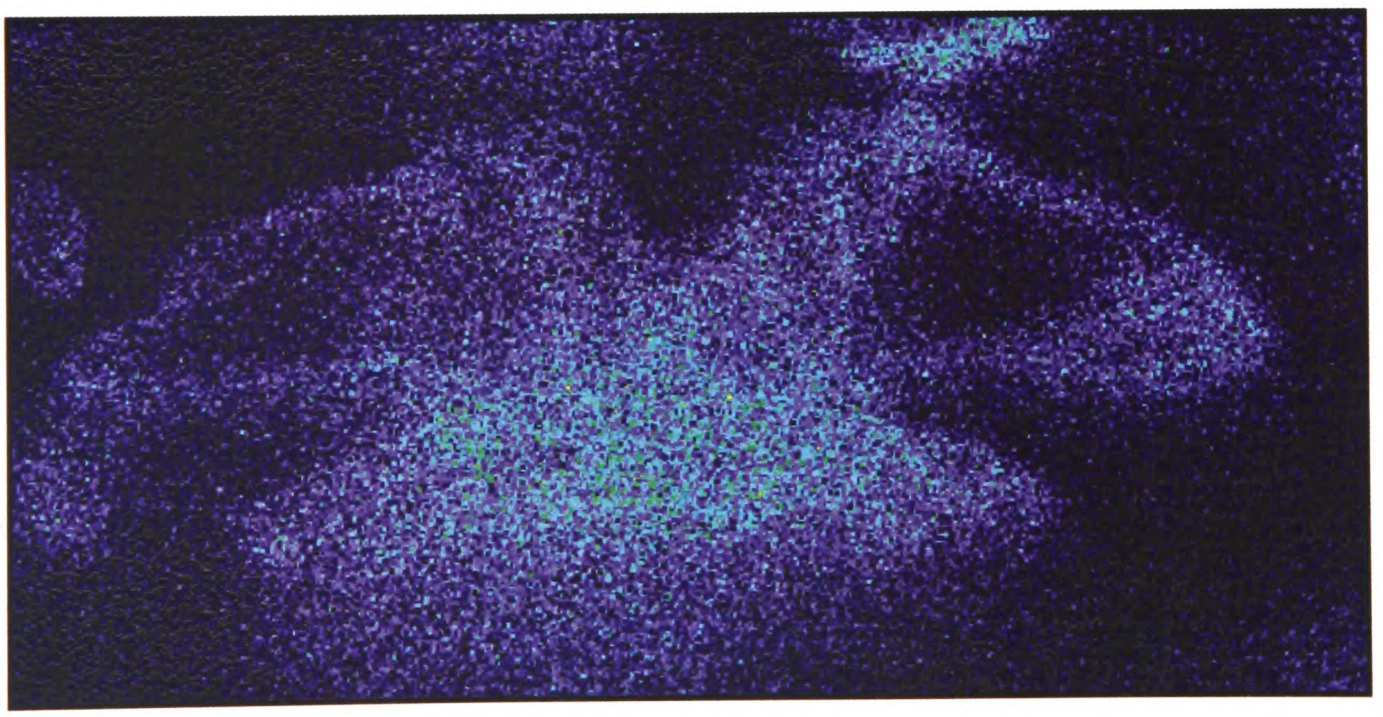

Figure 21. Top: *C. pelagicus* crystal structure (white highlights R-units and grey represents V-units). **Bottom**: Microprobe intensity image of Mg distribution in a sectioned *C. pelagicus* coccolith. Bright colours represent high Mg, dark colours represent low Mg.

To investigate whether the potential inhomogeneities indicated in the flow-through dissolution experiments, and hinted at using the electron microprobe, could be explained by the V-R mechanism it is necessary to understand how dissolution is progressing within the FT-TRA system. If indeed the complex FT-TRA data are linked to a multi-stage dissolution process, corresponding to the chemical compositions of the individual crystallographic units, the different units (V and R) should dissolve at different rates. Imaging of a single coccolith through dissolution is not possible under a conventional light microscope because the individual coccolith units are sized comparably with the wavelength of light. Furthermore, when wishing to sequentially dissolve a sample it is important to use a technique which does not require surface coating (such as conventional SEM). It was decided to image the coccoliths using Atomic Force Microscopy (AFM) which has two major advantages; firstly, the system is open to the air so dissolution can be undertaken in-situ, and secondly AFM produces three-dimensional data for the coccoliths, so the dissolution could be observed in all dimensions.

5.11 Investigating Coccolith Dissolution Using Atomic Force Microscopy

AFM is a high-resolution form of microscopy based on measurement of the interaction between a scanning probe and the samples surface. A silicone cantilever, the end of which is etched precisely into a tip with a curvature of radius ~10 nm, is moved back and forth across the sample, scanning in a series of parallel lines from one edge to the opposite edge (Figure 22). Topography encountered by the tip causes the soft cantilever to bend up or down. Displacement of the cantilever causes the laser beam incident upon its upper surface to be deflected. Because the incident beam has a vector component in the same direction at the length of the lever, flexing of the lever causes a change in the angle of reflectance. The displacement is amplified over the distance it travels to the photodiode receiver (analogous

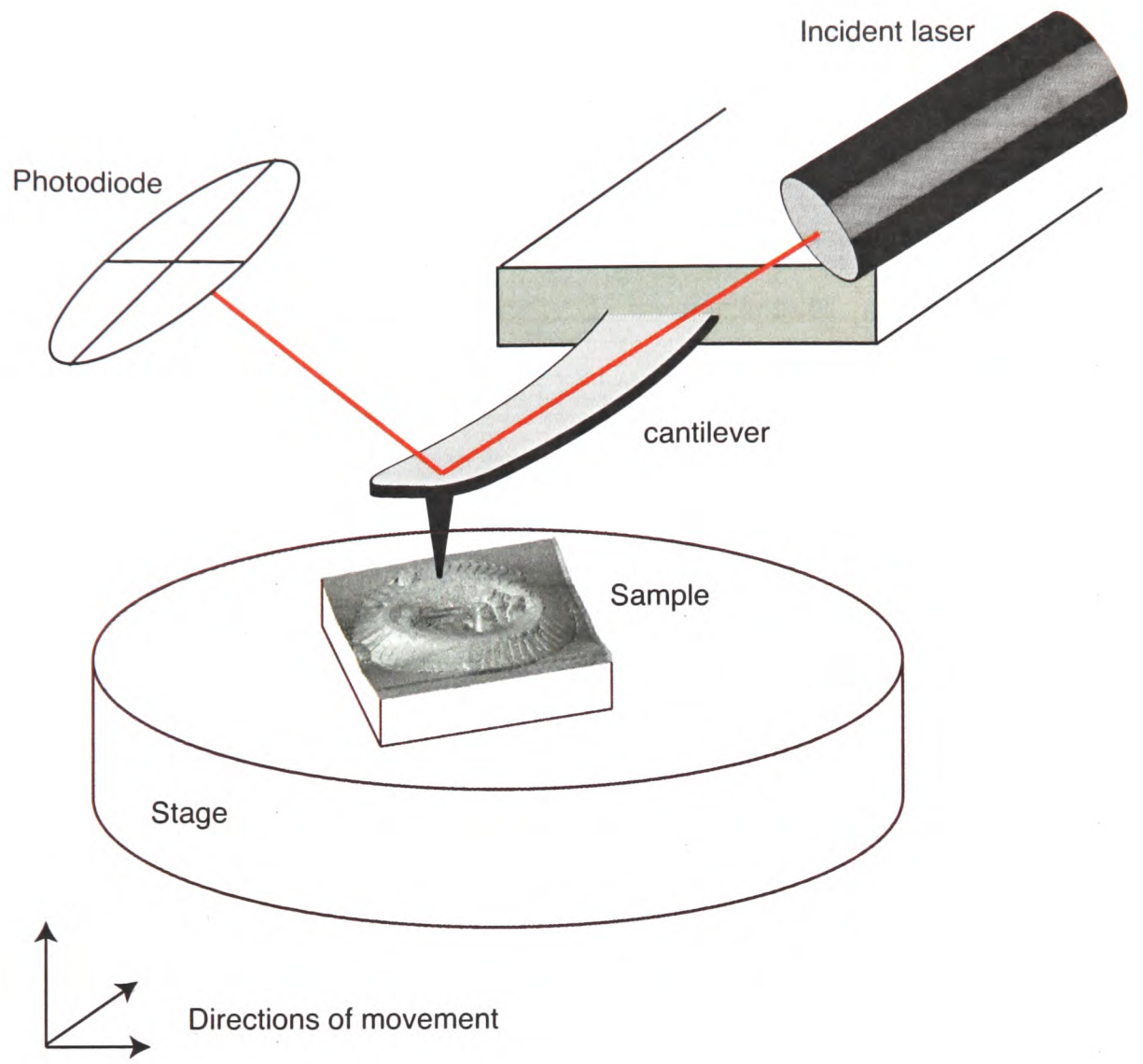

Figure 22. Outline of an Atomic Force Microscope (AFM). See text for explanation. Re-drawn and modified from www.farmfak.uu.se.

to twisting ones wristwatch subtly on a sunny day and moving the reflected point of light over a large distance). The photodiode matrix and laser position will initially be organised in such a way that the laser provides equal stimulation to two halves of the photodiode matrix (i.e. falls between two detectors). When the beam is deflected, one half of the diode matrix will receive more light and produce a stronger signal than the other, and a rapid feed-back loop will respond by moving the stage (upon which the sample is mounted) up or down to again zero the difference between the two photodiode signals. This vertical movement (controlled by the voltage applied to a piezoelectric tube) is recorded, and over a few minutes, a topographic image of the whole sample is produced.

5.11.1 AFM Sample Preparation and Imaging

Four studies have so far examined coccolith structure using AFM (Henriksen et al., 2003, Henriksen et al., 2004a, Henriksen et al., 2004c, Takahashi-Shimase and Nakashima, 2004), but only one of these has attempted to look at whole coccolith shape change during dissolution (Takahashi-Shimase and Nakashima, 2004). A major factor when designing an AFM dissolution experiment is how best to mount the sample to prevent it from moving, but avoiding embedding the sample in a resin such that the surface exposed to the dissolution liquid is limited. Furthermore, it is not ideal to introduce an adhesive substrate as one might for SEM analysis because the solvents associated with the adhesive layer may interfere with the dissolution. A further consideration is to avoid the use of excessive insulating material such as a plastic dissolution chamber, because the build-up of static will interact with the AFM lever, reducing image quality. Our investigations found it was best to prepare samples by placing a hydrophobic silica pad onto a glass slide, and deposit onto that a coccolith sample held in ethanol (which subsequently evaporates). The hydrophobic nature of the silica pad allowed rapid and complete supply and removal of the weak dissolution acid, whilst the hydrophilic calcite surface ensured interaction between the coccolith and the acid. No lateral movement of the coccoliths occurred in response to the acid flushing. The dissolution experiments were undertaken by optically recognising a complete coccolith (again *C. pelagicus*) lying parallel to the silica surface (recognised by the coccolith's simple oval shape in reflected light), then lowering the probe and imaging the coccolith. The probe is then lifted vertically and a droplet of the acid (pH 3.5 to allow highly controlled dissolution now that elemental mobility is not an issue) pipetted over the area containing the imaged coccolith. The acid was left for x minutes and then removed with the corner of an absorbent wipe. The probe was again lowered and a further image made. This process was repeated until full dissolution is was reached. One limitation of using this method, rather than continuously flowing fluid over the sample, was that during the later stages of dissolution small parts of the coccolith can become detached and 'stick' to the probe causing

streakiness in the imaging as observed in a number of the figures presented here. Coccoliths were cleaned for organic material as described in section 4.8.

5.11.2 AFM Dissolution Results

Figure 23 presents five three-dimensionally projected AFM images from a 25-minute dissolution of *C. pelagicus* in pH 3.5 HNO_3. Steps one to four show the dissolution of the distal shield progressing inwards from the outer edge. Step five then shows dissolution of the inner distal shield area leaving a rim of calcite. The same images have been presented as averaged cross-sections in Figure 24 (note the vertical exaggeration). These cross sections have been produced by averaging the line profiles of eight diameters distributed (rotationally) evenly around the coccolith's centre point. This process described the averaged shape change, but not a true area cross-section change because the coccolith is elliptical, and here the line profiles have all been superimposed on the longest diameter of the coccolith. It is evident from Figure 24 that dissolution of the distal shield begins on the upper surface (the rhomb face) of the V-unit and progresses without significant dissolution of the R-unit (the central area of the distal shield), then once complete the distal shield R-unit dissolved leaving the proximal shield. Howeverm on close examination of the V and R units after the first 2.5 minutes of dissolution both appear to be forming etch-pits, the initial stage of dissolution (Figure 25). One could therefore describe three phases of dissolution for the distal shield, first the removal of a soluble surface phase, secondly the dissolution of a moderately soluble V-unit, then finally the dissolution of the resistant distal shield R-unit, leaving the underside of the proximal shield exposed.

Figure 23. Three dimensional images plotted from measurements made during the dissolution of *C.pelagicus*. Distal shield facing upwards. Steps 1 to 5 represent progressively greater dissolution over ~25 minutes.

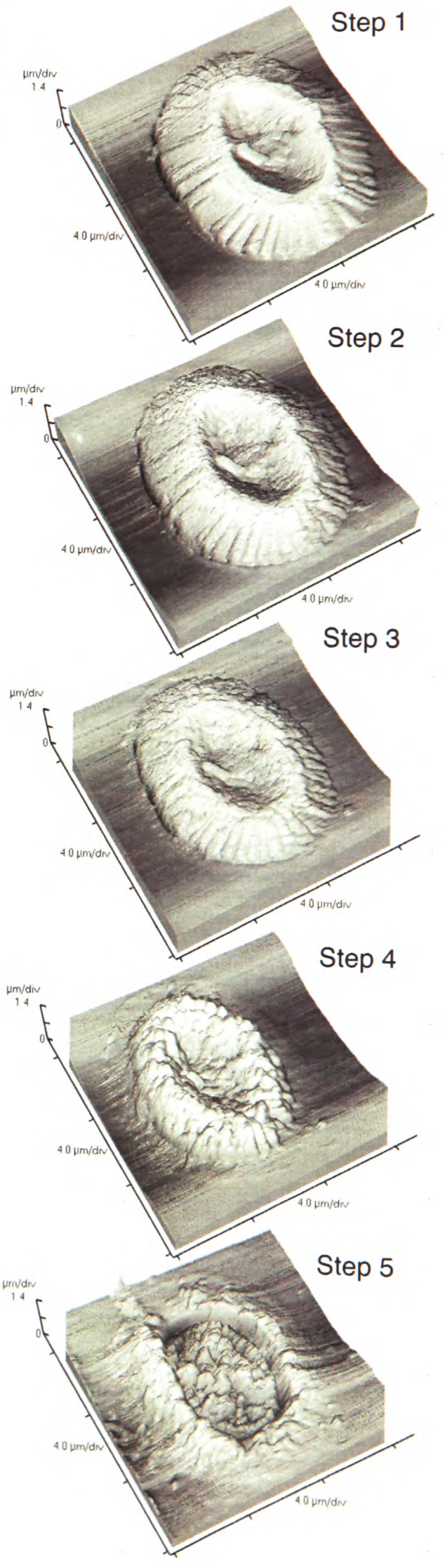

Further experiments were undertaken looking at the dissolution of the proximal shield (Figure 26). Here the R-units dissolve first from the circumference inwards, leaving the central area (V-units) which then dissolves leaving the underside of the distal shield visible. The contrasting order of unit dissolution between the distal and proximal shield experiments suggests that the process is unlikely to be controlled only by the crystallographic-unit's chemistry, and may instead be controlled by the kinetics of the different areas of the crystals, or an alternative chemical distribution. It also appears that the proximity of the shield to the substrate plays an important part in the rate of dissolution.

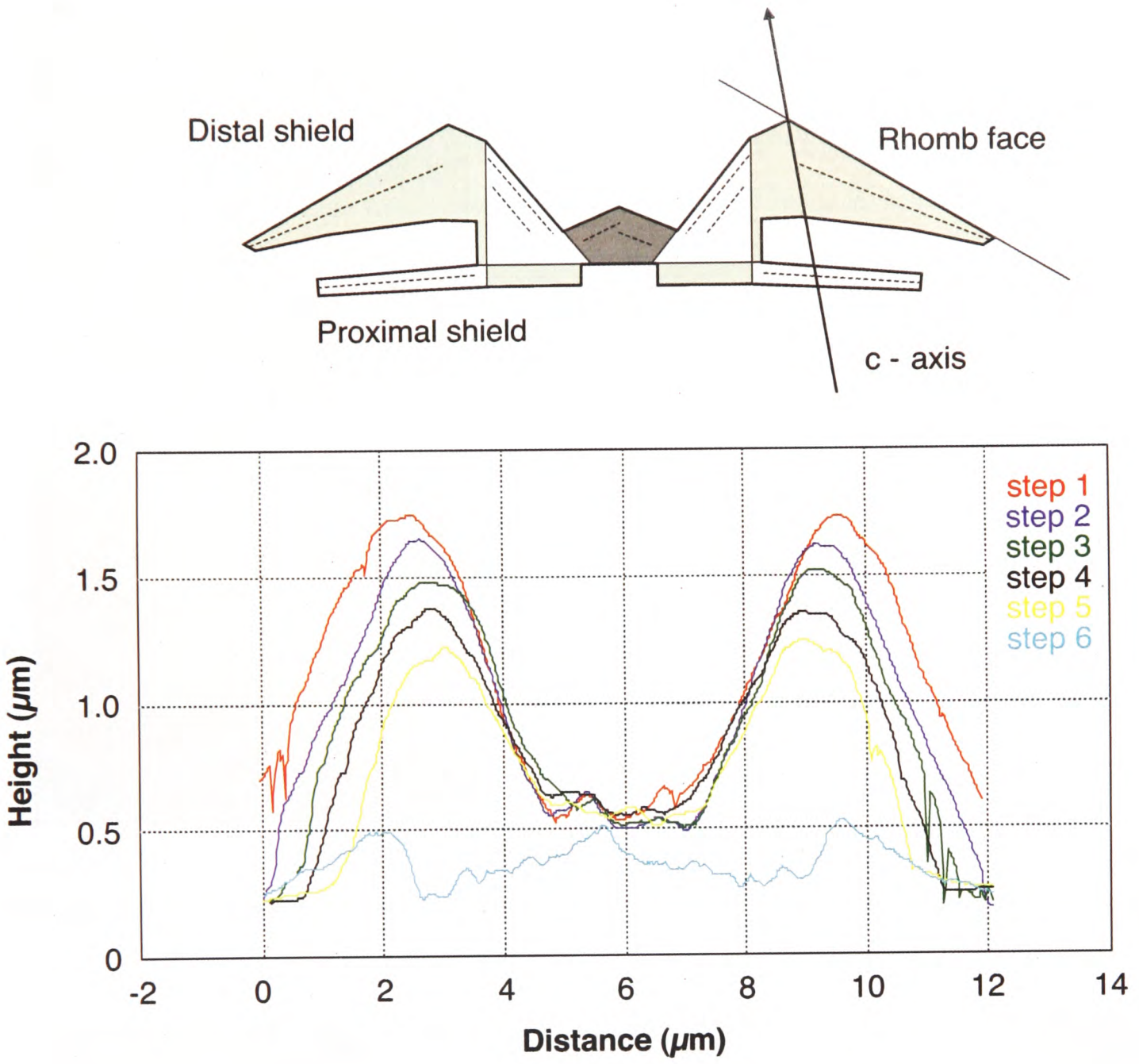

Figure 24. Top: V and R unit structure of an idealised coccolith produced by *C. pelagicus*. From Henriksen et el. (2003). Bottom: Averaged cross-sections showing the 5-step dissolution of *C. pelagicus*. Cross sections were produced by averaging eight equally spaced diameters sections through the 3-D dissolution data shown in Figure 23.

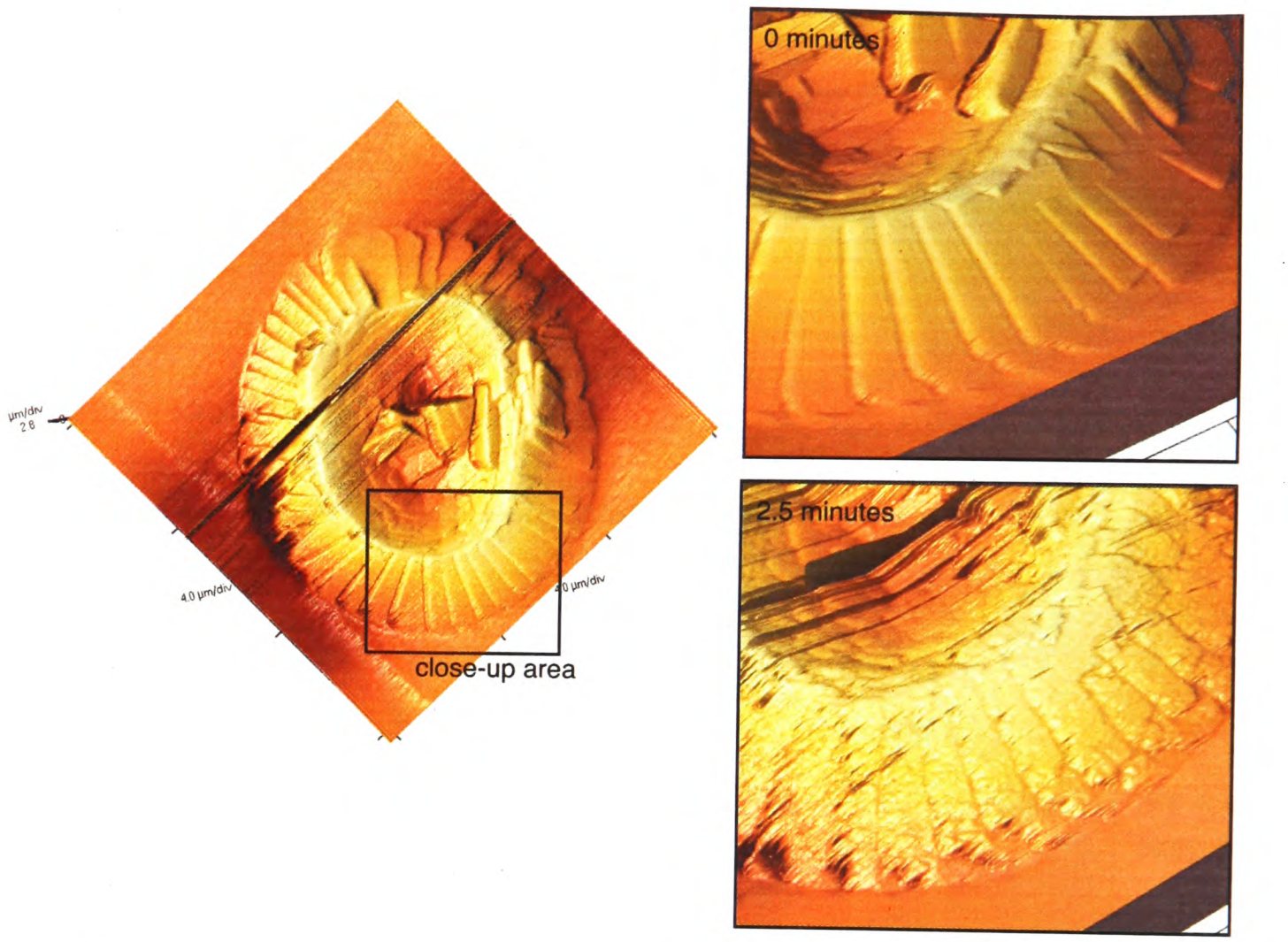

Figure 25. Close-up AFM images of the *C. pelagicus* surface after 0 and 2.5 minutes of dissolution. After 2.5 minutes etch-pits have begun to develop across the whole surface of the coccolith, into both V and R units.

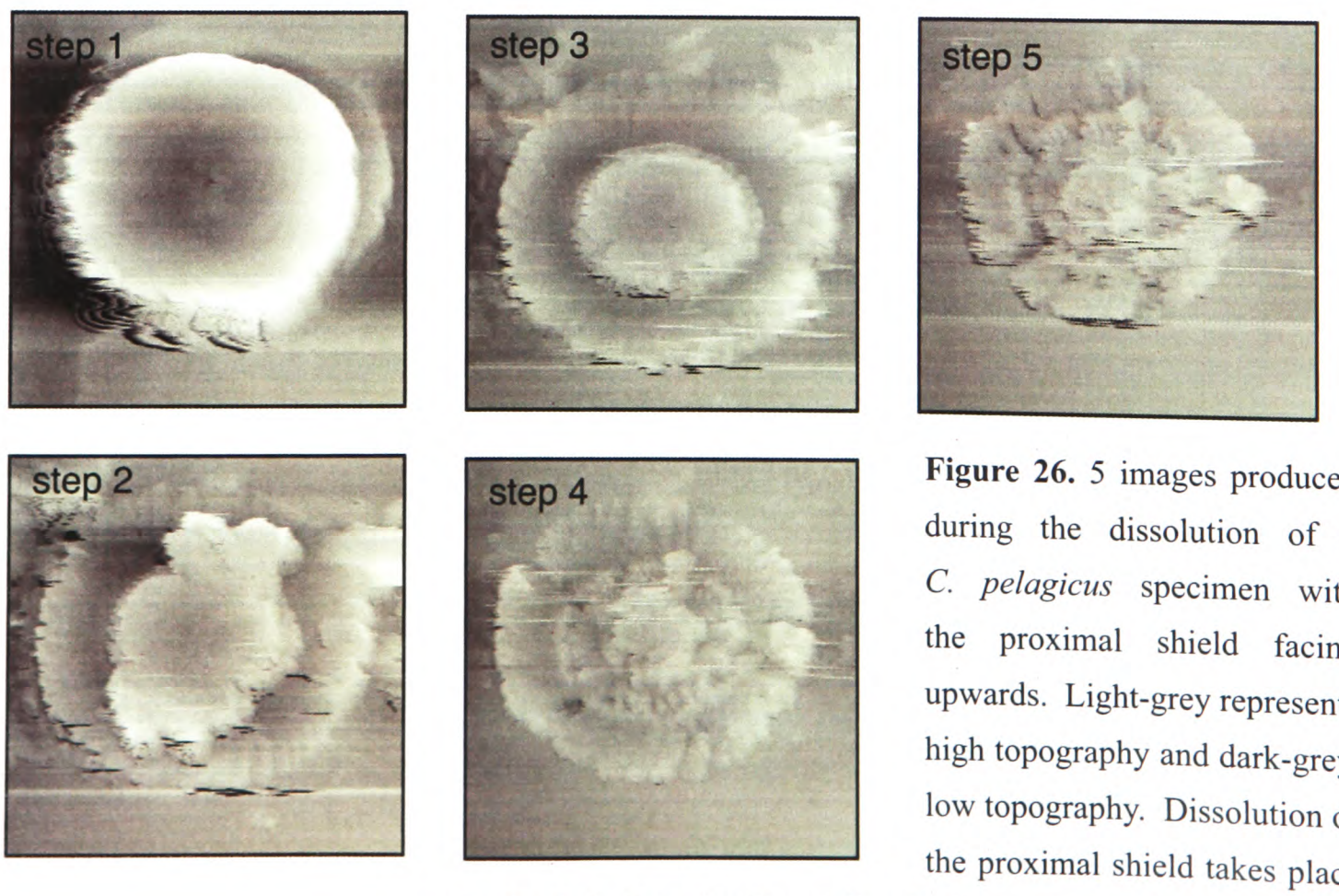

Figure 26. 5 images produced during the dissolution of a *C. pelagicus* specimen with the proximal shield facing upwards. Light-grey represents high topography and dark-grey, low topography. Dissolution of the proximal shield takes place completely before significant dissolution occurs on the distal shield.

5.12 FT-TRA Pitfalls and Future Development

An important caveat when considering the FT-TRA results presented in this chapter is the poor reproducibility of data, apparently a consequence of machine drift in the ICP-MS. As described in section 4.5, modification of the technique developed by Harding et al. (2006) to FT-TRA assumes that machine drift occurs linearly throughout the experiment. This assumption is flawed in a number of areas. Firstly, in batch experiments the assumption that drift occurs linearly is based on the fact that Ca will be building up on the focusing cones as the solution enters the ICP-MS at a constant rate because the sample has a constant concentration. This is not applicable to FT-TRA where the sample concentration is changing throughout the dissolution. Secondly, ICP-MS drift can be affected by many factors other than sample build-up on the focussing cones, for example, as a result of oscillations in temperature, gas flow, and non-uniformity in the sample introduction system. Figure 27 displays the count-intensity measured for Mg, Sr, Cd Zn and their Ca pairs over ~ 1 hour drawing a 20 ppm Ca multi-element standard at 0.1 ml min^{-1}, starting with freshly cleaned cones (which would normally be primed with a calcium standard to prevent the initial rapid count-intensity loss). Although Figure 27 shows that the majority of the standard drift can be described by a linear interpolation between the values measured at the start and end of an hour long analysis, it is also evident that shorter period variability occurs. It is possible that the non-linearity of machine drift could explain the poor-reproducibility of trace-element/Ca ratios, negating the need to invoke inhomogeneities in the coccolith calcite.

In light of the ICP-MS drift discussion it seems likely that, to obtain higher quality FT-TRA data, experiments should be undertaken using a mass spectrometer suitable for use with a mixture of internal standards simultaneously.

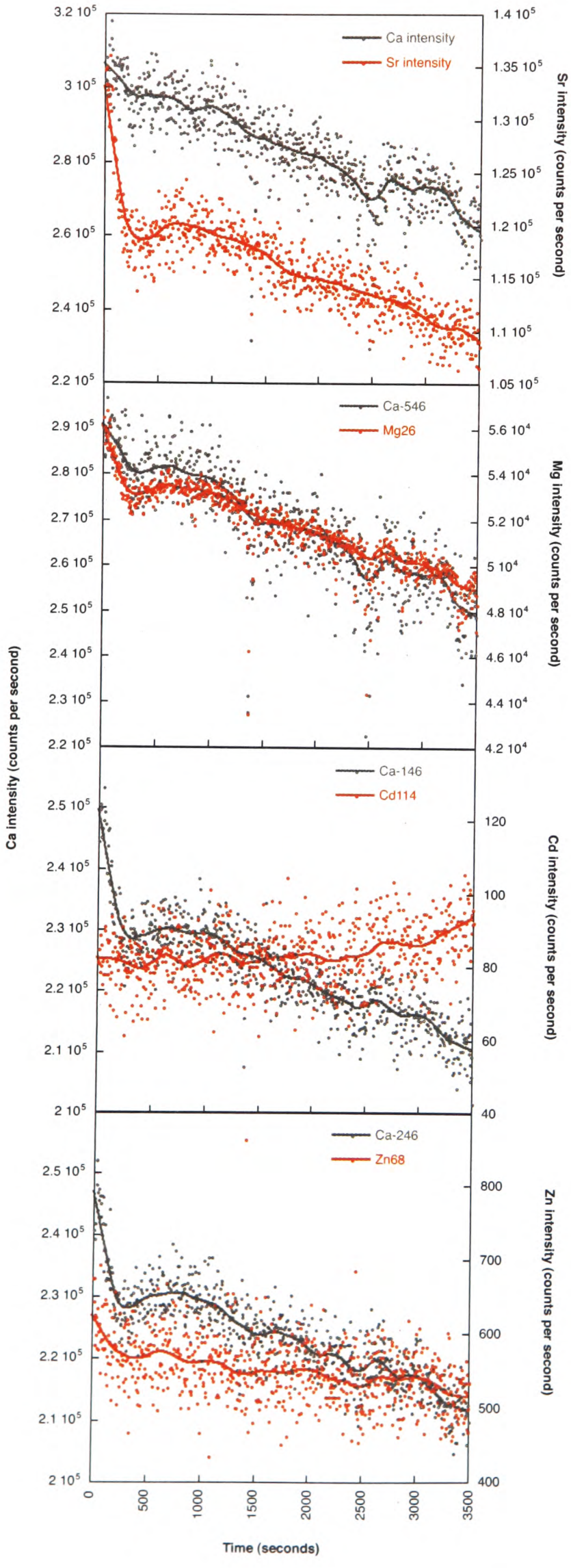

Figure 27. Quadrapole ICP-MS Ca, Sr, Mg, Cd and Zn intensities measured over 3500 seconds of continuous analysis of a well mixed multi-element standard (20 ppm Ca). The composition of the liquid being analysed is constant, therefore the variability must be a result of machine drift.

5.13 Discussion and Conclusions

This study has provided new insight into the function and value of FT-TRA, developing and documenting significant advances in the technique, as well as providing recommendations for future improvement. Initial values for *C. pelagicus* trace-element/Ca ratios are reported, and for the first time, detailed morphological and chemical data throughout whole coccolith dissolution has been presented.

Previously our understanding of coccolith trace-element compositions has essentially been limited to experimental and field measurement of Sr/Ca (e.g. Stoll et al., 2002a, Stoll and Schrag, 2001). Multiple Sr/Ca investigations have allowed a broad appreciation of inter-species variation and a number of the factors influencing the incorporation of Sr into coccoliths. In a study of coccolith Mg/Ca Stoll et al. (2001) examined the problems associated with cleaning cultured coccoliths to allow accurate Mg/Ca measurements. The authors concluded that *E. huxleyi* Mg/Ca was likely to be ≤ 0.2 mmol/mol, but when using the cleaning protocol which they had developed, a repeatable value could not be obtained. Since FT-TRA was initially developed to allow the cleaning of samples without the re-sorbtion of contaminant elements to the sample, FT-TRA could provide an ideal answer to the problem of sample cleaning. The likely reason for Stoll et al. (2001) failing to make accurate Mg/Ca measurements in coccoliths is that there would be significant re-sorbtion of contaminants to the large surface area presented by the minute and complexly ornamented coccoliths, in the same way that the large charged surface area of clays contaminates sedimentary calcite samples. When analysing foraminiferal calcite, self-contamination does not represent a major obstacle to trace-element measurement for two reasons, firstly because the 'large' foraminifera fragments have a considerably lower surface-area/volume ratio and therefore a smaller relative surface area to sorb contaminants, and secondly, as a result of the lower surface-area/volume ratio the samples can undergo a 'weak acid leach' to strip the surface of contaminants with only minimal dissolution of the sample; a similar process performed

	Sr/Ca (mmol/ mol)	Mg/Ca (mmol/ mol)	Ba/Ca (μmol/mol)	Mn/Ca (μmol/mol)	Cd/Ca (μmol/mol)	Zn/Ca (μmol/mol)
Culture medium value	8.60	4763.80	60.90	1.60	0.20	29.60
Coccolith calcite value	3.20	< 0.05	< 0.30	< 1.00	3.40-2.90	650.00-400.00
Exchange coefficient (K_D)	0.37	< 1.05 x10^{-5}	< 4.93 x10^{-3}	< 0.63	17.00-14.50	21.96-13.51

Table 1. Exchange coefficients of elements into *C. pelagicus* calcite, calculated from batch-measured culture-medium composition and flow-through measured *C. pelagicus* coccolith composition.

on coccoliths would result in a high degree of (or even total) dissolution. FT-TRA has allowed us to leach surface contaminants in a controlled environment and make first-order measurements of *C. pelagicus* trace-element chemistry. There results are presented in Table 1.

The distribution coefficients (K_D) presented for *C. pelagicus* coccoliths contrast with those known for foraminiferal calcite. Figure 28 presents the *C. pelagicus* data provided in Table 1 together with distribution coefficients for foraminiferal calcite and inorganic calcite [data from (Dromgoole and Walter, 1990, Hartley and Mucci, 1996, Kitano et al., 1980, Tesoriero and Pankow, 1996)]. Inorganic calcite data represent values obtained at the lowest observed crystal growth rates, and therefore closely approximate equilibrium values. Arrows represent extension of error bars to zero. It is clear that coccoliths, foraminifera and inorganic calcite incorporate trace elements very differently. This is perhaps not surprising because they are each precipitated under very different conditions. Seawater, although more than saturated with respect to $CaCO_3$, under normal conditions does not precipitate $CaCO_3$. This is primarily a result of the high seawater Mg concentration which acts as a kinetic inhibitor, increasing the solubility of calcite beyond that favourable for precipitation. The K_D values quoted for inorganic calcite therefore refer to experiments undertaken

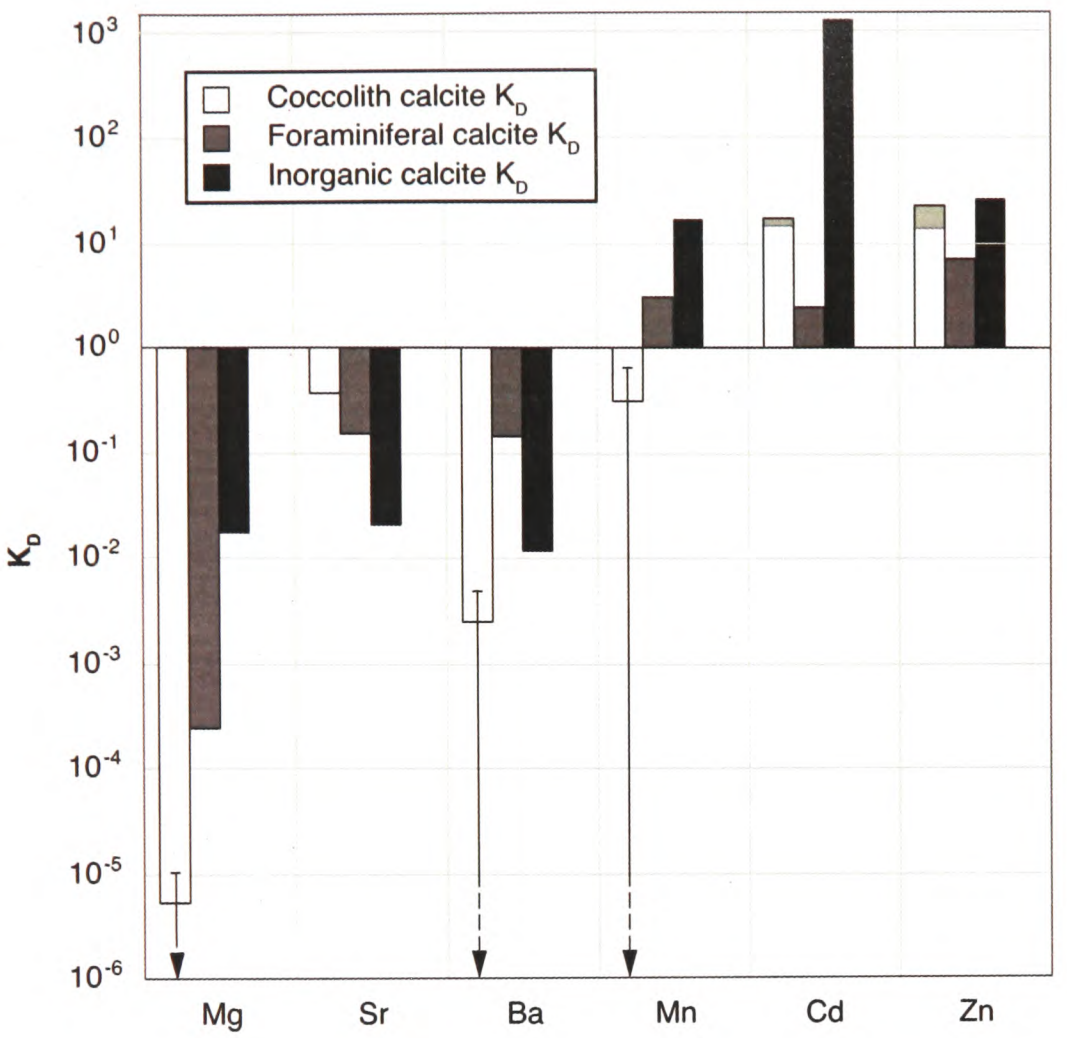

Figure 28. Distribution coefficients (K_D) measured in *C. pelagicus* coccoliths (this study), foraminifera and inorganic calcite. Where K_D = $(element/Ca)_{solid}/(element/Ca)_{liquid}$. Where present, error bars represent the low precision associated with flow-though analysis. The grey boxes at the end of the Cd and Zn coccolith calcite bars represent the maximum and minimum values recorded within one sample. Inorganic calcite data from; Dromgoole and Walter (1990), Hartley and Mucci, (1996), Kiano et al. (1980), and Tesoriero and Pankow (1996). Foraminiferal data from Rickaby et al. (2006).

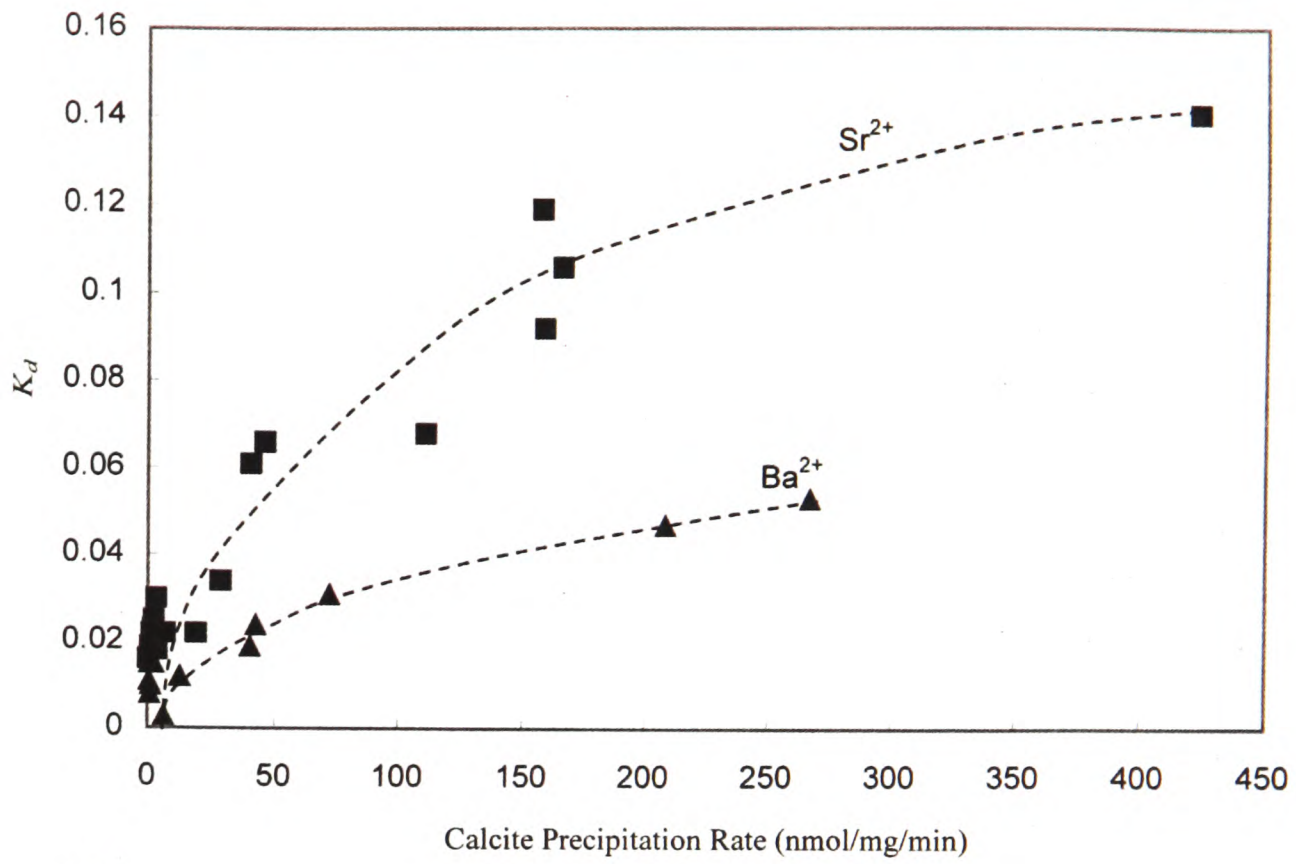

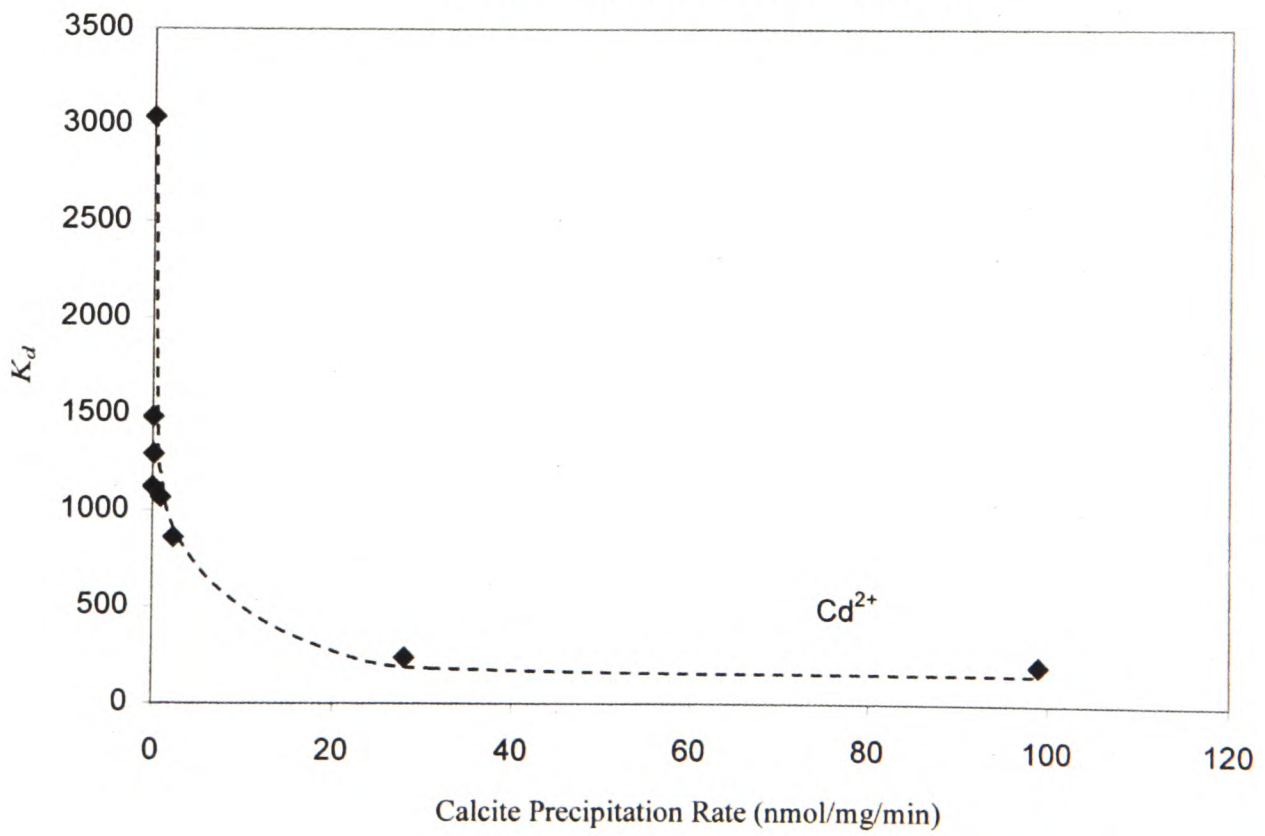

Figure 29. Elemental Distribution coefficients of Sr, Ba and Cd into $CaCO_3$ with increasing crystal growth rate. From Wang, YF; Xu (2001) and Tesoriero and Pankow (1996).

from a solution low in Mg. To allow themselves to precipitate calcite, foraminifera and coccolithophores have to modify the seawater. Foraminifera precipitate their calcite from an engulfed vacuole of ambient water and are believed to modify the chemistry in one of, or a combination of two ways; firstly, by pumping Mg out of the vacuolated seawater, or secondly by reducing the pH of the seawater (Erez, 2003). It is unlikely that the latter could explain the difference between foraminiferal and inorganic distribution coefficients because the primary response would be to change the precipitation rate, bringing the K_D values towards one [i.e. accentuate the expression of their compatibility with calcite (Figure

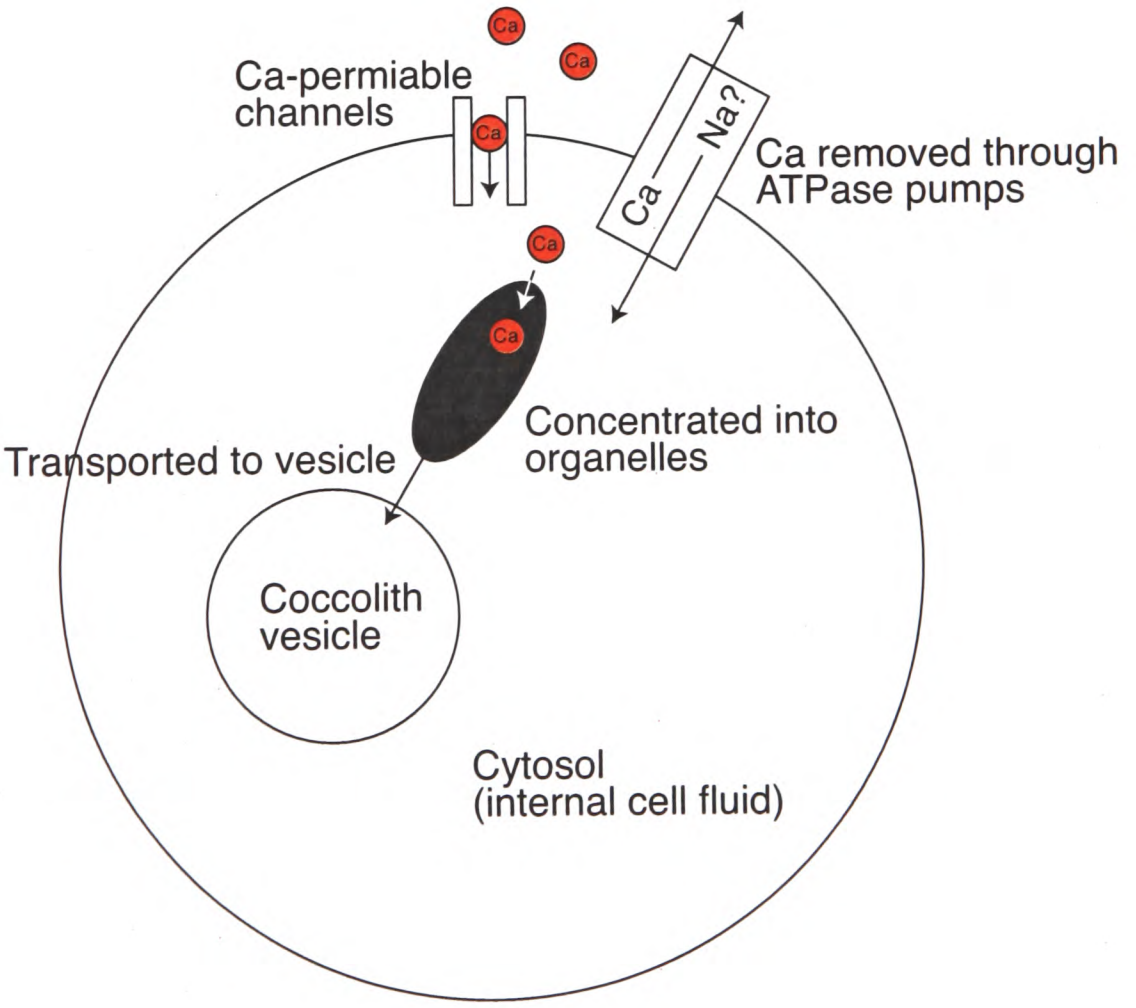

Figure 30. Coccolithophore calcification occurs intracellularly, and as a result all ions incorporated into the coccolith must pass through the cell wall, organelles in the cytoplasm and the vesicle wall. Each of these steps is likely to play some part in the elemental fractionation from seawater recorded in the coccolith calcite. This figure highlights possible biochemical pathways within the coccolithophore.

29)]. Although this result is consistent with K_D values for Sr, Ba, Mn, Cd and Mn, it is not consistent with Mg. However, if calcification is made possible by pumping Mg out of the vesicle, the trace-element K_D values of foraminifera (as presented in Figure 28) are entirely consistent with those of inorganic calcite; where Mg decreases, and consequently, because the $CaCO_3$ precipitation rate increases, the K_D values of the other elements move towards one. A consistent and robust explanation of trace-element incorporation during coccolith calcification is less straightforward because of the complex biological involvement.

Coccolithophore calcification is intracellular, and as such physiology and biochemistry exert strong controls over the transport of ions to the site of calcification (Figure 30). The transport mechanisms and pathways involved in moving Ca and $C_{inorganic}$ (CO_3^{2-} or HCO_3^-) to the site of calcification are very poorly understood, however a minimum requirement is that the substrates involved in calcification pass through two membranes; the cell wall, and the membrane surrounding the coccolith-forming vesicle. Considering fractionation at these two steps and during the precipitation of calcite, a number of mechanisms, can, and have been, proposed to explain the Sr/Ca composition and growth-rate dependence in coccolith calcite.

- **Fractionation during calcite precipitation**. The most simple, and therefore first potential fractionation to be considered is that occurring during the precipitation of calcite from a fluid. It has been demonstrated that there exists a fractionation against Sr during the inorganic precipitation of $CaCO_3$, and that this fractionation decreases under elevated growth-rate (Tesoriero and Pankow, 1996). Stoll et al. (Stoll et al., 2002b) compared the Sr/Ca growth-rate data from cultured *E. huxleyi* with model data fitted to the inorganic precipitation experiments and demonstrated that only if a high Sr/Ca existed in the fluid phase could this mechanism explain coccolith Sr/Ca. However the authors rejected this mechanism because no evidence existed for elevated Sr/Ca within the cell. More recent data from Ho et al. (2003) supports this assumption.

- **Fractionation during active transport**. Rickaby at al. (2002) proposed that calcification-rate dependent Sr/Ca fractionation could occur during active transport against the concentration gradient into the coccolith forming vesicle. The authors suggested that because carrier proteins bind Ca ions more strongly than Sr ions as a result of Ca's marginally higher charge density, Ca is more efficiently transported at lower concentrations, with the result that the rate of increase of Ca transport slows as it nears saturation whilst Sr transport continues to increase rapidly. This would cause an increased Sr/Ca within the coccolith vesicle, and subsequently in the coccolith.

- **Fractionation as a result of Sr enrichment**. It is likely that Ca initially enters the cell through ion channels in the cell wall (Brownlee and Taylor, 2004). Ion channels are protein structured pores that selectively allow ions, based on their ionic radius and charge, to pass down an osmotic gradient through cell membranes. The similar ionic radii of Ca, Sr and Ba result in comparable, but rarely identical, relative transport rates of these ions through Ca channels, with membranes from different organisms allowing transport of these elements at different relative rates (e.g. Lin and Spencer, 2001, Very and Davies, 2000). Because Sr and Ca would be expected to enter the cell in similar proportions to those of seawater, but are incorporated into the coccolith in a ratio lower than that of seawater, it is likely that Sr builds up in the coccolithophore forming vesicle, and ultimately the cellular Sr/Ca, and Sr uptake into the coccolith may therefore increase with an increased degree of calcification. Consideration of this, and the two previous mechanisms, lead to the question; why is Ba not elevated in coccolith calcite (Table 1), and coccolithophore cells (Fisher et al., 1991), as might be inferred through analogy with Sr? I propose that the answer to this is that the cell-wall Ca channels undergo partial blocking due to the high external Mg concentration of seawater, which causes a very significant reduction of Ba flowing through the channels. In most investigations of Ca channel flow,

external Mg concentrations are low, because membranes isolated from terrestrial plants or animals have been examined. Despite investigation under such conditions, it has been shown that an external [Mg] of 1 mmol/L (less than 2% of seawater [Mg]), can cause a seven-fold reduction in Ba transport in relation to Ca through Ca-channels (Serrano et al., 2000). Assuming this transport scales with increasing [Mg], under seawater [Mg] (53 mmol/L), Ba flux would be expected to approach zero. Similar results have been observed in response to Co-blocking (Hagiwara et al., 1974), although the Co concentrations required to cause considerable changes to the I

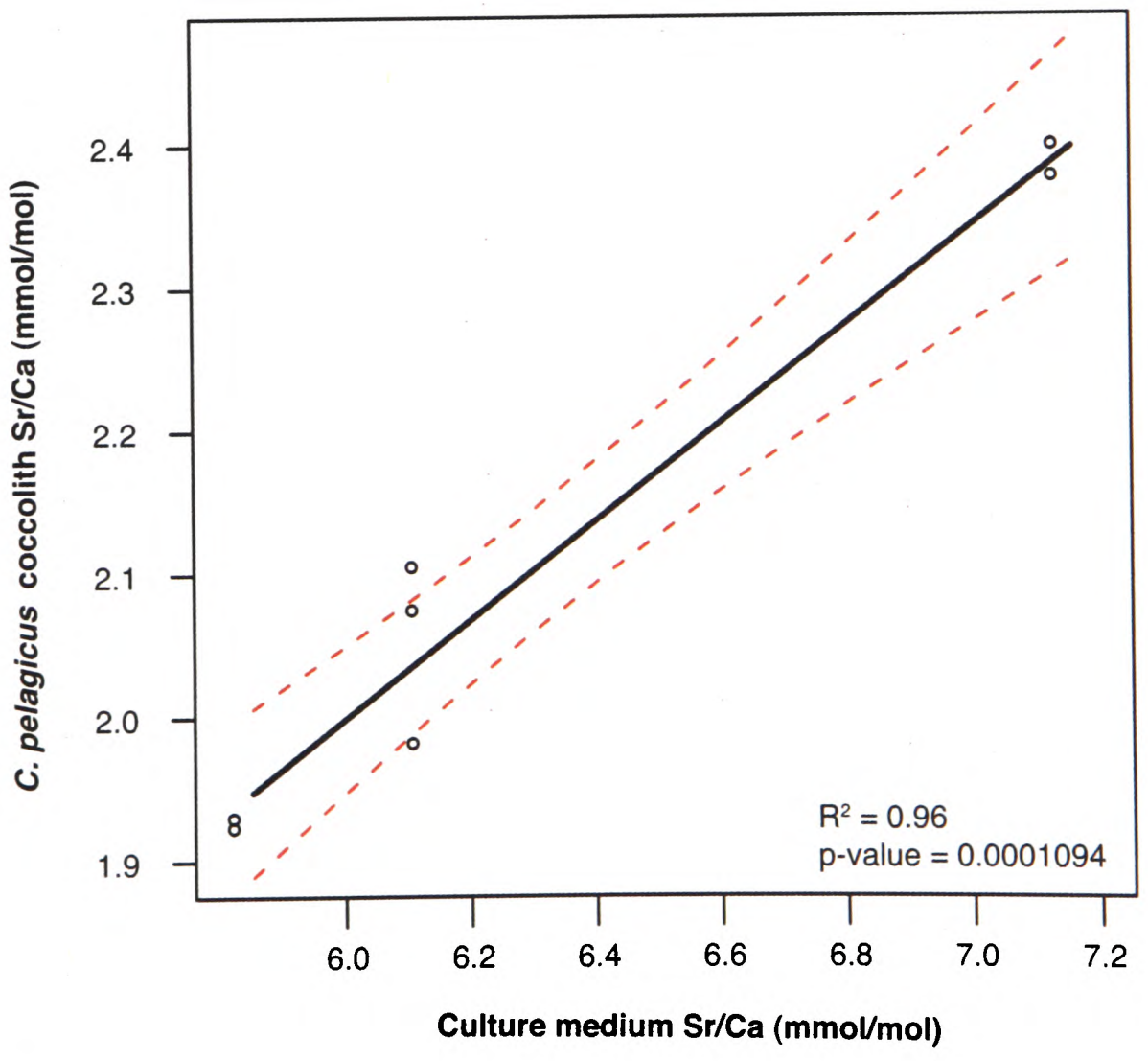

Figure 31. Sr/Ca ratios measured in *C. pelagicus* coccoliths cultured in filtered seawater media with artificially modified Sr/Ca. Points represent measurements made on replicate cultures, with variability between cultures cultured at common seawater Sr/Ca likely resulting from differences in growth-rates. The straight line represents the linear best fit, with an R^2 of 0.96, and red lines represent the 95% confidence intervals.

Although each of the above mechanisms are capable of explaining the nutrient governed coccolithophore growth-rate control over Sr/Ca, and potentially the direct correlation between culture medium Sr/Ca and coccolith Sr/Ca observed in *E. huxleyi* by Langer et al. (2006) and *C. pelagicus* in this study (Figure 31), these mechanisms are inconsistent with the observation that coccolith Sr/Ca does not vary with irradiance-induced changes in calcification rate (Langer et al., 2006, Stoll et al., 2002b, Stoll et al., 2002c). Langer et al. (2006) therefore propose two alternative mechanisms by which coccolith Sr/Ca could be controlled by nutrient availability rather than growth-rate per se:

- **Fractionation due to variable DIC transport**. Assuming the flux of Sr into the coccolith vesicle is greater than its rate of incorporation into the calcite lattice, Sr will build up in the vesicle until some equilibrium value is reached. Langer et al. (2006) argued that the equilibrium coccolith-vesicle [Sr] would be proportional to the [Sr] external to the cell, thereby satisfying the requirement that coccolith Sr/Ca correlates linearly with seawater Sr/Ca. The authors then suggest that if nutrient-dependent protein transport of DIC (CO_3^{2-} or HCO_3^-) controlled the saturation state of the vesicle with respect to $CaCO_3$, and therefore the vesicle [Ca] under which the precipitation can occur, and if DIC transport into the vesicle was related to nutrient availability, nutrients could control the [Ca] when calcification occurred. Because $[Sr]_{vesicle}$ would remain constant at its equilibrium value, the saturation state could control the $[Ca]_{vesicle}$ and therefore coccolith Sr/Ca.

- **Polysaccharide-concentration controlled Fractionation**. The second mechanism proposed by Langer et al. (2006) is that polysaccharides, carbohydrates known to be intimately associated with the calcification process (Henriksen et al., 2004b, Marsh, 2003) and known to be produced in high concentrations during times of nutrient limitation (Engel et al., 2004), strongly bind Sr, thereby limiting the availability

of Sr for incorporation into the $CaCO_3$ lattice. If polysaccharide production is proportional to nutrient availability, this mechanism could result in lower Sr/Ca in nutrient-poor conditions and elevated Sr/Ca in nutrient replete conditions.

The former of these mechanisms can be tested by measuring the Sr/Ca of coccoliths formed under different [DIC]. DIC availability is known to regulate calcification (Buitenhuis et al., 1999), and therefore if coccolith Sr/Ca is controlled by vesicle saturation state, Sr/Ca should vary with culture medium [DIC]. However, measurements made on *E. huxleyi* samples cultured at different [DIC], supplied by Ingrid Zondervan, did not show an increasing Sr/Ca with increasing [DIC] (Figure 32). The only mechanisms proposed to date, consistent with all observations, is that of a polysaccharide-concentration controlled Sr/Ca fractionation. This mechanism could also be consistent with the observation that different species record different Sr/Ca because different coccolithophore species are known to have different types and concentrations of

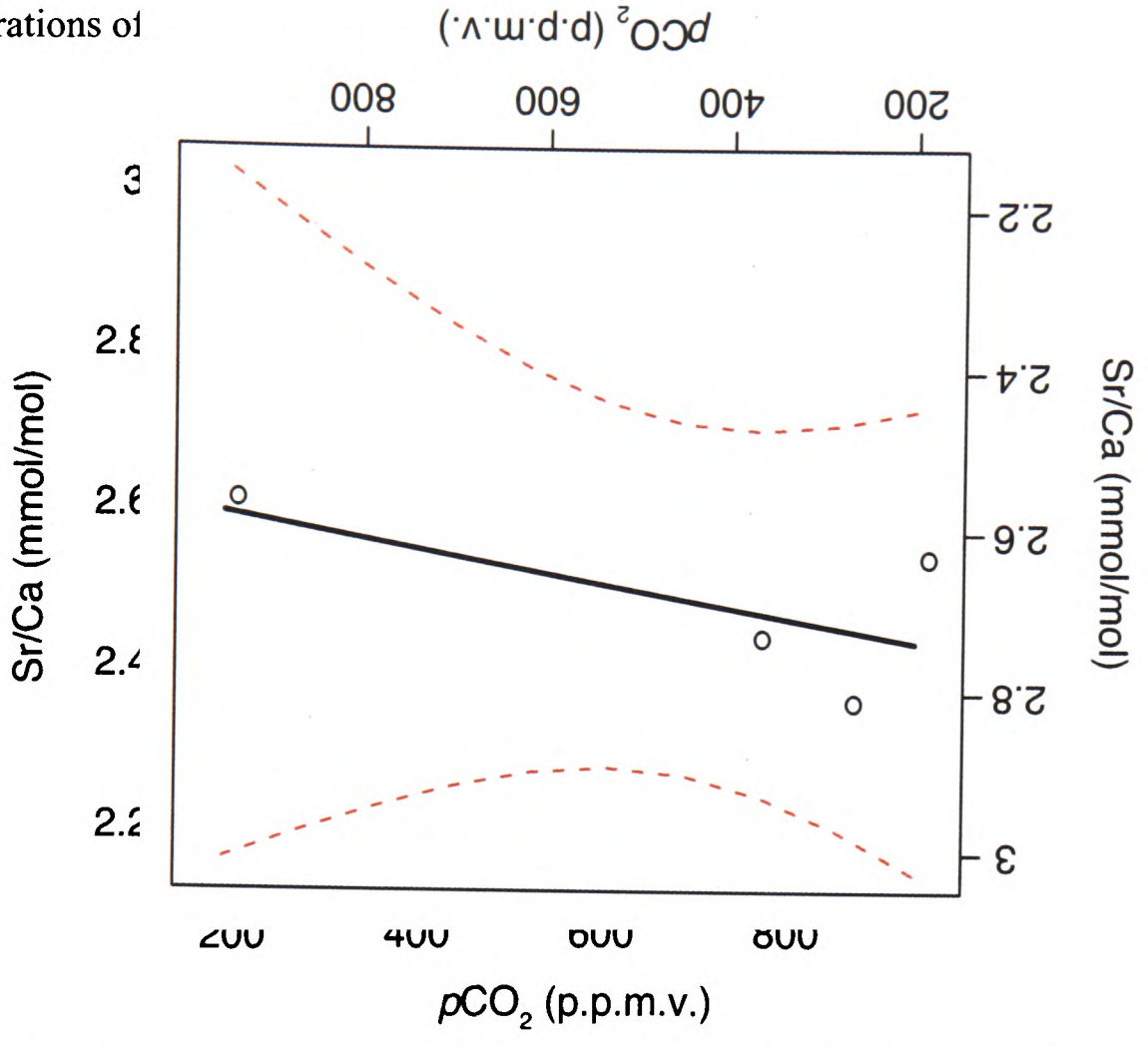

Figure 32. Sr/Ca measurements made on *E. huxleyi* coccoliths cultured at different pCO_2 levels, and therefore different [DIC] but with constant pH. The straight line represents a best fit linear model, and the red lines the 95% confidence intervals of the fit. Samples cultured by Ingrid Zondervan.

Considering the proposed mechanism of coccolith Sr/Ca control, and cellular coccolithophore element data (Ho et al., 2003, Fisher et al., 1991), it is possible to make some prediction about the incorporation and behaviour of elements other than Sr into coccolithophore calcite. Only Ca, Sr and Ba are believed to pass readily through Ca-channels. Given the high [Mg] of seawater, and the Ba-flux response of Ca-channels to Mg-blocking (Serrano et al., 2000), it logically follows, and has been experimentally shown, that coccolithophore [Ba] is low (Fisher et al., 1991). Furthermore, the requirement of high Ca-flux into the cell for calcification, together with the observation that Sr passively traces Ca (even under high external [Mg]) through most biological processes, explains the ample observations of high coccolithophore calcite Sr/Ca. Of the remaining elements analysed, all play important roles in cell biochemistry, and as such their concentrations will be carefully regulated by the coccolithophore. Other than [Mg], cellular concentrations of these elements are all at least two orders of magnitude lower than [Sr]. Table 2 presents concentrations for the elements of interest from Ho et al. (2003).

	C (µmol/L x10^7)	**Ca (µmol/L x10^7)**	**Sr (µmol/L)**	**Mg (µmol/L)**	**Mn (µmol/L)**	**Cd (µmol/L)**	**Zn (µmol/L)**
***E. huxleyi* (cell+ liths)**	3.10 (1.10)	1.90	44000	18000	940	48	50
***G. oceanica* (cell + liths)**	3.11 (0.89)	1.80	39000	18000	990	43	57
Average marine phytoplankton	1.27	0.00005	327	127329	364	12	96

Table 2. *E. huxleyi* and *G. oceanica* total coccolithophore cell and coccosphere elemental compositions, together with values for an average of ten non-coccolithophorid marine phytoplankton. Carbon values in brackets represent measurements made after the coccolithosphere has been removed by fuming with HCL. Data from Ho et al. (2003).

Coccolithophore data presented in Table 2, other than those in parenthesis, represents measurements made on bulk samples containing both cellular and carbonate material. Because we know the carbon concentrations before and after removal of the coccoliths by fuming with HCl, and that the molar ratio of carbon and calcium in coccoliths is essentially one, we can calculate that the coccolithophore Ca concentration minus the contribution from coccoliths, as -2.00 and -4.25 mol/L for *E. huxleyi* and *G. oceanica* respectively. It is unclear whether the cellular carbon values after HCl fuming were calculated with or without correction for the associated volume change [~50% volume change, assuming a typical *E. huxleyi* coccolithophore and sphere volume to be 65 μm^3, and coccolith volume to be 1.8 μm^3 (from Chapter 2), and assuming there to be 20 coccoliths per cell (Fernandez et al., 1993)]. This volume change may explain why the calculated Ca concentration becomes negative after acid fuming. The Sr/Ca of the untreated coccolithophores are 2.3 and 2.2 mmol/mol for *E. huxleyi* and *G. oceanica* respectively (Ho et al., 2003). Without knowledge of the growth-rate and temperature under which these coccolithophores were grown, it is not possible to calculate the cellular [Sr], however because the $Sr/Ca_{cell+lith}$ is similar to that measured in coccoliths of these species (Stoll et al., 2002c), it is reasonable to assume that most of the Sr measured by Ho et al. (2003) is associated with the coccoliths, and therefore that cellular [Sr] is similar to that of other marine phytoplankton (average of 10 species from Ho et al. (2003) = 327 μmol/L). The inference that cellular coccolithophore [Sr] is not abnormally elevated with respect to other marine phytoplankton, suggests that Sr is not building up in the cell as a result of high influx but low incorporation in to $CaCO_3$, indicating that discrimination against Sr is not occurring during active transport into the cell, but is instead either being excluded prior to entry into the cell, or concentrated in the coccolith vesicle and released to the surrounding seawater as the vesicle fuses with the cell-wall and the coccolith is extruded.

Without knowledge of the exact mechanisms involved in the transport and incorporation of Ca, CO_3 and substituted elements into coccolith calcite, it is impossible to make accurate

predictions about coccolith trace-element behaviour. However, given the high cellular concentration of Mg in coccolithophores and other marine phytoplankton, it is perhaps surprising that higher coccolith Mg/Ca have not been measured.

In light of the discussed results, it is important to consider what sedimentary coccolith trace-element chemistry might tell us about the past, and therefore where to focus future research. Since cellular [Mg], [Mn], [Zn] and [Cd] are likely to be under precise biological regulation, assuming an incorporation mechanism into $CaCO_3$ which 'sample' the whole-cell chemistry, these elements have the potential to act independently from seawater concentrations as proxies for past cell biochemistry. Mg, Mn, Zn and Cd are known to play important roles in photosynthesis, and in the case of Zn, in many diverse enzyme-dependent reactions. As such, the concentration of these elements in coccolithophore calcite, amongst other things, may record past photosynthetic or reproductive activity. Mg's utilisation extends to almost every aspect of cell biology, but is of particular importance in metabolism and all reactions requiring the release of energy from ATP. Consequently, coccolith Mg/Ca could conceivably vary under different growth-rate and nutrient regimes. Finally, although I have argued that Ba is potentially prevented from entering the cell in high concentrations due to Ca-channel blocking, under lowered external [Mg], Ba fluxes may increase. Due to the similarity in Ca and Ba chemistry, if entering the cell through Ca-channels, it seems quite possible that Ba would be incorporated readily into coccolith calcite. Therefore, coccolith Ba/Ca could act as a proxy for past seawater [Mg], which could be a valuable tool in answering questions surrounding palaeo-$Mg/Ca_{seawater}$ and the long-term cycling between calcite and aragonite precipitating seas. It is important, now, that coccolith polysaccharides are further investigated to test whether the Sr/Ca-growth-rate mechanism proposed by Langer et al. (2006) is robust, and to consider the affinity of the coccolith-polysaccharides for elements other than Sr and Ca.

In addition to providing information about bulk-coccolith trace-element chemistry, FT-TRA has allowed us to explore inhomogeneities in the distribution of trace-elements

within coccoliths. FT-TRA has been used together with microprobe and AFM analysis to provide a picture of these possible inhomogeneities. It is evident from these analyses that coccoliths dissolve in a very organised manner, and that the Cd, Zn and possibly even Sr element/calcium ratios evolve throughout dissolution in such a way that indicates non-uniformity. AFM allows us to say that if inhomogeneities do exist they are not directly associated with just the V and R units, however because the technique only allows imaging of one shield at a time, and requires that the sample is mounted on a surface, thereby distorting the dissolution, it is not possible to associate these potential inhomogeneities with specific regions of the whole coccolith.

AFM investigation into the morphometric evolution of *C. pelagicus* through dissolution has not only provided information to assist in our understanding of FT-TRA data, but also provides a framework for analysing the state of *C. peagicus* as a dissolution proxy, and provides further evidence for the surprising resistance of coccoliths to dissolution (Beaufort et al., 2007, Frenz and Henrich, 2007).

5.14 Future Work

It would now be valuable to culture coccolithophores in media spiked with high levels of individual elements (other than Ca) to test whether incorporation is proportional to culture-medium elemental concentrations, and to allow micro-probe or NanoSIMS examination of the location of these enriched elements within the coccolithophore. Further, dissolution experiments could examine whether the solubility of the coccoliths is affected by the elevated element incorporation. Additional AFM work may be employed to investigate the relative solubility of coccoliths produced by different coccolithophore species, and by examining samples with and without H_2O_2 treatment, to help understand the role of the organic coating in limiting dissolution, and its control over ballasting and the carbonate pump.

5.15 Bibliography

BEAUFORT, L., PROBERT, I. AND BUCHET, N. (2007) Effects of acidification and primary production on coccolith weight: Implications for carbonate transfer from the surface to the deep ocean. Geochemistry Geophysics Geosystems, 8, doi:10.1029/2006GC001493.

BENWAY, H. M., HALEY, B. A., KLINKHAMMER, G.AND MIX, A. C. (2003) Adaptation of a flow-through leaching procedure for Mg/Ca paleothermometry. Geochemistry Geophysics Geosystems, 4. doi:10.1029/2002GC000312.

BOYLE, E. A. (1981) Cadmium, zinc, copper, and barium in foraminifera tests. Earth and Planetary Science Letters, 53, 11-35.

BROWNLEE, C. AND TAYLOR, A. (2004) Calcification In Coccolithophores: A Cellular Perspective, In: Coccolithophores: from molecular processes to global impact, Berlin, Springer.

BUITENHUIS, E. T., DE BAAR, H. J. W. AND VELDHUIS, M. J. W. (1999) Photosynthesis and calcification by *Emiliania huxleyi* (*Prymnesiophyceae*) as a function of inorganic carbon species. J. Phycol., 35, 949-959.

DIDYMUS, J. M., YOUNG, J. R. AND MANN, S. (1994) Construction and morphogenesis of the chiral ultrastructure of coccoliths from the marine alga *Emiliania-Huxleyi*. Proceedings of the Royal Society of London Series B-Biological Sciences, 258, 237-245.

DROMGOOLE, E. L. AND WALTER, L. M. (1990) Iron and manganese incorporation into calcite - effects of growth-kinetics, temperature and solution chemistry. Chemical Geology, 81, 311-336.

EGGINS, S., SPERO, H., RUSSELL, A., ALFORD, S., DOO, S., KUROYANAGI, A., DA ROCHA, R. E. AND SADEKOV, A. Y. (2007) Controls on Mg/Ca variation in planktonic foraminifera: insights from microanalysis of laboritory cultures *Orbulina universa*. Eos Trans. AGU, 88, Fall Meet. Suppl., Abstract PP41E-03.

ENGEL, A., DELILLE, B., JACQUET, S., RIEBESELL, U., ROCHELLE-NEWALL, E., TERBRUGGEN, A. AND ZONDERVAN, I. (2004) Transparent exopolymer particles and dissolved organic carbon production by *Emiliania huxleyi* exposed to different CO_2 concentrations: a mesocosm experiment. Aquatic Microbial Ecology, 34, 93-104.

EREZ, J. (2003) The source of ions for biomineralization in foraminifera and their implications for paleoceanographic proxies. Biomineralization, 54, 115-149.

FERNANDEZ, E., BOYD, P., HOLLIGAN, M. AND HARBOUR, D. S. (1993) Production of Organic and Inorganic Carbon within a Large-Scale Coccolithophore Bloom in the

Northeast Atlantic-Ocean. Marine Ecology-Progress Series, 97, 271-285.

FISHER, N. S., GUILLARD, R. R. L. AND BANKSTON, D. C. (1991) The accumulation of barium by marine-phytoplankton grown in culture. Journal of Marine Research, 49, 339-354.

FRENZ, M. AND HENRICH, R. (2007) Carbonate dissolution revealed by silt grain-size distribution: comparison of Holocene and Last Glacial Maximum sediments from the pelagic South Atlantic. Sedimentology, 54, 391-404.

HAGIWARA, S., FUKUDA, J. AND EATON, D. C. (1974) Membrane currents carried by Ca, Sr, and Ba in barnacle muscle-fiber during voltage clamp. Journal of General Physiology, 63, 564-578.

HALEY, B. A. AND KLINKHAMMER, G.(2002) Development of a flow-through system for cleaning and dissolving foraminiferal tests. Chemical Geology, 185, 51-69.

HARDING, D. J., ARDEN, J. W. AND RICKABY, R. E. M. (2006) A method for precise analysis of trace element/calcium ratios in carbonate samples using quadrupole inductively coupled plasma mass spectrometry. Geochemistry Geophysics Geosystems, 7, doi:10.1029/2005GC001093.

HARTLEY, G. AND MUCCI, A. (1996) The influence of pCO_2 on the partitioning of magnesium in calcite overgrowths precipitated from artificial seawater at 25 degrees and 1 atm total pressure. Geochimica Et Cosmochimica Acta, 60, 315-324.

HENRIKSEN, K., STIPP, S. L. S., YOUNG, J. R. AND BOWN,R. (2003) Tailoring calcite: Nanoscale AFM of coccolith biocrystals. American Mineralogist, 88, 2040-2044.

HENRIKSEN, K., STIPP, S. L. S., YOUNG, J. R. AND MARSH, M. E. (2004a) Biological control on calcite crystallization: AFM investigation of coccolith polysaccharide function. American Mineralogist, 89, 1709-1716.

HENRIKSEN, K., STIPP, S. L. S., YOUNG, J. R. AND MARSH, M. E. (2004b) Polysaccharides in coccolith biomineralization: Site-specific interaction with the calcite surface. Geochimica Et Cosmochimica Acta, 68, A202-A202.

HENRIKSEN, K., YOUNG, J. R., BOWN,R. AND STIPP, S. L. S. (2004c) Coccolith biomineralisation studied with atomic force microscopy. Palaeontology, 47, 725-743.

HO, T. Y., QUIGG, A., FINKEL, Z. V., MILLIGAN, A. J., WYMAN, K., FALKOWSKI,G. AND MOREL, F. M. M. (2003) The elemental composition of some marine phytoplankton. Journal of Phycology, 39, 1145-1159.

KITANO, Y., OKUMURA, M. AND IDOGAKI, M. (1980) Abnormal cehaviors of copper(II) and zinc ions in parent solution at the early stage of calcite formation. Geochemical Journal, 14, 167-175.

KLINKHAMMER, G. P., HALEY, B. A., MIX, A. C., BENWAY, H. M. AND CHESEBY, M. (2004) Evaluation of automated flow-through time-resolved analysis of foraminifera for Mg/Ca paleothermometry. Paleoceanography, 19, doi:10.1029/2004PA001050.

KUNIOKA, D., SHIRAI, K., TAKAHATA, N., SANO, Y., TOYOFUKU, T. AND UJIIE, Y. (2006) Microdistribution of Mg/Ca, Sr/Ca, and Ba/Ca ratios in Pulleniatina obliquiloculata test by using a NanoSIMS: Implication for the vital effect mechanism. Geochemistry Geophysics Geosystems, 7, doi:10.1029/2006GC001280.

LANGER, G., GUSSONE, N., NEHRKE, G., RIEBESELL, U., EISENHAUER, A., KUHNERT, H., ROST, B., TRIMBORN, S. AND THOMS, S. (2006) Coccolith strontium to calcium ratios in *Emiliania huxleyi*: The dependence on seawater strontium and calcium concentrations. Limnology and Oceanography, 51, 310-320.

LIN, Y. C. J. AND SPENCER, A. N. (2001) Calcium currents from jellyfish striated muscle cells: preservation of phenotype, characterisation of currents and channel localisation. Journal of Experimental Biology, 204, 3717-3726.

MARCHITTO, T. M., CURRY, W. B. AND OPPO, D. W. (2000) Zinc concentrations in benthic foraminifera reflect seawater chemistry. Paleoceanography, 15, 299-306.

MARSH, M. E. (1999) Coccolith crystals of *Pleurochrysis carterae*: crystallographic faces, organization, and development. Protoplasma, 207, 54-66.

MARSH, M. E. (2003) Regulation of $CaCO_3$ formation in coccolithophores. Comparative Biochemistry and Physiology B-Biochemistry AND Molecular Biology, 136, 743-754.

MORSE, J. W. AND MACKENZIE, F. T. (1990) Geochemistry of sedimentary carbonates, Amsterdam ; Oxford, Elsevier.

PAQUETTE, J. AND REEDER, R. J. (1995) Relationship between surface-structure, growth-mechanism, and trace-element incorporation in calcite. Geochimica Et Cosmochimica Acta, 59, 735-749.

REEDER, R. J. (1996) Interaction of divalent cobalt, zinc, cadmium, and barium with the calcite surface during layer growth. Geochimica Et Cosmochimica Acta, 60, 1543-1552.

RICKABY, R. E. M., SCHRAG, D. P., ZONDERVAN, I. AND RIEBESELL, U. (2002) Growth rate dependence of Sr incorporation during calcification of *Emiliania huxleyi*. Global Biogeochemical Cycles, 16, doi:10.1029/2001GB001408.

RICKABY, R. E. M., STOLL, H., HENDERIKS, J., SHAW, S. AND ELDERFIELD, H. (2006) Blooming coccolithophores. Geochimica Et Cosmochimica Acta, 70, Supplement 1 A533.

SERRANO, J. R., DASHTI, S. R., PEREZ-REYES, E. AND JONES, S. W. (2000) Mg^{2+} block unmasks Ca^{2+}/Ba^{2+} selectivity of alpha 1G T-type calcium channels. Biophysical Journal, 79, 3052-3062.

STIPP, S. L., HOCHELLA, M. F., PARKS, G. A. AND LECKIE, J. O. (1992) Cd2+ Uptake by calcite, solid-state diffusion, and the formation of solid-solution - interface processes observed with near-surface sensitive techniques (Xps, Leed, and Aes). Geochimica Et

Cosmochimica Acta, 56, 1941-1954.

STOLL, H. M., ENCINAR, J. R., ALONSO, J. I. G., ROSENTHAL, Y., PROBERT, I. AND KLAAS, C. (2001) A first look at paleotemperature prospects from Mg in coccolith carbonate: Cleaning techniques and culture measurements. Geochemistry Geophysics Geosystems, 2, doi:10.1029/2000GC000144.

STOLL, H. M., KLAAS, C. M., PROBERT, I., ENCINAR, J. R. AND ALONSO, J. I. G. (2002a) Calcification rate and temperature effects on Sr partitioning in coccoliths of multiple species of coccolithophorids in culture. Global and Planetary Change, 34, 153-171.

STOLL, H. M., ROSENTHAL, Y. AND FALKOWSKI,(2002b) Climate proxies from Sr/ Ca of coccolith calcite: Calibrations from continuous culture of *Emiliania huxleyi*. Geochimica Et Cosmochimica Acta, 66, 927-936.

STOLL, H. M. AND SCHRAG, D.(2001) Sr/Ca variations in Cretaceous carbonates: relation to productivity and sea level changes. Palaeogeography Palaeoclimatology Palaeoecology, 168, 311-336.

STOLL, H. M., ZIVERI, P., GEISEN, M., PROBERT, I. AND YOUNG, J. R. (2002c) Potential and limitations of Sr/Ca ratios in coccolith carbonate: new perspectives from cultures and monospecific samples from sediments. Philosophical Transactions of the Royal Society of London Series a-Mathematical Physical and Engineering Sciences, 360, 719-747.

TAKAHASHI-SHIMASE, K. AND NAKASHIMA, S. (2004) Shape changes of calcareous nannofossils upon aqueous dissolution as revealed by atomic force microscope measurements. Geophysical Research Letters, 31, doi:10.1029/2004GL020416.

TESORIERO, A. J. AND PANKOW, J. F. (1996) Solid solution partitioning of Sr^{2+}, Ba^{2+}, and Cd^{2+} to calcite. Geochimica Et Cosmochimica Acta, 60, 1053-1063.

VERY, A. A. AND DAVIES, J. M. (2000) Hyperpolarization-activated calcium channels at the tip of Arabidopsis root hairs. Proceedings of the National Academy of Sciences of the United States of America, 97, 9801-9806.

WANG, Y. F. AND XU, H. F. (2001) Prediction of trace metal partitioning between minerals and aqueous solutions: A linear free energy correlation approach. Geochimica Et Cosmochimica Acta, 65, 1529-1543.

YOUNG, J., DAVIS, S., BOWN,AND MANN, S. (1999) Coccolith Ultrastructure and Biomineralisation. Journal of Structural Biology, 126, 195-215.

YOUNG, J. R., DIDYMUS, J. M., BOWN,R., PRINS, B. AND MANN, S. (1992) Crystal assembly and phylogenetic evolution in heterococcoliths. Nature, 356, 516-518.

Obtaining Species-Specific Coccolith Calcification and Chemistry: a Conceptual Solution

6

In Chapter 1 it was argued that two advances must be made before the proxy-potential of coccolith trace-element geochemistry can be fully realised. Firstly, a technique is required to allow the cleaning of coccoliths for clays. Secondly, a method, which can efficiently obtain species-specific chemistry, must be conceived. The technique described in Chapter 3 provided an answer to the first problem, however the second problem remains unsolved. This chapter presents a conceptual answer to the remaining question, together with a statistical validation of the proposed technique.

Chapter 1 introduced the efforts that have been made to produce species-specific coccolith Sr/Ca and isotopic records. Here we will consider these methods in more detail. The first documented attempt to purify coccolith sediment for chemical analysis was made by Stoll and Ziveri (2002), who developed a technique based on repeated decanting and settling. Using this method the authors achieved "separation of sediment fractions whose carbonate is highly dominated (>70% but in most cases >90%) by coccoliths from a single species". These separated fractions displayed $\delta^{18}O$ and $\delta^{13}C$ values varying by up to 1.5 ‰ and 2.5 ‰ respectively, demonstrating a first-order separation of the chemical signatures of the different species. Stoll (2005) further developed this method by attempting to quantify the mass of calcium carbonate attributed to each coccolithophore species, based on species counts and coccolith volume estimates. The calculated mass was then exploited to assign a

chemical signature to each species. Using this technique, Stoll (2005) produced oxygen and carbon isotopic records over the Paleocene Eocene Thermal Maximum and concluded that similarities in the records produced by different species indicated only small species isotopic offsets. However, culture experiments in which the inter-species variability in coccolith isotopic composition was examined indicate that these conclusions are not necessarily valid when considering modern-day samples (Dudley et al., 1980; Ziveri et al., 2003). Errors in coccolith volume estimates (Young and Ziveri, 2000), and temporal variation in coccolith mass may explain the disparity between the down-core and cultured range of coccolith oxygen and carbon isotopic values.

More recently, a method has been developed to hand-pick the coccoliths of individual species using a sharpened tungsten needle (Stoll et al., 2007a; Stoll et al., 2007b; Stoll et al., 2007c). Using this method, 12 to 20 coccoliths (~1.8 to 3.0 ng of calcium carbonate) are isolated and mounted in epoxy and their Sr/Ca analysed with an ion probe. This technique reveals a considerably greater range of Sr/Ca values than those measured in subsamples produced by filtering, settling and decanting, demonstrating that more information exists

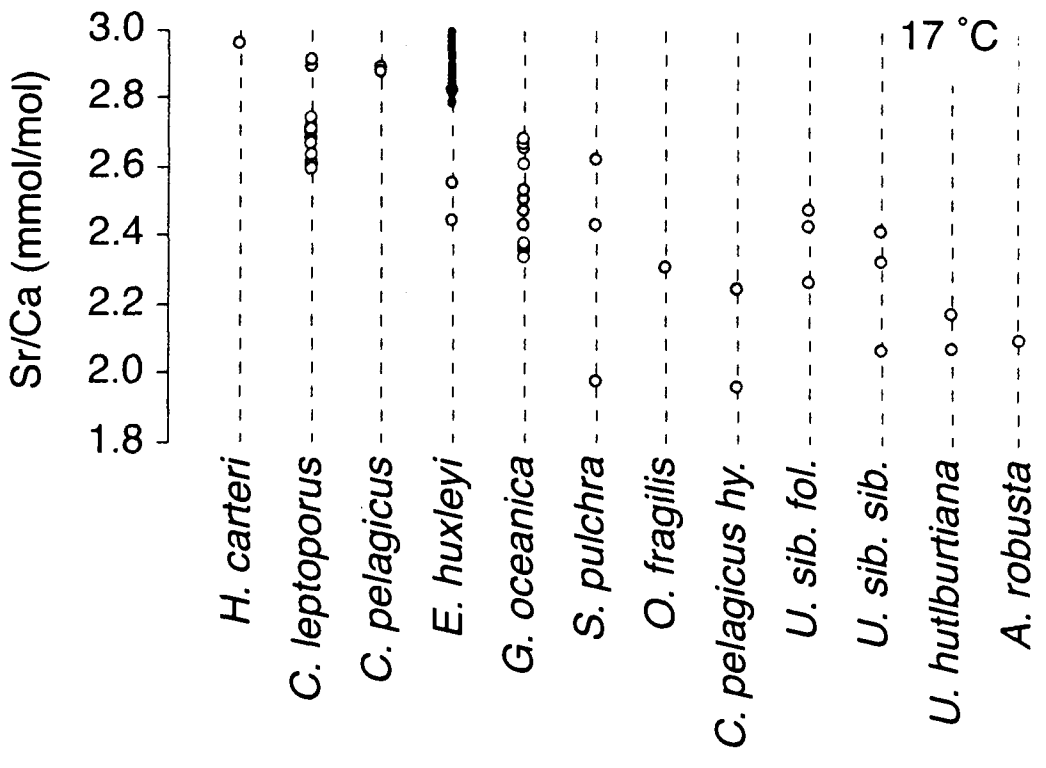

Figure 1. Sr/Ca of 12 different coccolithophore species cultured under identical temperature and nutrient conditions. From Stoll et al. (2002)

within down-core species specific Sr/Ca than has previously been utilised (the disparity in cultured coccolith Sr/Ca between different species is highlighted in Figure 1). Although individual coccolith picking has the potential to highlight interspecific differences in coccolith chemistry, it is slow and compromised by the small coccolith populations studied. Such a method is therefore unsuitable for producing high resolution, high precision geochemical records, particularly if the coccoliths of interest are produced by small species such as *E. huxleyi* and *Gephyrocapsa*.

The final method which attempts to achieve physical separation of species, developed by Minoletti et al. (Minoletti et al., 2001; and submitted), utilises microfiltration and strong ultrasonic treatment to produce monospecific samples of coccoliths produced by certain large Cretaceous species. This technique represents a significant step forward, but its application remains limited to coccoliths produced by a small number of species.

6.2 A New Methodology for the Determination of Species-Specific Down-Core Coccolith Geochemistry and Calcification

I propose a technique by which examination of the coccolith-assemblage, carbonate-mass and geochemistry, of multiple fractions from a size-restricted sub-sample can allow calculation of the mass and chemical composition of each species within that sample. This technique relies on forming a number of linear simultaneous equations equal to the number of species in the sub-sample, to allow calculation of the average mass of each species from absolute-species counts and the mass of carbonate in each fraction. The newly calculated average mass of each species in each fraction would then be combined with the chemistry and relative species counts from each fraction, to calculate the species-specific chemistry. The function and validity of this method are explained in more detail over the following paragraphs.

To prepare a tightly constrained size fraction of sediment containing a small number of species [three or four (Stoll and Ziveri, 2002)] one would apply a bubble-agitated filter procedure. Preliminary examination using polarising light microscopy would indicate how many species each sample contained. A method of settling and decanting (Stoll and Bains, 2003), if intra-species size variations are small, or otherwise bubble-agitated filtering and re-mixing, could then be applied to produce x sub-samples, where x is equal to the number of species in the sample, each containing a unique fraction of the different species. For every subsample, the relative proportion and number of liths-per-gram for each species in a known sample mass will be quantified using a polarised light microscope (after preparation of slides by filtering, spraying or settling from different water column heights, to achieve a uniform distribution of species), and the trace metal and isotopic composition of the sub-sample measured with mass spectrometry. The mass of $CaCO_3$ in each fraction could then be measured by weighing, before and after acidification (see Chapter 2). At this stage we would have x^2 species counts, x geochemical measurements, and x measurements of $CaCO_3$ mass. We can then produce x independent linear equations from the absolute species counts and measurements of $CaCO_3$ mass, and solve them simultaneously to find the average coccolith mass for each species in each sample. This first step is in itself of great value, and will allow down-core calculations of individual species calcification change, furthering the work discussed in Chapter 2, and bringing us closer to a species-wide understanding of calcification under ocean-acidification. The equations below highlight how the average coccolith mass for each species would be obtained, and a worked example following this technique is presented in appendix E.

If a, b and c are the absolute number of three species in a size-restricted sample that has been split into three fractions (Fractions 1, 2 and 3) with different proportions of each species (species x, y and z), and $Species_x$, $Species_y$ and $Species_z$, have unknown coccolith mass', referred to as $SM_{(x,y\ or\ z)}$, we can form three linear equations in which $Species_{(x,y\ or\ z)}$mass' are the only unknowns:

Fraction 1:

$$a_1 \cdot SM_x + b_1 \cdot SM_y + c_1 \cdot SM_z = \text{fraction1 } CaCO_3 \text{ mass}$$

Fraction 2:

$$a_2 \cdot SM_x + b_2 \cdot SM_y + c_2 \cdot SM_z = \text{fraction2 } CaCO_3 \text{ mass}$$

Fraction 3:

$$a_3 \cdot SM_x + b_3 \cdot SM_y + c_3 \cdot SM_z = \text{fraction3 } CaCO_3 \text{ mass}$$

The three equations can then be solved by substitution, or matrix methods, to calculate the average mass of a coccolith produced by Species' x, Species' y, and Species' z. An alternative methodology which could be used to gain the same result, if it were evident that errors associated with absolute species counts are prohibitively large, would be to perform the calculations from relative species counts and the average coccolith mass (i.e. the fraction's $CaCO_3$ mass divided by the number of $CaCO_3$ particles in the sample), as obtained by weighing and Coulter Counter analysis (see Chapter 2).

Once the average mass of coccoliths belonging to each species has been calculated, a similar method can be applied to calculate the species-specific chemistry:

If a, b and c are the relative proportions of three species in a size-restricted sample that has been split into three fractions (Fractions 1, 2 and 3) with different proportions of each species, and Species x, Species y and Species z have known mass' (referred to as $SM_{(x,y \text{ or } z)}$, see above for how this was calculated) but unknown chemistry (for example Sr/Ca or $\delta^{18}O$, referred to as $SC_{(x,y \text{ or } z)}$), we can form three linear equations where $Species_{(x,y,z)}$ chemistries are the only unknowns:

Fraction 1:

$$a_1 \cdot SM_x \cdot SC_x + b_1 \cdot SM_y \cdot SC_y + c_1 \cdot SM_z \cdot SC_z = \text{bulk fraction1 geochemistry}$$

Fraction 2:

$$a_2 \cdot SM_x \cdot SC_x + b_2 \cdot SM_y \cdot SC_y + c_2 \cdot SM_z \cdot SC_z = \text{bulk fraction2 geochemistry}$$

Fraction 3:

$$a_3 \cdot SM_x \cdot SC_x + b_3 \cdot SM_y \cdot SC_y + c_3 \cdot SM_z \cdot SC_z = \text{bulk fraction3 geochemistry}$$

The three equations can then be solved to calculate Species' x, Species' y, and Species' z trace-element or isotope chemistry.

6.3 Species-Specific Coccolith Chemistry: Proof of Concept

The proposed technique for obtaining species-specific coccolith chemistry relies on three criteria; the ability to produce subsamples containing different species compositions, the ability to accurately quantify the relative composition of each species, and the ability to accurately measure the chemistry of the different sub-samples. Stoll and Bains (2003) demonstrate that the relative proportion of species from within a single sample can be altered simply, utilising microfiltration, decanting and settling, and that the difference between Sr/Ca of these sub-fractions is systematically altered (Figure 2).

Accurate quantification of sub-sample population composition would be undertaken following well recognised sample preparation techniques, and counting with a polarized light

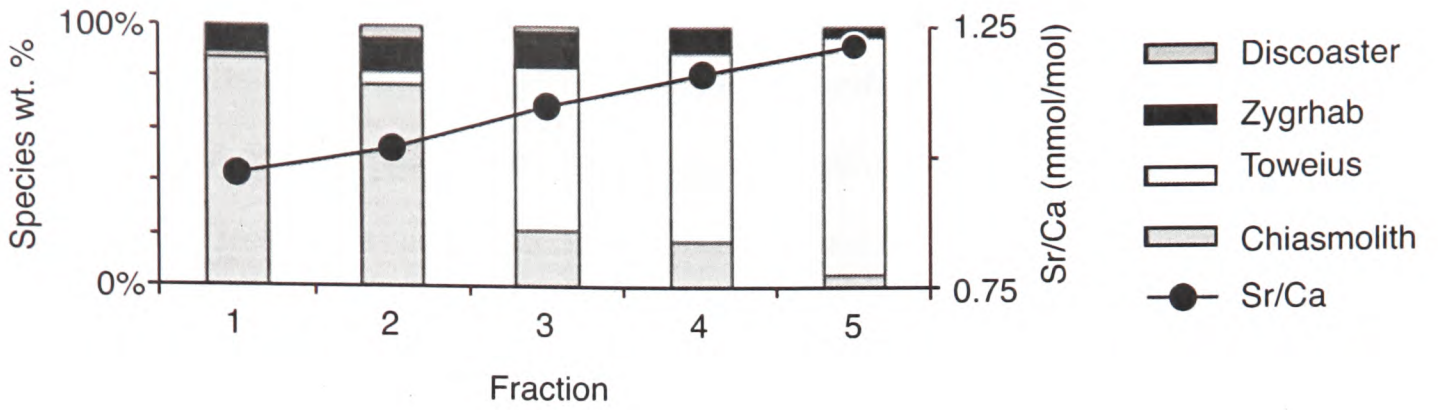

Figure 2. Weight percent of five different species calculated from species counts and measurements of coccolith diameter following the method of Young and Ziveri (2000) within five settling-split sample fractions of a sample (bars). Sr/Ca measurements on each sample fraction (black circles). This figure demonstrates how relative coccolith species-abundance can be altered, and how this is reflected in Sr/Ca measurements. Modified from Stoll and Bains (2003).

microscope. Because a restricted range of coccolith species would be analysed, population counts of ~300 coccoliths should constrain the relative species composition to within 1% (Fisher et al., 1943). The errors associated with absolute species counts are less well constrained than they are for relative species counts. Therefore, if it was evident that these errors were too large to allow the useful application of this method, a modified technique could be used, in which only relative species counts were necessary. To do this, instead of working out the average coccolith mass for each species using the total mass of calcite in the fraction, it would be possible to use the Coulter Counter method described in Chapter 2 to obtain the average coccolith mass (across all species). Knowing the average coccolith mass (across all species), and the relative proportion of each species it is possible to again produce simultaneous equations which can be solved to calculate species-specific coccolith mass. A major advantage of this method of plankton geochemical analysis over that based on foraminifera is that for no greater effort, large samples can be analysed. Large sample size allows analytical-repetition, and very precise trace-element, isotope and mass measurements to be made. Replicate measurements made using the Oxford ICP-MS facilities, would allow measurement with Sr/Ca reproducibility better than 1% and $\delta^{13}C$ and $\delta^{18}O$ reproducibility better than ±1.00‰.

To test the propagation of errors associated with the application of this method, Monte Carlo simulations have been produced to describe the distribution of standard deviations associated with the solution of three linear simultaneous equations. To do this, programs were written to record the standard deviation of 1000 solutions of a randomly generated set of results (where geochemical measurement values fell within the upper and lower limits of Sr/Ca or $\delta^{18}O$, and $CaCO_3$ mass fell between 1 and 10 units), each with the addition of an error, produced from a normal distribution over two standard deviations (where two standard deviations equals 1% for relative species counts, 2% for absolute species counts, 1% for Sr/Ca analyses and 1‰ for oxygen isotopes. The error associated with weighing is considered to be negligible, because the size of samples can be large, and unlimited replicate measurements can be made). This routine was run 10,000 to 30,000 times with randomly produced data sets containing species counts and geochemical results. The cumulative relative standard deviations (RSDs) for coccolith mass and Sr/Ca calculations are plotted in Figure 3. The modal RSDs falls between 1.4% and 1.6% for both analyses. Propagation of the modal RSD values give a combined error of between 2.0 and 2.3%, well within the errors commonly associated with biogeochemical analysis.

6.4 Implications

The technique I have proposed could be used to solve a number of exciting problems. One example of the method's application would be in the creation of a growth-rate correction for alkenone $\delta^{13}C$ CO_2 estimates by measuring Sr/Ca in coccoliths produced by the alkenone-forming coccolithophore species (*E. huxleyi* or *Gephyrocapsa* species, depending on sediment age). This correction has the potential to produce a step-improvement in alkenone-$\delta^{13}C$ estimates of past pCO_2. This is of great importance because our inability to accurately constrain past pCO_2 is one of the major issues holding back both palaeo and future climate science. At present we have high resolution atmospheric CO_2 levels dating back 650 kyr

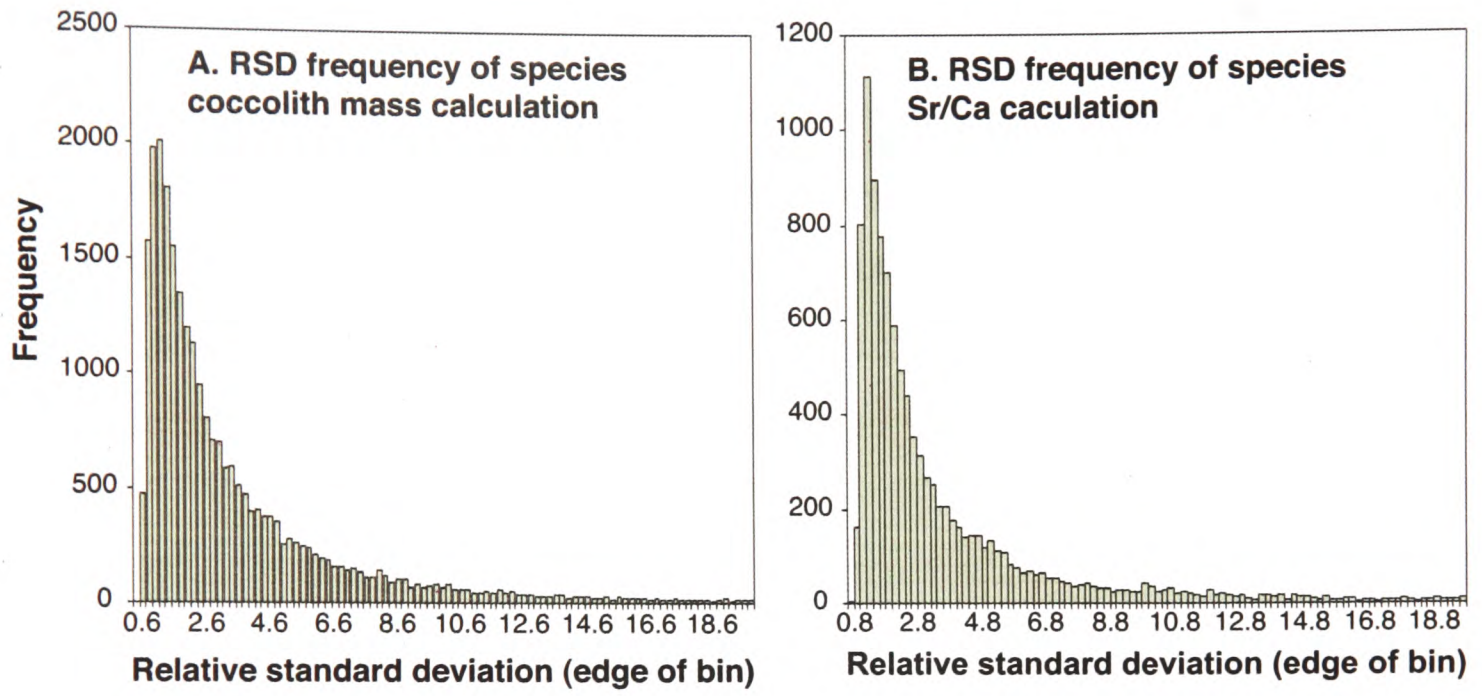

Figure 3. Monte Carlo simulations modelling the relative standard deviations (RSDs) of solutions to three simultaneous equations for **A.** coccolith mass and **B.** coccolith Sr/Ca. RSDs pertaining to coccolith mass calculations have been calculated allowing the fraction and coccolith mass' to fall between 1 and 10 units. Absolute species counts were assigned random errors taken from a normal distribution over two standard deviations, where two standard deviations equals 2% of the absolute count value. No error was assigned to weight measurements, because the potential to utilise large samples size and numerous replicate measurements would render the error negligible. Sr/Ca RSDs were calculated for results falling between 1 and 3 mmol/mol, produced by applying random errors following a normal distribution about the result over two standard deviations, where two standard deviations = 1% for relative species counts, and 1% for Sr/Ca measurements. Note that 3.2% and 2.9% of the data from the coccolith-mass and coccolith-Sr/Ca simulations respectively have an RSD greater than 20, but have been excluded from the plot for clarity.

from ice-core data (Siegenthaler et al., 2005). For older time intervals, our knowledge of atmospheric CO_2 variability relies on boron isotopic records obtained from foraminifera (e.g. Pearson and Palmer, 2000; Sanyal et al., 1995), alkenone (and other organic matter) based records of carbon isotopic fractionation by phytoplankton (e.g. Pagani, 2002), leaf stomatal indices (e.g. Royer et al., 2001), palaeosol carbonate $\delta^{13}C$ values (e.g. Tanner et al., 2001) and identification of sodium carbonate nahcolites (Lowenstein and Demicco, 2006). Each of these proxies is limited by the range of environmental and/or physiological factors to which they also respond.

Of those described above, the two tools most commonly used to reconstruct pre-icecore pCO_2 are changes in the ratio of boron isotopes incorporated into the calcium carbonate tests of planktonic foraminifera ($\delta^{11}B$), and changes in the carbon isotope fractionation (ε_p) by haptophytes as recorded by the carbon isotopic composition of alkenones. Foraminiferal $\delta^{11}B$ acts as a proxy for seawater pH, one of the variables needed to constrain the carbonate system. However, very precise pH measurements on samples free from dissolution, as well as knowledge of the dissolved inorganic carbon concentration, or a constraint on the ocean alkalinity, are required to reconstruct past CO_2 using this technique. No technique presently exists to accurately estimate past [DIC] or alkalinity.

Alkenones are long-chained organic molecules, produced by a narrow range of haptophyte species, including *Emiliania huxleyi* and *Gephyrocapsa oceanica*. The concentration of dissolved CO_2 during growth is a primary control on carbon isotope fractionation during photosynthesis, and thus the stable carbon isotopic composition of algal matter and algal-derived lipids (Wong and Sackett, 1978). Because alkenones are preserved readily in the sedimentary record, their isotopic composition potentially provides a very valuable palaeo-pCO_2 proxy. However, a number of factors other than pCO_2 control the carbon isotopic signature of alkenones, including: cell geometry, the active transport of inorganic carbon into the cell, and cellular growth rate (Bidigare et al., 1997; Jasper and Hayes, 1990; Laws et

al., 1995; Pancost and Pagani, 2006; Popp et al., 1998) (Figure 4). Taking into account these factors, the total isotopic fractionation recorded by the organic matter (ε_p) can be expressed as:

$$\varepsilon_p = \varepsilon_t + (\varepsilon_f - \varepsilon_t)\,(1 - ((\mu C)/(kC_e))$$

where ε_t represents the fractionation during transport, ε_f is the fractionation during Rubisco-mediated fixation; k is a rate constant representing the diffusion of CO_2 into and out of the cell, C and C_e are the CO_2 concentration internal and external to the cell respectively, and μ is the growth rate. The assumptions inherent in this equation have been tested using a range of phytoplankton grown under diverse conditions (Bidigare et al., 1997; Laws et al., 1997; Popp et al., 1998) (Figure 4). The experiments demonstrate that ε_p varies linearly with μ/pCO_2, but following a different gradient for each different organism. This implies

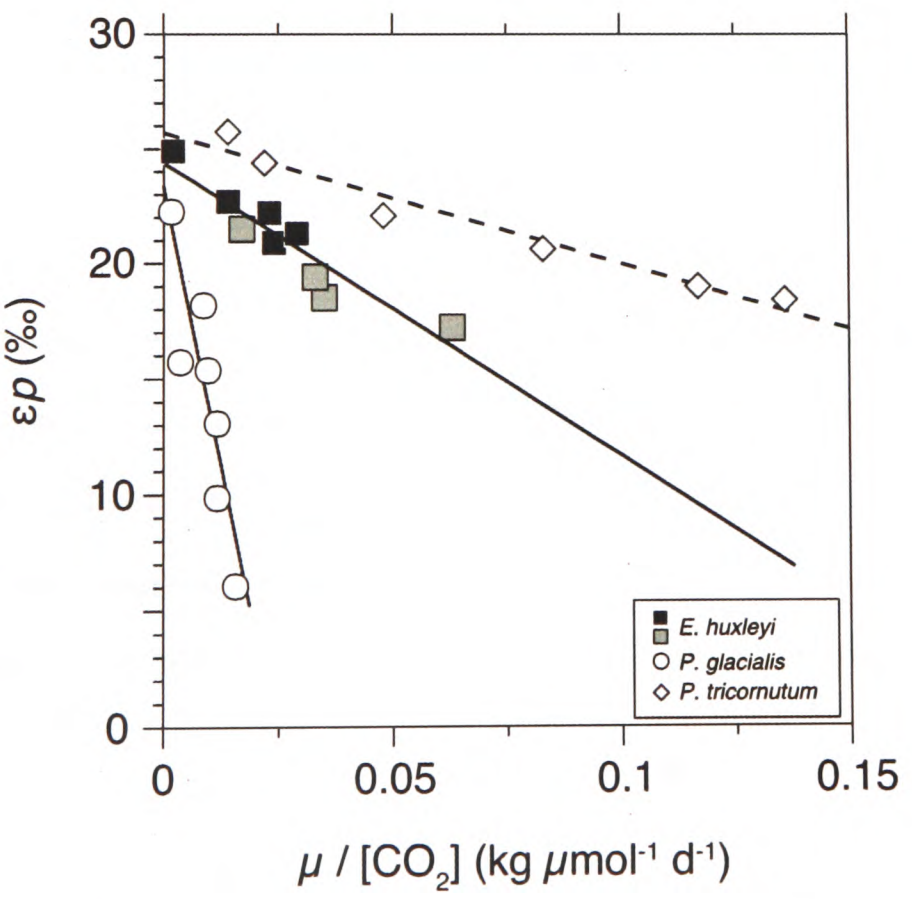

Figure 4. εp against $\mu/[CO_2]$ measured in three plankton species, *tricornutum*, *glacialis* and *E. huxleyi* (the only coccolithophore) during chemostat cultures. Re-drawn from Pancost and Pagani (2006), originally from Popp et al. (1998).

that for individual algal species, pCO_2 and growth rate are the main variables controlling the isotopic fractionation of organic matter. Down-core measurement of *E. huxleyi* and *Gephyrocapsa* coccolith Sr/Ca should allow the reconstruction of growth-rate in the same samples as those providing the alkenone $\delta^{13}C$, enabling a growth-rate correction of pCO_2 estimates and therefore greatly improved palaeo-pCO_2 reconstruction.

6.5 Species Specific Coccolith $\delta^{18}O$

A further example of how this proposed technique could be applied to palaeoclimatology is in the measurement of species-specific coccolith $\delta^{18}O$. This would allow a valuable $\delta^{18}O$ dataset to be built up in areas and cores where foraminifera are rare or significantly dissolved, as well as increasing the temporal resolution of $\delta^{18}O$ in previously analysed cores. Monte Carlo simulations have again been run to calculate the errors associated with this analysis. These simulations indicate a modal RSD for these measurements of between 1.8 and 2.1%, well within the typical errors associated with this kind of analysis. Species-specific coccolith $\delta^{18}O$ data has the potential to provide sea-level and temperature information at resolutions far in excess of those possible from foraminiferal $\delta^{18}O$ analysis, as a consequence of the smaller coccolith size. Furthermore, coccoliths appear to be more resistant to dissolution than are foraminifera (Beaufort et al., 2007; Frenz and Henrich, 2007) making them ideal for studying past periods of ocean acidification where foraminifera suffer from dissolution or extinction (for example the PETM). This would allow us to significantly improve our understanding of temperature and ice-volume change during periods of elevated pCO_2.

6.6 Conclusion

With the further development of cleaning procedures for sedimentary coccoliths, a large number of applications are likely to emerge requiring the ability to measure the chemistry of coccoliths produced by specific species. The method I propose here would allow the rapid production of a variety of data. However, inherent in the technique is the multiplication of many individual errors. Until a method has been developed to physically isolate individual coccoliths of any species, perhaps through the future development of flow-cytometry methods, I believe that the ideas presented here describe an exciting tool capable of breaking through the barrier of species-separation that has significantly limited the application of coccolith-geochemistry for the last 20 years.

6.7 Bibliography

BEAUFORT, L., PROBERT, I., AND BUCHET, N., 2007, Effects of acidification and primary production on coccolith weight: Implications for carbonate transfer from the surface to the deep ocean: Geochemistry Geophysics Geosystems, v. 8, doi:10.1029/2006GC001493.

BIDIGARE, R.R., FLUEGGE, A., FREEMAN, K.H., HANSON, K.L., HAYES, J.M., HOLLANDER, D., JASPER, J.P., KING, L.L., LAWS, E.A., MILDER, J., MILLERO, F.J., PANCOST, R., POPP, B.N., STEINBERG, P.A., AND WAKEHAM, S.G., 1997, Consistent fractionation of C-13 in nature and in the laboratory: Growth-rate effects in some haptophyte algae: Global Biogeochemical Cycles, v. 11, 279-292.

DUDLEY, W.C., DUPLESSY, J.C., BLACKWELDER, P., AND BRAND, L., 1980, Coccoliths in Pleistocene-Holocene nannofossil assemblages: Nature, v. 285,222-223.

FISHER, R.A., CORBET, A.S., AND WILLIAMS, C.B., 1943, The relation between the number of species and the number of individuals in a random sample of an animal population: The Journal of Animal Ecology, v. 12,42-58.

FRENZ, M., AND HENRICH, R., 2007, Carbonate dissolution revealed by silt grain-size distribution: comparison of Holocene and Last Glacial Maximum sediments from the pelagic South Atlantic: Sedimentology, v. 54,391-404.

JASPER, J. P. AND HAYES, J. M., 1990, A carbon isotope record of CO_2 levels during the late Quaternary: Nature, v. 347, 462-464.

LAWS, E.A., BIDIGARE, R.R., AND POPP, B.N., 1997, Effect of growth rate and CO_2 concentration on carbon isotopic fractionation by the marine diatom *Phaeodactylum tricornutum*: Limnology and Oceanography, v. 42,1552-1560.

LAWS, E.A., POPP, B.N., BIDIGARE, R.R., KENNICUTT, M.C., AND MACKO, S.A., 1995, Dependence of phytoplankton carbon isotopic composition on growth-rate and $[CO_2]_{(Aq)}$ - theoretical considerations and experimental results: Geochimica Et Cosmochimica Acta, v. 59,1131-1138.

LOWENSTEIN, T.K., AND DEMICCO, R.V., 2006, Elevated Eocene atmospheric CO_2 and its subsequent decline: Science, v. 313,1928-1928.

MINOLETTI, F., GARDIN, S., NICOT, E., RENARD, M., AND SPEZZAFERR, S., 2001, Mise au point d'un protocole experimental de separation granulometrique d'assemblages de nannofossiles calcaires; applications paleoecologiques et geochimiques: Bulletin de la Sociètè Gèologique de France, v. 172,437-446.

MINOLETTI, F., HERMOSO, M., AND GRESSIER, V., submitted, A separation protocol for micron-sized particles: Applications in palaeoceanography and calcareous

nannoplankton biogeochemistry.

PAGANI, M., 2002, The alkenone-CO_2 proxy and ancient atmospheric carbon dioxide: Philosophical Transactions of the Royal Society of London Series a-Mathematical Physical and Engineering Sciences, v. 360,609-632.

PANCOST, R., AND PAGANI, M., 2006, Controls on the carbon isotopic compositions of lipids in marine environments, *in* Volkman, J., ed., The Handbook of Environmental Chemistry, Volume 2 Series: Marine Organic Matter: Biomarkers, Isotopes and DNA, Springer, Germany,209-249.

PEARSON, P.N., AND PALMER, M.R., 2000, Atmospheric carbon dioxide concentrations over the past 60 million years: Nature, v. 406,695-699.

POPP, B.N., LAWS, E.A., BIDIGARE, R.R., DORE, J.E., HANSON, K.L., AND WAKEHAM, S.G., 1998, Effect of phytoplankton cell geometry on carbon isotopic fractionation: Geochimica Et Cosmochimica Acta, v. 62,69-77.

ROYER, D.L., WING, S.L., BEERLING, D.J., JOLLEY, D.W., KOCH, P.L., HICKEY, L.J., AND BERNER, R.A., 2001, Paleobotanical evidence for near present-day levels of atmospheric CO_2 during part of the tertiary: Science, v. 292,2310-2313.

SANYAL, A., HEMMING, N.G., HANSON, G.N., AND BROECKER, W.S., 1995, Evidence for a higher ph in the glacial ocean from boron isotopes in foraminifera: Nature, v. 373,234-236.

SIEGENTHALER, U., STOCKER, T.F., MONNIN, E., LUTHI, D., SCHWANDER, J., STAUFFER, B., RAYNAUD, D., BARNOLA, J.M., FISCHER, H., MASSON-DELMOTTE, V., AND JOUZEL, J., 2005, Stable carbon cycle-climate relationship during the late Pleistocene: Science, v. 310,1313-1317.

STOLL, H., SHIMIZU, N., AREVALOS, A., MATELL, N., BANASIAK, A., AND ZEREN, S., 2007a, Insights on coccolith chemistry from a new ion probe method for analysis of individually picked coccoliths: Geochemistry Geophysics Geosystems, v. 8, doi:10.1029/2006GC001546.

STOLL, H.M., 2005, Limited range of interspecific vital effects in coccolith stable isotopic records during the Palaeocene Eocene thermal maximum: Paleoceanography, v. 20, doi:10.1029/2004PA001046.

STOLL, H.M., AND BAINS, S., 2003, Coccolith Sr/Ca records of productivity during the Paleocene-Eocene thermal maximum from the Weddell Sea: Paleoceanography, v. 18, doi:10.1029/2002PA000875.

STOLL, H.M., SHIMIZU, N., ARCHER, D., AND ZIVERI, P., 2007b, Coccolithophore productivity response to greenhouse event of the Paleocene-Eocene Thermal Maximum: Earth and Planetary Science Letters, v. 258,192-206.

STOLL, H.M., AND ZIVERI, P., 2002, Separation of monospecific and restricted coccolith assemblages from sediments using differential settling velocity: Marine

Micropaleontology, v. 46,209-221.

STOLL, H.M., ZIVERI, P., SHIMIZU, N., CONTE, M., AND THEROUX, S., 2007c, Relationship between coccolith Sr/Ca ratios and coccolithophore production and export in the Arabian Sea and Sargasso Sea: Deep-Sea Research Part Ii-Topical Studies in Oceanography, v. 54,581-600.

TANNER, L.H., HUBERT, J.F., COFFEY, B.P., AND MCINERNEY, D.P., 2001, Stability of atmospheric CO_2 levels across the Triassic/Jurassic boundary: Nature, v. 411,675-677.

WONG, W.W., AND SACKETT, W.M., 1978, Fractionation of stable carbon isotopes by marine-phytoplankton: Geochimica Et Cosmochimica Acta, v. 42,1809-1815.

YOUNG, J.R., AND ZIVERI, P., 2000, Calculation of coccolith volume and its use in calibration of carbonate flux estimates: Deep-Sea Research Part II -Topical Studies in Oceanography, v. 47,1679-1700.

ZIVERI, P., STOLL, H., PROBERT, I., KLASS, C., GEISEN, M., GANSSEN, G., AND YOUNG, J., 2003, Stable isotope vital effects in coccolith calcite: Earth and Planetary Science Letters, v. 210,137-149.

Conclusions and Future Work

7

7.1 Summary

This thesis has examined the physiological response and potential geochemical application, of coccoliths to past and future environmental change. As discussed, the importance of coccolithophores, in terms of oceanic carbon-cycling, results from their prolific production of $CaCO_3$. Although coccolithophores constitute only a minor component of the total organic carbon production in the oceans, the coccoliths they produce account for around a third of all $CaCO_3$ being formed in the surface ocean today, and considerably more of that produced at times in the geological past. Coccoliths are therefore one of the most important players in the carbonate counter-pump, and one of the most valuable potential recorders of geochemical palaeoenvironmental data.

Chapter 2 explored the calcification response of coccolithophores to rising atmospheric CO_2 levels, since the beginning of the European Industrial Revolution around 230 years ago, and to predicted values for the end of this century. The down-core approach utilised in this study, the first examination of natural coccolith mass change over such short time intervals, indicated that the average mass of a coccolith in the Sub-Arctic North Atlantic had increased by almost 40% since 1780 A.D., and that this change correlates closely with the increase

in concentration of CO_2 in the atmosphere. To interpret this change as a true calcification increase, rather than an increase in coccolith mass at the expense of the number of coccoliths produced, a collaborative laboratory project was set up, as part of which I examined the volumes of coccoliths collected from cultures maintained under a variety of CO_2 conditions. These measurements demonstrated that coccolith volume change accounts for the majority of the increase in particulate inorganic carbon production by the coccolithophore *E. huxleyi* under elevated pCO_2 and therefore that the increase in mass of sedimentary coccoliths since 1780 is likely to represent an increase in total $CaCO_3$ production. A second observation from the culture experiments is that coccolithophore cells, as well as coccoliths, increase in volume as CO_2 is elevated, and that the associated organic and inorganic carbon production rates increase in proportion to each other. This finding is significant because, considering just coccolithophore production, the increased carbon fixation we observe in response to elevated pCO_2 will not change the balance of the organic-carbon and inorganic-carbon marine pumps, and therefore will have no net effect on CO_2 drawdown. This conclusion contrast with that of many previous studies, which have suggested that coccolithophore calcification will decrease under elevated CO_2 levels, and therefore will allow the surface ocean to store more anthropogenic CO_2 than if calcification remained constant. However, what this study does not allow us to confirm is whether, because coccolithophores account for a significantly larger proportion of total marine inorganic-carbon production than they do marine organic-carbon production, such an increased growth will be paralleled by an increased primary production of other marine organisms. If not, will the increased calcification by coccolithophores tip the whole-ecosystem organic-carbon:inorganic-carbon balance in favour of reduced atmospheric CO_2 drawdown?

Chapters 3 and 4 focused on the development of a new technique to facilitate the separation of sedimentary coccoliths from associated clay-grains. This new technique represents a significant step forward in the use of coccolith chemistry as a palaeo-reconstruction tool, because contamination by detrital clay minerals has so far prevented the geochemical

community from accessing the potential wealth of palaeoenvironmental trace-element data recorded within coccolith calcite. The global distribution, dissolution-resistance and mixed-layer production habitat of coccoliths, together with their small size, should make them ideal high-resolution geochemical recorders of surface-ocean environmental change. However, the last point, their small size, has also prevented widescale geochemical analysis. The technique described in Chapter 3 of this thesis exploits the contrasting birefringent and fluorescent properties of coccoliths in comparison to clay-grains, to allow separation using flow-cytometry. When applied to sedimentary material from the North-East Atlantic, this technique produced an order-of-magnitude drop in sample Al, Fe, Mg and Mn concentrations, and a break-down of correlation between Mg and Mn/Ca, and Al and Fe/Ca ratios, indicating that the measured Mg and Mn values were no longer associated with clay contamination, i.e. the sorted samples were clay-clean.

The fifth chapter of this thesis examined coccolith chemistry through continuous dissolution analysis, following the technique conceived by Haley and Klinkhammer (2002). So far, results using this technique have only been published by one research group, and subsequently, after fabricating a similar system in Oxford, we had the opportunity to validate their method and consider ways to further-improve the analyses. It was discovered that peaks in Ca concentration occurring at intervals throughout the sample dissolution related to step-changes in the pH of the acid used for dissolution, rather than the dissolution of distinct phases within the sample as had previously been thought. In light of this observation, it is recommended that future flow-through time-resolved analysis, undertaken using a quaternary gradient pump, use acid of a constant pH to dissolve samples rather then attempting to change the pH of the acid during the analysis. Following this recommendation, it was found that the FT-TRA system could wash away a number of contaminants, allowing the measurement of preliminary values for the exchange coefficients of element/Ca ratios into the calcite produced by *C. pelagicus*, with respect to the chemistry of the culture medium. These K_D values are; Sr/Ca = 0.37, Mg/Ca < 1.05×10^{-5}, Ba/Ca < 4.93×10^{-3}, Mn/Ca <0.63, Cd/Ca = 17.00-14.50

and Zn/Ca = 21.96-13.51. The possibility that some of the complex element/Ca curves obtained during continuous dissolution reflect a non-uniform distribution of elements within the calcified structure of a single coccolith has been considered. This idea was explored using atomic force microscopy, where it was shown that dissolution of a single coccolith progresses in an organised fashion, dissolving the crystal units making up the perimeter-region of the coccolith's exposed shield before dissolving the units making up the central area. Contrastingly however, the very first step of dissolution is not unit-selective, and is manifest as small etch-pit formation over the entire exposed coccolith surface. The inability to image the proximal and distal shields of a single coccolith simultaneously prevented conclusive determination of whether chemical inhomogeneity plays a governing roll in the morphological progression of dissolution, and therefore a full understanding of the chemical evolution recorded during flow-through analysis.

Chapter 6 then addressed the outstanding problem of sedimentary coccolith species separation to allow the construction of geochemical records unbiased by changes in species-composition. The solution I present to this problem relies on solving a matrix of chemical data to deconvolve the chemistries of the individual species from a number of bulk sediment measurements. This technique would inherently suffer from larger errors than would exist if large samples, containing only coccoliths produced by a single-species could be produced, however, presently such samples can not be obtained. Using the proposed method, I calculate that single species chemistries with modal relative standard deviations of between 2 and 2.3% for Sr/Ca analysis and 1.8 and 2.1% for $\delta^{18}O$ analysis could be obtained. These standard deviations fall well within the associated errors of biogeochemical analysis. Additionally, the method I describe could be utilised to estimate down-core calcification changes within coccoliths produced by a single coccolithophore species, and as such add significantly to our understanding of how coccolithophores have responded, and will continue to respond, to increasing levels of atmospheric CO_2.

7.2 Future Work

The results summarised above represent a significant step forward in our understanding of how coccolithophore calcification may react to further-elevated CO_2 levels, and how we might be able to use sedimentary coccoliths to investigate similar situations which have occurred in the past. However, we are still far from reaching a comprehensive understanding of the mechanisms involved in these processes.

Regarding the issues surrounding the phytoplankton calcification response to ocean-acidification, an important next step will be to understand how individual species have reacted to anthropogenic ocean-acidification over the last two centuries within the real ocean, allowing us to build up a consistent understanding of the group-wide response, and ultimately the ecosystem response to a perturbed future carbonate system. Many questions have been raised regarding the applicability of small-scale culture experiments to whole-oceanic problems. A particular worry is whether present culture experiments have allowed organisms time to adapt to the enforced condition, and therefore whether the results would differ if the cultures were maintained under those conditions for longer periods of time. In light of these concerns, I believe that the approach described in Chapter 2; looking for signs of a calcification response in the natural environment, is of great value, and should be a major focus for future study. One possible way to extend this work would be to utilise the method presented by Beaufort (2005) to examine individual coccolith birefringence, as a proxy for coccolith mass. Application of this technique would allow development of an understanding of the variability between the calcification responses of different species, an important parameter for biogeochemical modelling. New ultra-high sedimentation-rate cores need to be obtained from a variety of oceanic regimes, sampling coastal waters as well as the open ocean. The remains of organisms preserved in those cores should be analysed at a species level, perhaps employing the technique described in Chapter 6 to elucidate their physiological and chemical response to decreasing sea-water pH. However, just to understand

how calcification is changing is not enough. We need to know what is happening, and what will continue to happen, to organic-carbon as well as inorganic carbon-production as pCO_2 rises. It is clear that we cannot directly measure these changes in sedimentary samples, because the organic structures are not well preserved after burial, however it may be possible to use carbonate and biomarker chemistry to investigate these issues. Single-species coccolith Sr/Ca could tell us about nutrient availability, whilst concomitant carbonate $\delta^{13}C$ or organic-mater nitrogen isotope measurements could tell us about nutrient utilisation.

To produce global records of primary-production change and calcification over the last 250 years would be a major advance, but would still only be the first step in understanding the CO_2 feedback associated with changes in the relative 'strengths' of the organic-carbon and inorganic-carbon marine pumps. This is because ultimately it is not the production, but the export of these two carbon-products out of the seasonally mixed layer that regulates the air-sea CO_2 exchange. To understand the export efficiency of organic and inorganic carbon, we first need to fully understand the processes by which export occurs, whether through faecal pellets, transparent exopolymers or any of a number of other processes. With this in mind, we need to understand the role played by bio-minerals in changing the density of sinking particles and how this may influence the amount of organic and inorganic-carbon transported to depth.

The biological-response to ocean-acidification is as pressing a problem as it is poorly-understood. So far all that the community has done is to demonstrate that the phytoplankton response to elevated CO_2 levels is complex. We now need laboratory experiments performed under a common protocol, and the production of spatially and biologically rich datasets from ultra-high sedimentation cores, to allow the development of drastically improved biogeochemical models.

Considering now how we might improve our geochemical understanding and application of coccoliths, to answer palaeoenvironmental questions, the challenges are somewhat more clearly defined. We have demonstrated a technique that can be used to reliably sort coccolith samples from contaminating detrital clays, but we have been unable to confirm whether the subsequently measured chemistry represents pure-coccolith trace-element values. Large-volume flow-cytometry sorts are now needed to produce large samples upon which the various steps involved in the standard foraminiferal cleaning procedure can be performed. Measurement of samples cleaned to varying degrees will indicate if and where further contamination exists, and allow for the first time, confident down-core measurement of multiple-element/Ca ratios in coccoliths. These steps will then have to be combined with methods capable of obtaining data from coccoliths produced by single coccolithophore species, potentially through the application of the technique described in Chapter 6, to tackle new and exciting palaeoclimatological questions.

To fully understand what biomineral chemistry can tell as about past environmental change, we need to understand the controls exerted by biomineralisation over trace-element and isotope incorporation into crystals. The results presented in Chapter 5 allude to a non-uniform distribution of substituted elements even in one of the most basic biomineral constructions, a coccolith. New nano-analytical techniques such as NanoSIMS, combined with careful culturing of samples under a variety of chemical and environmental conditions, will allow us to test the existence and extent of the proposed inhomogeneity. Elemental maps of the distribution of substitutions within biominerals will need to be combined with genetic and proteonomic investigations of the biomineralisation mechanisms and pathways. Once this has been achieved, knowledge of biological element selectivity can be combined with a thermodynamic understanding of substitute partitioning into minerals, and new palaeo-proxies can be conceived and utilised with confidence.

7.3 Bibliography

BEAUFORT, L. (2005) Weight estimates of coccoliths using the optical properties (birefringence) of calcite. Micropaleontology, 51, 289-297.

HALEY, B. A. & KLINKHAMMER, G.(2002) Development of a flow-through system for cleaning and dissolving foraminiferal tests. Chemical Geology, 185, 51-69.

Appendix A: Ocean Acidification Data

Average values and 1σ errors for sample calcite mass, particle number and average calcite particle mass measured in RAPID-21-12-B. Data are presented as double-page spreads. Hyphens represent sample depths at which data was not collected.

Depth (cm.b.s.f.)	Age (Calender years A.D.)	Ave. coccolith mass x 10^{-10} g	Ave. coccolith mass error (1 σ)
0.25	2004.0	0.1219	0.0060
0.75	2001.8	0.1680	0.0269
1.25	1999.7	-	-
1.75	1997.5	0.1754	0.0399
2.25	1995.3	0.1294	0.0125
2.75	1993.1	0.1477	0.0310
3.25	1991.0	0.1635	0.0285
3.75	1988.8	-	-
4.25	1986.6	-	-
4.75	1984.4	0.1137	0.0232
5.25	1982.3	0.0979	0.0169
5.75	1980.1	0.1314	0.0048
6.25	1977.9	-	-
6.75	1975.7	0.1247	0.0164
7.25	1973.6	0.1040	0.0260
7.75	1971.4	0.1279	0.0172
8.25	1969.2	0.1321	0.0418
8.75	1967.0	0.1171	0.0186
9.25	1964.9	0.1231	0.0299
9.75	1962.7	0.1073	0.0158
10.25	1960.5	0.1038	0.0100
10.75	1958.3	0.1184	0.0273
11.25	1956.2	0.0966	0.0117
11.75	1954.0	0.2356	0.0507
12.25	1951.8	0.1302	0.0070
12.75	1949.7	0.0999	0.0162
13.25	1947.5	0.1264	0.0411
13.75	1945.3	0.0909	0.0101
14.25	1943.1	0.1061	0.0158
14.75	1941.0	0.1234	0.0150
15.75	1936.6	0.1449	0.0156
15.75	1936.6	0.1145	0.0059
16.25	1934.4	0.0988	0.0075
16.75	1932.3	0.1050	0.0314
17.25	1930.1	-	-
17.75	1927.9	0.1155	0.0101

Ave. sample calcite mass (x 10^{-10} g)	Ave. coccolith mass error (1 σ)	No. $CaCO_3$ particles	No. $CaCO_3$ particles error (1 σ)
81116	721	66538	3221
47530	351	28293	4527
23582	121	24942	16968
76832	572	43800	9952
74143	549	57314	5495
40173	367	27202	5705
26537	522	16233	2793
-	-	32044	3994
-	-	83205	7196
113055	709	99415	20280
99338	1853	101503	17357
104063	1088	79191	2771
16037	707	-	-
80738	507	64741	8498
33558	375	32254	8058
139982	638	109467	14719
116426	580	88103	27878
66352	412	56660	8972
72193	593	58628	14226
63314	540	58996	8650
94220	649	90810	8713
68613	629	57972	13362
71883	596	70444	8483
51156	702	21717	4660
96900	407	74425	3979
63103	465	63176	10203
74953	429	59275	19242
82295	784	90493	10004
105492	703	99428	14819
104554	697	84761	10314
72543	365	50047	5377
89390	606	78103	3984
69391	583	70207	5251
89473	462	85212	25453
63362	627	-	-
102161	739	88481	7721

Depth (cm.b.s.f.)	Age (Calender years A.D.)	Ave. coccolith mass x 10^{-10} g	Ave. coccolith mass error (1 σ)
18.25	1925.7	0.0974	0.0005
18.75	1923.6	0.0983	0.0130
19.25	1921.4	-	0.0230
19.75	1919.2	-	-
20.25	1917.0	0.1546	0.0440
20.75	1914.9	0.1178	0.0201
21.25	1912.7	0.1198	0.0173
21.75	1910.5	0.1387	0.0139
22.25	1908.3	0.1104	0.0101
22.75	1906.2	0.1151	0.0106
23.25	1904.0	0.1467	0.0200
23.75	1901.8	0.1084	0.0178
24.25	1899.7	0.0915	0.0148
25.75	1893.1	-	-
25.25	1895.3	0.1411	0.0172
25.75	1893.1	0.1400	0.0313
26.25	1891.0	0.1227	0.0110
26.75	1888.8	0.1112	0.0153
27.25	1886.6	0.1083	0.0068
27.75	1884.4	0.0933	0.0090
28.25	1882.3	0.1096	0.0111
28.75	1880.1	0.0958	0.0136
29.25	1877.9	0.1121	0.0364
29.75	1875.7	0.0867	0.0184
30.25	1873.6	0.1194	0.0170
30.75	1871.4	0.0947	0.0092
31.25	1869.2	0.1168	0.0240
31.75	1867.0	0.1457	0.0228
32.25	1864.9	0.1162	0.0125
32.75	1862.7	-	-
33.25	1860.5	0.1170	0.0088
33.75	1858.3	0.1134	0.0158
34.25	1856.2	0.1437	0.0257
34.75	1854.0	0.1085	0.0151
35.25	1851.8	-	-
35.75	1849.7	0.0866	0.0108
36.25	1847.5	0.1277	0.0278
36.75	1845.3	0.0817	0.0089
37.25	1843.1	0.0873	0.0065
37.75	1841.0	0.1063	0.0099
38.25	1838.8	0.0859	0.0144
38.75	1836.6	-	-
39.25	1834.4	0.1427	0.0491
39.75	1832.3	0.1031	0.0066
40.25	1830.1	0.1368	0.0417
40.75	1827.9	0.0839	0.0099
41.25	1825.7	0.0942	0.0591
41.75	1823.6	0.1196	0.0098
42.25	1821.4	0.0927	0.0345

Ave. sample calcite mass (x 10^{-10} g)	Ave. coccolith mass error (1 σ)	No. $CaCO_3$ particles	No. $CaCO_3$ particles error (1 σ)
163329	858	167740	19675
79129	561	80514	10616
90410	395	55597	7847
92692	528	52458	5361
63860	718	41306	11742
125025	812	106152	18111
112627	515	94038	13571
58821	602	42410	4229
76166	418	68979	6304
52220	773	45362	4089
33279	351	22680	3088
75993	356	70107	11502
75837	502	82868	13382
69520	587	-	-
50898	361	49276	5987
117912	1008	36348	8112
71293	287	96115	8570
84365	656	64117	8826
103639	608	77907	4865
121846	452	111123	10735
113906	513	93243	9429
74027	510	118914	16807
142527	669	66018	21411
93318	728	164405	34814
89096	666	78172	11078
133858	407	94111	9093
77532	491	114609	23569
132487	596	53207	8306
5122738	27365	114008	12193
129887	657	138907	49756
92146	430	111038	8355
39612	356	81286	11296
105590	633	27573	4922
114547	373	97301	13526
89751	46973	89888	8597
53370	269	103635	12947
62250	525	41796	9077
135389	593	76147	8313
63765	656	155138	11469
69376	291	59967	5590
93723	551	80798	13533
80825	2410	-	-
96144	273	56640	19507
24325	422	93230	5584
128636	554	17781	5424
131775	759	153353	18075
149838	46053	139906	21156
64272	411	125245	10225
34282	1570	69369	25293

Depth (cm.b.s.f.)	Age (Calender years A.D.)	Ave. coccolith mass x 10^{-10} g	Ave. coccolith mass error (1 σ)
42.75	1819.2	-	-
43.25	1817.0	0.0789	0.0132
43.75	1814.9	0.1014	0.0182
44.25	1812.7	0.1069	0.0234
44.75	1810.5	0.1333	0.0237
45.25	1808.3	0.0952	0.0040
45.75	1806.2	0.1367	0.0172
46.25	1804.0	0.1301	0.0216
46.75	1801.8	0.0954	0.0214
47.25	1799.7	-	-
47.75	1797.5	0.1091	0.0057
48.25	1795.3	0.1182	0.0261
48.75	1793.1	0.0996	0.0177
49.25	1791.0	0.1155	0.0187
49.75	1788.8	-	-
50.25	1786.6	0.1088	0.0329
50.75	1784.4	0.1228	0.0173
51.25	1782.3	0.0938	0.0282
51.75	1780.1	-	-
52.25	1777.9	0.0992	0.0104
52.75	1775.7	-	-
53.25	1773.6	-	-
53.75	1771.4	-	-
54.15	1769.7	-	-

Ave. sample calcite mass (x 10^{-10} g)	Ave. coccolith mass error (1 σ)	No. $CaCO_3$ particles	No. $CaCO_3$ particles error (1 σ)
105771	476	57996	8190
106577	664	133981	22438
96190	640	105120	18897
31972	503	89959	19604
98478	787	23984	4267
69308	377	103493	4309
38914	435	50704	6365
61543	513	29918	4968
150793	695	64480	14421
114929	478		27485
70186	566	105347	5380
58462	310	59356	13076
117782	773	58711	10422
34142	331	101981	16453
145473	411	-	-
65287	9818	133754	11440
133566	571	53162	7478
47466	294	142341	42723
97645	406	23878	4325
107867	599	98477	10298
11132	438	130727	14149
71893	631	5484	3740
63091	676	79465	11083
-	-	76494	6028

Appendix B: Flow-Through Data Processing Software

This appendix holds an annotated version of the Visual Basic software written to process the ICP-MS output resulting from FT-TRA analysis. Code is in black, and annotations in red. Detailed annotations have been provided to assist with the future adaptation of the software.

```
Sub FlowThrough()
Specifies the name of the procedure

Below the necessary variable names and type are declared
Dim Blank As Variant
Dim Std1a As Variant
Dim Std1b As Variant
Dim Std1c As Variant
Dim Std2a As Variant
Dim Std2b As Variant
Dim Std2c As Variant
Dim Std1aRatios(8, 1) As Variant
Dim Std1bRatios(8, 1)  As Variant
Dim Std1cRatios(8, 1)  As Variant
Dim Std2aRatios(8, 1)  As Variant
Dim Std2bRatios(8, 1)  As Variant
Dim Std2cRatios(8, 1)  As Variant
Dim Std1Mean(8, 1)  As Variant
Dim Std2Mean(8, 1)  As Variant
Dim DeviationsFromMeanStd1a(8, 1)  As Variant
Dim DeviationsFromMeanStd1b(8, 1)  As Variant
Dim DeviationsFromMeanStd1c(8, 1)  As Variant
Dim DeviationsFromMeanStd2a(8, 1)  As Variant
Dim DeviationsFromMeanStd2b(8, 1)  As Variant
Dim DeviationsFromMeanStd2c(8, 1)  As Variant
Dim StdConcentrationMean(8, 1)  As Variant
Dim DeviationFromStdConcentrationMean(8, 1) As Variant
Dim Std1SlopeArray(8, 1) As Variant
Dim Std2SlopeArray(8, 1) As Variant
Dim Std1Intensity(8, 1) As Variant
Dim Std2Intensity(8, 1) As Variant
Dim Std1Std2Slope(8, 1) As Variant
Dim StdIntensityForReplicate(8, 1) As Variant
Dim CorrectedReplicateRatio(8, 1) As Variant
Dim Replicate(16, 1) As Variant
Dim ReplicateRatio(8, 1) As Variant
```

```
Dim RatioCorrection(8, 1) As Variant
Dim MassCorrection(8, 1) As Variant
Dim WorksheetArray(13, 1) As Variant
Dim WorksheetArray2(13, 1) As Variant
Dim Std1ConcMean(16, 1) As Variant
Dim Std2ConcMean(16, 1) As Variant
Dim DeviationsFromMeanStd1aConc(16, 1) As Variant
Dim DeviationsFromMeanStd1bConc(16, 1) As Variant
Dim DeviationsFromMeanStd1cConc(16, 1) As Variant
Dim DeviationsFromMeanStd2aConc(16, 1) As Variant
Dim DeviationsFromMeanStd2bConc(16, 1) As Variant
Dim DeviationsFromMeanStd2cConc(16, 1) As Variant
Dim ConcGuess(16, 1) As Variant
Dim Std1ConcIntensity(16, 1) As Variant
Dim Std1Std2ConcSlope(16, 1) As Variant
Dim PredictedReplicateIntensity(16, 1) As Variant
Dim Std2ConcIntensity(16, 1) As Variant
Dim InitialConcGuess(16, 1) As Variant
Dim Std2Equivalent(16, 1) As Variant
Dim Std1ConcSlope(16, 1) As Variant
Dim Std2ConcSlope(16, 1) As Variant
Dim DeviationFromStdConcentrationMean2(16, 1) As Variant
```

The next three sets of lines are where the initial values are assigned to necessary variables.

Reads into the 'NoReplicates' valiable the number of replicates the samples contain from a user specified value on the Excel input page.

```
NoReplicates = Worksheets("Settings").Cells(6, 1).Value
```

Reads into the 'NoSamplesInRun' variable the number of samples to be processed from a user specified value on the Excel input page.

```
NoSamplesInRun = Worksheets("Settings").Cells(10, 1).Value
```

The following 13 lines assign the names of the Excel sheets that are to contain the processed data output to thirteen lines in a two-dimensional array.

```
WorksheetArray(1, 1) = "Sample 1"
WorksheetArray(2, 1) = "Sample 2"
WorksheetArray(3, 1) = "Sample 3"
WorksheetArray(4, 1) = "Sample 4"
WorksheetArray(5, 1) = "Sample 5"
WorksheetArray(6, 1) = "Sample 6"
WorksheetArray(7, 1) = "Sample 7"
WorksheetArray(8, 1) = "Sample 8"
WorksheetArray(9, 1) = "Sample 9"
WorksheetArray(10, 1) = "Sample 10"
WorksheetArray(11, 1) = "Sample 11"
WorksheetArray(12, 1) = "Sample 12"
WorksheetArray(13, 1) = "Sample 13"
```

The following 13 lines assign the names of the Excel sheets that contain the raw input data to thirteen lines in a two-dimensional array.

```
WorksheetArray2(1, 1) = "Input Sample 1"
WorksheetArray2(2, 1) = "Input Sample 2"
WorksheetArray2(3, 1) = "Input Sample 3"
WorksheetArray2(4, 1) = "Input Sample 4"
WorksheetArray2(5, 1) = "Input Sample 5"
WorksheetArray2(6, 1) = "Input Sample 6"
WorksheetArray2(7, 1) = "Input Sample 7"
WorksheetArray2(8, 1) = "Input Sample 8"
WorksheetArray2(9, 1) = "Input Sample 9"
WorksheetArray2(10, 1) = "Input Sample 10"
WorksheetArray2(11, 1) = "Input Sample 11"
WorksheetArray2(12, 1) = "Input Sample 12"
WorksheetArray2(13, 1) = "Input Sample 13"
```

This first 'For To' statement is the start of a loop that will run all of the enclosed codes a number of times equal to the number of samples to be processed.

```
For counter = 1 To NoSamplesInRun
```

This equation reads into the variable 'StartOfSample' the cell at which the data relating to the sample currently being processed begins. This will subsequently act as a reference point. E.g. when the variable 'counter' (which holds a value relating to the number of the sample currently being processed) is 1, then the cell pertaining to the start of the sample is: (1-1)*133 + 1 =1. When 'counter' equals 2, then the starting point to read in the data is cell 134.

```
StartOfSample = (counter - 1) * 133 + 1
```

This statement reads into 16 positions of a two dimensional array 'Blank' the intensities measured for each element in the blank.

```
Blank = Range(Worksheets("Input Std Data").Cells(StartOfSample + 3, 2),
    Worksheets("Input Std Data").Cells(StartOfSample + 18, 2))
```

This statement reads into 16 positions of a two dimensional array 'Sta1a' the intensities measured for each element in first 25ppm Ca standard.

```
Std1a = Range(Worksheets("Input Std Data").Cells(StartOfSample + 22, 2),
    Worksheets("Input Std Data").Cells(StartOfSample + 37, 2))
```

This statement reads into 16 positions of a two dimensional array 'Sta1b' the intensities measured for each element in first 50ppm Ca standard.

```
Std1b = Range(Worksheets("Input Std Data").Cells(StartOfSample + 41, 2),
    Worksheets("Input Std Data").Cells(StartOfSample + 56, 2))
```

This statement reads into 16 positions of a two dimensional array 'Sta1c' the intensities measured for each element in first 100ppm Ca standard.

```
Std1c = Range(Worksheets("Input Std Data").Cells(StartOfSample + 60, 2),
    Worksheets("Input Std Data").Cells(StartOfSample + 75, 2))
```

The following three statements read into three arrays the element intensities for the second set of standards (run after a sample).

```
Std2a = Range(Worksheets("Input Std Data").Cells(StartOfSample + 79, 2),
    Worksheets("Input Std Data").Cells(StartOfSample + 94, 2))
Std2b = Range(Worksheets("Input Std Data").Cells(StartOfSample + 98, 2),
    Worksheets("Input Std Data").Cells(StartOfSample + 113, 2))
Std2c = Range(Worksheets("Input Std Data").Cells(StartOfSample + 117, 2),
    Worksheets("Input Std Data").Cells(StartOfSample + 132, 2))
```

Here a 'For To' loop cycles through the positions relating to the different elements in the standard and blank arrays, subtracting the blank value from the standard value.

```
For i = 1 To 16
   Std1a(i, 1) = Std1a(i, 1) - Blank(i, 1)
   Std1b(i, 1) = Std1b(i, 1) - Blank(i, 1)
   Std1c(i, 1) = Std1c(i, 1) - Blank(i, 1)

   Std2a(i, 1) = Std2a(i, 1) - Blank(i, 1)
   Std2b(i, 1) = Std2b(i, 1) - Blank(i, 1)
   Std2c(i, 1) = Std2c(i, 1) - Blank(i, 1)
Next i
```

This 'For To' loop cycles through the nested code for a number of times equal to the number of replicates in the sample. In this loop 'i' is the counter.

```
For i = 1 To NoReplicates
```

This statement loops along a row of cells reading into an array 'Replicate' the intensities for each measured element for the replicate currently being processed.

```
    For y = 1 To 16
       Replicate(y, 1) = Worksheets(WorksheetArray2(counter, 1)).Cells(i + 2, y +
            1).Value
    Next y
```

Here a 'For To' loop cycles through the positions relating to the different elements in the 'Replicate' and 'Blank' arrays, subtracting the blank value from the standard value.

```
    For y = 1 To 16
       Replicate(y, 1) = Replicate(y, 1) - Blank(y, 1)
    Next y
```

The following section corrects the element values for linear drift during the analysis. To do this we first calculate a linear regression through the measured standards of different concentration for the set of standards run before and after the sample using the equation:

Slope = sample covariance/sample variance
= (sum of (deviations from average x multiplied by deviations from average y) divided by no. data points) Divided by (sum of deviations from x (squared), divided by no data points))

Because the zero concentration there will be zero measured intensity the y-intercept is know to be zero.

First we must find the mean standard intensity from the three measured standards before and after the sample was analysed.

```
For x = 1 To 16
   Std1ConcMean(x, 1) = (Std1a(x, 1) + Std1b(x, 1) + Std1c(x, 1)) / 3
   Std2ConcMean(x, 1) = (Std2a(x, 1) + Std2b(x, 1) + Std2c(x, 1)) / 3
```

To work out the varience we need to know the deviations of measurement from the mean, as assigned to the variables 'DeviationsFromStd*Concs).

```
DeviationsFromMeanStd1aConc(x, 1) = Std1a(x, 1) - Std1ConcMean(x, 1)
DeviationsFromMeanStd1bConc(x, 1) = Std1b(x, 1) - Std1ConcMean(x, 1)
DeviationsFromMeanStd1cConc(x, 1) = Std1c(x, 1) - Std1ConcMean(x, 1)
```

We find the modulus of the values to give us only positive deviations.

```
DeviationsFromMeanStd1aConc(x, 1) = Sqr(DeviationsFromMeanStd1aConc(x, 1)
      * DeviationsFromMeanStd1aConc(x, 1))
DeviationsFromMeanStd1bConc(x, 1) = Sqr(DeviationsFromMeanStd1bConc(x, 1)
      * DeviationsFromMeanStd1bConc(x, 1))
DeviationsFromMeanStd1cConc(x, 1) = Sqr(DeviationsFromMeanStd1cConc(x, 1)
      * DeviationsFromMeanStd1cConc(x, 1))

DeviationsFromMeanStd2aConc(x, 1) = Std2a(x, 1) - Std2ConcMean(x, 1)
DeviationsFromMeanStd2bConc(x, 1) = Std2b(x, 1) - Std2ConcMean(x, 1)
DeviationsFromMeanStd2cConc(x, 1) = Std2c(x, 1) - Std2ConcMean(x, 1)

DeviationsFromMeanStd2aConc(x, 1) = Sqr(DeviationsFromMeanStd2aConc(x, 1)
      * DeviationsFromMeanStd2aConc(x, 1))
DeviationsFromMeanStd2bConc(x, 1) = Sqr(DeviationsFromMeanStd2bConc(x, 1)
      * DeviationsFromMeanStd2bConc(x, 1))
DeviationsFromMeanStd2cConc(x, 1) = Sqr(DeviationsFromMeanStd2cConc(x, 1)
      * DeviationsFromMeanStd2cConc(x, 1))
```

In addition to the pulse intensity measured by ICP-MS for the standards (the y-axis used in calculating the slop) we need also to know the x-axis i.e. the Actual concentration of the element in the standard, as ascertained by standard addition.

The concentrations in the 100ppm Ca standard are as follows:

Ca = 105.4 ppm
U = 0.0061 ppb
Cd = 0.04 ppb
Zn = 0.801 ppb
Ba = 0.974 ppb
Mn = 11.3 ppb
Mg = 0.366 ppm
Sr = 0.333 ppm

Al = 0.05ppm (nominally but used here)

Using the above concentrations we can calculate the deviations from the mean in the standard. We analyse three standard concentration, 50ppm Ca, 75ppm Ca and 100ppm Ca, therefore the mean will be the elemental concentration in the 50ppm Ca standard and the deviation will be the equivalent concentration in a 25ppm Ca standard, or the 100ppm value divided by 4:

```
DeviationFromStdConcentrationMean2(1, 1) = (105.4 / 4)
DeviationFromStdConcentrationMean2(2, 1) = (0.0061 / 4 / 1000)
DeviationFromStdConcentrationMean2(3, 1) = (105.4 / 4)
DeviationFromStdConcentrationMean2(4, 1) = (0.04 / 4 / 1000)
DeviationFromStdConcentrationMean2(5, 1) = (105.4 / 4)
DeviationFromStdConcentrationMean2(6, 1) = (0.801 / 4 / 1000)
DeviationFromStdConcentrationMean2(7, 1) = (105.4 / 4)
DeviationFromStdConcentrationMean2(8, 1) = (0.974 / 4 / 1000)
DeviationFromStdConcentrationMean2(9, 1) = (105.4 / 4)
DeviationFromStdConcentrationMean2(10, 1) = (11.3 / 4 / 1000)
DeviationFromStdConcentrationMean2(11, 1) = (105.4 / 4)
DeviationFromStdConcentrationMean2(12, 1) = (0.366 / 4)
DeviationFromStdConcentrationMean2(13, 1) = (105.4 / 4)
DeviationFromStdConcentrationMean2(14, 1) = (0.333 / 4)
DeviationFromStdConcentrationMean2(15, 1) = (105.4 / 4)
DeviationFromStdConcentrationMean2(16, 1) = 0.05
```

We now have all the data necessary to calculate the standard slopes of the using the formula 'Slope = sample covariance/sample variance'.

```
Std1ConcSlope(x, 1) = (((DeviationFromStdConcentrationMean2(x, 1) * Deviation
    sFromMeanStd1aConc(x, 1)) + (DeviationFromStdConcentrationMean2(x,
    1) * DeviationsFromMeanStd1cConc(x, 1))) / 3) / ((2 * ((DeviationFromStd
    ConcentrationMean2(x, 1) * DeviationFromStdConcentrationMean2(x,
    1)))) / 3)
Std2ConcSlope(x, 1) = (((DeviationFromStdConcentrationMean2(x, 1) * Deviation
    sFromMeanStd2aConc(x, 1)) + (DeviationFromStdConcentrationMean2(x,
    1) * DeviationsFromMeanStd2cConc(x, 1))) / 3) / ((2 * ((DeviationFromStd
    ConcentrationMean2(x, 1) * DeviationFromStdConcentrationMean2(x,
    1)))) / 3)
```

No we know the slopes of the two sets of standards and therefore the plain of how pulse intensity correlates with concentration we can iteratively match the measured intensity of each element in each replicate with the 2-d plain of values and therefore work out what element concentration that intensity corresponds to.

Before we start the iteration we need to guess at the initial values. Out initial guess for the concentration is that which we would see if the replicate was run at the same time at the first set of standards. This value is read into the array variable 'InitialConcGuess'.

```
InitialConcGuess(x, 1) = Replicate(x, 1) / Std1ConcSlope(x, 1)
```

We must convert this concentration guess into an intensity as described the slope of the

final standards:

Std2Equivalent(x, 1) = Std2ConcSlope(x, 1) * InitialConcGuess(x, 1)

We can then describe the slope of the line joining these two point:

Std1Std2ConcSlope(x, 1) = (Std2Equivalent(x, 1) - Replicate(x, 1)) / NoReplicates

Using the above described slope we can calculate what the elemental intensity would be if tour initial concentration guess was correct.

PredictedReplicateIntensity(x, 1) = Std1Std2ConcSlope(x, 1) * i + Replicate(x, 1)

We pass the initial guess of cencentratin into a variable which will be iteratively changed until it provides us with a pulse intensity calculated form the concentration values that matches the measured intensity. We then know the concentration of elements in the standard.

ConcGuess(x, 1) = InitialConcGuess(x, 1)

The first part of the iteration is to ascertain if our guess at the intensity is avove or below the actual measured intensity – we will then be able to iterate with positive or negative steps as required. This is thested in the following 'If... Then' statement.

If PredictedReplicateIntensity(x, 1) > Replicate(x, 1) Then

'Do... while' loop repeatedly decrements the guessed concentration by 0.0005 ppm until it provides an intensity value below measured intensity value. At that point we know that out guessed concentration is within 0.0005 ppm of the real value.

```
Do While PredictedReplicateIntensity(x, 1) > Replicate(x, 1)
  ConcGuess(x, 1) = ConcGuess(x, 1) - 0.0005

  Std1ConcIntensity(x, 1) = Std1ConcSlope(x, 1) * ConcGuess(x, 1)
  Std2ConcIntensity(x, 1) = Std2ConcSlope(x, 1) * ConcGuess(x, 1)

  Std1Std2ConcSlope(x, 1) = (Std2ConcIntensity(x, 1) - Std1ConcIntensity(x,
    1)) / NoReplicates

PredictedReplicateIntensity(x, 1) = Std1Std2ConcSlope(x, 1) * i + Std1ConcIntensity(x, 1)

  Loop
```

Because we require accuracy better than 0.0005 ppm for concentration we then add then step value back onto the guess, so that the guess is again higher than the measured intensity and proceed to iteratively home in on the concentration using progressively smaller and smaller step. This process is repeated in each of the following eight loops with smaller and smaller step values.

```
PredictedReplicateIntensity(x, 1) = Replicate(x, 1) + 0.0005
ConcGuess(x, 1) = ConcGuess(x, 1) + 0.0005

Do While PredictedReplicateIntensity(x, 1) > Replicate(x, 1)
  ConcGuess(x, 1) = ConcGuess(x, 1) - 1e-05
```

```
    Std1ConcIntensity(x, 1) = Std1ConcSlope(x, 1) * ConcGuess(x, 1)
    Std2ConcIntensity(x, 1) = Std2ConcSlope(x, 1) * ConcGuess(x, 1)

    Std1Std2ConcSlope(x, 1) = (Std2ConcIntensity(x, 1) - Std1ConcIntensity(x,
      1)) / NoReplicates

    PredictedReplicateIntensity(x, 1) = Std1Std2ConcSlope(x, 1) * i +
      Std1ConcIntensity(x, 1)

Loop
        PredictedReplicateIntensity(x, 1) = Replicate(x, 1) + 1e-05
        ConcGuess(x, 1) = ConcGuess(x, 1) + 1e-05


Do While PredictedReplicateIntensity(x, 1) > Replicate(x, 1)
  ConcGuess(x, 1) = ConcGuess(x, 1) - 1e-07

    Std1ConcIntensity(x, 1) = Std1ConcSlope(x, 1) * ConcGuess(x, 1)
    Std2ConcIntensity(x, 1) = Std2ConcSlope(x, 1) * ConcGuess(x, 1)

    Std1Std2ConcSlope(x, 1) = (Std2ConcIntensity(x, 1) - Std1ConcIntensity(x,
      1)) / NoReplicates
    PredictedReplicateIntensity(x, 1) = Std1Std2ConcSlope(x, 1) * i +
      Std1ConcIntensity(x, 1)

Loop
    PredictedReplicateIntensity(x, 1) = Replicate(x, 1) + 1e-07
    ConcGuess(x, 1) = ConcGuess(x, 1) + 1e-07


Do While PredictedReplicateIntensity(x, 1) > Replicate(x, 1)
  ConcGuess(x, 1) = ConcGuess(x, 1) - 1e-09

    Std1ConcIntensity(x, 1) = Std1ConcSlope(x, 1) * ConcGuess(x, 1)
    Std2ConcIntensity(x, 1) = Std2ConcSlope(x, 1) * ConcGuess(x, 1)

    Std1Std2ConcSlope(x, 1) = (Std2ConcIntensity(x, 1) - Std1ConcIntensity(x,
      1)) / NoReplicates

    PredictedReplicateIntensity(x, 1) = Std1Std2ConcSlope(x, 1) * i +
      Std1ConcIntensity(x, 1)

Loop
  PredictedReplicateIntensity(x, 1) = Replicate(x, 1) + 1e-09
          ConcGuess(x, 1) = ConcGuess(x, 1) + 1e-09
```

```
Do While PredictedReplicateIntensity(x, 1) > Replicate(x, 1)
   ConcGuess(x, 1) = ConcGuess(x, 1) - 1e-11

   Std1ConcIntensity(x, 1) = Std1ConcSlope(x, 1) * ConcGuess(x, 1)
   Std2ConcIntensity(x, 1) = Std2ConcSlope(x, 1) * ConcGuess(x, 1)

   Std1Std2ConcSlope(x, 1) = (Std2ConcIntensity(x, 1) - Std1ConcIntensity(x,
      1)) / NoReplicates

   PredictedReplicateIntensity(x, 1) = Std1Std2ConcSlope(x, 1) * i +
      Std1ConcIntensity(x, 1)

Loop
   PredictedReplicateIntensity(x, 1) = Replicate(x, 1) + 1e-11
   ConcGuess(x, 1) = ConcGuess(x, 1) + 1e-11


Do While PredictedReplicateIntensity(x, 1) > Replicate(x, 1)
   ConcGuess(x, 1) = ConcGuess(x, 1) - 1e-13

   Std1ConcIntensity(x, 1) = Std1ConcSlope(x, 1) * ConcGuess(x, 1)
   Std2ConcIntensity(x, 1) = Std2ConcSlope(x, 1) * ConcGuess(x, 1)
   Std1Std2ConcSlope(x, 1) = (Std2ConcIntensity(x, 1) - Std1ConcIntensity(x,
      1)) / NoReplicates

   PredictedReplicateIntensity(x, 1) = Std1Std2ConcSlope(x, 1) * i +
      Std1ConcIntensity(x, 1)

Loop
   PredictedReplicateIntensity(x, 1) = Replicate(x, 1) + 1e-13
   ConcGuess(x, 1) = ConcGuess(x, 1) + 1e-13


Do While PredictedReplicateIntensity(x, 1) > Replicate(x, 1)
   ConcGuess(x, 1) = ConcGuess(x, I) - 1e-15

   Std1ConcIntensity(x, 1) = Std1ConcSlope(x, 1) * ConcGuess(x, 1)
   Std2ConcIntensity(x, 1) = Std2ConcSlope(x, 1) * ConcGuess(x, 1)

   Std1Std2ConcSlope(x, 1) = (Std2ConcIntensity(x, 1) - Std1ConcIntensity(x,
      1)) / NoReplicates

   PredictedReplicateIntensity(x, 1) = Std1Std2ConcSlope(x, 1) * i +
      Std1ConcIntensity(x, 1)

Loop
```

```
PredictedReplicateIntensity(x, 1) = Replicate(x, 1) + 1e-15
        ConcGuess(x, 1) = ConcGuess(x, 1) + 1e-15


Do While PredictedReplicateIntensity(x, 1) > Replicate(x, 1)
  ConcGuess(x, 1) = ConcGuess(x, 1) - 1e-18

  Std1ConcIntensity(x, 1) = Std1ConcSlope(x, 1) * ConcGuess(x, 1)
  Std2ConcIntensity(x, 1) = Std2ConcSlope(x, 1) * ConcGuess(x, 1)

  Std1Std2ConcSlope(x, 1) = (Std2ConcIntensity(x, 1) - Std1ConcIntensity(x,
    1)) / NoReplicates

  PredictedReplicateIntensity(x, 1) = Std1Std2ConcSlope(x, 1) * i +
    Std1ConcIntensity(x, 1)
  Loop
  PredictedReplicateIntensity(x, 1) = Replicate(x, 1) + 1e-18
        ConcGuess(x, 1) = ConcGuess(x, 1) + 1e-18


Do While PredictedReplicateIntensity(x, 1) > Replicate(x, 1)
  ConcGuess(x, 1) = ConcGuess(x, 1) - 1e-21

        Std1ConcIntensity(x, 1) = Std1ConcSlope(x, 1) * ConcGuess(x, 1)
        Std2ConcIntensity(x, 1) = Std2ConcSlope(x, 1) * ConcGuess(x, 1)

        Std1Std2ConcSlope(x, 1) = (Std2ConcIntensity(x, 1) - Std1ConcIntensity(x,
          1)) / NoReplicates

        PredictedReplicateIntensity(x, 1) = Std1Std2ConcSlope(x, 1) * i +
Std1ConcIntensity(x, 1)

        Loop
```

We now repeat he same process as above, but for when the initial guess was lower than the measured concentration, so we add a step each time.

```
Else

        Do While PredictedReplicateIntensity(x, 1) < Replicate(x, 1)
          ConcGuess(x, 1) = ConcGuess(x, 1) + 0.0005

          Std1ConcIntensity(x, 1) = Std1ConcSlope(x, 1) * ConcGuess(x, 1)
          Std2ConcIntensity(x, 1) = Std2ConcSlope(x, 1) * ConcGuess(x, 1)

          Std1Std2ConcSlope(x, 1) = (Std2ConcIntensity(x, 1) - Std1ConcIntensity(x,
                1)) / NoReplicates
```

```
        PredictedReplicateIntensity(x, 1) = Std1Std2ConcSlope(x, 1) * i +
                Std1ConcIntensity(x, 1)

    Loop

    PredictedReplicateIntensity(x, 1) = Replicate(x, 1) - 0.0005
    ConcGuess(x, 1) = ConcGuess(x, 1) - 0.0005

    Do While PredictedReplicateIntensity(x, 1) < Replicate(x, 1)
       ConcGuess(x, 1) = ConcGuess(x, 1) + 1e-05

       Std1ConcIntensity(x, 1) = Std1ConcSlope(x, 1) * ConcGuess(x, 1)
       Std2ConcIntensity(x, 1) = Std2ConcSlope(x, 1) * ConcGuess(x, 1)

       Std1Std2ConcSlope(x, 1) = (Std2ConcIntensity(x, 1) - Std1ConcIntensity(x,
                1)) / NoReplicates

       PredictedReplicateIntensity(x, 1) = Std1Std2ConcSlope(x, 1) * i +
                Std1ConcIntensity(x, 1)


    Loop

    PredictedReplicateIntensity(x, 1) = Replicate(x, 1) - 1e-05
    ConcGuess(x, 1) = ConcGuess(x, 1) - 1e-05

    Do While PredictedReplicateIntensity(x, 1) < Replicate(x, 1)
       ConcGuess(x, 1) = ConcGuess(x, 1) + 1e-07

       Std1ConcIntensity(x, 1) = Std1ConcSlope(x, 1) * ConcGuess(x, 1)
       Std2ConcIntensity(x, 1) = Std2ConcSlope(x, 1) * ConcGuess(x, 1)

       Std1Std2ConcSlope(x, 1) = (Std2ConcIntensity(x, 1) - Std1ConcIntensity(x,
                1)) / NoReplicates

       PredictedReplicateIntensity(x, 1) = Std1Std2ConcSlope(x, 1) * i +
                Std1ConcIntensity(x, 1)

    Loop

       PredictedReplicateIntensity(x, 1) = Replicate(x, 1) - 1e-07
                ConcGuess(x, 1) = ConcGuess(x, 1) - 1e-07

    Do While PredictedReplicateIntensity(x, 1) < Replicate(x, 1)
       ConcGuess(x, 1) = ConcGuess(x, 1) + 1e-09

       Std1ConcIntensity(x, 1) = Std1ConcSlope(x, 1) * ConcGuess(x, 1)
       Std2ConcIntensity(x, 1) = Std2ConcSlope(x, 1) * ConcGuess(x, 1)
```

```
        Std1Std2ConcSlope(x, 1) = (Std2ConcIntensity(x, 1) - Std1ConcIntensity(x,
            1)) / NoReplicates

        PredictedReplicateIntensity(x, 1) = Std1Std2ConcSlope(x, 1) * i +
            Std1ConcIntensity(x, 1)

    Loop

        PredictedReplicateIntensity(x, 1) = Replicate(x, 1) - 1e-09
            ConcGuess(x, 1) = ConcGuess(x, 1) - 1e-09

    Do While PredictedReplicateIntensity(x, 1) < Replicate(x, 1)
        ConcGuess(x, 1) = ConcGuess(x, 1) + 1e-11

        Std1ConcIntensity(x, 1) = Std1ConcSlope(x, 1) * ConcGuess(x, 1)
        Std2ConcIntensity(x, 1) = Std2ConcSlope(x, 1) * ConcGuess(x, 1)

        Std1Std2ConcSlope(x, 1) = (Std2ConcIntensity(x, 1) - Std1ConcIntensity(x,
        1)) / NoReplicates

        PredictedReplicateIntensity(x, 1) = Std1Std2ConcSlope(x, 1) * i +
        Std1ConcIntensity(x, 1)

    Loop

    PredictedReplicateIntensity(x, 1) = Replicate(x, 1) - 1e-11
    ConcGuess(x, 1) = ConcGuess(x, 1) - 1e-11

    Do While PredictedReplicateIntensity(x, 1) < Replicate(x, 1)
        ConcGuess(x, 1) = ConcGuess(x, 1) + 1e-13

        Std1ConcIntensity(x, 1) = Std1ConcSlope(x, 1) * ConcGuess(x, 1)
        Std2ConcIntensity(x, 1) = Std2ConcSlope(x, 1) * ConcGuess(x, 1)

        Std1Std2ConcSlope(x, 1) = (Std2ConcIntensity(x, 1) - Std1ConcIntensity(x.
        1)) / NoReplicates

        PredictedReplicateIntensity(x, 1) = Std1Std2ConcSlope(x, 1) * i +
        Std1ConcIntensity(x, 1)

    Loop
    PredictedReplicateIntensity(x, 1) = Replicate(x, 1) - 1e-13
    ConcGuess(x, 1) = ConcGuess(x, 1) - 1e-13

    Do While PredictedReplicateIntensity(x, 1) < Replicate(x, 1)
        ConcGuess(x, 1) = ConcGuess(x, 1) + 1e-15
```

```
        Std1ConcIntensity(x, 1) = Std1ConcSlope(x, 1) * ConcGuess(x, 1)
        Std2ConcIntensity(x, 1) = Std2ConcSlope(x, 1) * ConcGuess(x, 1)

        Std1Std2ConcSlope(x, 1) = (Std2ConcIntensity(x, 1) - Std1ConcIntensity(x,
        1)) / NoReplicates

        PredictedReplicateIntensity(x, 1) = Std1Std2ConcSlope(x, 1) * i +
        Std1ConcIntensity(x, 1)

    Loop

        PredictedReplicateIntensity(x, 1) = Replicate(x, 1) - 1e-15
                ConcGuess(x, 1) = ConcGuess(x, 1) - 1e-15

    Do While PredictedReplicateIntensity(x, 1) < Replicate(x, 1)
        ConcGuess(x, 1) = ConcGuess(x, 1) + 1e-18

        Std1ConcIntensity(x, 1) = Std1ConcSlope(x, 1) * ConcGuess(x, 1)
        Std2ConcIntensity(x, 1) = Std2ConcSlope(x, 1) * ConcGuess(x, 1)

        Std1Std2ConcSlope(x, 1) = (Std2ConcIntensity(x, 1) - Std1ConcIntensity(x,
                1)) / NoReplicates
        PredictedReplicateIntensity(x, 1) = Std1Std2ConcSlope(x, 1) * i +
                Std1ConcIntensity(x, 1)

    Loop

        PredictedReplicateIntensity(x, 1) = Replicate(x, 1) - 1e-18
                ConcGuess(x, 1) = ConcGuess(x, 1) - 1e-18

    Do While PredictedReplicateIntensity(x, 1) < Replicate(x, 1)
        ConcGuess(x, 1) = ConcGuess(x, 1) + 1e-21

        Std1ConcIntensity(x, 1) = Std1ConcSlope(x, 1) * ConcGuess(x, 1)
        Std2ConcIntensity(x, 1) = Std2ConcSlope(x, 1) * ConcGuess(x, 1)

        Std1Std2ConcSlope(x, 1) = (Std2ConcIntensity(x, 1) - Std1ConcIntensity(x,
                1)) / NoReplicates

        PredictedReplicateIntensity(x, 1) = Std1Std2ConcSlope(x, 1) * i +
                Std1ConcIntensity(x, 1)

    Loop

End If
```

The values held in the array variable 'CncGuess' are now estimated correctly to the

nearest 10e-21ppm, so can be transferred the output sheet. Here we move the values from the array variable into individual variables with more meaningful names to help keep the code transparent.

```
CalciumConcentration1 = ConcGuess(1, 1)
CalciumConcentration2 = ConcGuess(3, 1)
CalciumConcentration3 = ConcGuess(5, 1)
CalciumConcentration4 = ConcGuess(7, 1)
CalciumConcentration5 = ConcGuess(9, 1)
CalciumConcentration6 = ConcGuess(11, 1)
CalciumConcentration7 = ConcGuess(13, 1)
CalciumConcentration8 = ConcGuess(15, 1)
UraniumConcentration = ConcGuess(2, 1)
CadmiumConcentration = ConcGuess(4, 1)
ZinkConcentration = ConcGuess(6, 1)
BariumConcentration = ConcGuess(8, 1)
ManganeseConcentration = ConcGuess(10, 1)
MagnesiumConcentration = ConcGuess(12, 1)
StrontiumConcentration = ConcGuess(14, 1)
AluminiumConcentration = ConcGuess(16, 1)
```

The program now loops back for the next element

```
Next x
```

Here the final concentrations are passed to the output sheet. The primary Ca values are averaged from the 8 different times Ca has been measured

```
Worksheets(WorksheetArray(counter, 1)).Cells(i + 3, 2).Value =
(CalciumConcentration1 + CalciumConcentration2
+ CalciumConcentration3 + CalciumConcentration4 + CalciumConcentration5 +
CalciumConcentration6 + CalciumConcentration7 + CalciumConcentration8) / 8
```

For all elements the ppm value is outputted onto the output sheet and then the trace-element/calcium ratios are worked out as pairs between each element and it's neighbouring calcium on the spreadsheet.

```
Worksheets(WorksheetArray(counter, 1)).Cells(i + 3, 11).Value =
        UraniumConcentration
Worksheets(WorksheetArray(counter, 1)).Cells(i + 3, 12).Value =
        CadmiumConcentration
Worksheets(WorksheetArray(counter, 1)).Cells(i + 3, 13).Value =
        ZinkConcentration
Worksheets(WorksheetArray(counter, 1)).Cells(i + 3, 14).Value =
        BariumConcentration
Worksheets(WorksheetArray(counter, 1)).Cells(i + 3, 15).Value =
        ManganeseConcentration
Worksheets(WorksheetArray(counter, 1)).Cells(i + 3, 16).Value =
        MagnesiumConcentration
Worksheets(WorksheetArray(counter, 1)).Cells(i + 3, 17).Value =
        StrontiumConcentration
Worksheets(WorksheetArray(counter, 1)).Cells(i + 3, 18).Value =
```

```
            AluminiumConcentration

        Worksheets(WorksheetArray(counter, 1)).Cells(i + 3, 20).Value =
            CalciumConcentration1
        Worksheets(WorksheetArray(counter, 1)).Cells(i + 3, 21).Value =
            CalciumConcentration2
        Worksheets(WorksheetArray(counter, 1)).Cells(i + 3, 22).Value =
            CalciumConcentration3
        Worksheets(WorksheetArray(counter, 1)).Cells(i + 3, 23).Value =
            CalciumConcentration4
        Worksheets(WorksheetArray(counter, 1)).Cells(i + 3, 24).Value =
            CalciumConcentration5
        Worksheets(WorksheetArray(counter, 1)).Cells(i + 3, 25).Value =
            CalciumConcentration6
        Worksheets(WorksheetArray(counter, 1)).Cells(i + 3, 26).Value =
            CalciumConcentration7
        Worksheets(WorksheetArray(counter, 1)).Cells(i + 3, 27).Value =
            CalciumConcentration8


The process now loops back for the next replicate
    Next i
The code now loops back for the next sample
Next counter

'End sub' denotes the end of the procedure.
End Sub
```

Appendix C: Estimation of *C. pelagicus* Surface Area to Volume Ratio

A first-order estimation of the surface area to volume ratio of a single coccolith produced by *C. pelagicus* has been calculated from the SEM image of a cross section through a *C. pelagicus* coccolith displayed below.

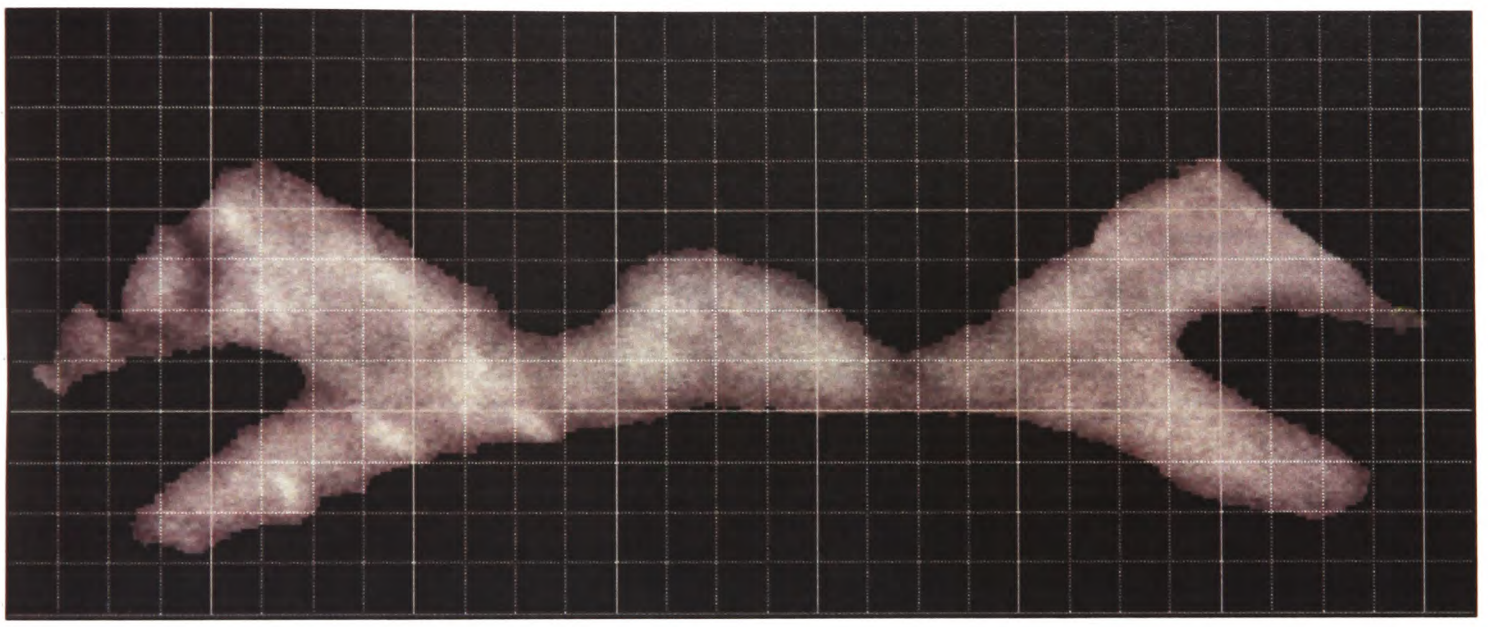

It has been assumed that the coccolith is circular in the plane of the shields. The outline length is 80 units and the area 42 units, giving a surface area to volume ratio of 1.9.

Appendix D: Culture Medium Chemical Composition

	Ca (ppm)	Mg (ppm)	Sr (ppm)	Ba (ppb)	Mn (ppb)	Cd (ppb)	Zn (ppb)
Culture Medium Concentration	435.50	1257.20	8.19	90.85	0.94	0.21	21.05

Element concentrations measured in the culture medium. Measurements were made by diluting the sample 10 times for Ca, Mn, Cd and Zn analysis and 1000 times for Ca, Mg and Sr analysis, then performing standard addition. The table below presents the same data but ratioed to Ca, and using the units mmol or μmol/mol

	Mg/Ca (mmol/mol)	Sr/Ca (mmol/mol)	Ba/Ca (μmol/mol)	Mn/Ca (μmol/mol)	Cd/Ca (μmol/mol)	Zn/Ca (μmol/mol)
Culture Medium ratio	4763.8	8.6	60.9	1.6	0.2	29.6

Appendix E: Worked Example to Accompany Chapter 6

This appendix presents a theoretical worked example demonstrating the method presented in Chapter 6, to allow calculation of species-specific coccolith chemistry.

This example begins by assuming that one has filtered the sediment sample of interest into a narrow size range (e.g. 2-4 μm), and that this size range contains only coccoliths of three species (species x, species y and species z). The sample has then been split by settling into three fractions, each containing a different proportion of the three species. Species counts are then performed upon these three fractions, weigh the mass of calcite in each fraction (weighing before and after acid addition to account for the non-$CaCO_3$ component of sediment), and analyse the bulk chemistry of each fraction.

The first step is then to work out the average coccolith mass of each species using the formula presented in Chapter 5:

Fraction 1:

$$a_1 \cdot SM_x + b_1 \cdot SM_y + c_1 \cdot SM_z = \text{fraction1 } CaCO_3 \text{ mass}$$

Fraction 2:

$$a_2 \cdot SM_x + b_2 \cdot SM_y + c_2 \cdot SM_z = \text{fraction2 } CaCO_3 \text{ mass}$$

Fraction 3:

$$a_3 \cdot SM_x + b_3 \cdot SM_y + c_3 \cdot SM_z = \text{fraction3 } CaCO_3 \text{ mass}$$

where a, b and c are the absolute counts of each of three species (x, y and z) with subscripts indicating to which fraction the counts belong, fraction(1, 2 or 3) $CaCO_3$ mass is the mass of

calcite measured in that fraction, and $SM_{(x, y \text{ or } z)}$ values are the species mass', the unknowns we want to solve these equations for.

If we assume the absolute species counts to be as follows, where a's represent the counts for species x, b's represent the counts for species y and c's represent the counts for species z, and the subscript 1 2 or 3 indicates in which of the three fractions the count has taken place:

$a_1 = 10000$	$b_1 = 800000$	$c_1 = 500000$
$a_2 = 200000$	$b_2 = 400000$	$c_2 = 300000$
$a_3 = 20000$	$b_3 = 600000$	$c_3 = 500000$

and the measured mass of $CaCO_3$ in each fraction to be:

Fraction1 $CaCO_3$	8000000 units
Fraction1 $CaCO_3$	6000000 units
Fraction1 $CaCO_3$	7000000 units

Then:

Fraction 1:

$$10000 \cdot SM_x + 800000 \cdot SM_y + 500000 \cdot SM_z = 8000000$$

Fraction 2:

$$200000 \cdot SM_x + 400000 \cdot SM_y + 300000 \cdot SM_z = 6000000$$

Fraction 3:

$$20000 \cdot SM_x + 600000 \cdot SM_y + 500000 \cdot SM_z = 7000000$$

The equations can be solved for the individual average species mass' (SM'), giving:

$SM_x = 8.42$ units

$SM_y = 5.42$ units

$SM_z = 7.16$ units

We now know the average coccolith mass (calcification) of the three species in the sample. At this stage we could use the results to look at species-specific changes in calcification, over a period of environmental change such as the Anthropocene (and therefore elaborating on the results presented in Chapter 2), or we could go further and calculate the species-specific chemistry (i.e. Sr/Ca or oxygen isotopes). To do this we need to know the average coccolith mass of each species (obtained from the above calculations), relative species counts (already obtained to allow the above calculations), and the bulk chemistry of the three fractions. We can then use the equations presented in Chapter 5:

Fraction 1:

$$a_1 \cdot SM_x \cdot SC_x + b_1 \cdot SM_y \cdot SC_y + c_1 \cdot SM_z \cdot SC_z = \text{bulk geochemistry measured in fraction1}$$

Fraction 2:

$$a_2 \cdot SM_x \cdot SC_x + b_2 \cdot SM_y \cdot SC_y + c_2 \cdot SM_z \cdot SC_z = \text{bulk geochemistry measured in fraction2}$$

Fraction 3:

$$a_3 \cdot SM_x \cdot SC_x + b_3 \cdot SM_y \cdot SC_y + c_3 \cdot SM_z \cdot SC_z = \text{bulk geochemistry measured in fraction3}$$

where a, b and c are the relative proportions of three species in fractions 1, 2 and 3 (denoted by subscripts) with different proportions of each species, and Species x, Species y and Species z have known mass' ($MS_{(x,y \text{ and } z)}$ = 8.42, 5.42 and 7.16 units respectively) but unknown

chemistry (for example Sr/Ca or $\delta^{18}O$, referred to as $SC_{(x,y\ or\ z)}$).

If the relative species counts are:

$a_1 = 0.34$	$b_1 = 0.25$	$c_1 = 0.41$
$a_2 = 0.87$	$b_2 = 0.08$	$c_2 = 0.05$
$a_3 = 0.13$	$b_3 = 0.72$	$c_3 = 0.15$

and:

bulk geochemistry measured in fraction1 =	1.471 units
bulk geochemistry measured in fraction3 =	1.677 units
bulk geochemistry measured in fraction3 =	3.565 units

then we can form the equations:

Fraction 1:

$$0.34 \cdot 8.42 \cdot SC_x + 0.25 \cdot 5.42 \cdot SC_y + 0.41 \cdot 7.16 \cdot SC_z = 1.471$$

Fraction 2:

$$0.87 \cdot 8.42 \cdot SC_x + 0.08 \cdot 5.42 \cdot SC_y + 0.05 \cdot 7.16 \cdot SC_z = 1.677$$

Fraction 3:

$$0.13 \cdot 8.42 \cdot SC_x + 0.72 \cdot 5.42 \cdot SC_y + 0.15 \cdot 7.16 \cdot SC_z = 3.565$$

which can be solved to give:

$SC_x = 0.181$ units

$SC_y = 0.886$ units

$SC_z = -0.084$ units

These values are therefore the individual chemistries of the coccoliths of the three species x, y and z.